TECHNISCHE UNIVERSITÄT WIEN
Vienna | Austria

ESEA
Institut für Energiesysteme und Elektrische Antriebe

Dissertation

Vertical Volt/var chain control as part of the *LINK*-based holistic architecture

carried out for the purpose of obtaining the degree of Doctor technicae (Dr. techn.), submitted at TU Wien, Faculty of Electrical Engineering and Information Technology, by

.....

Daniel-Leon Schultis

Mat.Nr.: 1131268

under the supervision of

Associate Prof. Dipl.-Ing. Dr.techn. Albana Ilo

Institute of Energy Systems and Electrical Drives, E370

Vienna, June 2021

Reviewed by

.....	.....
Prof. Goran Strbac	Univ.Prof. Dr.-Ing. Wolfgang Gawlik
Imperial College London	TU Wien

Acknowledgements

I sincerely thank my thesis supervisor Albana Ilo for her outstanding support and the time she invested in guiding me through the broad topic of smart grids. She has inspired me to turn away from partial views and approach power systems from a holistic perspective.

I appreciate the continuous support from my parents, Eva-Martina and Hans-Wolfgang, who always encouraged me to go my own way.

Furthermore, I thank Wolfgang Gawlik and Manfred Schrödl for providing the resources of the Institute of Energy Systems and Electrical Drives necessary to conduct my studies.

Thank you, Lena, for always motivating me to complete this thesis and standing by me in times I was mainly occupied by work.

For my daughter Marie-Leonie.

Abstract

Volt/var management is one of the most fundamental power system processes that enables the reliable and efficient operation of the electricity grids. Nowadays, the massive connection of renewable and distributed generation and the electrification of other sectors give rise to new challenges and opportunities that call for an adaption of the traditional Volt/var control schemes. Recently, different local controls, such as cos$\varphi(P)$- and $Q(U)$-control of photovoltaic inverters and on-load tap changers in distribution substations, have emerged to mitigate voltage limit violations at the low voltage level. However, the local controls of photovoltaic inverters provoke uncontrolled reactive flows in the superordinate grids challenging their operation. Attempts to coordinate them require large-scale data sharing leading to cybersecurity issues. As a result, the integration of distributed and renewable energy sources is stalling, even though it is needed more than ever to decarbonise the economy under today's climate change condition.

The *LINK*-based holistic architecture incorporates all power system levels, including customer plants, into a standardised structure. It perceives Smart Grids in two axes: horizontal axis including very high and high voltage grids; and vertical axis including the high, medium and low voltage grids and the customer plants. The secondary control is the basic instrument for coordinating the operation throughout the entire Smart Grid. This thesis focuses on the Volt/var secondary control chain process in the vertical axis.

A comprehensive and systematic study is conducted to analyse the Volt/var behaviour in the presence of the recently emerged and newly introduced control strategies. Results show that cos$\varphi(P)$- and $Q(U)$-control of photovoltaic inverters and on-load tap changers in distribution substations are insufficient to meet the social and technical requirements of future Smart Grids. In contrast, the newly introduced $X(U)$-control in radial structures combined with Q-Autarkic customer plants maintain voltage limit compliance reliably, effectively, and efficiently while preserving the interests of all involved stakeholders. Additionally, it is found that the voltage limits in radial structures (e.g. medium voltage) are deformed by the voltage drops in the subordinate grids (e.g. low voltage). The deformation degree depends on the low voltage feeders' properties: the greater the feeder impedance and the number of connected customer plants, the more intensive is the deformation. The lumped grid models are extended by a new parameter, the "boundary voltage limits", to consider the limit deformation. It allows verifying voltage limit compliance at the low voltage level by conducting load flow analysis at the medium voltage level.

Kurzfassung

Das Spannungs- und Blindleistungs-Management ist einer der grundlegendsten Prozesse des Stromversorgungssystems, der den zuverlässigen und effizienten Betrieb der Netze ermöglicht. Heutzutage führt der massive Anschluss von erneuerbarer und dezentraler Erzeugung und die Elektrifizierung anderer Sektoren zu neuen Herausforderungen und Chancen, die eine Anpassung der traditionellen Regelungsstrategien erfordern. Deshalb wurden in jüngster Vergangenheit verschiedene lokale Regelungen, wie die cosφ(P)- und Q(U)-Regelung von Photovoltaik-Wechselrichtern und regelbare Ortsnetztransformatoren, eingeführt, welche den Verletzungen der Spannungsgrenzwerte im Niederspannungsnetz entgegenwirken sollen. Die lokalen Regelung der Photovoltaik-Wechselrichter führen jedoch zu unkontrollierten Blindleistungsflüssen in den übergeordneten Netzebenen, welche ihren Betrieb erschweren. Ihre Koordinierung würde einen immensen Datenaustausch benötigen, welcher die Cybersicherheit gefährdet. Infolgedessen stockt die Integration dezentraler und erneuerbarer Energiequellen, obwohl sie mehr denn je erforderlich ist, um die Wirtschaft unter den heutigen Bedingungen des Klimawandels zu dekarbonisieren.

Die *LINK*-basierte ganzheitliche Architektur gliedert alle Ebenen des Stromversorgungssystems, einschließlich der Kundenanlagen, in eine standardisierte Struktur ein. Sie erfasst Smart Grids in zwei Achsen: die Horizontale, welche Höchst- und Hochspannungsnetze beinhaltet, und die Vertikale, welche Hoch-, Mittel- und Niederspannungsnetze sowie Kundenanlagen beinhaltet. Die Sekundärregelung bildet das grundlegende Instrument für den koordinierten Betrieb des gesamten Smart Grids. Diese Dissertation beschäftigt sich mit der Spannungs-/Blindleistungs-Kettenregelung in der vertikalen Achse.

Das Netzverhalten unter den kürzlich eingeführten und neu vorgeschlagenen Regelungsstrategien wird in einer umfangreichen und systematischen Studie analysiert. Die Ergebnisse zeigen, dass die cosφ(P)- und Q(U)-Regelung von Photovoltaik-Wechselrichtern sowie die regelbaren Ortsnetztransformatoren nicht die sozialen und technischen Anforderungen zukünftiger Smart Grids erfüllen. Im Gegensatz dazu gewährleisten die X(U)-Regelung und ihre Kombination mit Q-Autarken Kundenanlagen die Einhaltung der Spannugsgrenzwerte zuverlässig, effektiv und effizient, während die Interessen aller beteiligten Akteure gewahrt bleiben. Außerdem zeigt sich, dass die Spannungsgrenzen in radialen Strukturen (z. B. Mittelspannungsnetze) durch die Spannungsabfälle in den untergeordneten Netzen (z. B. Niederspannungsnetze) verformt werden. Der Verformungsgrad hängt von den Eigenschaften der

Niederspannungs-Stichleitungen ab: Je höher die Leitungsimpedanz und die Anzahl der angeschlossenen Kundenanlagen, desto stärker ist die Verformung. Die konzentrierten Modelle der Niederspannungsnetze werden um einen neuen Parameter, die "Grenzspannungsgrenzen", erweitert, um die Verformung der Spannungsgrenzen zu berücksichtigen. Die Grenzspannungsgrenzen ermöglichen die Überprüfung der Einhaltung der Spannungsgrenzwerte auf der Niederspannungsebene durch Lastflussanalysen auf der Mittelspannungsebene.

Table of Contents

1 Introduction

Volt/var management is one of the most fundamental power system processes that enables the reliable and efficient operation of the electricity grids. It is used to ensure compliance with voltage limits and to keep the power factor close to one. Both the elimination of voltage limit violations and the minimisation of the reactive power flows extend the active power transfer capability of the grid. In other words, an appropriate Volt/var control increases the utilisation of the electrical infrastructure, thus lowering the need for grid reinforcement.

The massive connection of renewable and distributed generation and the electrification of other sectors gave rise to new challenges and opportunities that call for an adaption of the traditional Volt/var control schemes. Deteriorated power quality and uncontrolled interactions between the systems operated by different stakeholders are recognised as the main problems to be solved by future smart grids (Sun et al. 2019). Meanwhile, the ability of distributed energy resources to participate in the Volt/var process (Bollen and Sannino 2005) and the active role of customer plants (Schweiger et al. 2020) introduce new control opportunities. Numerous approaches are discussed in the literature that focus on certain grid parts, devices or control strategies without embedding the proposed concepts into a holistic architecture. The result is a jungle of individual solutions for individual issues that do not fit into one another to establish the optimum of the overall system.

This thesis introduces the Volt/var chain process in the framework of the *LINK*-based holistic architecture. Chapter 2 presents the relevant aspects of the existing architecture, including the underlying paradigm and model, the architecture components and structure, different architectural levels, and the chain control strategy. Chapter 3 focuses on the Volt/var chain process. Firstly, the corresponding physical and technical fundamentals are explained. The state-of-art is reviewed by presenting the traditional Volt/var control and the recently introduced control strategies from the holistic view of the power system. A clear problem statement is given that underlines the necessity of a holistic approach for Volt/var control. The generalised *LINK*-based Volt/var chain control is presented in great detail. Different Volt/var control setups are analysed by conducting load flow simulations in vertical power system axes. The investigated control setups are evaluated to provide a clear picture of their individual strengths and weaknesses. A general guideline and a step-by-step procedure for setting up the effective Volt/var chain control for specific vertical axes are presented.

2 *LINK*-based holistic architecture

The electricity supply structure changes radically because of many distributed generation units, each with the possibility of interfering with the system operation at all voltage levels, and the electrification of other sectors. The utilisation of the added flexibility necessitates a new architecture that should guarantee to perform as expected by unifying their whole structure and systematising operational tasks. It should handle the scalability of the system and minimise the complexity.

By definition, a *holistic power system architecture* is an architecture where all relevant components of the power system are merged into one single structure. These components could comprise of the following:

- Electricity producer (regardless of technology or size, e.g. big power plants, distributed generations, etc.),
- Electricity storage (regardless of technology or size, e.g. pumped power plants, batteries, etc.),
- Electricity grid (regardless of voltage level, e.g. high, medium and low voltage grid),
- Customer plants, and
- Electricity market.

The holistic architecture unifies all interactions within the power system itself, between the network-, generation- and storage operators, consumers and prosumers, and the market, thus creating the possibility to harmonise them without compromising data privacy and cybersecurity. It facilitates all necessary processes for a reliable, economical, and environmentally friendly operation of smart power systems. It allows a clear description of the relationships between different actors and creates conditions to go through the transition phase without causing problems. It enables the integration of local energy communities and sector coupling (ETIP SNET 2019).

2.1 *LINK*-Paradigm and the associated holistic model

By definition, the *LINK*-Paradigm is a set of one or more Electrical Appliances (ElA), i.e. a grid part, storage or producer device, the controlling schema, and the interface (Ilo 2016a). Fig. 2.1 shows the overview of the *LINK*-Paradigm.

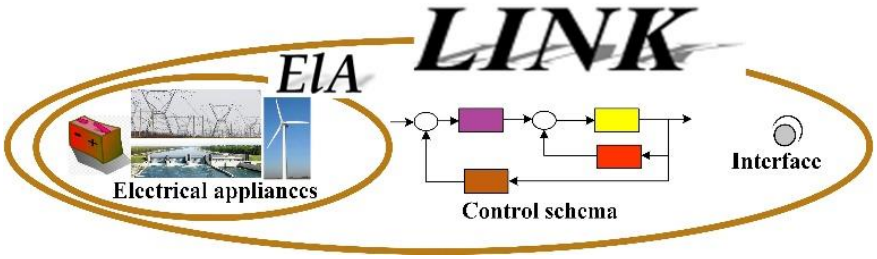

Fig. 2.1 Overview of the *LINK*-Paradigm. (Ilo 2019)

The *LINK*-Paradigm is used as an instrument to design a *LINK*-based holistic architecture. It facilitates modelling of the entire power system from High (HV) to Low Voltage (LV) levels, including Customer Plants (CP). It enables the description of all power system operation processes such as load-generation balance, voltage assessment, dynamic security, price- and emergency-driven demand response, etc. (Vaahedi 2014). The *LINK*-Paradigm is fundamental to the holistic technical and market-related smart grid models with large shares of Distributed Energy Resources (DER). Fig. 2.2a shows the holistic technical model, i.e. the *Energy Supply Chain Net* (Ilo 2013), which illustrates the links' compositions and their relative position in space, both horizontally and vertically. In the horizontal axis, the interconnected HV grids are arranged. They are owned and operated by Transmission System Operators (TSO). Medium Voltage (MV), LV and CP grids, including the HV grid to which the MV grid is connected, are set vertically. MV and LV grids are owned and operated by the Distribution System Operators (DSO), while customers own the CPs.

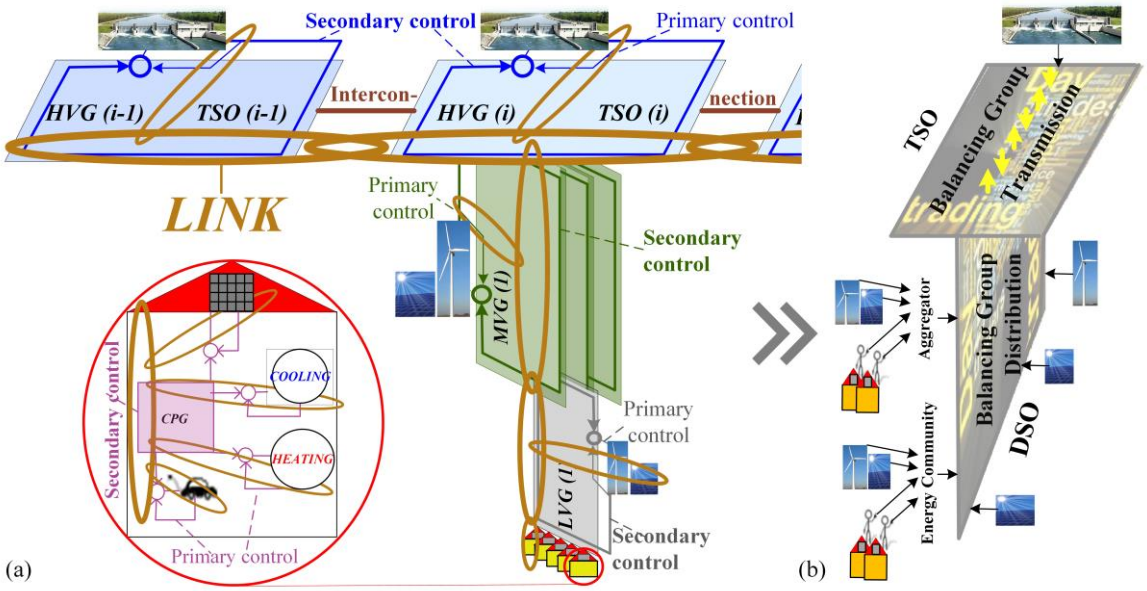

Fig. 2.2 Overview of the holistic models: (a) technical; (b) market-related. (Ilo 2019)

By definition, an *Energy Supply Chain Net* is a set of automated power grids intended for chain links (abbreviated as links), which fit into one another to establish a flexible and reliable electrical connection. Each individual link or link bundle operates autonomously and has contractual arrangements with other relevant boundary links or link bundles.

The holistic model associated with the energy market is derived from the holistic technical model as shown in Fig. 2.2b. The whole energy market consists of coupled market areas (balancing groups) at the horizontal and vertical axes. TSOs operate on the horizontal axis of the holistic market model, while DSOs operate on the vertical ones. Based on this model, TSOs and DSOs will communicate directly with the whole market to ensure a congestion-free distribution grid operation and take over the task of load-production balance. The owners of DER and the prosumers (producers and consumers of electricity) may participate directly in the market or via aggregators or local energy communities (Ilo et al. 2019). The creation of the local retail markets attracts the demand response bids and stimulates investment in the local energy communities.

2.2 Architecture components and structure

Based on the *LINK*-Paradigm are defined three independent architecture elements: Grid-, Producer- and Storage-Link.

2.2.1 Grid-Link

The Grid-Link is defined as a composition of a grid part, called Link-Grid, the corresponding Secondary Control (SC), and the interface, Fig. 2.3a.

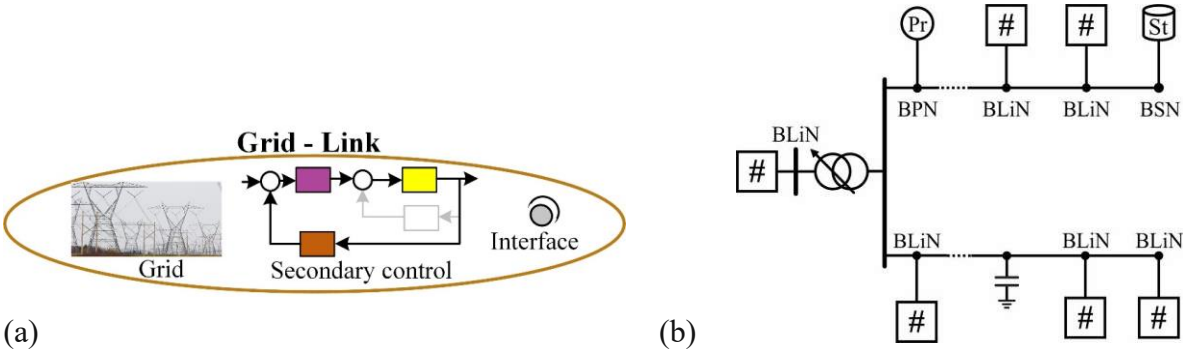

Fig. 2.3 Grid-Link: (a) overview; (b) electrical scheme.

The Link-Grid refers to electrical equipment, such as lines/cables, transformers, and Reactive Power Devices (RPD), connected directly to each other, forming an electrical unity. The size of the Link-Grid size is variable and defined from the area where the SC is set up. Therefore, the Link-Grid may include one subsystem, e.g. the Supplying Transformer (STR) and the

feeders supplied from it, or a part of the sub-transmission network, as long as the SC is set up on the respective area. As a result, depending on its size, the Link-Grid may represent the HV, MV, LV and even the CP grid. Fig. 2.3b shows an overview of a typical Link-Grid. Each Link-Grid has many Boundary Link Nodes (BLiN) through which it connects neighbouring Link-Grids. The neighbouring Link-Grids are represented by the symbol [#]. Producer- and Storage-Links exchange power with the Link-Grid through their Boundary Producer Nodes (BPN) and Boundary Storage Nodes (BSN), respectively.

By definition, the Link-Grid is upgraded with SC for both major power system entities, i.e. frequency and voltage. Fig. 2.4a and b show the Hertz/Watt (HzW**SC**) and Volt/var Secondary Control (Vv**SC**) of a typical Grid-Link.

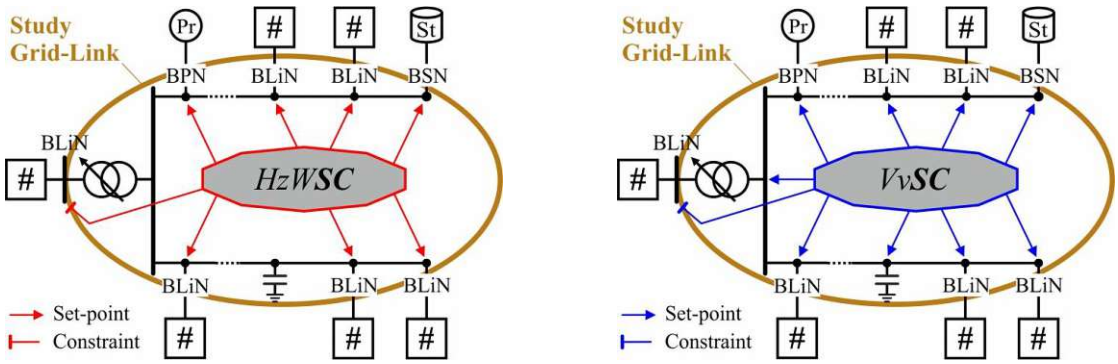

Fig. 2.4 Overview of secondary control: (a) Hertz/Watt; (b) Volt/var.

The SC algorithm needs to fulfil technical issues and calculate the set-points for the connected elements by respecting the dynamic constraints necessary to enable a stable operation. The Link-Grid's facilities, i.e. transformers and RPDs, are mostly upgraded with Primary (PC), Direct (DiC) or Local Control (LC) (see §3.1.5). Thus, the SC sends set-points to the Link-Grid's facilities and all elements connected at the boundary nodes.

2.2.2 Producer-Link

The Producer-Link is defined as a composition of an electricity production facility, such as a generator, Photovoltaic (PV) system, etc., its PC, and the interface, Fig. 2.5a.

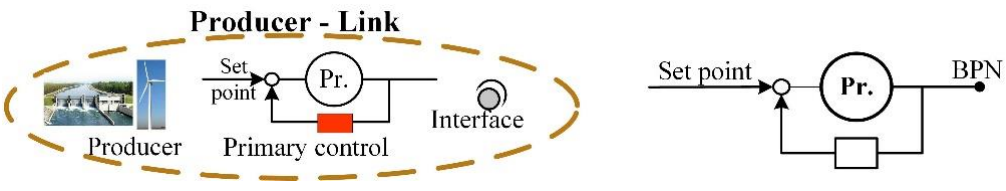

(a) (b)

Fig. 2.5 Producer-Link: (a) overview; (b) electrical scheme.

Fig. 2.5b shows the electrical scheme of the Producer-Link. Each Producer-Link is connected to a Link-Grid through the BPN.

2.2.3 Storage-Link

The Storage-Link is defined as a composition of a storage facility, such as the generator of a pumped power plant, batteries, etc., its PC, and the interface, Fig. 2.6a.

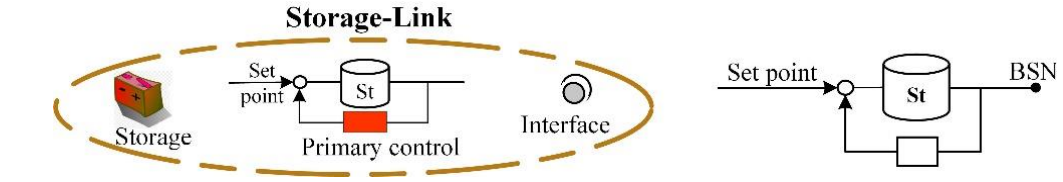

Fig. 2.6 Storage-Link: (a) overview; (b) electrical scheme.

Fig. 2.6b shows the electrical scheme of the Storage-Link. Each Storage-Link is connected to a Link-Grid through the BSN.

2.2.4 Structure

Data privacy and significant data transfer are among the biggest challenges that smart grid technologies are facing today. The distributed *LINK*-based architecture meets these challenges, as its fundamental principle is to forbid access to all resources by default, allowing access only through well-defined boundary points via interfaces. Fig. 2.7 shows an overview of the *LINK*-based holistic architecture's structure.

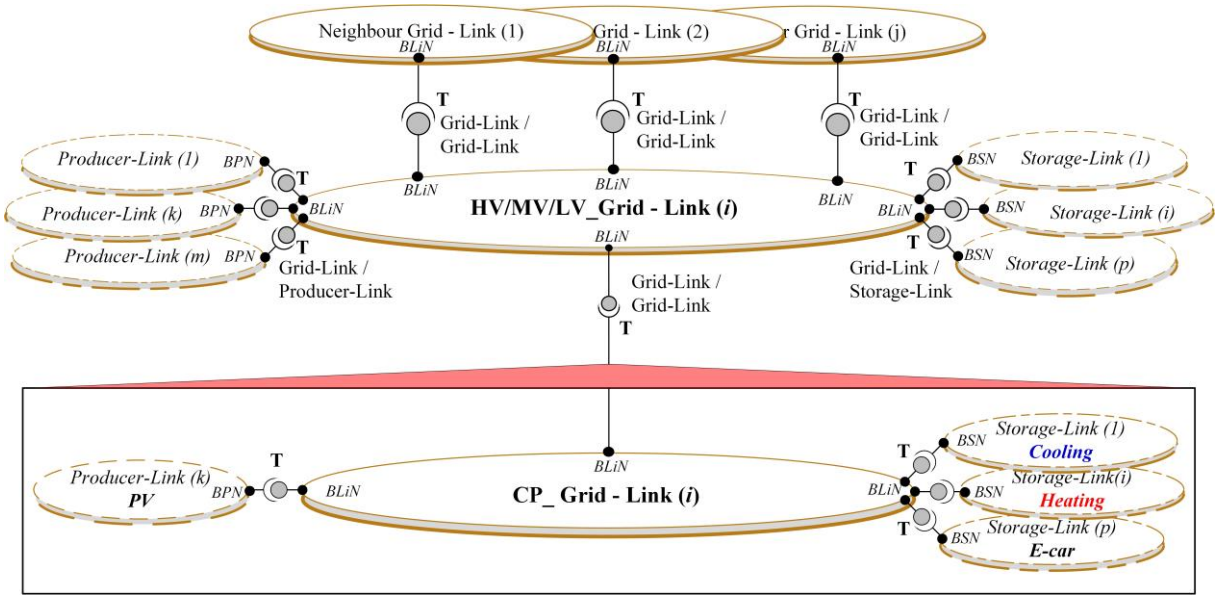

Fig. 2.7 Overview of the *LINK*-based holistic architecture's structure.

Each Link, i.e. Producer-, Storage- and Grid-Link, acts as a black-box that exchanges a predefined minimum data set with the neighbouring Links through the corresponding technical interfaces, which are designated as "T". The structure shown in Fig. 2.7 consists of two parts: the HV/MV/LV part and the CP part. The different stakeholders, operating and owning the different parts, have to communicate via external interfaces that are subject to data privacy and cybersecurity. In the HV/MV/LV part, all Links are operated by different stakeholders. Due to this similarity, they are presented one above the other. Customer plants are shown separately from the rest of the Smart Grids, as they act as vertically integrated utilities (Ilo et al. 2019). The grid is the central element that connects producers and storages across the entire Smart Grids. Producer- and Storage-Links communicate with the Grid-Links via technical interfaces. Neighbouring Grid-Links also communicate with each other via technical interfaces. The different Link types available in the same CP have internal interfaces that are neither subject to data privacy nor cybersecurity, as they have the same owner.

2.3 Architectural levels

The architecture of complex systems usually has several architectural levels representing different degrees of abstraction on which the system can be modelled. The technical/functional and the holistic level are described below.

2.3.1 Technical/functional level

The technical/functional architectural level includes the conjunction of all three architecture components, i.e. Grid-, Producer- and Storage-Links, in the HV, MV, LV and CP levels, Fig. 2.8.

The HV_Grid-Link is set up on the HV grid part. The Producer- and Storage-Links electrically connected to this grid part communicate through the technical interfaces. The neighbouring Grid-Links, such as HV and MV, communicate via the technical interfaces as well. The MV and LV_Grid-Links are set up on the MV and LV grid parts, respectively. The Producer- and Storage-Links electrically connected to these grid parts communicate through the technical interfaces. The neighbouring Grid-Links, such as HV, MV, LV and CP, also communicate via technical interfaces. The same structure is repeated at the CP level. The CP_Grid-Link is set up on the CP grid. The Producer-Links, e.g. rooftop PV-facilities, and Storage-Links, e.g. the battery of an Electric Vehicle (EV), electrically connected to this grid, communicate through the technical interfaces. LV_Grid-Link is usually the sole neighbour of a CP_Grid-Link, which also communicates through the technical interfaces.

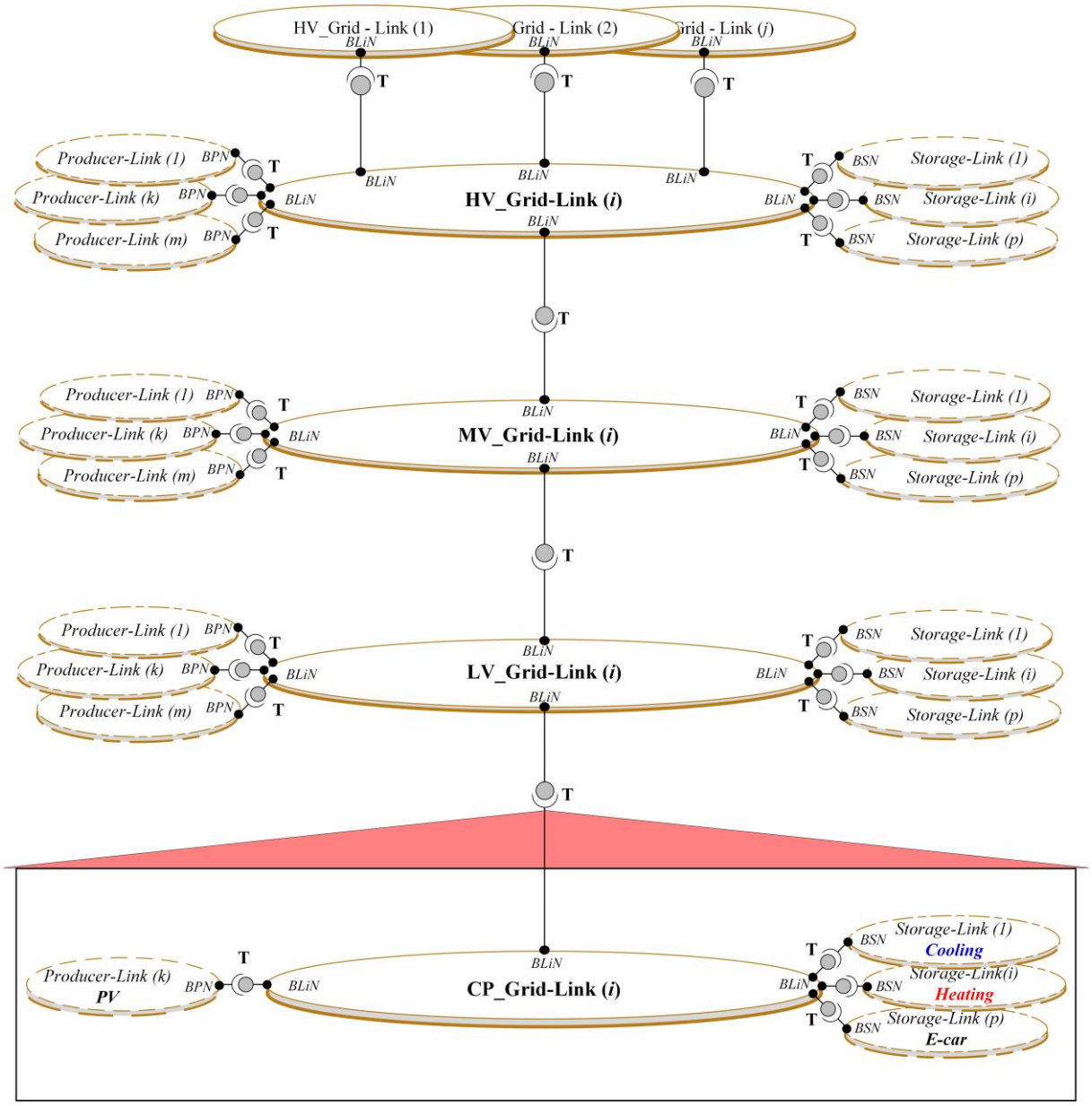

Fig. 2.8 Technical/functional architectural level of the *LINK*-based holistic architecture.

2.3.2 Holistic level

The holistic architecture level is the core of the *LINK*-based architecture, Fig. 2.9. It comprises the Smart Grids and the electricity market. The market surrounds the generalised architecture and communicates with it through the market interfaces, which are designated as "M", by exchanging aggregated meter readings, external schedules, etc. (Ilo 2017). At this architectural level, the CP_Grid-Links are removed from the generalised presentation because they are too small to participate directly in the whole market. They may participate in the market through aggregators or energy communities (Ilo et al. 2019). For the sake of privacy and cybersecurity, the market interfaces are designed apart from technical interfaces.

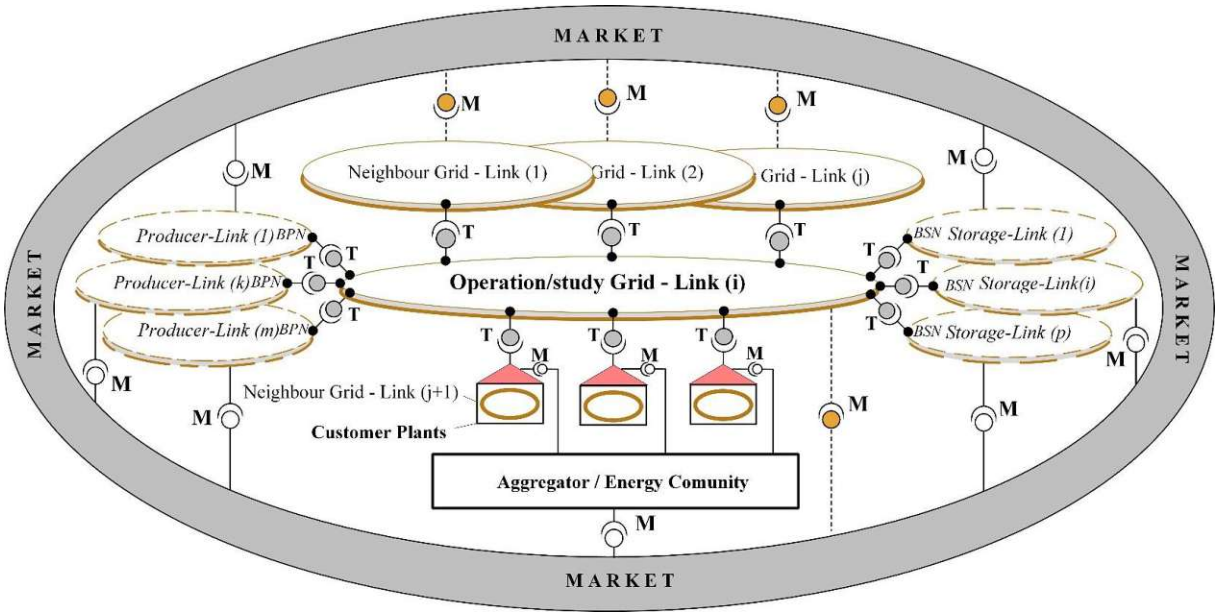

Fig. 2.9 Holistic architectural level of the *LINK*-based holistic architecture. (Ilo 2019)

2.4 Chain control strategy

The *LINK*-based holistic architecture's standardised structure enables a compact and precise representation of the control strategy, which is designed as a chain net. The most popular control strategies are local, primary, and secondary control, which are mainly used in transmission systems. In contrast, the chain net control strategy constitutes a coordinated control set including direct, primary, and secondary control loops throughout the entire Smart Grid.

Secondary control loops are the instruments enabling the coordination and reliable operation of the Grid-Links in the whole Smart Grid.

Each of the SCs in the set calculates the corresponding set-points by respecting the dynamic constraints of neighbouring Grid-Links.

2.4.1 Horizontal axis

The interconnected very-high and high voltage grids are arranged in the horizontal axis (X-axis) of the power system. Fig. 2.10 shows the secondary control chain in the horizontal axis with details of the HV_Grid-Link *i*, which includes one Hertz/Watt and one Volt/var secondary control.

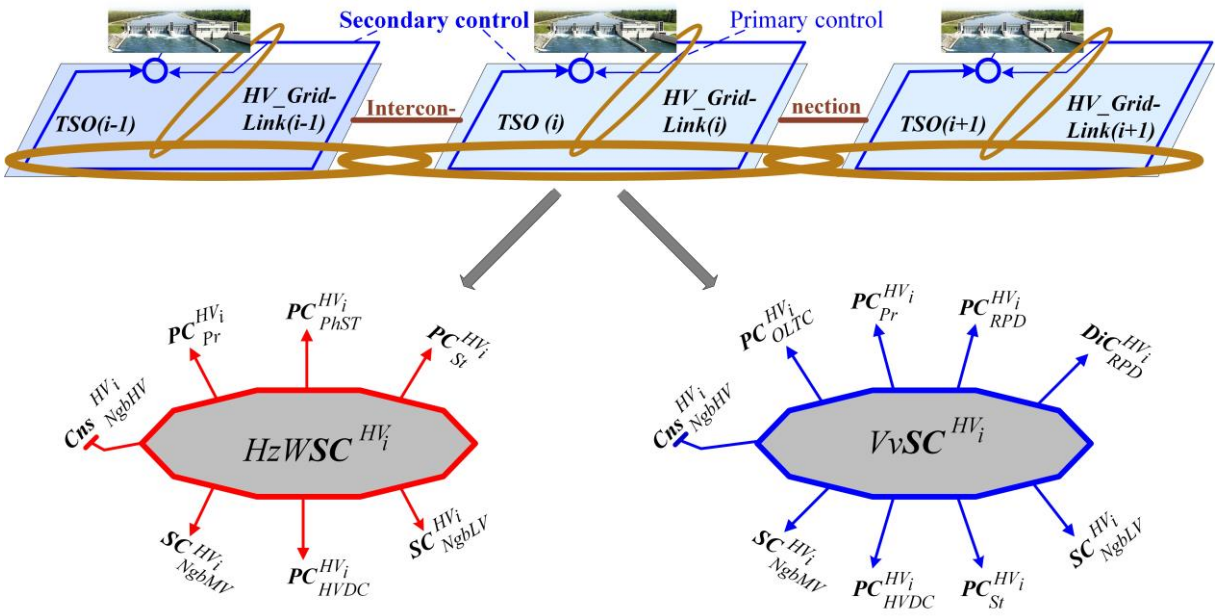

Fig. 2.10 Horizontal secondary control chain with details of the Hertz/Watt and Volt/var secondary controls in HV_Grid-Link *i*.

2.4.1.1 Hertz/Watt secondary control

HzW**SC** calculates set-points for four different types of appliances, i.e. Phase-Shifting Transformers (PhST), producers, storages and High Voltage Direct Current (HVDC) facilities, and two types of neighbouring Grid-Links, i.e. medium and low voltage. The active power flows in the transmission lines determine the constraints to be respected between the HV_Grid-Links. Equation (2.1) presents the horizontal HzW**SC** chain. It is designed as the union of all SCs, including the corresponding subset of primary controls, the subset of secondary controls of neighbouring Grid-Links, and the related constraints.

$$HzW\boldsymbol{SC}_{Chain}^{X-axis} = \bigcup_{i=1}^{M}\{HzW\boldsymbol{SC}^{HV_i}(\boldsymbol{PC}_{PhST}^{HV_i}, \boldsymbol{PC}_{Pr}^{HV_i}, \boldsymbol{PC}_{St}^{HV_i}, \boldsymbol{PC}_{HVDC}^{HV_i}, \boldsymbol{SC}_{NgbMV}^{HV_i}, \boldsymbol{SC}_{NgbLV}^{HV_i}, \boldsymbol{Cns}_{NgbHV}^{HV_i})\} \quad (2.1)$$

Where $HzW\boldsymbol{SC}_{Chain}^{X-axis}$ is the chain of Hertz/Watt secondary controls in the horizontal power system axis; $HzW\boldsymbol{SC}^{HV_i}$ is the Hertz/Watt secondary control of the HV_Grid-Link *i*; *M* is the number of HV_Grid-Links in the horizontal power system axis; $\boldsymbol{PC}_{PhST}^{HV_i}$ are the primary controls of the phase-shifting transformers included in the HV_Grid-Link *i*; $\boldsymbol{PC}_{Pr}^{HV_i}$ are the primary controls of the Producer-Links connected to the HV_Grid-Link *i*; $\boldsymbol{PC}_{St}^{HV_i}$ are the primary controls of the Storage-Links connected to the HV_Grid-Link *i*; $\boldsymbol{PC}_{HVDC}^{HV_i}$ are the primary controls of the HVDC facilities included in the HV_Grid-Link *i*; $\boldsymbol{SC}_{NgbMV}^{HV_i}$ are the secondary controls of

the neighbouring MV_Grid-Links; $\boldsymbol{SC}_{NgbLV}^{HV_i}$ are the secondary controls of the neighbouring LV_Grid-Links; and $\boldsymbol{Cns}_{NgbHV}^{HV_i}$ are the dynamic constraints of neighbouring HV_Grid-Links.

2.4.1.2 Volt/var secondary control

Vv**SC** calculates set-points for five different types of appliances, i.e. On-Load Tap Changers (OLTC), producers, storages, RDPs and HVDC facilities, and two types of neighbouring Grid-Links, i.e. medium and low voltage. The reactive power flow in tie lines and the voltage in boundary nodes determine the constraints to be respected between the HV_Grid-Links. Equation (2.2) presents the horizontal Vv**SC** chain. Similarly to the HzW**SC** chain, it is designed as the union of all SCs, including the corresponding subset of primary and direct controls, the subset of secondary controls of neighbouring Grid-Links, and the related constraints.

$$\boldsymbol{VvSC}_{Chain}^{X-axis} = \cup_{i=1}^{M}\{\boldsymbol{VvSC}^{HV_i}(\boldsymbol{PC}_{OLTC}^{HV_i}, \boldsymbol{PC}_{Pr}^{HV_i}, \boldsymbol{PC}_{St}^{HV_i}, \boldsymbol{PC}_{RPD}^{HV_i}, \boldsymbol{DiC}_{RPD}^{HV_i}, \boldsymbol{PC}_{HVDC}^{HV_i}, \boldsymbol{SC}_{NgbMV}^{HV_i}, \boldsymbol{SC}_{NgbLV}^{HV_i}, \boldsymbol{Cns}_{NgbHV}^{HV_i})\} \quad (2.2)$$

Where $\boldsymbol{VvSC}_{Chain}^{X-axis}$ is the chain of Volt/var secondary controls in the horizontal power system axis; $\boldsymbol{VvSC}^{HV_i}$ is the Volt/var secondary control of the HV_Grid-Link *i*; $\boldsymbol{PC}_{OLTC}^{HV_i}$ are the primary controls of the transformers with OLTC included in the HV_Grid-Link *i*; and $\boldsymbol{DiC}_{RPD}^{HV_i}$ are the direct controls of the reactive power devices included in the HV_Grid-Link *i*.

2.4.2 Vertical axis

The vertical axis (Y-axis) of the power system includes the HV, MV, LV and CP grids. They are owned and operated by DSOs and customers, respectively. Fig. 2.11 shows the secondary control chain in the vertical axis with details of the W**SC** and Vv**SC** in Grid-Link *i*. As the frequency is a global variable, its monitoring and control continue to be carried out by the TSO. The Grid-Links operators on the Y-axis, such as DSOs and customers, focus on the Demand-Production balance using W**SC** within their operation area in predefined time intervals. They monitor and control both the voltage and the reactive power using Vv**SC** because they are local variables.

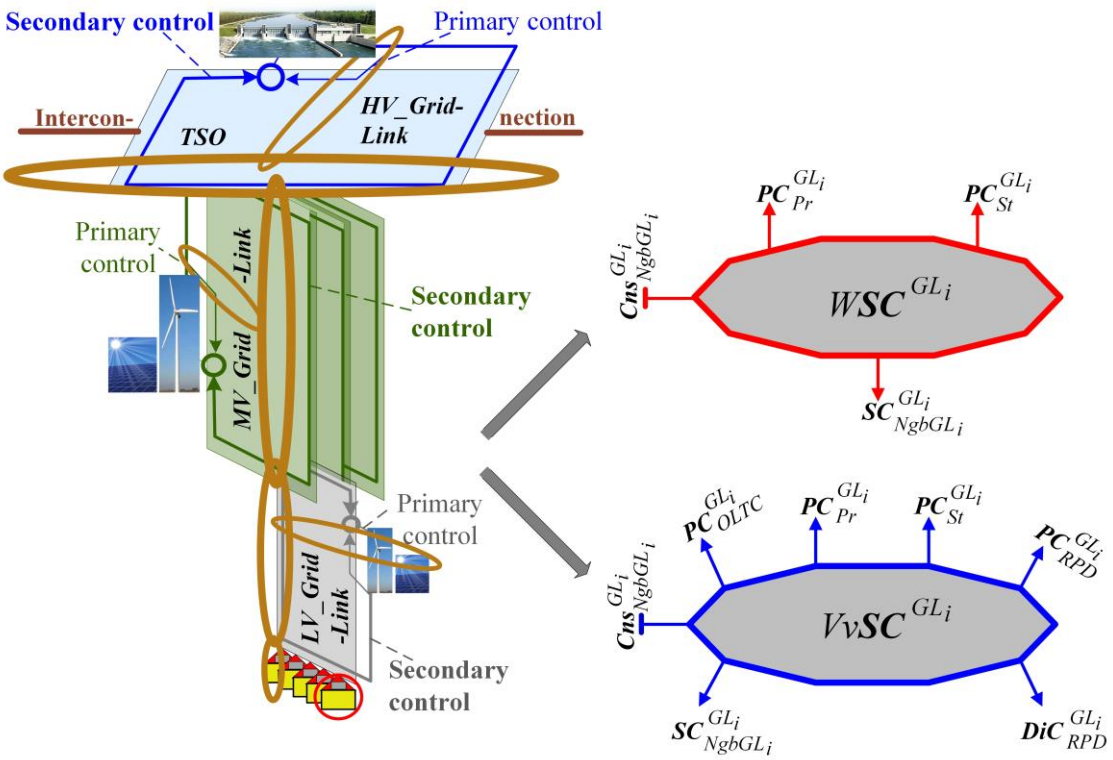

Fig. 2.11 Vertical secondary control chain with details of the Watt and Volt/var secondary controls in Grid-Link *i*.

2.4.2.1 Watt secondary control

W**SC** calculates set-points for two different types of appliances, i.e. producers and storages, and neighbouring Grid-Links. The coordination with the superordinate Grid-Links is realised by respecting the corresponding constraints. Equation (2.3) presents the vertical W**SC** chain. It is designed as the union of all SCs, including the corresponding subset of primary controls, the subset of secondary controls of neighbouring Grid-Links, and the related constraints.

$$\boldsymbol{WSC}_{Chain}^{Y-axis} = \bigcup \left\{ \begin{matrix} \boldsymbol{HzWSC}^{HV}(\boldsymbol{PC}_{PhST}^{HV}, \boldsymbol{PC}_{Pr}^{HV}, \boldsymbol{PC}_{St}^{HV}, \boldsymbol{PC}_{HVDC}^{HV}, \boldsymbol{SC}_{NgbMV}^{HV}, \boldsymbol{SC}_{NgbLV}^{HV}, \boldsymbol{Cns}_{NgbHV}^{HV}) \\ \bigcup_{i=1}^{N} \{\boldsymbol{WSC}^{GL_i}(\boldsymbol{PC}_{Pr}^{GL_i}, \boldsymbol{PC}_{St}^{GL_i}, \boldsymbol{SC}_{NgbGL_i}^{GL_i}, \boldsymbol{Cns}_{NgbGL_i}^{GL_i})\} \end{matrix} \right\} \quad (2.3)$$

Where

$GL_i \in \{MV, LV, CP\}$;
$NgbGL_i \in \{HV, MV, LV, CP\}$;

$\boldsymbol{WSC}_{Chain}^{Y-axis}$ is the chain of Watt secondary controls in the vertical power system axis; N is the number of MV, LV and CP_Grid-Links in the vertical power system axis; $\boldsymbol{WSC}^{GL_i}$ is the Watt secondary control of the Grid-Link *i*; $\boldsymbol{PC}_{Pr}^{GL_i}$ are the primary controls of the Producer-Links connected to the Grid-Link *i*; $\boldsymbol{PC}_{St}^{GL_i}$ are the primary controls of the Storage-Links connected to

the Grid-Link *i*; $\boldsymbol{SC}_{NgbGL_i}^{GL_i}$ are the secondary controls of the neighbouring Grid-Links; and $\boldsymbol{Cns}_{NgbGL_i}^{GL_i}$ are the dynamic constraints of neighbouring Grid-Links.

2.4.2.2 Volt/var secondary control

Vv**SC** calculates set-points for four different types of appliances, i.e. OLTCs, producers, storages, RPDs, and neighbouring Grid-Links. The reactive power flow between the Grid-Links and the voltages in the boundary nodes determine the constraints to be respected by the Vv**SC**. Equation (2.4) presents the vertical Vv**SC** chain. It is designed as the union of all SCs, including the corresponding subset of primary and direct controls, the subset of secondary controls of neighbouring Grid-Links, and the related constraints.

$$\boldsymbol{VvSC}_{Chain}^{Y-axis} = \tag{2.4}$$

$$\bigcup \begin{Bmatrix} \boldsymbol{VvSC}^{HV}(\boldsymbol{PC}_{OLTC}^{HV}, \boldsymbol{PC}_{Pr}^{HV}, \boldsymbol{PC}_{St}^{HV}, \boldsymbol{PC}_{RPD}^{HV}, \boldsymbol{DiC}_{RPD}^{HV}, \boldsymbol{PC}_{HVDC}^{HV}, \boldsymbol{SC}_{NgbMV}^{HV}, \boldsymbol{SC}_{NgbLV}^{HV}, \boldsymbol{Cns}_{NgbHV}^{HV}) \\ \bigcup_{i=1}^{N}\{\boldsymbol{VvSC}^{GL_i}(\boldsymbol{PC}_{OLTC}^{GL_i}, \boldsymbol{PC}_{Pr}^{GL_i}, \boldsymbol{PC}_{St}^{GL_i}, \boldsymbol{PC}_{RPD}^{GL_i}, \boldsymbol{DiC}_{RPD}^{GL_i}, \boldsymbol{SC}_{NgbGL_i}^{GL_i}, \boldsymbol{Cns}_{NgbGL_i}^{GL_i})\} \end{Bmatrix}$$

Where $\boldsymbol{VvSC}_{Chain}^{Y-axis}$ is the chain of Volt/var secondary controls in the vertical power system axis; $\boldsymbol{VvSC}^{GL_i}$ is the Volt/var secondary control of the Grid-Link *i*; $\boldsymbol{PC}_{OLTC}^{GL_i}$ are the primary controls of the transformers with OLTC included in the Grid-Link *i*; $\boldsymbol{PC}_{RPD}^{GL_i}$ are the primary controls of the RPDs included in the Grid-Link *i*; and $\boldsymbol{DiC}_{RPD}^{GL_i}$ are the direct controls of the RPDs included in the Grid-Link *i*.

2.5 Chains of Smart Grid operation

In order to ensure a reliable power supply, the power system operator employs a number of processes, including monitoring, Volt/var control, load-generation balancing, load-frequency control, price- and emergency-driven demand response, power recovering, reserve monitoring, and static and dynamic stability. The *LINK*-based holistic architecture allows executing these processes as chains of operation, thus minimising the necessary data transfer and increasing the resiliency of the system by design. The focus of this thesis is set on the Volt/var chain process in the vertical power system axis, which is described and analysed in detail in §3.

3 Volt/var chain process

"Simplicity is the ultimate sophistication."

Leonardo da Vinci

Physically, the voltage is a local quantity that differs in each node of the electricity grid, as it varies along with the power transfer and the characteristics of the grid. Due to their strong coupling, the reactive power has always been used to control the voltage in transmission grids, originating the term Volt/var process. Reactive power is produced and consumed by diverse appliances distributed throughout the power system and operated by different stakeholders, making Volt/var control an extremely complex issue by its very nature. The overall control strategy should be designed with special care to reduce the complexity of the resulting Volt/var chain to facilitate the management.

3.1 Fundamentals of Volt/var process

The design of an appropriate Volt/var control requires fundamental knowledge on the behaviour of the grid, the existent reactive power sources and sinks, reactive power compensation, and the available control variables and concepts.

3.1.1 Volt/var and Volt/Watt interrelations

Flows of active and reactive power through the grid modify the node voltages in magnitude and angle, and vice versa. The two bus system shown in Fig. 3.1 is considered to clarify the interrelations between power flows and voltages. The complex impedance $\underline{Z}$ represents a series-connected grid component such as a line segment or transformer. The complex voltages and apparent power flows are designated by $\underline{U}_1$, $\underline{U}_2$ and $\underline{S}_1$, $\underline{S}_2$, respectively, and the complex current by $\underline{I}$.

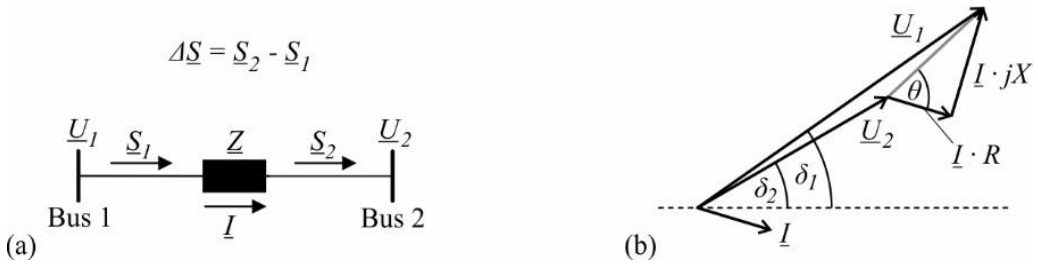

Fig. 3.1 Two bus system: (a) Circuit diagram; (b) Vector diagram.

The variables shown in Fig. 3.1 are expressed as in Equations (3.1) to (3.3).

$$\underline{Z} = Ze^{j\theta} = R + jX \tag{3.1}$$

$$\underline{U_1} = U_1 e^{j\delta_1} \tag{3.2a}$$

$$\underline{U_2} = U_2 e^{j\delta_2} \tag{3.2b}$$

$$\delta = \delta_2 - \delta_1 \tag{3.2c}$$

$$\underline{S_1} = P_1 + jQ_1 \tag{3.3a}$$

$$\underline{S_2} = P_2 + jQ_2 \tag{3.3b}$$

Where Z, θ are the magnitude and angle of the complex impedance; R, X are the resistive and reactive part of the complex impedance; U_1, δ_1 and U_2, δ_2 are the magnitudes and angles of the complex voltages at buses 1 and 2, respectively; δ is the voltage angle difference between both buses; And P_1, Q_1 and P_2, Q_2 are the active and reactive power flowing into and out of the impedance, respectively. The impedance itself consumes active (ΔP) and reactive power (ΔQ) in the form of power losses, as shown in Equation (3.4).

$$\Delta P = P_1 - P_2 = I^2 \cdot R = \frac{P_2^2 + Q_2^2}{U_2^2} \cdot R \tag{3.4a}$$

$$\Delta Q = Q_1 - Q_2 = I^2 \cdot X = \frac{P_2^2 + Q_2^2}{U_2^2} \cdot X \tag{3.4b}$$

The exact interrelations between complex power flows and voltages at both sides of the impedance are given in Equation (3.5).

$$\underline{S_1} = \underline{U_1} \cdot \underline{I}^* = \frac{U_1^2}{Z} e^{j\theta} - \frac{U_1 \cdot U_2}{Z} e^{j(\theta-\delta)} \tag{3.5a}$$

$$\underline{S_2} = \underline{U_2} \cdot \underline{I}^* = \frac{U_1 \cdot U_2}{Z} e^{j(\theta+\delta)} - \frac{U_2^2}{Z} e^{j\theta} \tag{3.5b}$$

However, these formulas are unwieldy and do not enable an intuitive understanding of the interrelations between power flows and voltages. To estimate and understand the effect of power flows on the behaviour of transmission and distribution grids, simplifications are necessary. Different approximations are commonly made for transmission and distribution grids due to their distinct characteristics (R/X-ratio). The vector diagrams shown in Fig. 3.2 illustrate these approximations for both types of grids.

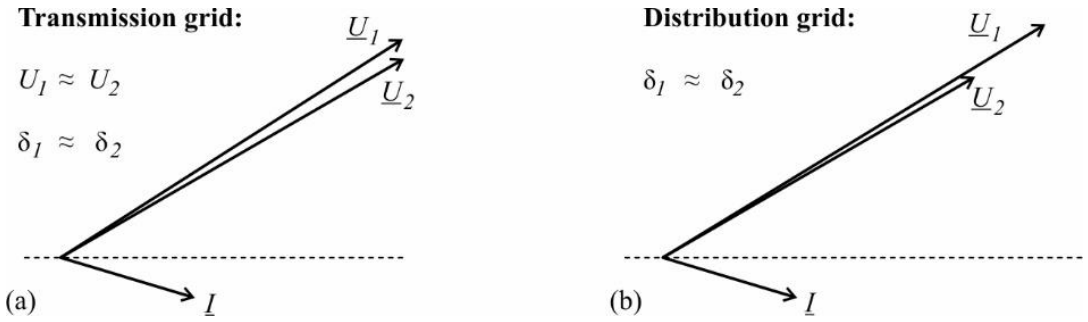

Fig. 3.2 Vector diagrams illustrating the approximations commonly made for different grids: (a) Transmission; (b) Distribution.

3.1.1.1 Transmission grids

Partitioning Equation (3.5b) into its real and imaginary part yields Equation (3.6).

$$P_2 = \frac{U_1 \cdot U_2}{Z}\cos(\theta + \delta) - \frac{U_2^2}{Z}\cos(\theta) \tag{3.6a}$$

$$Q_2 = \frac{U_1 \cdot U_2}{Z}\sin(\theta + \delta) - \frac{U_2^2}{Z}\sin(\theta) \tag{3.6b}$$

The sensitivities of the active and reactive power flows to the voltage magnitude and angle are usually used to describe the Volt/var interrelations in transmission grids. For small deviations in voltage magnitude, the changes in active and reactive power are given by Equation (3.7).

$$\frac{\partial P_2}{\partial U_2} = \frac{U_1}{Z}\cos(\theta + \delta) - \frac{2U_2}{Z}\cos(\theta) \tag{3.7a}$$

$$\frac{\partial Q_2}{\partial U_2} = \frac{U_1}{Z}\sin(\theta + \delta) - \frac{2U_2}{Z}\sin(\theta) \tag{3.7b}$$

For small deviations in voltage angle, the changes in active and reactive power are given by Equation (3.8).

$$\frac{\partial P_2}{\partial \delta_2} = -\frac{U_1 \cdot U_2}{Z}\sin(\theta + \delta) \tag{3.8a}$$

$$\frac{\partial Q_2}{\partial \delta_2} = \frac{U_1 \cdot U_2}{Z}\cos(\theta + \delta) \tag{3.8b}$$

Transmission grids are characterised by very low R/X-ratios, thus $\theta \approx 90°$. Regarding small differences in voltage magnitude ($U_1 \approx U_2$) and angle ($\delta_1 \approx \delta_2$) as shown in Fig. 3.2a allows approximating the voltage magnitude sensitivity of power flows, as shown in Equation (3.9).

$$\frac{\partial P_2}{\partial U_2} \approx 0 \tag{3.9a}$$

$$\frac{\partial Q_2}{\partial U_2} \approx -\frac{U_2}{Z} \tag{3.9b}$$

Meanwhile, the voltage angle sensitivity of power flows is approximated in Equation (3.10).

$$\frac{\partial P_2}{\partial \delta_2} \approx -\frac{U_1 \cdot U_2}{Z} \tag{3.10a}$$

$$\frac{\partial Q_2}{\partial \delta_2} \approx 0 \tag{3.10b}$$

Equations (3.9) and (3.10) indicate a strong relationship between active power flows and voltage angles; And between reactive power flows and voltage magnitudes. Hence, active and reactive power can be studied separately for many problems within transmission grids. Furthermore, Equation (3.9b) shows that reactive power cannot be transmitted over long distances, as this would require large voltage gradients (Kundur 1994).

3.1.1.2 Distribution grids

Distribution grids have much greater *R*/*X*-ratios than transmission grids. Thus, the approximation made for the impedance angle of transmission grids is no longer valid. As a result, the sensitivity considerations described above are not relevant to distribution grids. Therefore, the voltage drop equation, i.e. Equation (3.11), is used in the distribution level.

$$U_1 \cdot \cos(\delta) - U_2 = \frac{RP_2 + XQ_2}{U_2} \tag{3.11}$$

Assuming small differences in voltage angles ($\delta_1 \approx \delta_2$) as shown in Fig. 3.2b, which is justified in distribution grids (Sarkar et al. 2018), yields the approximate voltage drop equation shown in Equation (3.12).

$$\Delta U = U_1 - U_2 \approx \frac{RP_2 + XQ_2}{U_2} \tag{3.12}$$

This formula helps to understand the Volt/var and Volt/Watt behaviour of radial distribution grids, as it allows to estimate the voltage drops along the feeders caused by the active and reactive power part of the load.

3.1.2 Reactive power sources and sinks

All elements of the electric power system such as producers, storages, grid components, and consuming devices have reactive power capabilities. They produce or consume reactive power, thus acting as var-sources and -sinks, respectively.

- Producers and storages are mainly installed to contribute active power. However, they often include synchronous machines or power electronic converters whose reactive power contributions are controllable within the corresponding capability limits.

- The grid is the binding link between producers, storages and consuming devices. Its transformers and lines inherently contribute reactive power when they are energised and loaded. Additional RPDs are dispersed throughout the power system to increase the power factor and maintain acceptable voltages.
- Consuming devices convert electrical power into services for users. Their reactive power contributions are determined by the user, and the thermostatic controls that switch on and off the consuming devices.

3.1.2.1 Producers

Producers are electricity production facilities that convert primary energy into electrical energy. Traditionally, the demand was mainly supplied by the large thermal, nuclear and hydropower plants commonly referred to as conventional power plants. In recent years, the number of PV and Wind Turbine (WT) systems rapidly increased, constituting a significant share of the European electricity production nowadays (IEA 2020). The remaining producers, such as biofuel, solar- and geothermal, tidal power plants, etc., only slightly contribute to the overall electricity production. They are all summarised in this section under the term "others".

Conventional power plants

Conventional power plants utilise the thermal energy derived from fossil fuels and nuclear fission, and the kinetic energy of water. They use prime movers and Synchronous Machines (SM) to convert the primary energy first into mechanical and finally into electrical energy. Two main SM types are distinguished: Salient pole and cylindrical rotor. Salient pole SMs are commonly used in hydropower plants, while the cylindrical rotor ones are mainly used in thermal power plants (Oeding and Oswald 2011). Both convert the mechanical power at the prime mover side into active power at the grid side. The corresponding excitation systems allow regulating the machines' reactive power contributions within their P/Q capability limits. Fig. 3.3 shows the basic steady-state P/Q capability chart of the cylindrical rotor and salient pole SM for nominal terminal voltage (Binder 2012; Walker 1953).

In the over-excited area, the same restrictions limit the capabilities of both machine types: The maximal field current (1) and the maximal armature current (2). As the terminal voltage increases, the maximal field current narrows the capability chart, while the maximal armature current widens it (Walker 1953). Fig. 3.3a shows that the under-excited region of the cylindrical rotor machine is limited by the stator end-core heating (4). The higher the terminal voltage, the more reactive power can be absorbed without overheating the stator end-core (Alla et al. 2018). Regarding the salient pole machine, the under-excited area is restricted by the practical stability

limit (4) and the minimal field current (5); When the terminal voltage increases, both limits get less restrictive (Walker 1953). In addition to the generator-related limits, the prime mover restricts the maximal active power injection independent of the terminal voltage (3).

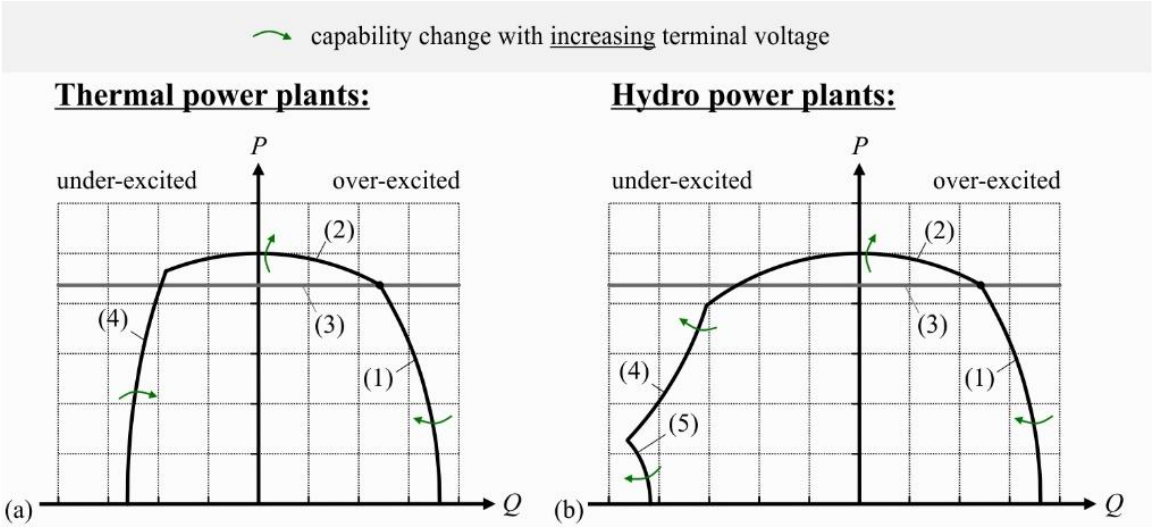

Fig. 3.3 Basic steady-state *P*/*Q* capability chart of different SM types for nominal terminal voltage: (a) Cylindrical rotor; (b) Salient pole.

PV systems

Photovoltaic systems basically consist of PV modules, filters and inverters. The modules convert the solar power into electrical Direct Current (DC) power that is further converted into Alternating Current (AC) active power by the associated inverter. From the Volt/var process-related point of view, the inverter is the key component of the PV system, as it may contribute reactive power to support the grid operation. Numerous topologies of self-commutated inverters are used for the grid connection of PV modules (Teodorescu et al. 2007). Depending on their topology and the used modulation strategy, most inverters are capable of providing reactive power (Poliseno et al. 2012). Voltage Source Converters (VSC) are the dominant inverter topology used for grid applications (Choi et al. 2017). Within their *P*/*Q* capability limits, their reactive power contributions can be controlled continuously and independently of the prevalent active power conversion. The basic steady-state *P*/*Q* capability chart of a VSC is shown in Fig. 3.4 for terminal voltages of 0.9, 1.0, and 1.1 p.u. (Albarracín and Alonso 2013; Arrillaga et al. 2009).

The *P*/*Q* capability of the VSC is limited by the maximum DC voltage (1) and the maximum current through the electronic switches (2). The maximum DC voltage significantly restricts the over-excited capability region of the inverter for high terminal voltages. Conversely, the maximum current through the electronic switches allows for increased power exchanges when

the terminal voltage is high. The PV module rating imposes additional restrictions on the active power capability of the producer unit.

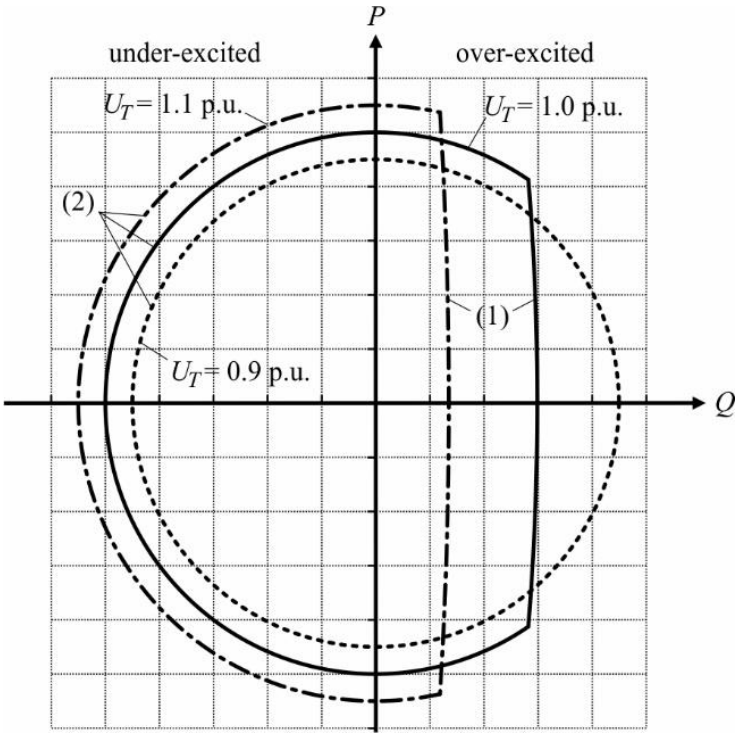

Fig. 3.4 Basic steady-state *P*/*Q* capability chart of a VSC for different terminal voltages.

WT systems

WT systems are generally divided into four distinct categories based on their machine and converter setup: Fixed-speed wind generator; Limited variable-speed wind generator; Doubly-Fed Induction Generator (DFIG); And Full-Converter Wind Generator (FCWG) (Sarkar et al. 2018; Vittal et al. 2019). Fixed- and limited variable-speed wind generators are directly connected induction generators that consume reactive power depending on wind speed and local voltage; Usually, fixed capacitors are added to supply the no-load reactive power demand at nominal voltage. The converter based WT systems provide more flexibilities. The rotors of the DFIGs are fed by back-to-back systems[1], allowing to independently control the active and reactive power contribution of the WT systems. Fig. 3.5 shows the steady-state *P*/*Q* capability chart of the DFIG for terminal voltages of 0.95, 1.00, and 1.05 p.u. (Schürhuber 2018).

The *P*/*Q* capabilities are restricted by the rated rotor voltage limit (1), rotor current de-rating at zero slip (2), rated rotor current limit (3), mechanical power limit of the wind turbine (4), and rated stator current limit (5) (Tian et al. 2013; Engelhardt et al. 2011). The rotor-related limits (1) – (3) tighten with an increasing terminal voltage while the rated stator current limit

[1] Machine-side VSC, DC link capacitor, and grid-side VSC.

widens. The FCWG may include an induction or synchronous generator connected to the grid through a back-to-back system. In this case, the WT is fully decoupled from the grid, and the resulting P/Q capability is determined by the grid side VSC, Fig. 3.4. The mechanical power limits of the WT further restrict the active power capability of the producer unit. Today, most fixed- and limited variable-speed wind generators have been replaced by DFIGs and FCWGs (Vittal et al. 2019).

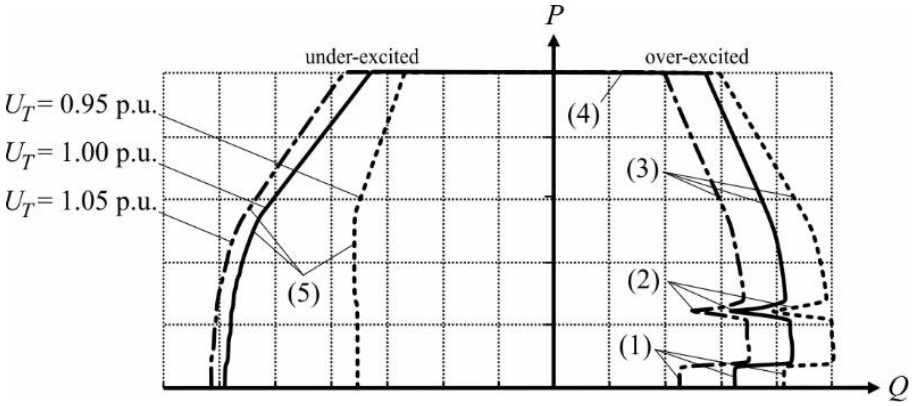

Fig. 3.5 Basic steady-state P/Q capability chart of a DFIG for different terminal voltages.

Others

The other producers, such as biofuel, solar- and geothermal, tidal power plants, etc., are mostly connected to the grid via SMs or VSCs (Sarkar et al. 2018). These producers have similar reactive power capabilities as conventional power plants and PV systems. If induction generators are used for the power conversion, the corresponding reactive power contributions cannot be controlled as those of fixed- and limited variable-speed wind generators.

3.1.2.2 Storages

Electrical storages convert electric energy from the power system into a form that can be stored, such as electrostatic, magnetic, kinetic, potential, (electro-) chemical, and thermal energy. From the perspective of the power system, they are categorised into storages that: A) do inject the energy back at the charging point; B) do not inject the energy back at the charging point; And C) reduce the energy consumption at the charging point in the near future (Ilo 2020). They are used for numerous applications, including portable devices, transport vehicles and stationary energy resources; Either for energy management or to improve power quality and reliability (Chen et al. 2009). However, their capability to provide reactive power is of primary interest for the Volt/var process. Numerous storage technologies exist, including pumped hydroelectric, compressed air, battery, thermal, superconducting magnetic energy storage, flywheels, fuel cells, capacitors, etc. Pumped hydroelectric and compressed air energy storages are connected

to the grid through synchronous machines, thus having similar *P*/*Q*-capabilities as conventional power plants. Basically, the diagrams shown in Fig. 3.3 can be mirrored to reflect the motor operating mode (Walker 1953). Meanwhile, batteries, flywheels, fuel cells and superconducting magnetic energy storage are connected via converters that determine their reactive power capabilities. If VSCs are used, the *P*/*Q*-chart shown in Fig. 3.4 is applicable.

3.1.2.3 Grid components

The grid comprises lines, transformers, reactive power devices, and HVDC systems.

Lines

Overhead lines and cables are used to transmit active and reactive power from producing to consuming devices. Due to their constructive form and physical configuration, they possess resistances, inductances and capacitances per unit length. The π-equivalent circuit shown in Fig. 3.6 is commonly used to model their behaviour in load flow studies.

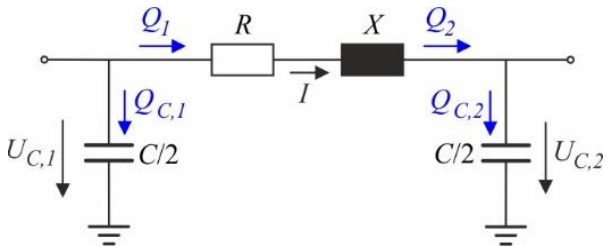

Fig. 3.6 Basic π-equivalent circuit of overhead lines and cables.

According to Equation (3.13a), the reactive power consumption of a line segment depends on the current through the series inductance.

$$Q_L = Q_1 - Q_2 = X \cdot I^2 \tag{3.13a}$$

$$Q_{C,1/2} = -\omega\, C/2 \cdot U_{C,1/2}^2 \tag{3.13b}$$

Meanwhile, its reactive power production depends on the voltages at the shunt capacitances, Equation (3.13b). Equation (3.13b) implies that a cable at the MV level produces much more reactive power than one at the LV level. Table 3.1 shows benchmark parameters of European overhead lines and underground cables calculated from the data provided in (CIGRE 2014a).

Overhead lines generally have much lower capacitances than cables. The *R*/*X*-ratio of the wires increases from the HV to the LV level. The capacitances are often neglected at the LV level as they produce only insignificant amounts of reactive power due to the low operating voltage (see Equation (3.13b)).

Table 3.1 Benchmark parameters of European overhead lines and underground cables.

Level	Installation	Nominal voltage	R'	X'	C'	R'/X'
		[kV]	[Ω/km]	[Ω/km]	[nF/km]	[-]
HV	Overhead	380	0,033	0,312	11,48	0,106
	Overhead	220	0,065	0,398	9,08	0,163
	Overhead	110	0,082	0,345	10,65	0,238
MV	Overhead	20	0,510	0,366	10,10	1,393
	Underground	20	0,501	0,716	151,17	0,670
LV	Overhead	0.4	0,492	0,285	-	1.726
	Underground	0.4	0,265	0,082	-	3.232

Transformers

Transformers are used in the electric power system to interconnect different grid parts and to connect producers and storages with the grid. Fig. 3.7 shows the basic equivalent circuit of a two-winding transformer. It includes the primary and secondary winding resistances (R_p and R_s) and leakage reactances (X_p and X_s), the magnetising reactance referred to the primary side (X_{mp}) and the ideal transformer.

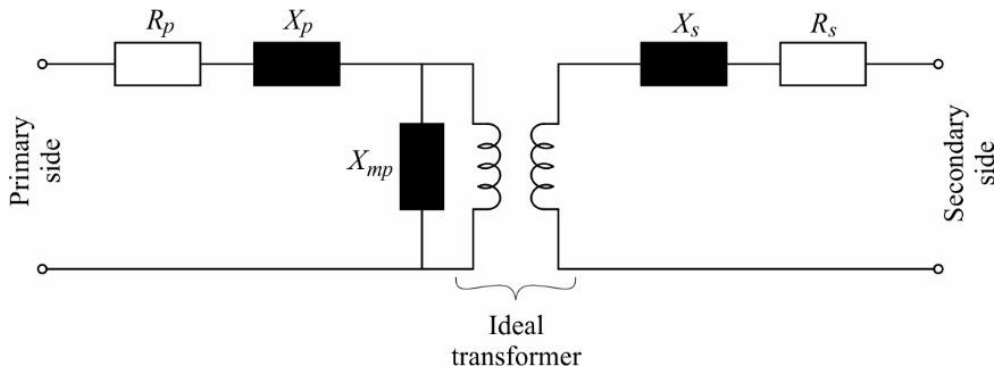

Fig. 3.7 Basic equivalent circuit of a two-winding transformer.

Transformers always consume reactive power depending on their loading: In no or low load conditions, the effect of the shunt magnetising reactance predominates, while in high load conditions, the impact of the series leakage reactance dominates (Kundur 1994).

Reactive power devices

RPDs are used for many purposes, including voltage control, load compensation, power flow control, damping of oscillations, and for improving voltage, transient and dynamic stability.

They are series- or shunt-connected. Series-connected RPDs are mainly[2] used for power flow control and oscillation damping. Meanwhile, the shunt-connected ones are primarily used for voltage control and load compensation. However, both types affect the reactive power flow and consequently the grid voltages. (Hingorani and Gyugyi 2000)

$$Q_{RPD} = Q_1 - Q_2 \tag{3.14}$$

Fig. 3.8 and Equations (3.14) to (3.18) illustrate the physical principles of reactive power contribution.

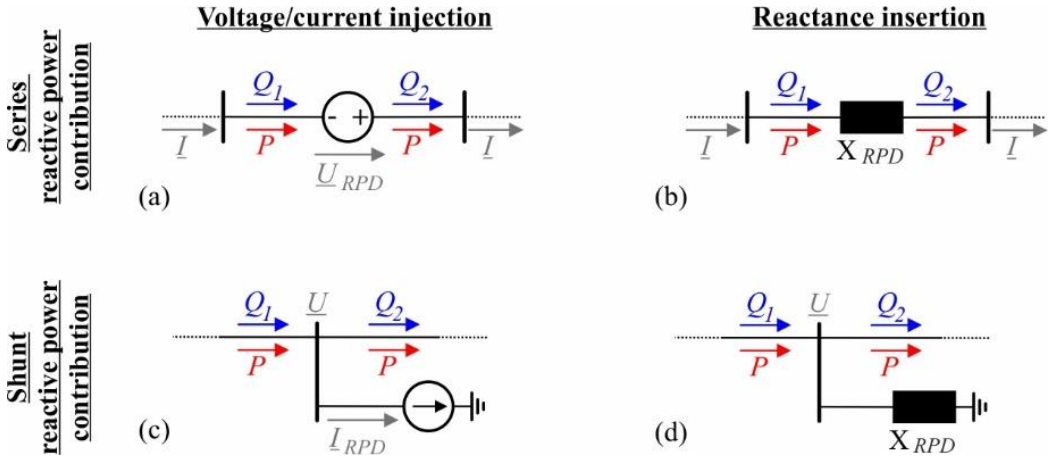

Fig. 3.8 Physical principles of reactive power contribution: (a) Series voltage injection; (b) Series reactance insertion; (c) Shunt current injection; (d) Shunt reactance insertion.

Fig. 3.8 a and b illustrate the principles of the series reactive power contribution. In Fig. 3.8a, a series voltage U_{RPD} is injected in quadrature to the line current I, provoking the reactive power contribution according to Equation (3.15).

$$Q_{RPD} = I \cdot U_{RPD} \tag{3.15}$$

In Fig. 3.8b, a series reactance X_{RPD} is inserted that contributes reactive power according to Equation (3.16).

$$Q_{RPD} = I^2 \cdot X_{RPD} \tag{3.16}$$

This formula is compliant with Equation (3.4b), which describes the reactive power losses of a series connected impedance. The shunt reactive power contribution principles are illustrated in Fig. 3.8c and d. In Fig. 3.8c, a shunt current I_{RPD} is injected in quadrature to the node voltage U, resulting in the reactive power contribution according to Equation (3.17).

$$Q_{RPD} = U \cdot I_{RPD} \tag{3.17}$$

[2] Series reactive power contribution is sometimes used in distribution level to secure the supply of factories against voltage dips (Zhang et al. 2006).

The inserted shunt reactance X_{RPD} shown in Fig. 3.8d contributes reactive power depending on the node voltage, Equation (3.18).

$$Q_{RPD} = U^2 / X_{RPD} \tag{3.18}$$

Numerous RPDs have been developed that take advantage of the physical principles outlined above.

Table 3.2 Overview of reactive power devices.

Principle	RPD	Acronym	Capability	Controllability
Shunt reactance insertion	Fixed shunt capacitor	-	Capacitive	None
	Fixed shunt reactor	-	Inductive	None
	Mechanically switched capacitor	MSC	Capacitive	Discrete
	Mechanically switched reactor	MSR	Inductive	Discrete
	Static var compensator	SVC	Both	Continuous
Shunt current injection	Static synchronous compensator	STATCOM	Both	Continuous
	Synchronous condenser	SyC	Both	Continuous
Series reactance insertion	Fixed series capacitor	-	Capacitive	None
	Thyristor-switched series capacitor	TSSC	Capacitive	Discrete
	Thyristor-switched series reactor	TSSR	Inductive	Discrete
	Thyristor-controlled series capacitor	TCSC	Capacitive	Continuous
	Thyristor-controlled series reactor	TCSR	Inductive	Continuous
Series voltage injection	Static synchronous series compensator	SSSC	Both	Continuous

Table 3.2 groups the most widely used ones according to the physical principle they rely on; Their reactive power capability and the corresponding controllability are also given. A detailed

description of the listed RPDs can be found in (Dixon et al. 2005) and (Hingorani and Gyugyi 2000).

Fixed shunt capacitors and reactors are permanently connected to the grid, while the mechanically switched ones (MSC and MSR, respectively) are connected via circuit breakers. MSCs are often split into smaller capacitor units to improve the smoothness of their control. As the constructional parameters determine their maximum capacitance, their reactive power capability strongly depends on the local voltage (see Equation (3.18)). For low voltages, i.e. when the reactive power support is most needed, their reactive power capability is very low. Static Var Compensators (SVC) employ Thyristor-Controlled Reactors (TCR), Thyristor-Switched Reactors (TSR) and Thyristor-Switched Capacitors (TSC) to continuously adjust their reactance. Therefore, analogously to the MSC, the SVC has deficient reactive power capabilities for low voltages.

Static Synchronous Compensators (STATCOM) are shunt-connected self-commutated converters whose output current can be continuously controlled independently of the terminal voltage. According to Equation (3.17), their reactive power capabilities decrease linearly with the terminal voltage, thus offering better voltage support for low voltages as the SVCs. Synchronous Condensers (SyC) are synchronous machines running without prime mover or mechanical load. They inject reactive currents in quadrature to the node voltage.

The fixed series capacitor produces reactive power depending on the square of the current flowing through it, Equation (3.16). It compensates for the line series inductance, reducing the effective reactive power loss (see Equation (3.4b)). In this regard, the fixed series capacitor acts self-regulating (Kundur 1994). The Thyristor-switched series capacitor (TSSC) and reactor (TSSR) consist of a series capacitor and reactor, respectively, shunted by a TSR. They allow for stepwise reactance control. Smoothly variable reactance is provided by both Thyristor-Controlled Series Capacitor (TCSC) and Reactor (TCSR), as they use thyristor-controlled reactors instead of the thyristor-switched ones.

The Static Synchronous Series Compensator (SSSC) resembles the STATCOM, except that it injects a voltage in series with the line, Equation (3.15). Its reactive power capability linearly depends on the line current.

Additional active power sources or storages may be connected at the DC side of STATCOMs and SSSCs, creating the ability to inject and absorb active power (Hingorani and Gyugyi 2000). This topic is not treated in this chapter because this ability is not related to the Volt/var control process.

HVDC systems

HVDC systems are used for long-distance active power transmission and to interconnect asynchronous AC systems. They basically comprise two transformers, two power electronic converters, and DC transmission lines (Alassi et al. 2019). The absence of capacitive charging effects at the DC lines allows the low-loss submarine, underground and overhead power transmission. Two main categories of HVDC converters are in use: Line-Commutated Converters (LCC) and VSCs. Both convert AC active power into DC one, and vice versa. However, their reactive power capabilities substantially differ from each other. The LCCs inherently consume reactive power of about 50 to 60% of the prevalent active power conversion. Therefore, supplementary reactive power sources are usually installed nearby the converter stations to compensate for the reactive power demand at nominal conditions. Meanwhile, the VSCs provide more flexibilities as they allow independent control of their reactive power contributions (see §3.1.2.1). The DC power lines add active power limits to the *P*/*Q* capability chart shown in Fig. 3.4. Today, LCCs still dominate the HVDC market. However, a shift towards VSC technology is already noticeable and expected for the future (Alassi et al. 2019).

3.1.2.4 Consuming devices

Consuming devices convert electric power into services for the users. They consume active power and contribute reactive power when they are switched on. Traditional consuming devices such as directly connected induction motors behave inductively. In contrast, many modern ones, such as switch-mode power supply loads with passive power factor correction, adjustable speed drives, compact fluorescent lamps, and Light Emitting Diodes (LED), show capacitive behaviour (Schultis and Ilo 2019a). When switched on, their power consumption depends on the supplying voltage (Preiss and Warnock 1978). In load flow studies, this voltage dependency is commonly modelled using the exponential or the polynomial (also called "ZIP") load model (Price et al. 1993; Arif et al. 2018). The polynomial load model relies on Equation (3.19).

$$P^{Dev}/P^{Dev}_{nom} = C^{Z,P} \cdot (U/U_{nom})^2 + C^{I,P} \cdot (U/U_{nom}) + C^{P,P} \tag{3.19a}$$

$$Q^{Dev}/Q^{Dev}_{nom} = C^{Z,Q} \cdot (U/U_{nom})^2 + C^{I,Q} \cdot (U/U_{nom}) + C^{P,Q} \tag{3.19b}$$

$$C^{Z,P} + C^{I,P} + C^{P,P} = C^{Z,Q} + C^{I,Q} + C^{P,Q} = 1 \tag{3.19c}$$

Where $C^{Z,P}$, $C^{I,P}$, $C^{P,P}$ and $C^{Z,Q}$, $C^{I,Q}$, $C^{P,Q}$ are the active and reactive power-related ZIP coefficients; P^{Dev}, Q^{Dev} and P^{Dev}_{nom}, Q^{Dev}_{nom} are the active and reactive power consumptions for the actual and nominal voltage, respectively; And U, U_{nom} are the actual and nominal supplying voltage, respectively. However, considering the power system's fractal structure (Ilo 2019), the

consuming devices themselves consist of several smaller elements, i.e., conductors, transformers, reactive power devices and active power appliances. Hence, they can be regarded as a grid part such as the CP or LV grid, but smaller in size.

3.1.3 Reactive power compensation

Reactive power compensation contains two aspects: load compensation and voltage support (Dixon et al. 2005).

3.1.3.1 Load compensation

Load compensation is traditionally used to locally supply the reactive power demand of industrial customer plants and consuming devices such as motors and discharging lamps (Riese 2012).

> The goal of load compensation is to increase the power factor of industrial CPs and consuming devices independent of their supplying voltage.

The reactive power demand of induction motors is locally supplied by capacitors connected at the CP level or directly at the device level. In the former case, the capacitor may supply the reactive power demand of many motors. Fig. 3.9a and b show an induction motor without and with load compensation at the device level, respectively. The motor is connected to a bus bar with the supplying voltage $\underline{U}$.

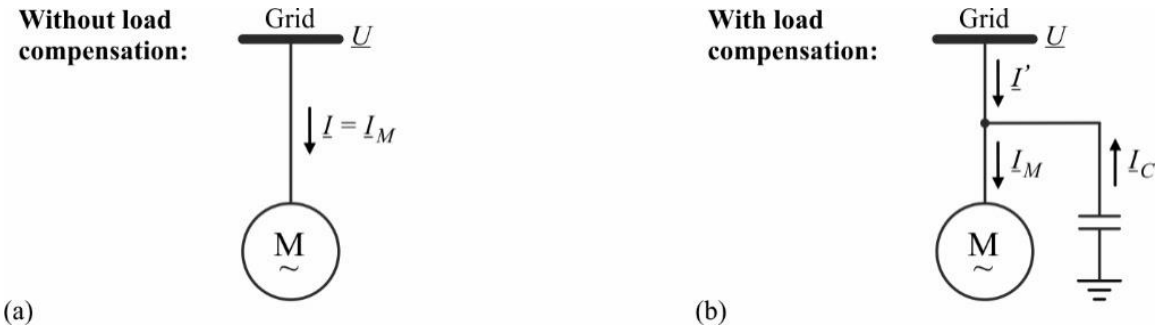

Fig. 3.9 Induction motor: (a) Without load compensation; (b) With load compensation at the device level.

Without load compensation, the current drawn from the grid $\underline{I}$ equals the current consumed by the motor $\underline{I_M}$, Equation (3.20a). When load compensation is used, the grid current $\underline{I}$ is composed of the motor $\underline{I_M}$ and the capacitor current $\underline{I_C}$, Equation (3.20b).

The vector diagrams of both cases are shown in Fig. 3.10. When no load compensation is applied, the grid current lags the voltage by a significant angle φ, leading to a poor power factor at the grid connection point, Fig. 3.10a.

$$\underline{I} = \underline{I}_M \tag{3.20a}$$

$$\underline{I}' = \underline{I}_M - \underline{I}_C \tag{3.20b}$$

Fig. 3.10b shows that the reactive current injection of the capacitor partly compensates for the consumption of the motor, decreasing the angle φ and thus improving the power factor at the bus bar. Furthermore, the magnitude of the grid current is reduced.

Fig. 3.10 Vector diagrams of induction motor: (a) Without load compensation; (b) With load compensation at the device level.

Load compensation reduces the reactive power flows in the grid and thus its loading, losses and voltage drop. The reduction of line and transformer loading increases the active power transfer capability of the electricity grid.

3.1.3.2 Voltage support

Reactive power is traditionally compensated at the HV and MV levels to maintain acceptable voltages and increase the power factor throughout the grid. The grid voltage and the reactive power flows are closely coupled. Therefore, they are controlled together in the course of the Volt/var process, described comprehensively in this chapter.

3.1.4 Volt/var control variables

The grid voltages are affected by the active and reactive power flows and the tap positions of various transformers. Active power is the good that should be transferred and distributed and does not serve to control the voltage. As a result, only two Volt/var control variables remain, i.e. the shunt var contributions that have a considerable indirect impact on the voltage and the tap positions of transformers that control it directly. Series var contributions as those of series-connected RPDs are usually not used for Volt/var control (see §3.1.2.3). Both the tap positions

of transformers and the shunt var contributions differ in their impact on the feeders' voltage profiles.

3.1.4.1 On-load tap changers

Tap changers are usually implemented in every transformer, but the OLTCs are typically available in power transformers, STRs and Line Voltage Regulators (LVR). Meanwhile, Distribution Transformers (DTR) usually have tap changers that can only be changed after de-energisation. The control of the tap position varies the transformer's transmission ratio, provoking a voltage magnitude jump. Fig. 3.11 illustrates the effect of an LVR's tap position on the voltage profiles of two distribution feeders. The change of the tap position shifts a part of the voltage profile mainly in parallel to the original one. This effect is denoted as the Displacement Effect (Ilo 2016b). The parallelism is usually inaccurate due to the voltage dependency of the consumption (see §3.1.2.4) and feeder losses (§3.1.2.3).

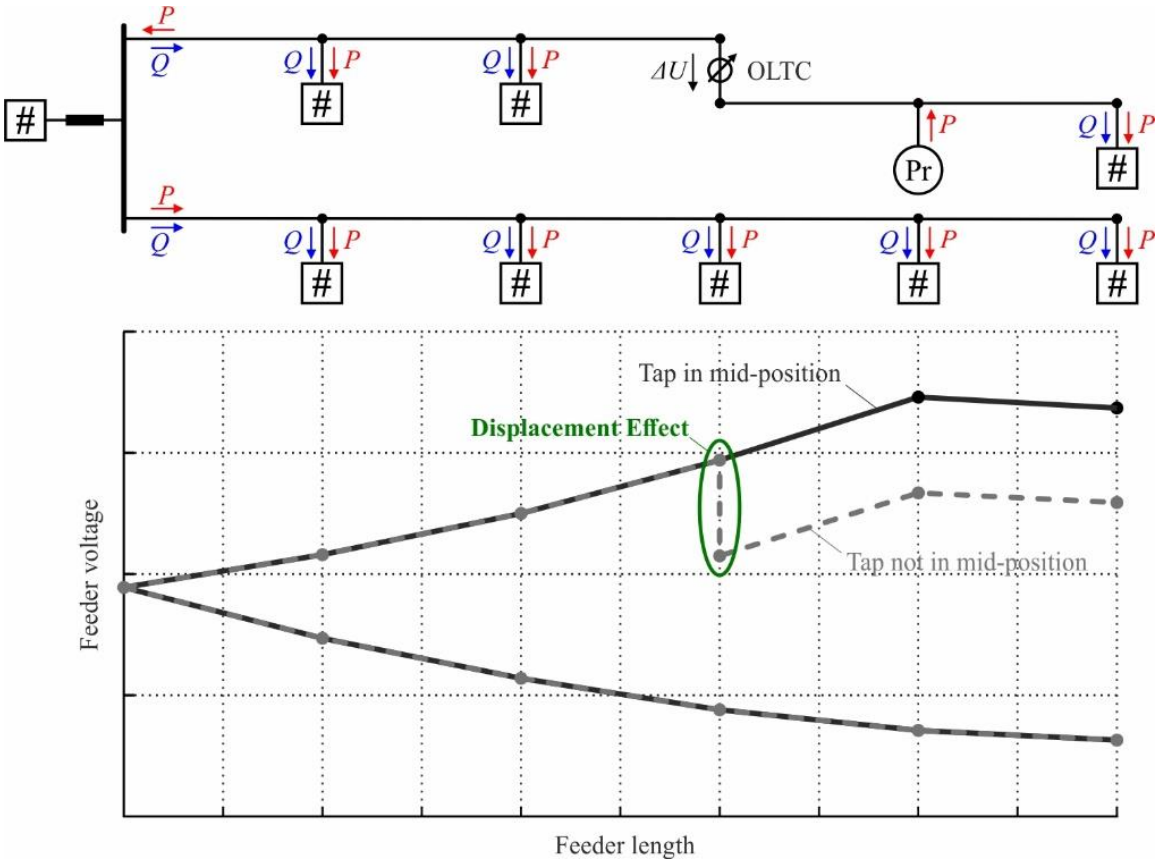

Fig. 3.11 Effect of an LVR's tap position on the voltage profiles of two distribution feeders.

3.1.4.2 Shunt var contributions

Shunt var contributions provoke reactive power flows through the grid that modify the grid voltages (see Equation (3.12)). Fig. 3.12 illustrates the effect of the var absorption of a shunt-

connected RPD on the voltage profiles of two distribution feeders. The change of the reactive power contribution has two effects on the resulting voltage profiles (Ilo 2016b):

- The Displacement Effect shifts the voltage at the supplying bus bar. As a consequence, the voltage profiles of both feeders are moved in parallel.
- The Push Down/Up Effect pushes the voltage profile down or up for inductive or capacitive var contributions, respectively. The maximal shift occurs at the connection point of the RPD. This effect rotates the voltage profile of the feeder to which the RPD is connected.

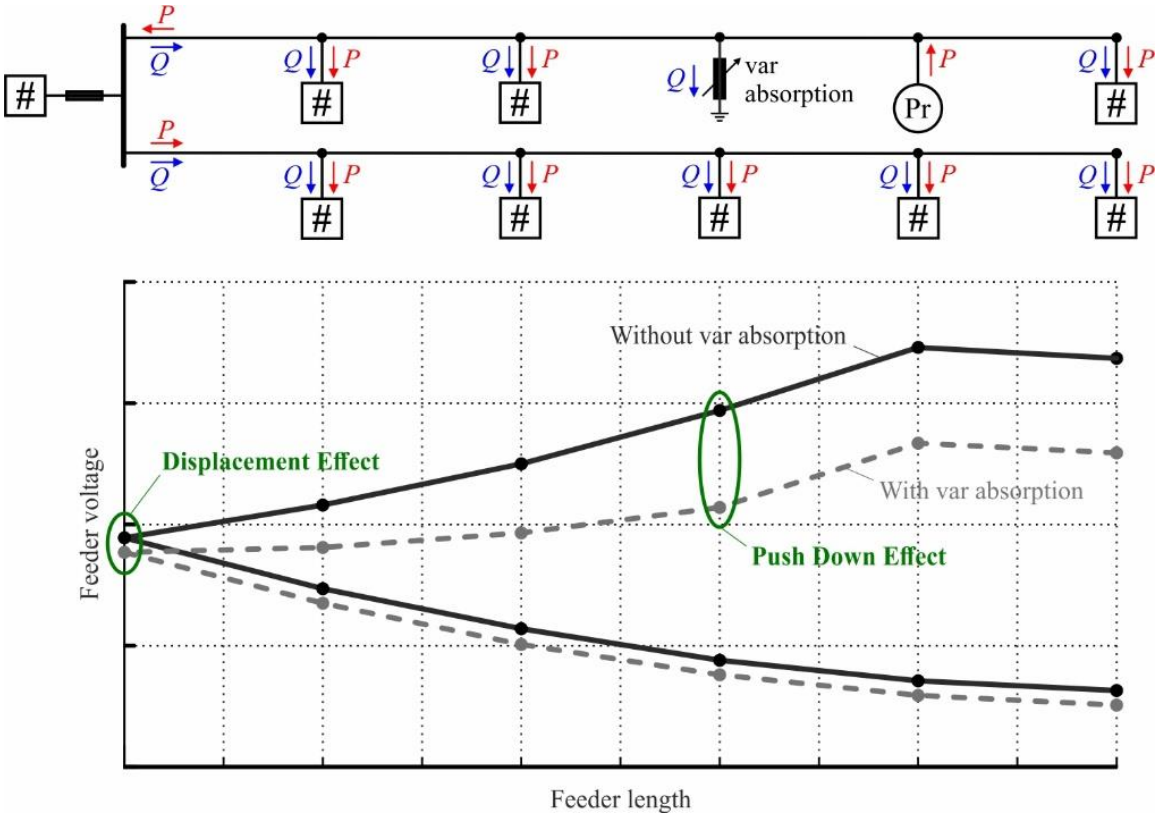

Fig. 3.12 Effects of the var absorption on the voltage profiles of two distribution feeders.

3.1.5 Volt/var control concepts

Volt/var control is an essential process for system operators to ensure the reliable and efficient operation of the power system. This process aims to operate the existing control variables to maintain acceptable voltages optimally. The management of the var contributions of producers, storages and RPDs is challenging due to their vast number, distributed nature, discrete or continuous adjustability, and the complexity of the physical laws that determine the overall system behaviour. Different parts of power systems are owned and operated by distinct stakeholders. Since the power system is a physical entity and the control actions within a particular grid part also impact the system behaviour in other parts of the grid, the overall

control strategy must be agreed between the involved stakeholders. Different concepts are used to control the available variables, including manual, local, primary, direct and secondary control.

3.1.5.1 Manual control

Manual Control (MC) is used to adjust discrete control variables such as the tap positions of transformers and the switch positions of mechanically switched capacitors. As a prerequisite, distributed measurements are collected via the Supervisory Control And Data Acquisition (SCADA) system and visualised in the control centre. On this basis, the operator manually initiates the control action required to achieve the desired system state. For example, the TSO recognises a deviation from the scheduled reactive power exchange with the neighbour transmission grid and manually changes the switch position of the remotely controlled MSC or authorises a crew to execute the command on site.

3.1.5.2 Local control

LC refers to control actions that are carried out locally without considering the holistic real-time behaviour of the relevant grid part. Its action path may be realised in open- or closed-loop. LC automatically adjusts the active/reactive power contributions of RPDs, storages and producers, and the tap positions of transformers based on local measurements or time schedules (Sun et al. 2019; Roytelman and Ganesan 1999; Farivar et al. 2015). It usually maintains a power system parameter, which is locally measured or calculated based on local measurements, equal to the desired value. The fixed control settings are calculated based on offline system analysis for typical operating conditions. Local controls are simple, reliable and quickly respond to changing operating conditions without the need for a communication infrastructure (Zhou et al. 2021; Nowak et al. 2020; Roytelman and Ganesan 2000).

3.1.5.3 Primary control

PC refers to control actions executed locally in a closed-loop: The input and output variables are the same. The output- or control variable is locally measured and continuously compared with the set-point received from the corresponding SC. The deviation from the set-point results in a signal that influences the valves or frequency, excitation current or reactive power, transformer tap positions, etc., in a primary-controlled power plant, transformer, and so on, such that the desired power is delivered or the desired voltage is reached.

3.1.5.4 Direct control

DiC refers to control actions performed locally in an open-loop, taking into account the real-time holistic behaviour of the corresponding grid part. The secondary control calculates the control action.

3.1.5.5 Secondary control

Secondary control refers to control variables that are calculated based on the current state of a control area. It fulfils a predefined objective function by respecting the constraints of electrical appliances (*P*/*Q* capabilities of generators, transformer rating, voltage limits, etc.). It calculates and sends the set-points to primary controls and the input variables to direct controls acting on its area.

3.1.6 Monitoring

The Volt/var process aims to maintain acceptable voltages and high power factors throughout the entire power system by managing the available reactive power resources and on-load tap changers. This management may be established by coordinated or uncoordinated control.

Operators use SCADA systems and, in many cases, also state estimators to observe the steady-state and specify set-points for the distributed control variables to maintain limit compliance within the observed area. The set-points may be calculated automatically by secondary controls or manually by the personnel of the control centres. In any case, the coordinated Volt/var control builds upon monitoring the power system.

In contrast, the uncoordinated control uses fixed control settings for the distributed control variables determined based on offline power system analysis.

3.2 Traditional Volt/var control

Traditionally, the power system was divided into two levels: Transmission, which includes the very high and high voltage level; And distribution, which includes the medium and low voltage levels. Customer demand was mainly met by the large thermal and hydropower plants connected at the transmission level. The traditional Volt/var applications were designed to cope with the resulting unidirectional power flows from transmission via distribution grid to the consuming devices connected at the customer plant level. Energy (EMS) and Distribution Management Systems (DMS) were used by the operators mostly in advisory mode, i.e. in open-loop. Local and manual controls are used to control the reactive power and voltage in very high, high and medium voltage grids. The low voltage grids were sufficiently dimensioned based on the estimated peak demand and the expected annual demand increase to guarantee acceptable

voltages in low voltage level. Fig. 3.13 shows an overview of the traditional devices equipped with Volt/var control units from the holistic view of the power system. The available control variables are highlighted in blue.

The synchronous machines located in the conventional power plants and pumped hydroelectric storages connected at the transmission level provide the basic means of voltage control. Their automatic voltage regulators act as local controls that maintain scheduled voltage set-points at the generator terminals. Additional RPDs are distributed throughout the transmission grids to maintain voltages and improve the power factor. Analogously to the generators of conventional power plants, synchronous condensers and static var compensators are mostly controlled to establish voltage set-points at their terminals. Due to their high purchasing and operating costs, the synchronous condensers have been widely replaced by static var compensators. Shunt reactors are typically used at long overhead lines to prevent the violation of the upper voltage limit caused by the line capacitances during light load conditions. They may be fixed and permanently connected or switched if less reactive power support is required during high load conditions. Fixed and mechanically switched capacitors are also used to supply the reactive power demand of overhead lines and subordinate distribution grids. The reactors and capacitors connected to the transmission grid are switched automatically, depending on locally measured quantities such as voltage, current and so on, or based on time schedules (LC). They may also be switched manually by the system operator (MC). The tap positions of power transformers affect the grid voltages and the reactive power exchanges between the transmission grids. They are controlled either locally to maintain one of the bus voltages or manually. HVDC systems were implemented with LCC technology, thus without the ability to adjust their reactive power contribution and to participate in Volt/var control actively. (Kundur 1994)

Voltage in the distribution level is controlled using the OLTC of supplying transformers, line voltage regulators and mechanically switched capacitor banks (Kundur 1994). The STR and line voltage regulators are locally controlled to maintain the voltages at their secondary buses or other nodes using line drop compensation. Mechanically switched capacitors are used for power factor correction and MV feeder voltage control. They are automatically switched depending on time clocks, terminal voltage, power factor, etc. The small hydropower plants are traditionally operated with a unity power factor (Xu et al. 2015).

Storages within the customer plants (mainly heating and cooling systems) do not participate in the Volt/var control process. Traditionally, no producers are connected at the CP level.

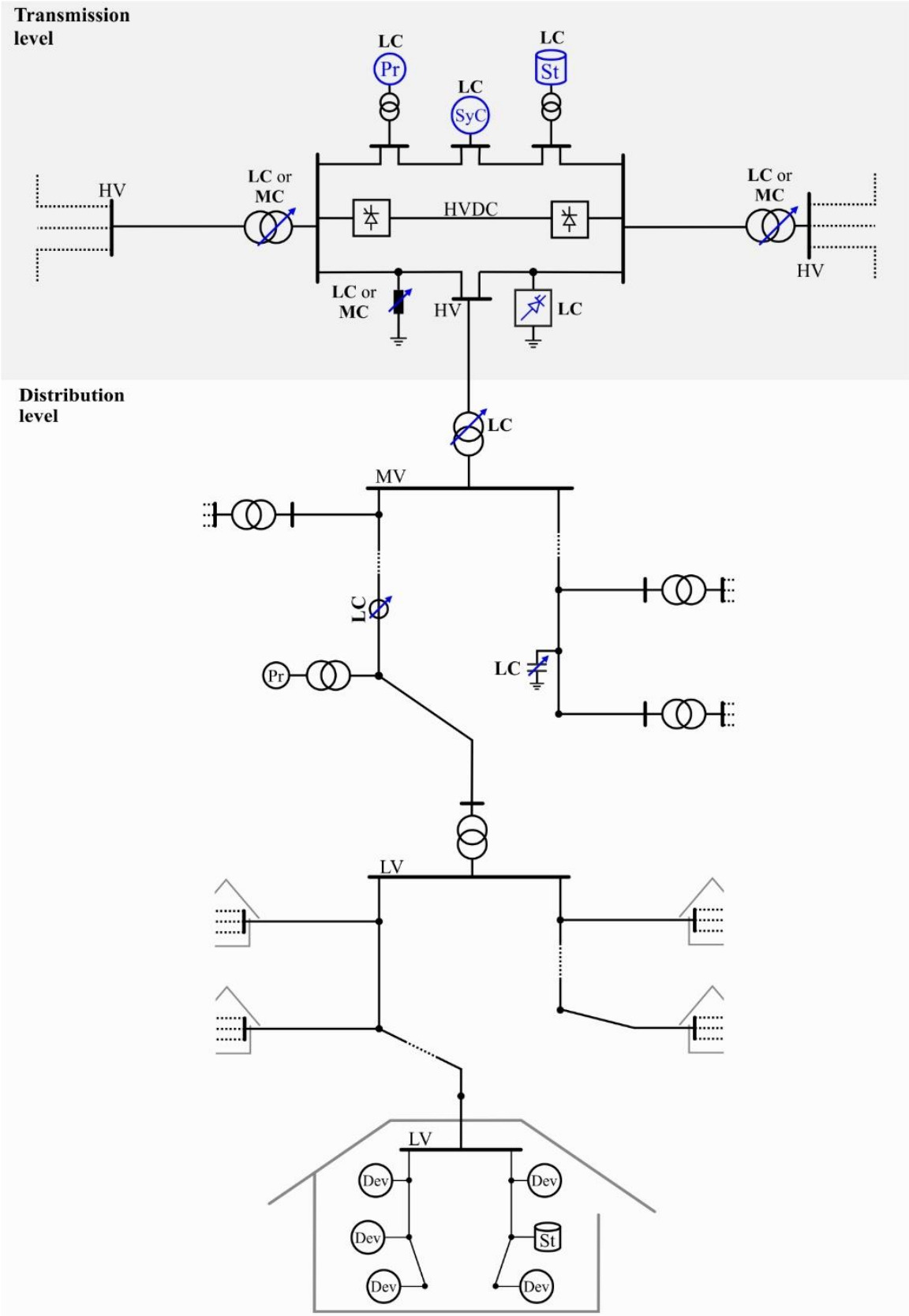

Fig. 3.13 Overview of the traditional Volt/var control from the holistic view of the power system.

3.3 Recently introduced control strategies

In recent years, many inverter-coupled producers, including PV and WT systems, have been installed across all grid levels. Their intensive and intermittent injections pose new challenges for the power system operation that call for an adaption of the traditional Volt/var control schemes. Fluctuating voltages, increased operations of discrete control variables, and bidirectional active power flows through the vertical power system axis are the consequence. The original dimensioning of low voltage grids is insufficient to cope with the simultaneous PV injections and the high consumption of EV chargers, making Volt/var control necessary also at the LV level. From here, the separate consideration of medium and low voltage grids became established to identify the Volt/var control requirements of both system levels. Meanwhile, CPs are implied in the low voltage level and not considered separately.

Up to now, the main strategy used to meet the new challenges was to increase the number of control variables. The inverter-coupled producers across all grid levels are equipped with local controls to utilise their reactive power capabilities for the Volt/var process. The rapid development in power electronics gave rise to new appliances such as FACTS devices and HVDC systems in VSC technology that opened up new control possibilities at the high voltage level. Furthermore, the upgrade of DTRs with OLTCs is considered as a potential measure to increase power system controllability. Most EMS and DMS still run in open-loop, and the settings of the local controls are calculated based on offline system analysis. The recent Volt/var control is overviewed in Fig. 3.14 from the holistic view of the power system.

The STATCOMs and VSCs of HVDC systems recently connected to the HV level are locally controlled to establish voltage or reactive power set-points (Xu et al. 2019; ENTSO-E 2019). The local controls of large WT and PV systems usually maintain constant reactive power, power factor or voltage set-points or adjust the reactive power contribution depending on the local voltage (Li et al. 2018).

Some of the small hydropower plants connected at the MV level are upgraded with local controls that enable the voltage or power factor control mode (Xu et al. 2015). Diverse storage technologies are installed, but they are usually not incorporated in the Volt/var process. The distributed PV and WT systems are mostly operated with fixed reactive power or power factor, or according to $\cos\varphi(P)$- or $Q(U)$-control characteristics.

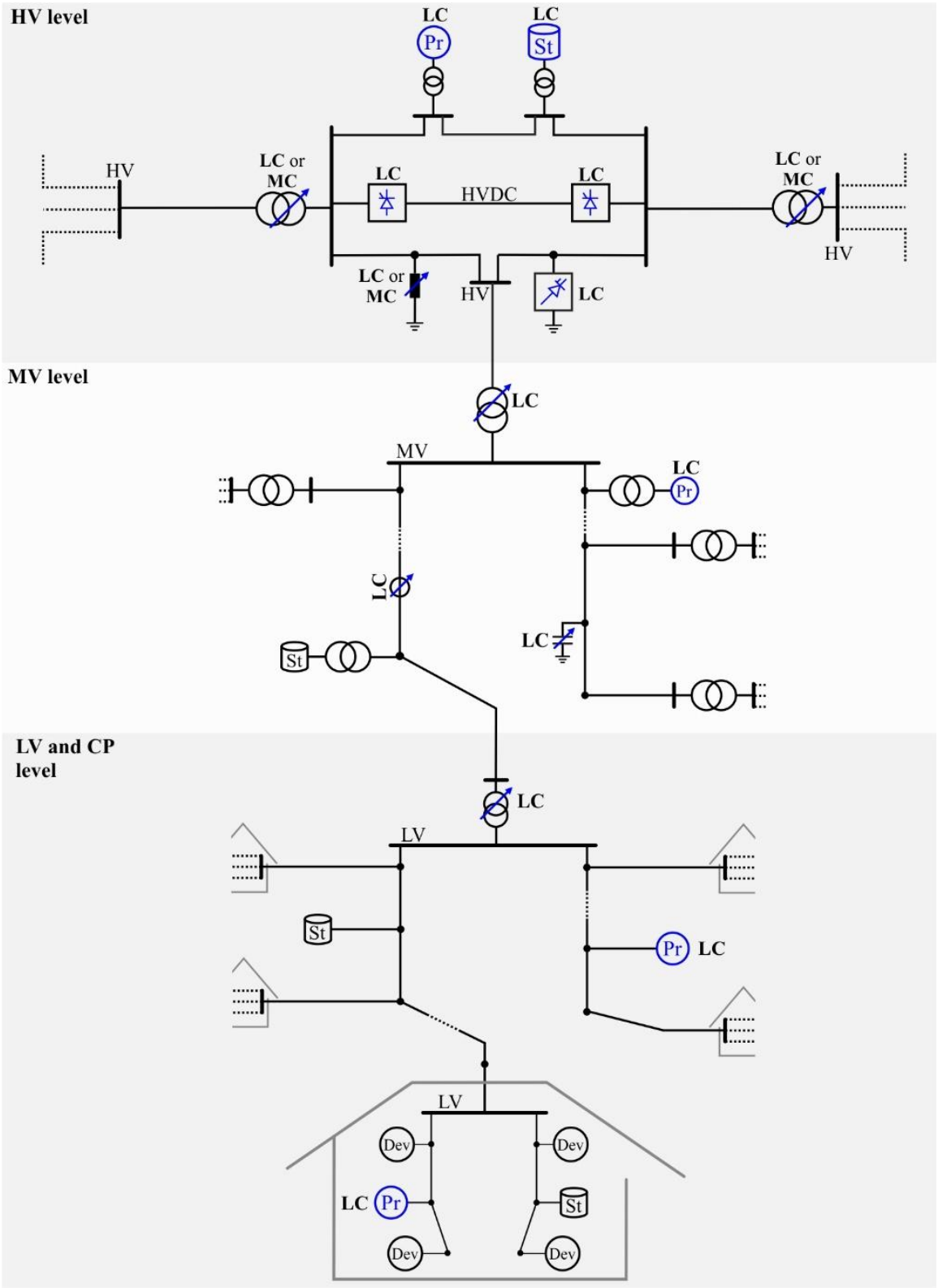

Fig. 3.14 Overview of the recent Volt/var control from the holistic view of the power system.

Local control of the PV systems' reactive power contributions (which are mostly located at the CP level) is used to maintain voltage limit compliance at the LV level. Constant reactive power, constant power factor, cos$\varphi(P)$- and $Q(U)$-control are the most common operating modes

(Bletterie et al. 2010). These modes have been further refined by including more local variables, e.g. cosφ(P,U) (Demirok et al. 2011), Q(U,P) (Zhang et al. 2017), cosφ(P,R/X) (Smith et al. 2011), and many more (Turitsyn et al. 2011). Fig. 3.15a shows the symbolic representation of a PV system with local Volt/var control connected to the CP grid. Alternatively to the control of PV systems, the DTR may be upgraded with an OLTC and locally controlled to maintain its secondary voltage close to a defined value. This measure may also be combined with the Q(U)-control of PV systems (Marggraf et al. 2017). EV chargers are increasingly installed at the CP level, but they are usually not integrated into the Volt/var process.

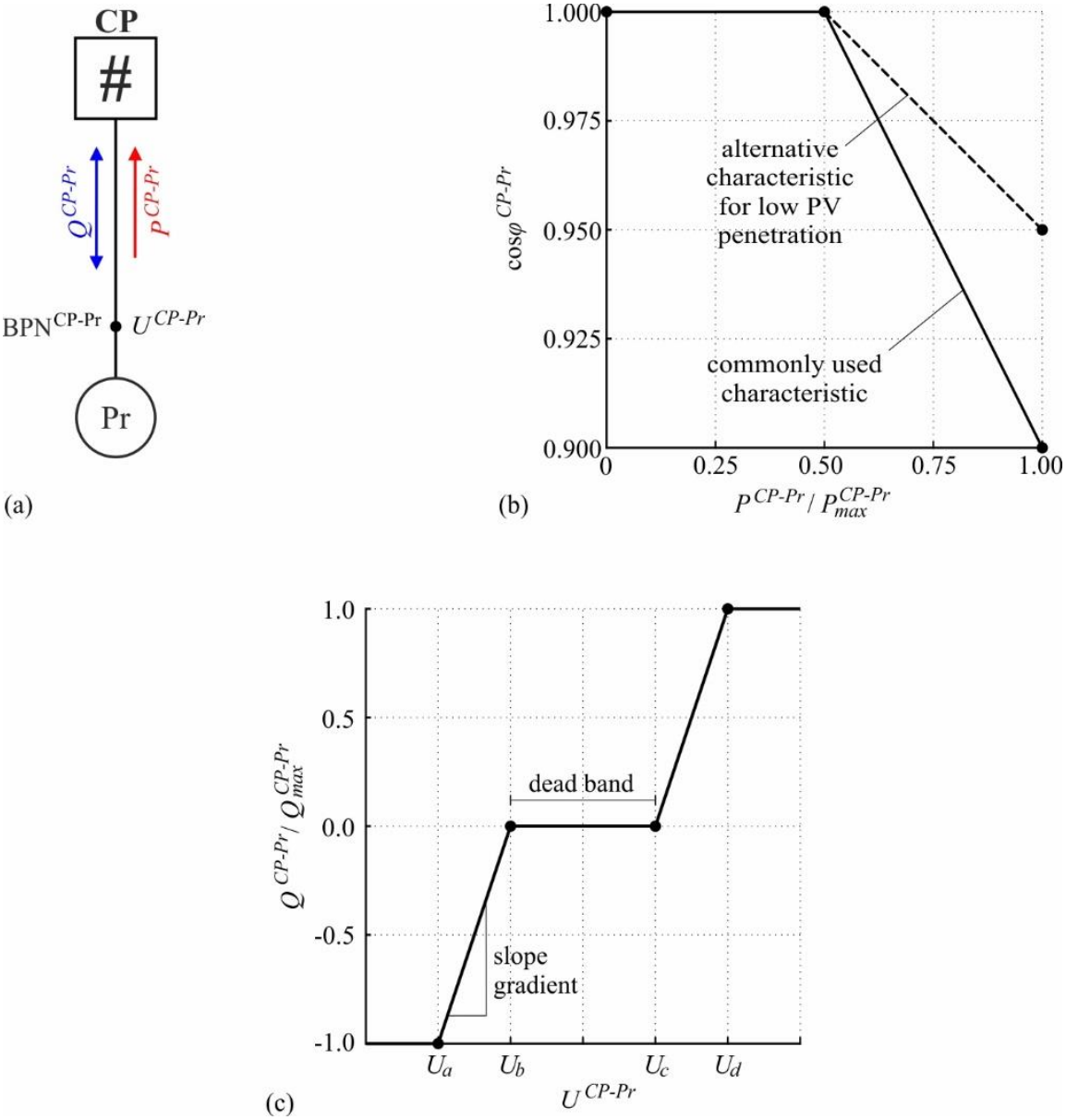

Fig. 3.15 Control strategies for PV inverters: (a) Symbolic representation of the PV system connected at the CP level; (b) Fundamental cosφ(P)-control characteristic; (c) Fundamental Q(U)-control characteristic.

3.3.1 cosφ(P)-control

A cosφ(P)-controlled inverter absorbs reactive power when the active injection exceeds a certain value, which is commonly set to 50 % of the maximal production. Usually, the power factor is reduced from 1.0 down to 0.9 inductive during periods of peak production. Alternatively, for low PV penetrations, it might be less decreased. The fundamental control characteristic is shown in Fig. 3.15b.

3.3.2 Q(U)-control

When Q(U)-control is applied, the PV inverter absorbs reactive power for high local voltages and injects reactive power for low ones, Fig. 3.15c. The parameters U_a, U_b, U_c, and U_d, are specified by the responsible Distribution System Operator (DSO) according to the prevalent grid conditions. The control parametrisation is discussed in detail in §A.2.1.

3.3.3 OLTC in the distribution substation

The on-load tap changer in the distribution substation modifies the voltage at the DTR secondary bus, thus shifting the voltage profiles of all LV feeders in parallel. It is usually primary controlled to adjust its tap position when the voltage error at a certain grid node deviates from the specified dead-band during a specified time delay (Choi and Moon 2009).

3.4 Problem statement

The local controls recently implemented at LV and CP level are insufficient to meet the technical and social requirements of future Smart Grids. The OLTC in the distribution substation is slow to operate and sensitive to the number of tap operations. It cannot react appropriately to the voltage fluctuations caused by the intermittent PV injections. Temporary voltage limit violations and unnecessary tap operations are the consequence, thus jeopardising the electrical equipment and shortening the transformer's durability (Hossain et al. 2016). The use of local cosφ(P)- and Q(U)-control provokes extensive uncontrolled reactive power flows throughout all grid levels (Ilo 2016b) and makes active power curtailment necessary to ensure supply quality and reliability (Tonkoski and Lopes 2011). Implementing cosφ(P)- and Q(U)-controls in PV systems intertwines the operation of the LV grids and customer plants (Ilo and Schultis 2019). Consequently, the reactive power is procured by non-market-based and – in the case of Q(U)-control – discriminatory procedures, which fundamentally contradicts (Directive EU 2019/944).

Although not implemented on a large scale yet, the necessity for the closed-loop coordination of the distributed control variables is widely recognised. The coordinated

automatic voltage regulation in transmission grids has already been studied in Italy, France, Belgium and Spain (Corsi et al. 2004). Still, the coordination between transmission and distribution grids has not been considered. Today, ENTSO-E proposes the use of secondary and primary controls for dynamic optimisation and voltage control at the high voltage level (ENTSO-E 2019). Furthermore, advanced DMS are emerging that allow – among many others – for the closed-loop Volt/var optimisation of distribution grids on a 24/7 basis (Carden and Popovic 2018). Few distribution utilities such as 'Inland Power and Light' and 'Clatskanie PUD' (Wilson and Bell 2004), 'Dominion Virginia Power' (Peskin et al. 2012), 'SCE' (Neal 2010), 'Duke Energy' (Belvin and Short 2012), and 'BC Hydro' (Dabic and Atanackovic 2015), have already implemented the closed-loop Volt/var control.

However, the lack of a holistic approach makes the large scale roll-out of the new control paradigms almost impossible. Coordination schemes that do not rely on a holistic approach consider the perspective of individual stakeholders (TSOs, DSOs, and customers) and optimise individual functionalities, thus leading to suboptimal solutions from the global view. European utilities supply about 260 million CPs, of which more than 99 % are connected at the LV level (Eurelectric 2013). Coordinating the reactive power contributions of millions of CPs results in a flood of data exchange that poses severe challenges to ICT (Rohjans et al. 2012), cybersecurity (Wang and Lu 2013) and data privacy (Zeadally et al. 2013).

3.5 Volt/var chain control

The *LINK*-Architecture allows splitting the horizontal and vertical power system axes into chains of locally optimised Links that interact with each other in a coordinated way (see §2.4). It accomplishes the Volt/var process by a chain control to increase the electrical infrastructure utilisation. Its effectiveness may be increased using an extended lumped grid model. Innovative control strategies at the LV and CP levels overcome the insufficiencies of the recently implemented control schemes.

3.5.1 Extension of the lumped grid model

The hardware of the system components builds the skeleton of the power system that determines its fundamental physical behaviour. Their accurate modelling is the basis of power system analysis and the prerequisite to study the effect of control strategies on the system behaviour. However, the power system is often referred to as the biggest and most complex human-made system existing on earth owned, operated or used by different stakeholders. Its complete modelling and simulation as a single entity are impracticable due to the related modelling effort,

the required computational resources and unknown system details. Therefore, power system analysis is restricted to relatively small grid parts and considers the connected neighbouring elements by lumped models. The lumped modelling of system parts is challenging as these parts usually include numerous elements with distinct characteristics and complex inter-dependencies.

3.5.1.1 Lumped modelling for power flow analysis

Power flow analysis is used to study the steady-state behaviour of grid parts. While the grid part under study is modelled in detail, lumped models represent the connected producers, storages, and neighbouring grid parts. Each lumped model corresponds to one of the following node-elements:

- ***PV* node-element**: The element's active power contribution and the voltage magnitude at its boundary node are specified for the regarded instant of time. Additional Q-limits may be defined. Typical examples include producers such as generators of conventional power plants and RPDs such as static var compensators and synchronous condensers.
- ***PQ* node-element**: The element's active and reactive power contributions are specified for the regarded instant of time, either independent of the voltage at the boundary node or as a function of it. Typical examples include producers such as PV and WT systems, storages, and neighbour Link-Grids.
- **Slack node-element**: The voltage magnitude and angle at its boundary node are specified for the regarded instant of time. For power flow analysis at MV, LV, and CP (and device) level, the superordinate grid is usually selected as the sole slack node-element. Meanwhile, at the HV level, the largest generator may be defined as the slack node-element, or the slack node-element may be divided between different large generators.

The specification of the PQ node-elements that represent entire system parts is of great uncertainty. Their active and reactive power contributions vary over time and node voltage. The time dependency mainly results from the behaviour of customers and thermostatic controls that switch on and off the consuming devices, from the weather conditions that determine the injection of renewable producers, and from the schedules of storages and thermal power plants. Meanwhile, the voltage dependency inheres the power system hardware itself and may be intensified by control schemes such as $Q(U)$.

3.5.1.2 Conventional model

Fig. 3.16 shows an overview of the conventional monitoring model. The grid part under study may apply to HV, MV or LV grids, Fig. 3.16a. Neighbouring grid parts are conventionally modelled as *PQ* node-elements specifying their $P(U)$ and $Q(U)$ behaviour for each regarded instant of time t, Fig. 3.16b. They are commonly represented by the "→" symbol in power flow analysis tools. No voltage limits are associated with the conventional lumped models of neighbouring grid parts. Instead, narrow voltage limits are associated with the study grid part to imply safety margins for the neighbouring ones, which are represented by lumped models. For example, a maximal voltage drop of ± 0.06 p.u. is expected to appear at the LV level under worst-case conditions. The MV grid is operated within voltage limits of ± 0.04 p.u. around the nominal value to ensure limit compliance at the LV level.

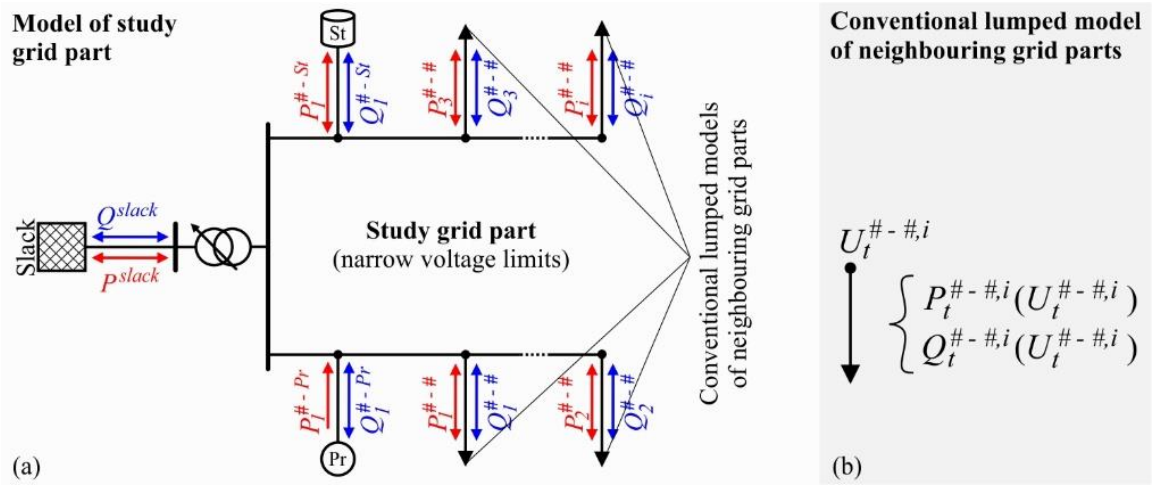

Fig. 3.16 Overview of the conventional monitoring model: (a) Detailed model of the study grid part; (b) Lumped model of neighbouring grid parts.

3.5.1.3 Extended model

The extended lumped model is explained in the following subsections by introducing the concept of Boundary Voltage Limits (BVL) and summarising all model components. Furthermore, the procedure used to calculate the extended lumped model of a Link-Grid is described, and a use case is presented.

Boundary voltage limits

Boundary voltage limits allow verifying voltage limit compliance within the elements represented by lumped models. The upper boundary voltage limits of producers, storages and Link-Grids are denoted as $\overline{BVL_t}^{\#-Pr}$, $\overline{BVL_t}^{\#-St}$, and $\overline{BVL_t}^{\#-\#}$, respectively, while the lower ones as $\underline{BVL_t}^{\#-Pr}$, $\underline{BVL_t}^{\#-St}$, and $\underline{BVL_t}^{\#-\#}$. The symbol # is replaced by the corresponding system

levels, i.e. HV, MV, LV or CP. The setup shown in Fig. 3.17 is analysed in detail to illustrate the variable BVLs of Link-Grids.

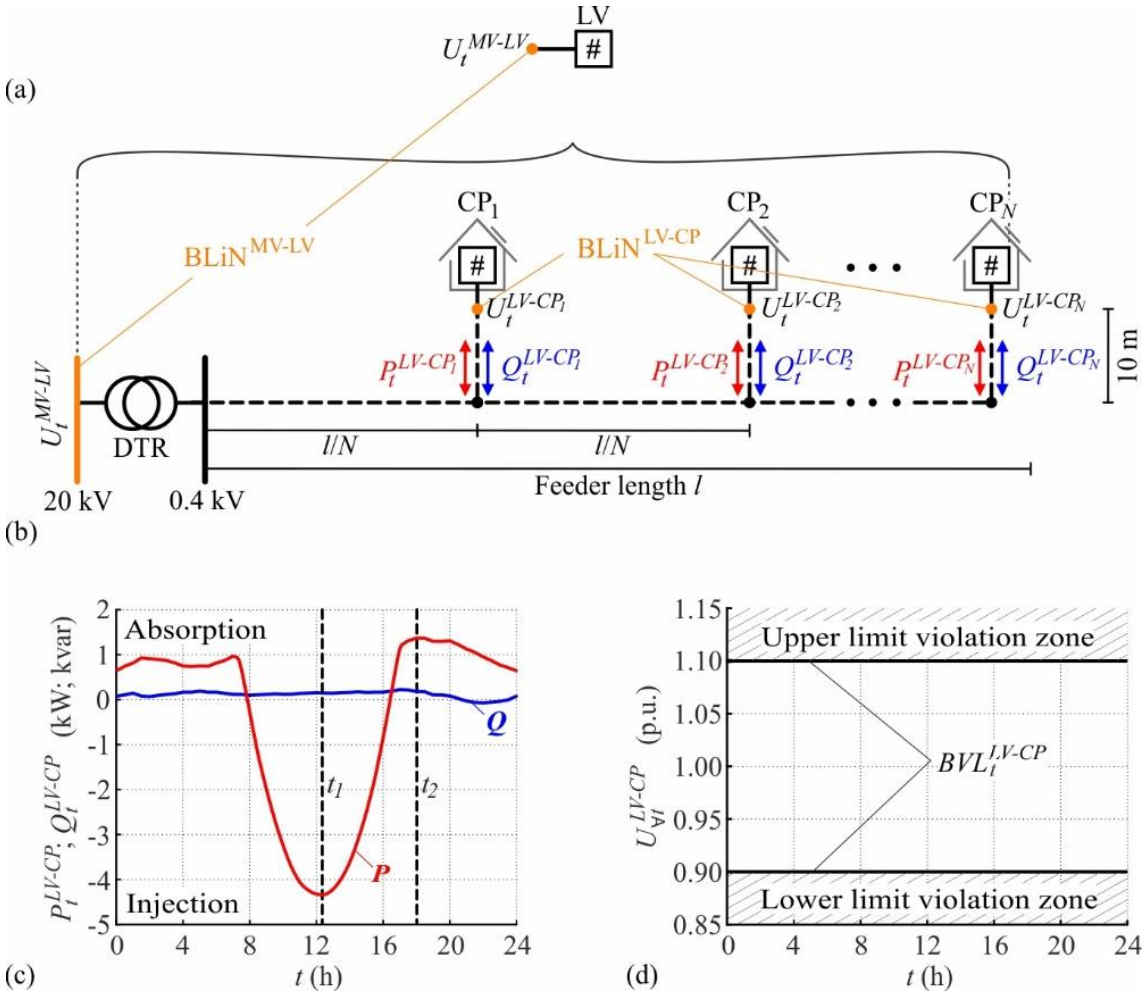

Fig. 3.17 Setup used to illustrate the occurrence of variable BVLs: (a) Lumped model of LV_Link-Grid; (b) LV_Link-Grid represented by the lumped model; (c) Power contributions of each CP; (d) Voltage limits at LV-CP boundary nodes.

Fig. 3.17a shows the lumped model of an LV_Link-Grid, which is intended to be used for load flow analysis at the MV level. Its boundary node to the MV level is denoted as BLiN^{MV-LV} and is associated with the corresponding upper and lower boundary voltage limits, i.e. the $\overline{BVL}_t^{MV-LV}$ and $\underline{BVL}_t^{MV-LV}$. The lumped model represents the LV and CP_Link-Grids sketched in Fig. 3.17b. N residential CP_Link-Grids are connected equidistantly along the LV feeder with the length l through the corresponding boundary nodes, i.e. the BLiN^{LV-CP}. Due to the included consuming devices and PV systems, they absorb and inject power depending on daytime. The load profiles shown in Fig. 3.17c are used to represent the power contributions of each CP. ZIP models are used to consider the voltage dependency of consuming devices. The

European grid codes set the corresponding limits, i.e. the $\overline{BVL}_t^{LV-CP}$ and $\underline{BVL}_t^{LV-CP}$, to ±10 % around nominal voltage (EN 50160:2010). This specification makes the boundary voltage limits of CP_Link-Grids appear time-constant, Fig. 3.17d.

The voltage profiles of the cable feeder (l = 1 km, N = 25) at $t_1 = 12{:}10$ and $t_2 = 18{:}00$ are shown in Fig. 3.18 for MV-LV boundary voltages that provoke violations of the upper and lower LV-CP boundary voltage limits.

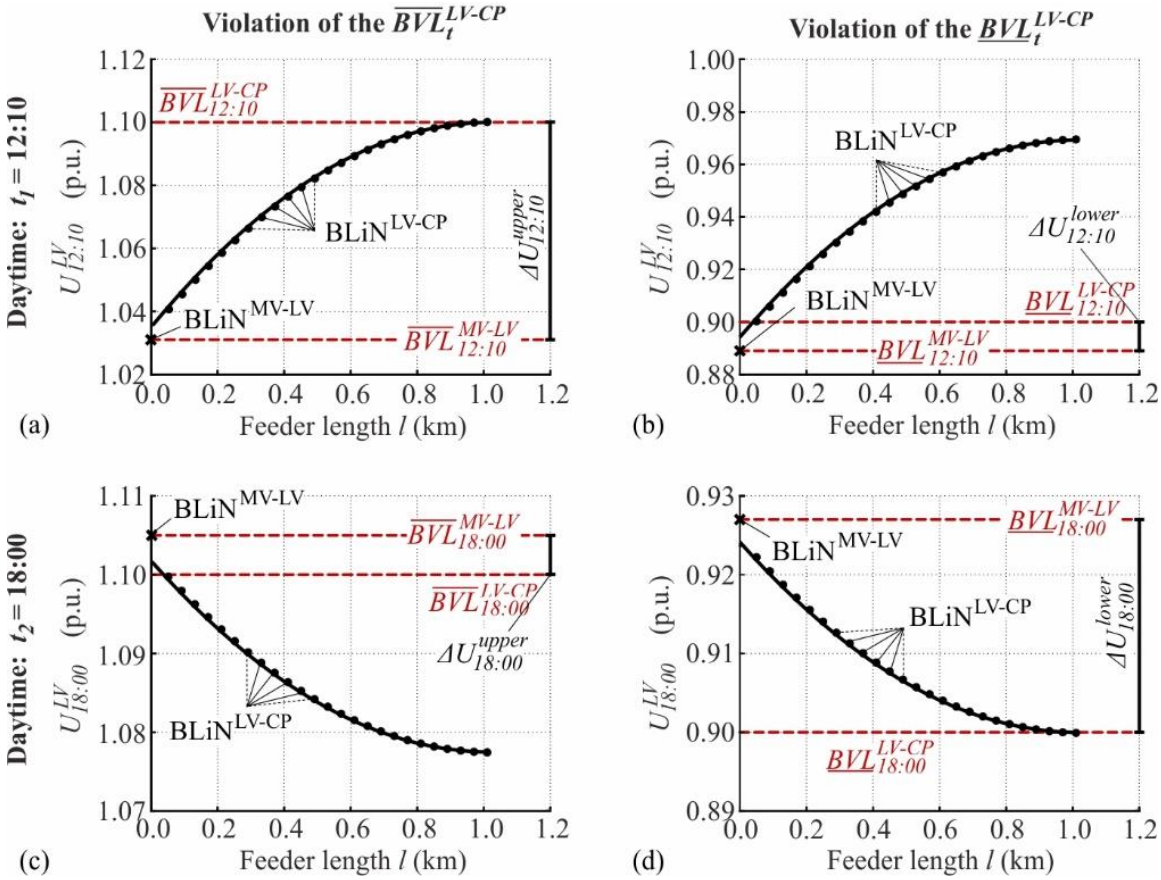

Fig. 3.18 Voltage profiles of the cable feeder (l = 1 km, N = 25) at t_1 and t_2 for MV-LV boundary voltages that provoke violations of the upper and lower LV-CP boundary voltage limits: (a) Upper limit at t_1; (b) Lower limit at t_1; (c) Upper limit at t_2; (d) Lower limit at t_2.

At 12:10, the $\overline{BVL}_{12:10}^{LV-CP}$ is violated by the backmost CP when the MV-LV boundary voltage exceeds 1.031 p.u., setting the $\overline{BVL}_{12:10}^{MV-LV}$ value accordingly, Fig. 3.18a and Equation (3.21a). When reducing the MV-LV boundary voltage to 0.889 p.u., the $\underline{BVL}_{12:10}^{LV-CP}$ is violated by the foremost CP, Fig. 3.18b. In this case, the lower limit is less restrictive at the BLiN^{MV-LV} than at the BLiN^{LV-CP}, Equation (3.21b).

At 18:00, the voltages decrease along the DTR and LV feeder, setting the upper and lower MV-LV boundary voltage limits to 1.105 and 0.927 p.u., respectively, Fig. 3.18c-d and Equation (3.22).

$$\overline{BVL}_{12:10}^{MV-LV} = \overline{BVL}_{12:10}^{LV-CP} - \left|\Delta U_{12:10}^{upper}\right| = 1.031 \text{ p.u.} \quad (3.21a)$$

$$\underline{BVL}_{12:10}^{MV-LV} = \underline{BVL}_{12:10}^{LV-CP} - \left|\Delta U_{12:10}^{lower}\right| = 0.889 \text{ p.u.} \quad (3.21b)$$

$$\overline{BVL}_{18:00}^{MV-LV} = \overline{BVL}_{18:00}^{LV-CP} + \left|\Delta U_{18:00}^{upper}\right| = 1.105 \text{ p.u.} \quad (3.22a)$$

$$\underline{BVL}_{18:00}^{MV-LV} = \underline{BVL}_{18:00}^{LV-CP} + \left|\Delta U_{18:00}^{lower}\right| = 0.927 \text{ p.u.} \quad (3.22b)$$

Calculating the load flows for the complete time horizon yields the variable upper and lower BVL_t^{MV-LV}-curves, Fig. 3.19.

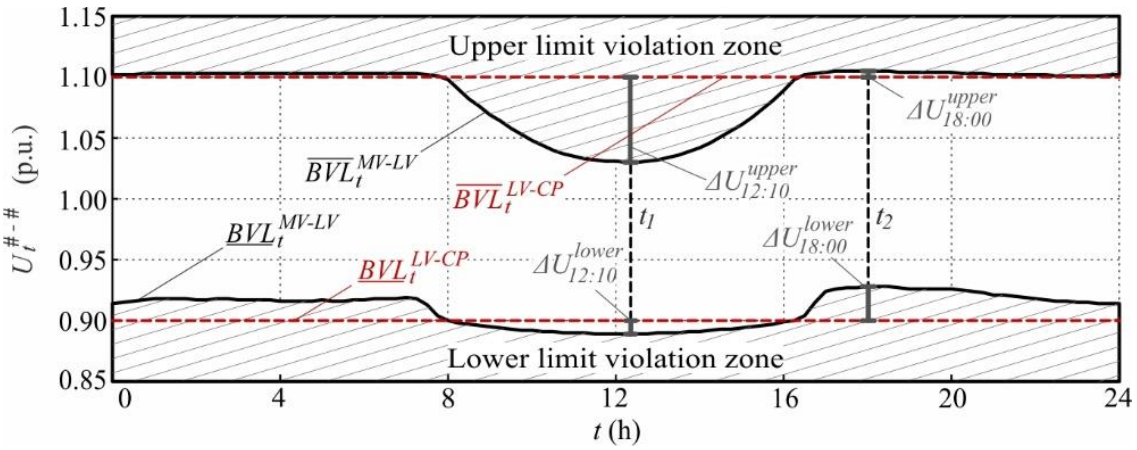

Fig. 3.19 Deformation of the boundary voltage limits by the internal voltage drops of the LV_Link-Grid (cable, $l = 1$ km, $N = 25$).

The injection around noontime significantly decreases the upper BVL of the lumped LV_Link-Grid model and slightly decreases the lower one. Vice versa, in times of consumption, both BVL are increased, tightening the admissible voltage band in total. The extend of limit curve deformation – between the $\text{BLiN}^{\text{MV-LV}}$ and the $\text{BLiN}^{\text{LV-CP}}$ – depends on the feeder parameters and the number of connected CPs. Fig. 3.20 shows the upper and lower BVL_t^{MV-LV} for overhead line and cable conductors and for different feeder lengths and CP numbers. The more CPs are connected, the tighter are the resulting BVL_t^{MV-LV}. The cable feeder is less restricted than the overhead line one, as it has lower series impedance. Long feeders are more restricted than short ones.

Components of the extended model

The *LINK*-based holistic architecture provides a systematic approach for power system modelling as it relies on the fractal feature of power systems (Ilo 2019). Fig. 3.21 shows an

overview of the extended monitoring model. The Link-Grid under study may apply to HV, MV, LV or CP_Link-Grids, or even to the conductors in consuming device level, Fig. 3.21a. Neighbouring Link-Grids are represented by the extended monitoring model, which complements the conventional one by two additional variables:

- Upper boundary voltage limit ($\overline{\text{BVL}}$);
- And lower boundary voltage limits ($\underline{\text{BVL}}$).

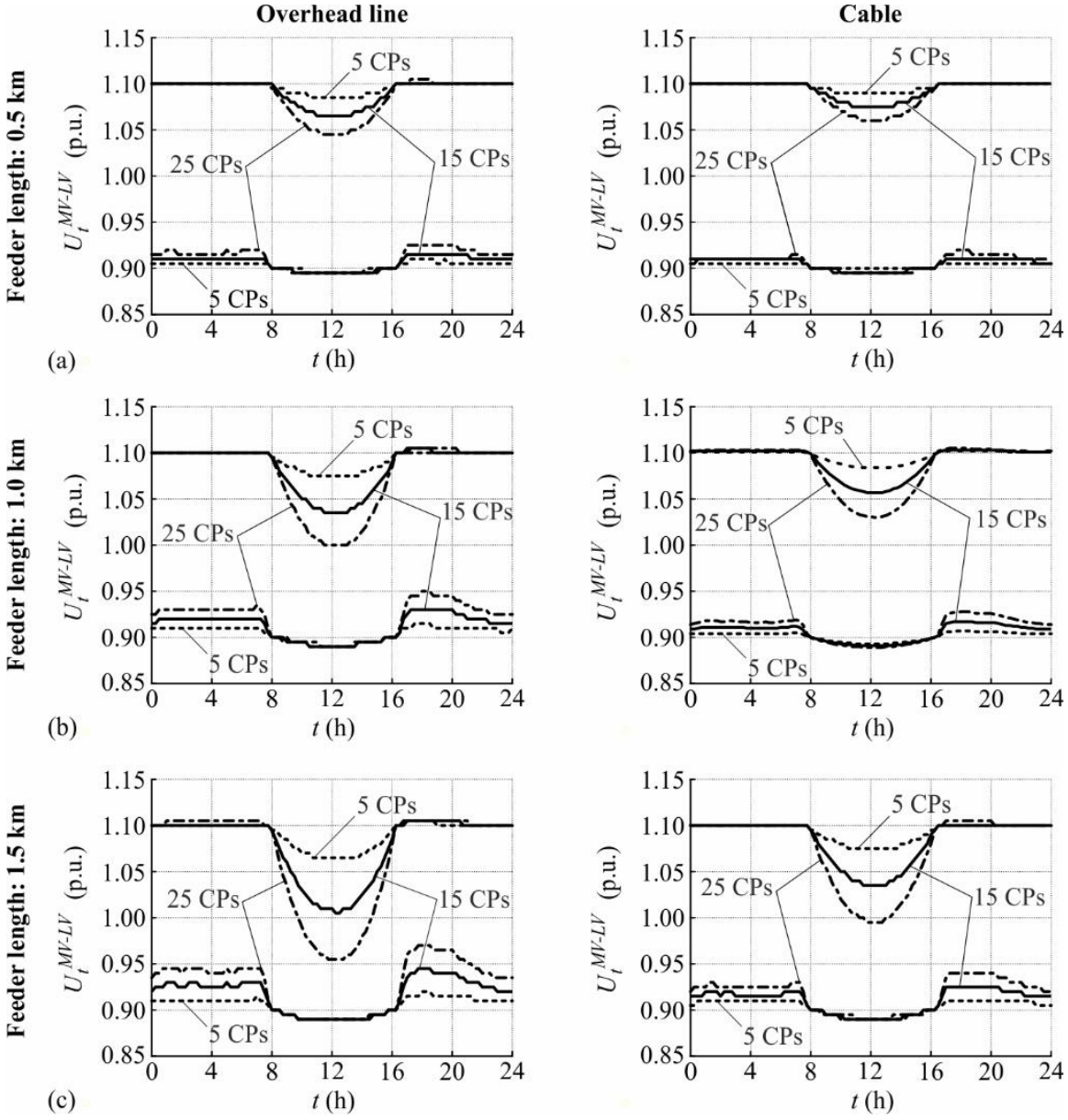

Fig. 3.20 Upper and lower BVL_t^{MV-LV} for 5, 15 and 25 connected CPs, for overhead line and cable conductors, and for different feeder lengths: (a) 0.5 km; (b) 1.0 km; (c) 1.5 km.

Fig. 3.21b shows the extended lumped model supplemented with the new changing boundary voltage limits. The neighbouring Link-Grids are represented by the "#" symbol to distinguish

between the conventional and the extended lumped model. Producers and Storages are connected through the BPNs and the BSNs, respectively.

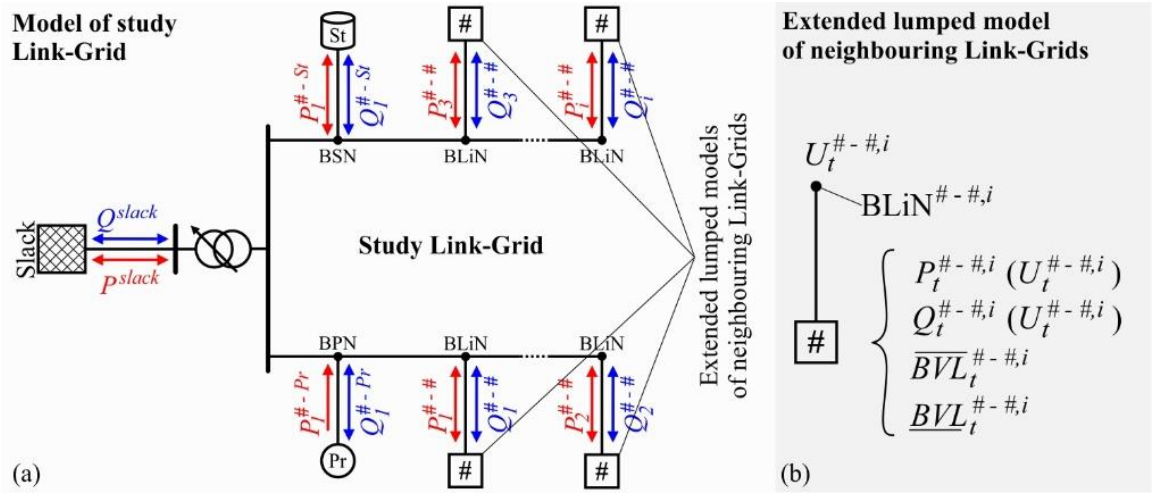

Fig. 3.21 Overview of the extended monitoring model: (a) Detailed model of the study Link-Grid; (b) Lumped model of neighbouring Link-Grids.

Detailed model of the study Link-Grid

The detailed Link-Grid model includes all existent lines, transformers, reactive power devices, and HVDC systems interconnected and parametrised to represent the grid part under study. The model is complemented with voltage limits for each node, representing the electrical equipment's insulation-related limits.

Extended lumped models of the connected elements

The lumped model behind each *PQ* node-element is complemented with the boundary voltage limits so that it includes the following information for each regarded instant of time:

- The **power contributions** as functions of the boundary voltage, i.e. $P_t(U_t)$ and $Q_t(U_t)$;
- And the boundary voltage limits, i.e. upper and lower BVL_t.

The **lumped producer models** reflect the behaviour of electricity production facilities. They inject active power and inject or absorb reactive power. Their boundary voltage limits, $BVL_t^{\#-Pr}$, are usually time-invariant and documented in the datasheet provided by the manufacturer.

The **lumped storage models** reflect the behaviour of storage facilities. They inject or absorb active and reactive power. Their boundary voltage limits, $BVL_t^{\#-St}$, are usually time-invariant and documented in the datasheet provided by the manufacturer.

The **lumped Link-Grid models** reflect the aggregate behaviour of neighbour Link-Grids and all thereto connected elements, i.e. producers, storages and further Link-Grids. They inject or absorb active and reactive power. Their boundary voltage limits, $BVL_t^{\#-\#}$, usually vary over time.

Fig. 3.22 exemplifies the lumped Link-Grid model using the LV_Link-Grid described in Fig. 3.17 (cable, l = 1 km, N = 25). The power contributions of the lumped model are defined for each instant of time and boundary voltage value. Each point (t, U) within the violation zones provokes voltage limit violations within the Link-Grid represented by the lumped model.

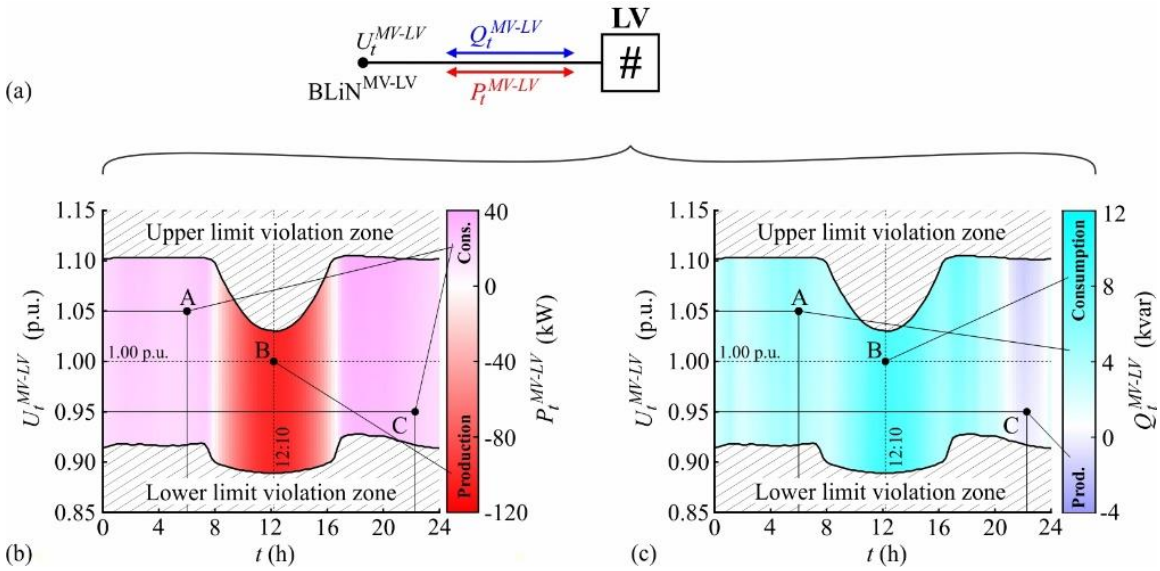

Fig. 3.22 Exemplary lumped LV_Link-Grid model: (a) Symbolic representation; (b) Active power contribution and BVL_t^{MV-LV}; (c) Reactive power contribution and BVL_t^{MV-LV}.

The active power behaviour is presented in the relevant zone between the upper and lower BVL_t^{MV-LV} using different colour shades from red for 120 kW injection to light violet for 40 kW absorption, Fig. 3.22b. The direction of the active power flow changes twice a day. From 00:00 to 8:00, the LV_Link-Grid draws active power from the MV level. At 6:00, for a boundary voltage of 1.05 p.u., it consumes 21.48 kW, case A. With the onset of a sunny day, PV systems begin to produce electricity. When the total production exceeds the total consumption, i.e. from 08:00 to 16:15, the active power changes the direction and flows from the LV to the MV level. It rises steadily to reach the maximum value at 12:10. For a voltage of 1.00 p.u. at the BLiN^{MV-LV}, the LV_Link-Grid injects 101.93 kW into the MV level, case B. With the offset of a sunny day, the electricity production of PV systems reduces to zero. When the produced electricity falls below the consumed one, i.e. from 16:15 to 24:00, the active power changes the direction and flows again from the MV to the LV level. At 22:10, for a boundary

voltage of 0.95 p.u., the lumped model consumes 21.94 kW, case C. Fig. 3.22c shows the reactive power behaviour in different colour shades from light blue for 4 kvar injection to cyan for 12 kvar consumption. Also, the reactive power changes the direction of flow twice a day. It flows from the MV into the LV level from 0:00 to 20:45, reaching values of 4.51 and 8.46 kvar in cases A and B, respectively. Later on, due to the capacitive nature of many modern consuming devices (mostly LED light bulbs), the reactive power changes the flow direction: It flows from the LV into the MV level until 23:30. Here, the boundary voltage has a noticeable impact on reactive power production. The lower the boundary voltage, the less reactive power is produced, amounting to 0.97 kvar in case C.

Fig. 3.23a and b show the power contributions for one specific boundary voltage and instant of time, respectively, cut out from the lumped model shown in Fig. 3.22. Case B is marked in both figures.

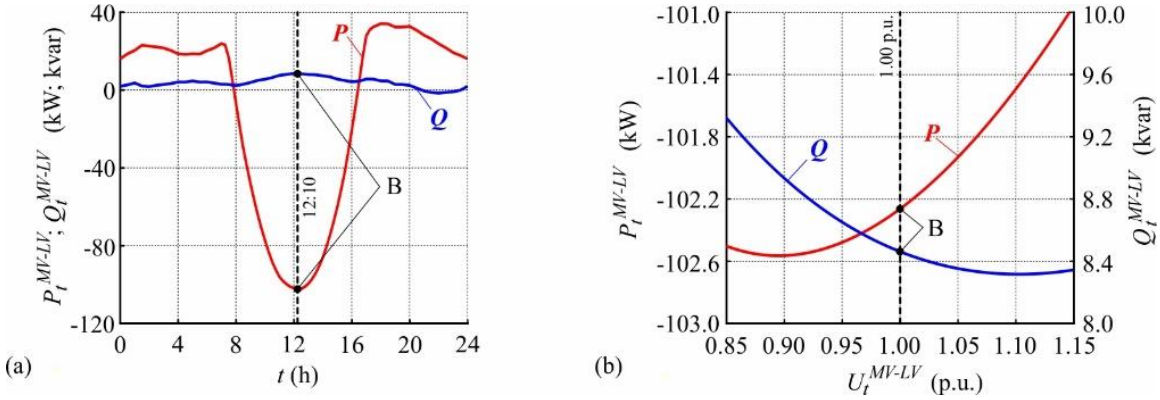

Fig. 3.23 Power contributions of the exemplary lumped Link-Grid model: (a) As functions of time for the boundary voltage of 1.00 p.u.; (b) As functions of boundary voltage at 12:10.

The time dependency of active and reactive power contributions appears similar to the one of the CPs shown in Fig. 3.17c, as only grid losses are added, Fig. 3.23a. The power contributions at 12:10 only slightly depend on the boundary voltage, Fig. 3.23b. Both the active power injection and the reactive power absorption decrease with increasing voltage.

Calculation procedure of the model components

The aggregate behaviour of any Link-Grid can be calculated if its structure and the behaviour of the connected elements are known. Fig. 3.24 illustrates the aggregation of the Link-Grid. The BLiN at which the Link-Grid is aggregated is designated as the “BLiN of aggregation”. The Link-Grid to be aggregated connects producers, storages, and neighbouring Link-Grids, Fig. 3.24a. Their lumped models include the power contributions as functions of boundary voltage and time and the corresponding boundary voltage limits.

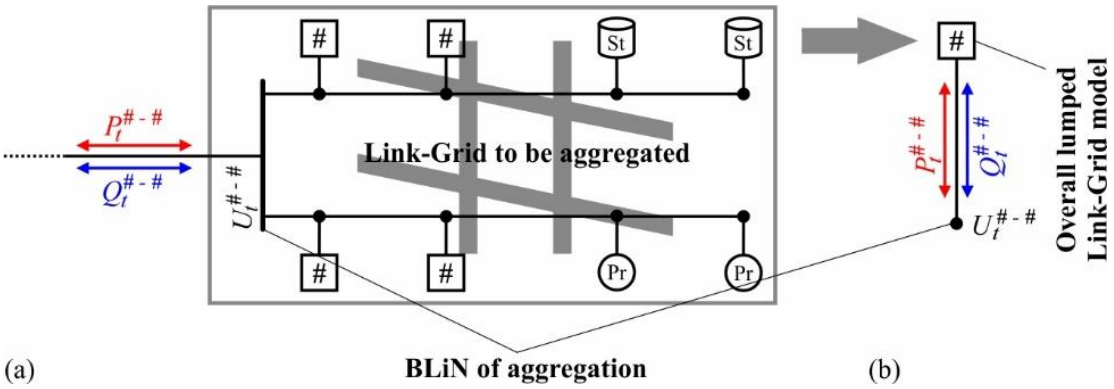

Fig. 3.24 Aggregation of a Link-Grid: (a) Link-Grid to be aggregated; (b) Overall lumped Link-Grid model.

Fig. 3.24b shows the aggregated Link-Grid, which is calculated by using the procedures described below.

1. Connect the slack node-element to the BLiN of aggregation.
2. Define the slack voltage range of interest, e.g. from 0.9 p.u. to 1.1 p.u., and the corresponding resolution, e.g. 0.01 p.u. steps.
3. Select one instant of time specified by the lumped models of the connected elements.
4. Repeat load flow simulations of the selected instant of time for all defined slack voltages, and record the *P*- and *Q*-values provided by the slack node-element. Furthermore, document all slack voltage values that provoke violations of:
   - The voltage limits of any node of the detailed Link-Grid model, i.e. the Link-Grid to be aggregated.
   - And the boundary voltage limits of any connected element.
5. Repeat steps 1 to 4 for all other instants of time specified by the lumped models of the connected elements.

This procedure yields the following results for each instant of time:

- The power contributions of the Link-Grid to be aggregated as functions of its boundary voltage;
- A set of slack voltage values that provoke violations of upper voltage limits either within the Link-Grid to be aggregated, or at the boundary node of any connected lumped model. This set of values is denoted as $U_{k,t}^{upper-viol.}$, where k indexes the different values within this set;
- And a set of slack voltage values that provoke violations of lower voltage limits either within the Link-Grid to be aggregated, or at the boundary node of any connected lumped

model. This set of values is denoted as $U_{m,t}^{lower-viol.}$, where m indexes the different values within this set.

Subsequently, the upper and lower boundary voltage limits of the lumped Link-Grid model are calculated using Equation (3.23).

$$\overline{BVL}_t^{\#-\#} = \min_k \left(U_{k,t}^{upper-viol.}\right) \tag{3.23a}$$

$$\underline{BVL}_t^{\#-\#} = \max_m \left(U_{m,t}^{lower-viol.}\right) \tag{3.23b}$$

The calculated power contributions and boundary voltage limits build the overall lumped Link-Grid model, which can be used to study the behaviour of the Link-Grid connected at the other side of the BLiN of aggregation.

Use case: Notification of boundary voltage limits

The extended monitoring model allows formulating use cases for the *LINK*-based monitoring chain process that apply in different timeframes, e.g. in day-ahead and real-time (Schultis and Ilo 2021).

Generalised use case

Due to the standardised structure of the *LINK*-based holistic architecture, the consideration of two Grid-Links is sufficient to formulate the generalised use case. Two cases are distinguished: Different System Operators (SO) operate the Grid-Links, and one SO operates the Grid-Links.

- Different operators operate the Grid-Links:

  This case is shown in Fig. 3.25, where SO_1 and SO_2, which may be different companies, operate Grid-Link_1 and Grid-Link_2, respectively. SO_1 calculates the BVLs at the boundary node to Grid-Link_2 and notifies them to SO_2. SO_2 sets the optimisation constraints[3] of its Volt/var Secondary Control accordingly.

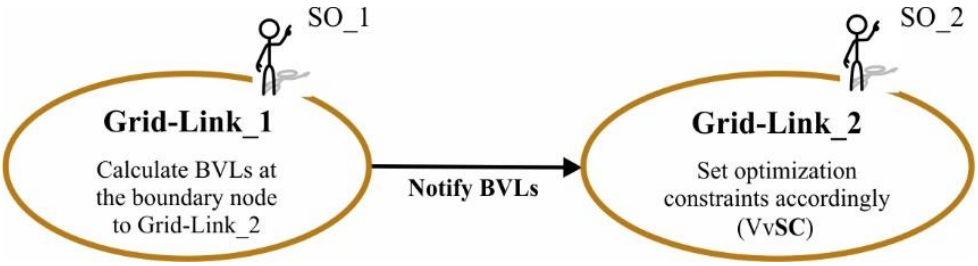

Fig. 3.25 Overview of the use case: Notification of boundary voltage limits when different SOs operate the Grid-Links.

[3] These constraints apply exclusively to the boundary node between Grid-Link_1 and Grid-Link_2.

- The same operator operates the Grid-Links.

  Fig. 3.26 shows the case where one SO, e.g. the DSO, operates both Grid-Links. Although the data of both Grid-Links are normally available in the same database, the state estimation may be performed by different applications and in different time intervals. The application estimating the state of Grid-Link_1 calculates the BVLs at the boundary node to Grid-Link_2 and notifies them to the application observing Grid-Link_2. The ***VvSC*** in Grid-Link_2 adapts its optimisation constraints accordingly.

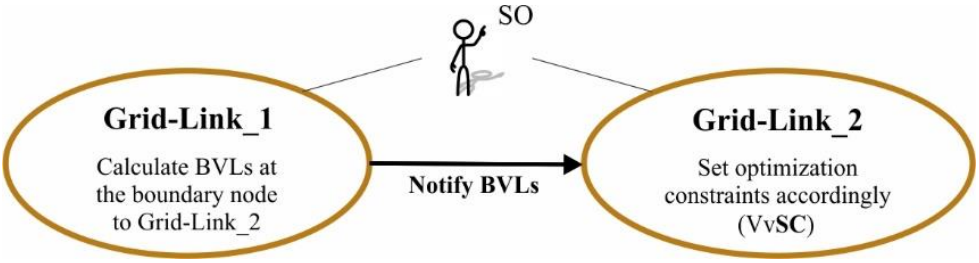

Fig. 3.26 Overview of the use case: Notification of boundary voltage limits when one SO operates the Grid-Links.

Day-ahead scheduling

SO_1 calculates the day-ahead schedule of the BVLs at the boundary node of Grid-Link_2 with sufficient resolution and notifies it to SO_2. SO_2 sets the (time-variant) optimisation constraints of its Vv**SC** for the next day accordingly.

Short-term adaptation

SO_1 recognises a deviation from its actual day-ahead schedule of the BVLs at the boundary node to Grid-Link_2, recalculates the corresponding BVLs and notifies them to SO_2. SO_2 updates the optimisation constraints of its Vv**SC** accordingly.

3.5.1.4 Conventional vs extended model

The use of time constant voltage limits to check the power flow results is not accurate. Voltage limits in radial structures (e.g. MV) are object to deformation due to the voltage drops in the subordinate grids (e.g. LV). The extent of this deformation depends on the properties of the LV feeders: The greater the feeder impedance and the number of connected customer plants, the more intensive is the deformation. In order to take the latter into account, the conventional lumped models of grid parts are extended with new parameters, i.e. the upper and lower boundary voltage limits. BVLs allow verifying voltage limit compliance within the study/operation Link-Grid and within the neighbouring Link-Grids, represented by lumped models in power flow analysis.

The presented use cases allow increasing the operational efficiency of Smart Grids by day-ahead scheduling and short-term (online) adaption of the boundary voltage limits.

3.5.2 General description of the Volt/var chain

The Volt/var chain control coordinates the available control variables using the secondary control (see §2.4) as the base instrument. Fig. 3.27 shows the generalised form of the Volt/var chain control wherein the Grid-Links are set upon four classical levels: HV, MV, LV and CP level. But, by definition, the Grid-Link size is variable (see §2.2.1). It may apply to the classical system levels and to a part of the grid that includes more than one system level, e.g. MV and LV. The LV and CP levels are distinguished to enable the consideration of different ownerships and stakeholder interests. While the automation and communication path is drawn in blue, the power flow path is black coloured. In its generalised form, the Volt/var chain control utilises all reactive power resources, including storages with reactive power capabilities across all system levels. The neighbour Grid-Links may act as additional control variables by accepting reactive power set-points. The $\boldsymbol{VvSCs}$ of the generalised Volt/var chain control are described in the following sections separately for the horizontal and vertical power system axis.

3.5.2.1 Horizontal

The transmission grids, i.e. the HV grids, lie within the horizontal axis (X-axis) of the power system. HV_Grid-Links are typically set upon the control areas of the TSOs. Equation (3.24) compactly represents the control variables and dynamic constraints of the horizontal Volt/var chain control.

$$\begin{aligned} &\boldsymbol{VvSC}_{Chain}^{X-axis} = \cup_{i=1}^{M}\{ \\ &\boldsymbol{VvSC}^{HV_i}(\boldsymbol{PC}_{OLTC}^{HV_i}, \boldsymbol{PC}_{Pr}^{HV_i}, \boldsymbol{PC}_{St}^{HV_i}, \boldsymbol{PC}_{RPD}^{HV_i}, \boldsymbol{DiC}_{RPD}^{HV_i}, \boldsymbol{PC}_{HVDC}^{HV_i}, \boldsymbol{SC}_{NgbHV}^{HV_i}, \\ &\qquad \boldsymbol{SC}_{NgbMV}^{HV_i}; \boldsymbol{Cns}_{NgbHV}^{HV_i})\} \end{aligned} \tag{3.24}$$

Where the $\boldsymbol{VvSC}^{HV_i}$ calculates in real-time:

- The voltage set-points for the primary controls $\boldsymbol{PC}_{OLTC}^{HV_i}$ of the power transformers included in the HV_Grid-Link *i* that have OLTC;
- The voltage and reactive power set-points for the primary controls $\boldsymbol{PC}_{Pr}^{HV_i}$ of the Producer-Links connected to the HV_Grid-Link *i*;
- The voltage and reactive power set-points for the primary controls $\boldsymbol{PC}_{St}^{HV_i}$ of the Storage-Links connected to the HV_Grid-Link *i*;

- The voltage, reactive power and switch position set-points for the primary $\boldsymbol{PC}_{RPD}^{HV_i}$ and direct controls $\boldsymbol{DiC}_{RPD}^{HV_i}$ of the RPDs included in the HV_Grid-Link *i*;
- The voltage and reactive power set-points for the primary controls $\boldsymbol{PC}_{HVDC}^{HV_i}$ of the HVDC converters included in the HV_Grid-Link *i*; and
- The reactive power set-points for the secondary controls $\boldsymbol{SC}_{NgbHV}^{HV_i}$ of the neighbouring HV_Grid-Links that act as var control variables.
- And the reactive power set-points for the secondary controls $\boldsymbol{SC}_{NgbMV}^{HV_i}$ of the neighbouring MV_Grid-Links;

While respecting:

- The reactive power constraints $\boldsymbol{Cns}_{NgbHV}^{HV_i}$ at the boundary nodes to the neighbouring HV_Grid-Links that act as var constraints.

3.5.2.2 Vertical

The vertical power system axis (Y-axis) comprises all system levels, i.e. HV, MV, LV and CP level. Equation (3.25) compactly represents the control variables and dynamic constraints of the vertical Volt/var chain control.

$$
\begin{aligned}
&\boldsymbol{VvSC}_{Chain}^{Y-axis} = \{ \\
&\boldsymbol{VvSC}^{HV}(\boldsymbol{PC}_{OLTC}^{HV}, \boldsymbol{PC}_{Pr}^{HV}, \boldsymbol{PC}_{St}^{HV}, \boldsymbol{PC}_{RPD}^{HV}, \boldsymbol{DiC}_{RPD}^{HV}, \boldsymbol{PC}_{HVDC}^{HV}, \boldsymbol{SC}_{NgbHV}^{HV}, \\
&\qquad \boldsymbol{SC}_{NgbMV}^{HV};\ \boldsymbol{Cns}_{NgbHV}^{HV}), \\
&\boldsymbol{VvSC}^{MV}(\boldsymbol{PC}_{OLTC}^{MV}, \boldsymbol{PC}_{Pr}^{MV}, \boldsymbol{PC}_{St}^{MV}, \boldsymbol{PC}_{RPD}^{MV}, \boldsymbol{DiC}_{RPD}^{MV}, \boldsymbol{SC}_{NgbLV}^{MV};\ \boldsymbol{Cns}_{NgbHV}^{MV}), \\
&\boldsymbol{VvSC}^{LV}(\boldsymbol{PC}_{OLTC}^{LV}, \boldsymbol{PC}_{Pr}^{LV}, \boldsymbol{PC}_{St}^{LV}, \boldsymbol{PC}_{RPD}^{LV}, \boldsymbol{DiC}_{RPD}^{LV}, \boldsymbol{SC}_{NgbCP}^{LV};\ \boldsymbol{Cns}_{NgbMV}^{LV}), \\
&\boldsymbol{VvSC}^{CP}\left(\boldsymbol{PC}_{Pr}^{CP}, \boldsymbol{PC}_{St}^{CP}, \boldsymbol{PC}_{RPD}^{CP}, \boldsymbol{DiC}_{RPD}^{CP};\ \boldsymbol{Cns}_{NgbLV}^{CP}\right)\}
\end{aligned}
\tag{3.25}
$$

HV level

The $\boldsymbol{VvSC}^{HV}$ calculates in real-time:

- The voltage set-points for the primary controls $\boldsymbol{PC}_{OLTC}^{HV}$ of the power transformers included in the HV_Grid-Link that have OLTC;
- The voltage and reactive power set-points for the primary controls $\boldsymbol{PC}_{Pr}^{HV}$ of the Producer-Links connected to the HV_Grid-Link;
- The voltage and reactive power set-points for the primary controls $\boldsymbol{PC}_{St}^{HV}$ of the Storage-Links connected to the HV_Grid-Link;
- The voltage, reactive power and switch position set-points for the primary $\boldsymbol{PC}_{RPD}^{HV}$ and direct controls $\boldsymbol{DiC}_{RPD}^{HV}$ of the RPDs included in the HV_Grid-Link;

- The voltage and reactive power set-points for the primary controls $\boldsymbol{PC}_{HVDC}^{HV}$ of the HVDC converters included in the HV_Grid-Link;
- The reactive power set-points for the secondary controls $\boldsymbol{SC}_{NgbHV}^{HV}$ of the neighbouring HV_Grid-Links that act as var control variables;
- And the reactive power set-points for the secondary controls $\boldsymbol{SC}_{NgbMV}^{HV}$ of the neighbouring MV_Grid-Links;

While respecting:

- The reactive power constraints $\boldsymbol{Cns}_{NgbHV}^{HV}$ at the boundary nodes to the neighbouring HV_Grid-Links that act as var constraints.

MV level

The $\boldsymbol{VvSC}^{MV}$ calculates in real-time:

- The voltage set-points for the primary controls $\boldsymbol{PC}_{OLTC}^{MV}$ of the supplying transformers and other transformers included in the MV_Grid-Link that have OLTC;
- The voltage and reactive power set-points for the primary controls $\boldsymbol{PC}_{Pr}^{MV}$ of the Producer-Links connected to the MV_Grid-Link;
- The voltage and reactive power set-points for the primary controls $\boldsymbol{PC}_{St}^{MV}$ of the Storage-Links connected to the MV_Grid-Link;
- The voltage, reactive power and switch position set-points for the primary $\boldsymbol{PC}_{RPD}^{MV}$ and direct controls $\boldsymbol{DiC}_{RPD}^{MV}$ of the RPDs included in the MV_Grid-Link;
- And the reactive power set-points for the secondary controls $\boldsymbol{SC}_{NgbLV}^{MV}$ of the neighbouring LV_Grid-Links;

While respecting:

- The reactive power constraints $\boldsymbol{Cns}_{NgbHV}^{MV}$ at the boundary node to the neighbouring HV_Grid-Link.

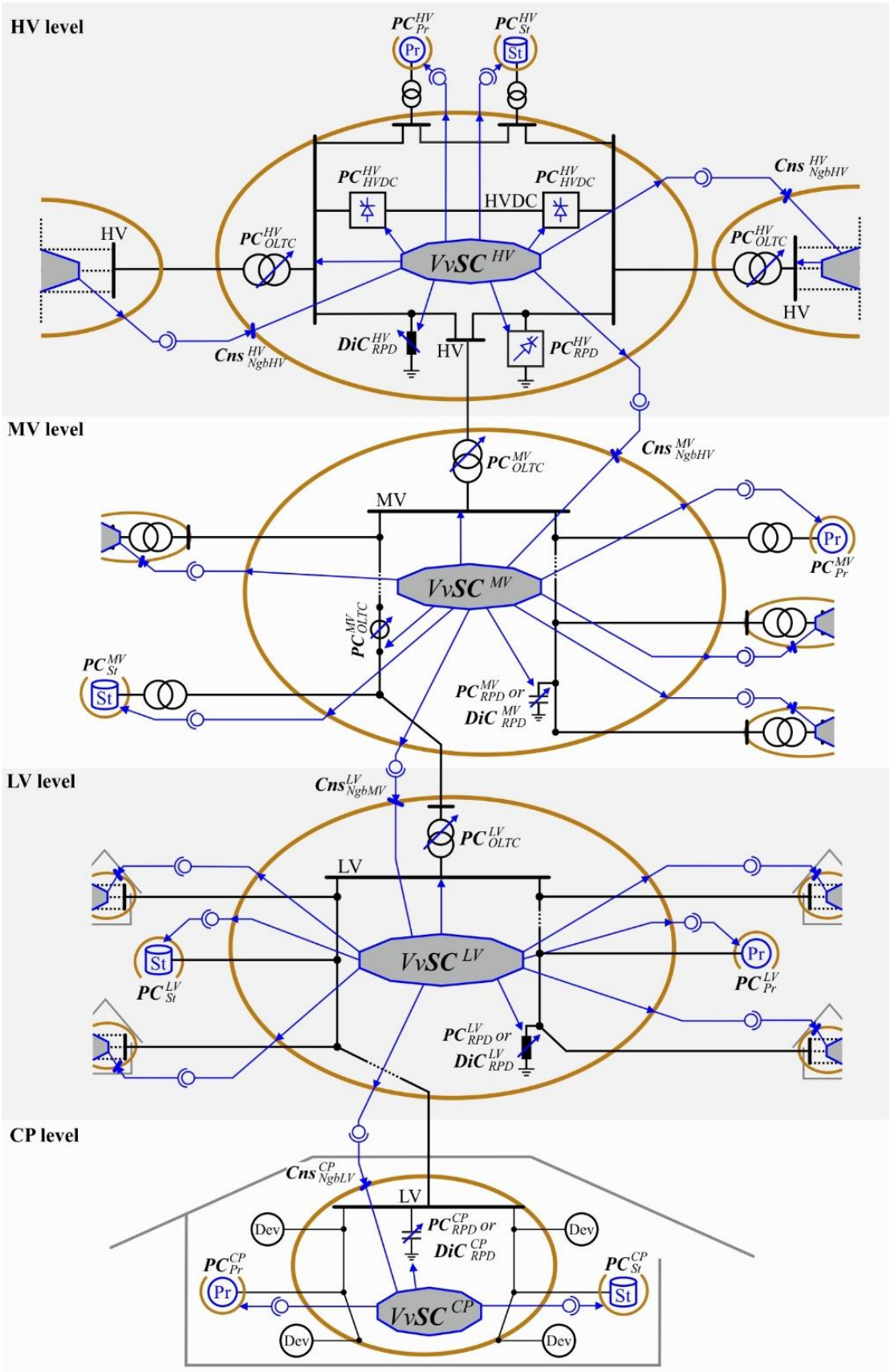

Fig. 3.27 Overview of the generalised Volt/var chain control from the holistic view of the power system.

LV level

The $\boldsymbol{VvSC^{LV}}$ calculates in real-time:

- The voltage set-points for the primary control $\boldsymbol{PC^{LV}_{OLTC}}$ of the distribution transformer included in the LV_Grid-Link (when it possesses an OLTC);
- The voltage and reactive power set-points for the primary controls $\boldsymbol{PC^{LV}_{Pr}}$ of the Producer-Links connected to the LV_Grid-Link;
- The voltage and reactive power set-points for the primary controls $\boldsymbol{PC^{LV}_{St}}$ of the Storage-Links connected to the LV_Grid-Link;
- The voltage, reactive power and switch position set-points for the primary $\boldsymbol{PC^{LV}_{RPD}}$ and direct controls $\boldsymbol{DiC^{LV}_{RPD}}$ of the RPDs included in the LV_Grid-Link;
- And the reactive power set-points for the secondary controls $\boldsymbol{SC^{LV}_{NgbCP}}$ of the neighbouring CP_Grid-Links;

While respecting:

- The reactive power constraints $\boldsymbol{Cns^{LV}_{NgbMV}}$ at the boundary node to the neighbouring MV_Grid-Link.

CP level

The $\boldsymbol{VvSC^{CP}}$ calculates in real-time:

- The voltage and reactive power set-points for the primary controls $\boldsymbol{PC^{CP}_{Pr}}$ of the Producer-Links connected to the CP_Grid-Link;
- The voltage and reactive power set-points for the primary controls $\boldsymbol{PC^{CP}_{St}}$ of the Storage-Links connected to the CP_Grid-Link;
- And the switch position set-points for the primary $\boldsymbol{PC^{CP}_{RPD}}$ and direct controls $\boldsymbol{DiC^{CP}_{RPD}}$ of the RPDs[4] included in the CP_Grid-Link;

While respecting:

- The reactive power constraint $\boldsymbol{Cns^{CP}_{NgbLV}}$ at the boundary node to the neighbouring LV_Grid-Link.

3.5.3 New Volt/var control strategy in LV and CP level

The *LINK*-Architecture stipulates that each Grid-Link operator should mainly use its own control devices to maintain acceptable voltages and power factor. Reactive power support from neighbour elements, such as Grid-, Producer- and Storage-Links, may be incorporated into the

[4] RDPs are commonly used in industrial CPs.

Volt/var control process when the internal resources are insufficient and when their installation is uneconomical. This idea gave rise to a new Volt/var control strategy: The $X(U)$-control.

3.5.3.1 Distributed and concentrated var contributions

The categorisation of the shunt var contribution into the distributed and concentrated type is introduced in (Ilo et al. 2018). Here, the associated effectiveness is analysed in two steps: Firstly, an unloaded single-phase feeder is used to study the fundamental impact of both var contribution types on the system behaviour; Several simplifications are made to enable the analytical investigation in closed-form. Secondly, simulations are conducted on the feeder in loaded conditions to validate the findings.

Definitions

The distributed and concentrated var contributions provoke distinct reactive power flows that differently affect the grid voltages.

Distributed var contributions

Per definition, the distributed var contributions are reactive power contributions at various nodes distributed throughout the length of the feeder, Fig. 3.28.

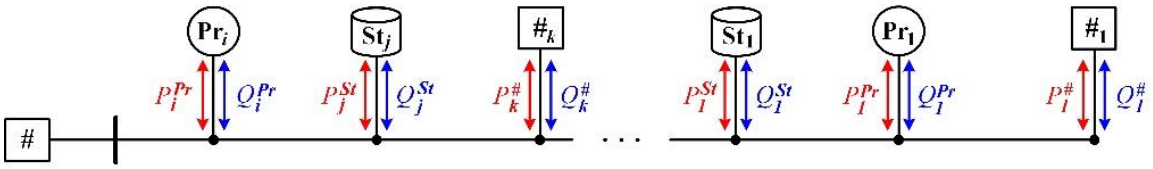

Fig. 3.28 Overview of the distributed var contributions.

Concentrated var contribution

Per definition, the concentrated var contribution is one reactive power contribution close to the end of the feeder, Fig. 3.29.

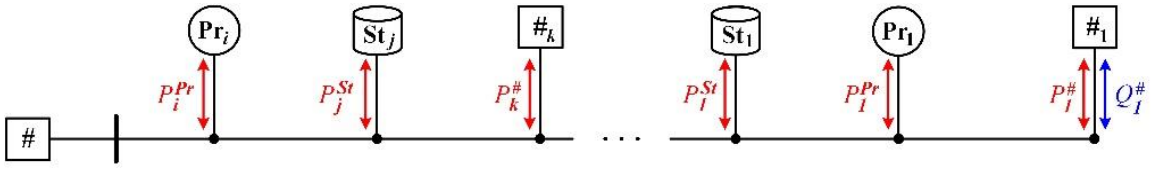

Fig. 3.29 Overview of the concentrated var contribution.

Behaviour of the unloaded feeder

The fundamental impact of both var contribution types on the voltage is analysed using an unloaded feeder, i.e. a feeder through which no active power flows. The feeder consists of N

line segments with the reactance X, $(N+1)$ nodes with the voltage U_i, and N connected CPs, Fig. 3.30 and Fig. 3.31. The active and reactive power losses of the line segments are neglected, and the node voltages are calculated with Equation (3.12) to enable the analysis of the feeder behaviour in closed-form.

Distributed var contributions

The unloaded feeder's behaviour in the presence of distributed var contributions is analysed using the setup shown in Fig. 3.30. The CPs connected at nodes $i \in [1; N]$ provoke distributed var contributions[5] Q^d. The Link-Grid connected at node $N+1$ contributes the reactive power Q^d_{total} required to satisfy the overall reactive power balance.

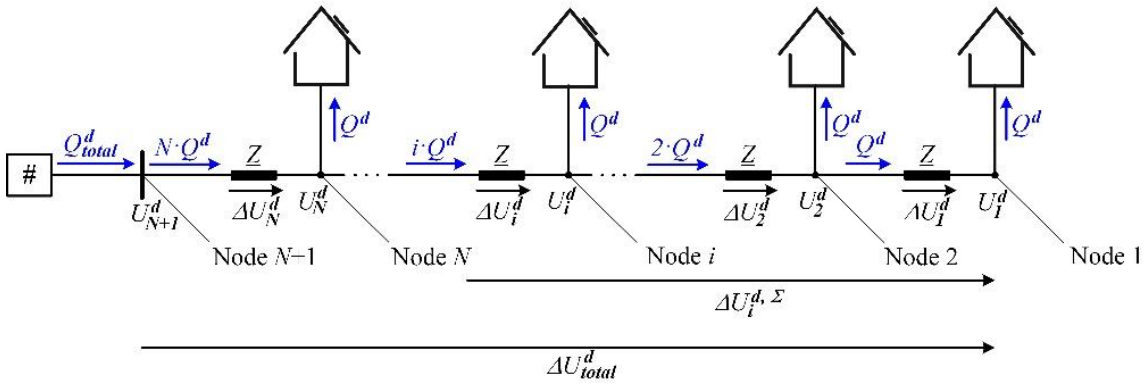

Fig. 3.30 Setup used to analyse the unloaded feeder's behaviour in the presence of distributed var contributions.

The voltage drop ΔU^d_k over the line segment k depends on its reactance, the reactive power flow $(k \cdot Q^d)$ through it, and the voltage of the corresponding node U^d_k, Equation (3.26).

$$\Delta U^d_k = \frac{(k \cdot Q^d) \cdot X}{U^d_k} \tag{3.26}$$

The voltage drop $\Delta U^{d,\Sigma}_k$ between node k and feeder end results from adding up the voltage drops over the intermediate line segments, Equation (3.27).

$$\Delta U^{d,\Sigma}_k = \sum_{i=1}^{k} \Delta U^d_i \tag{3.27}$$

For $k \in [2; N+1]$, the voltage U^d_k at node k is expressed by the voltage U^d_1 at feeder end and the voltage drop in between, Equation (3.28).

$$U_k = U^d_1 + \Delta U^{d,\Sigma}_{k-1} \tag{3.28}$$

[5] Positive algebraic sign for reactive power absorptions.

Combining Equation (3.26) to (3.28) yields the following recursive formula for the total voltage drop ΔU^d_{total} over the feeder with N line segments and distributed var contributions.

$$\Delta U^d_{total} = \Delta U^{d,\Sigma}_N = \frac{Q^d \cdot X}{U^d_1} + \sum_{i=2}^{N} \frac{i \cdot Q^d \cdot X}{U^d_1 + \Delta U^{d,\Sigma}_{i-1}} \tag{3.29}$$

As the losses are neglected, the total reactive power that flows into the feeder is given by Equation (3.30).

$$Q^d_{total} = N \cdot Q^d \tag{3.30}$$

Concentrated var contribution

The behaviour of the unloaded feeder is also analysed for the concentrated var contribution, Fig. 3.31. While the CPs connected at nodes $i \in [1; N]$ do not contribute any reactive power, the RPD connected at node $i = 1$ contributes6 the reactive power Q^c. As in the case with distributed var contributions, the Link-Grid connected at node $N + 1$ satisfies the overall reactive power balance.

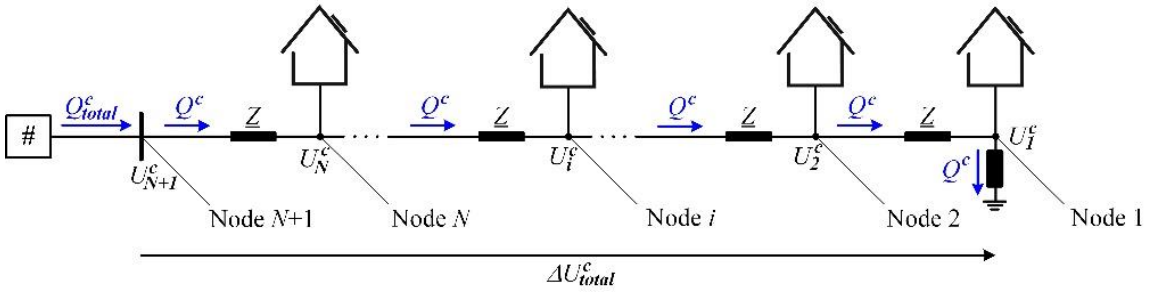

Fig. 3.31 Setup used to analyse the unloaded feeder's behaviour in the presence of one concentrated var contribution.

The total voltage drop ΔU^c_{total} over the feeder depends on the concentrated reactive power contribution Q^c, the feeder reactance $(N \cdot X)$ and the voltage at feeder end, Equation (3.31).

$$\Delta U^c_{total} = \frac{Q^c \cdot (N \cdot X)}{U^c_1} \tag{3.31}$$

The voltage of each node k is given by Equation (3.32).

$$U^c_k = U^c_1 + \frac{Q^c \cdot (k-1) \cdot X}{U^c_1} \tag{3.32}$$

As losses are neglected, the total reactive power that flows into the feeder equals the concentrated reactive power contribution, Equation (3.33).

$$Q^c_{total} = Q^c \tag{3.33}$$

Distributed vs concentrated var contributions

The var contribution types are compared by setting the same voltages at feeder end and feeder beginning as in Equation (3.34).

$$U_1^d = U_1^c = U_1 \tag{3.34a}$$

$$\Delta U_{total}^d = \Delta U_{total}^c = \Delta U_{total}^{d/c} \tag{3.34b}$$

Combining Equation (3.29), (3.31) and (3.34) yields the concentrated reactive power contribution that is required to achieve the same total voltage drop as the distributed ones as a function of the line segment number, Equation (3.35).

$$Q^c = \frac{Q^d}{N} \cdot \left(1 + \sum_{i=2}^{N} i \cdot \frac{U_1}{U_1 + \Delta U_{i-1}^{d,\Sigma}}\right) \tag{3.35}$$

Equations (3.30) to (3.35) allow calculating the total reactive power flowing into the feeder for the distributed and concentrated var contributions and the total voltage drop over the feeder, depending on the line segment number. The values used for the voltage at the feeder end and for the distributed var contributions are given in Table 3.3.

Table 3.3 Parameters used to analyse the behaviour of the unloaded feeder.

Var contribution	U_1	Q^d
Absorption	0.9 p.u.	0.5 kvar
Injection	1.1 p.u.	-0.5 kvar

The resulting curves are shown in Fig. 3.32a and b for exemplary LV feeder parameters[6] and for var absorptions and injections, respectively. The distributed var contributions require more reactive power in total than the concentrated one to achieve the same total voltage drop over the feeder. For example, regarding a feeder with 20 line segments and the var absorption case, the distributed var contributions provoke a total voltage drop and reactive power requirement of 0.076 p.u. and 10 kvar, respectively. Meanwhile, the concentrated var contribution requires only 5.05 kvar to achieve the same total voltage drop.

The unloaded feeder's voltage profiles resulting from the distributed and concentrated var contributions are calculated according to Equations (3.28) and (3.32) for the absorption and injection cases.

[6] The following parameters that correspond to a LV overhead line with a length of 100 m are used: $U_{nom} = 230$ V, $R = 0.03264\ \Omega$, $X = 0.03557\ \Omega$.

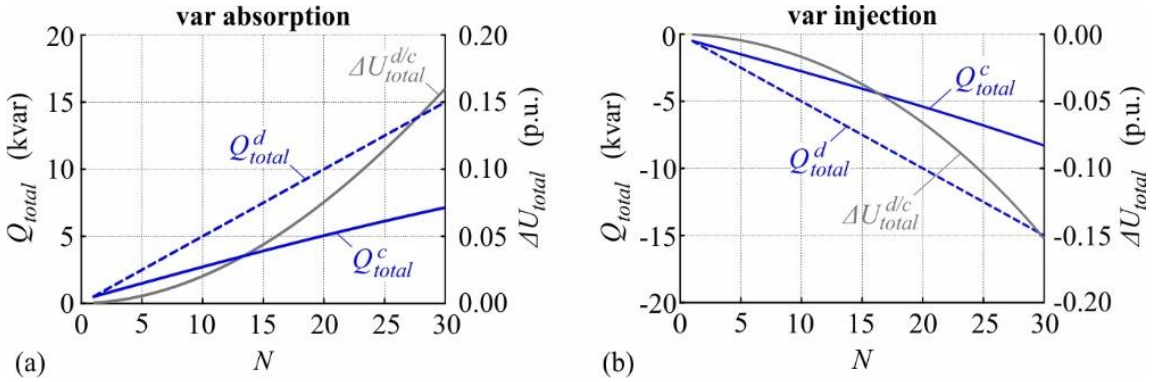

Fig. 3.32 Total voltage drop and reactive power requirement of the unloaded feeder for distributed and concentrated var contributions as functions of the line segment number: (a) Var absorption case; (b) Var injection case.

They are shown in Fig. 3.33 for the feeder with 20 line segments. The voltage profile has a curved shape when the var contributions are distributed, and a straight one when one concentrated var contribution is present. In the var absorption case, the total voltage drop of 0.076 p.u. appears as discussed above. The node voltages U_k^{none} without var contributions are constant along the feeder, as no active and reactive power flows through the line segments.

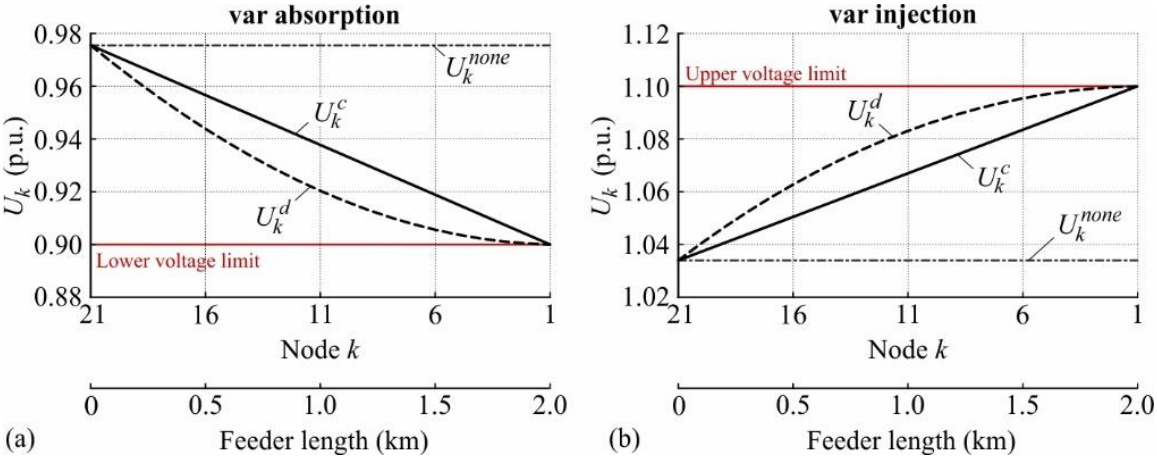

Fig. 3.33 The unloaded feeder's voltage profiles for no, distributed and concentrated var contributions: (a) Var absorption case; (b) Var injection case.

The impact of both var contribution types is calculated by Equation (3.36).

$$U^d_{k,imp} = U^d_k - U^{none}_k \tag{3.36a}$$

$$U^c_{k,imp} = U^c_k - U^{none}_k \tag{3.36b}$$

The curves describing the var contributions' impact have the same shape as the corresponding voltage profiles due to the constant voltages along the feeder without var contributions, Fig. 3.34. The distributed and concentrated var absorptions decrease the node voltages along the

feeder, while the var injections increase them. The largest impact appears at the feeder end in all cases.

The closed-form analysis of the unloaded LV feeder revealed the clear superiority of the concentrated var contribution as follows:

The concentrated var contribution provokes lower reactive power flows at the LV feeder beginning than the distributed ones to achieve the same total voltage drop over the feeder.

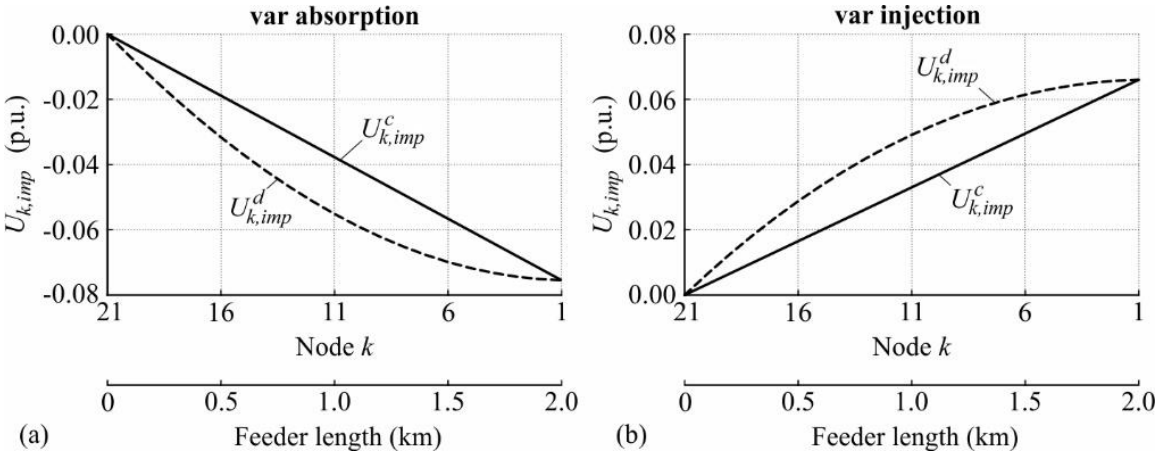

Fig. 3.34 Impact of the distributed and concentrated var contributions on the unloaded feeder's voltage profile: (a) Var absorption case; (b) Var injection case.

Behaviour of the loaded feeder

To verify the previous section's findings under more realistic conditions, the feeder behaviour is also analysed for loaded conditions. Therefore, load flow simulations are conducted for the var absorption and injection cases using the setups[7] shown in Fig. 3.35. Distributed and concentrated var contributions, as well as the case without any var contributions, are simulated.

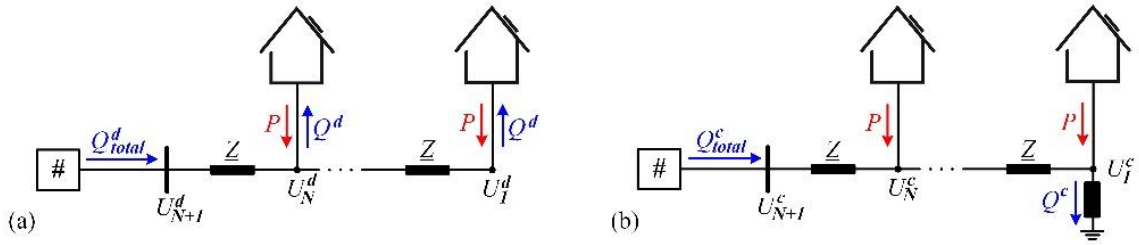

Fig. 3.35 Setup used to analyse the loaded feeder's behaviour in the presence of different var contributions: (a) Distributed; (b) Concentrated.

[7] Positive algebraic sign for active power injection and reactive power absorption.

The values used for the voltage at feeder beginning and for the distributed active and reactive power contributions are given in Table 3.4. In analogy with the analysis of the unloaded feeder, the concentrated reactive power contribution is always set to achieve the same total voltage drop as the distributed one, Equation (3.34b). Both the active and reactive power flows determine the behaviour of the loaded feeder.

Table 3.4 Parameters used to analyse the behaviour of the loaded feeder.

Var contribution	U_{N+1}	Q^d	P
Absorption	1.0 p.u.	0.5 kvar	0.7 kW
Injection	1.0 p.u.	-0.5 kvar	-0.7 kW

The impacts of both var contribution types are isolated according to Equations (3.37) and (3.38) to study their effects on the feeder behaviour.

$$\Delta U_{imp}^{d/c} = \Delta U_{total}^{d/c} - \Delta U_{total}^{none} \tag{3.37}$$

$$Q_{imp}^{d} = Q_{total}^{d} - Q_{total}^{none} \tag{3.38a}$$

$$Q_{imp}^{c} = Q_{total}^{c} - Q_{total}^{none} \tag{3.38b}$$

Where ΔU_{total}^{none} and Q_{total}^{none} are the total voltage drop and reactive power requirement at feeder beginning, respectively, when no reactive power is contributed by any element connected along the feeder. The corresponding curves are shown in Fig. 3.36a and b for the var absorption and injection cases, respectively.

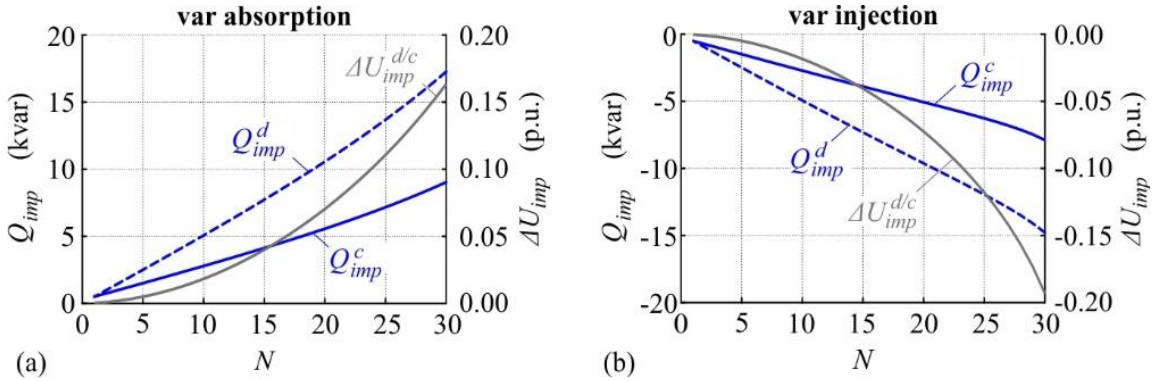

Fig. 3.36 Impact of the distributed and concentrated var contributions on the total voltage drop and reactive power requirement of the loaded feeder as functions of the line segment number: (a) Var absorption case; (b) Var injection case.

Fundamentally, the same behaviour is observed as for the unloaded feeder (see Fig. 3.32). The distributed var contributions always require more reactive power than the concentrated one, especially for high line segment numbers.

The loaded feeder's voltage profiles for no, distributed and concentrated var contributions are shown in Fig. 3.37a and b for the var absorption and injection case, respectively. The cases without any var contributions along the feeder clearly show the impact of the active power flows. The injections and absorptions of active power increase and decrease the node voltages, respectively. var contributions allow mitigating the voltage change caused by the active power flows. In comparison, the distributed var contributions cause relatively flat voltage profiles so that the maximum and minimum voltages appear at the feeder end for the var absorption and injection cases, respectively. Meanwhile, the concentrated var contribution provokes more curved profiles, wherein the maximum and minimum voltages appear somewhere along the feeder.

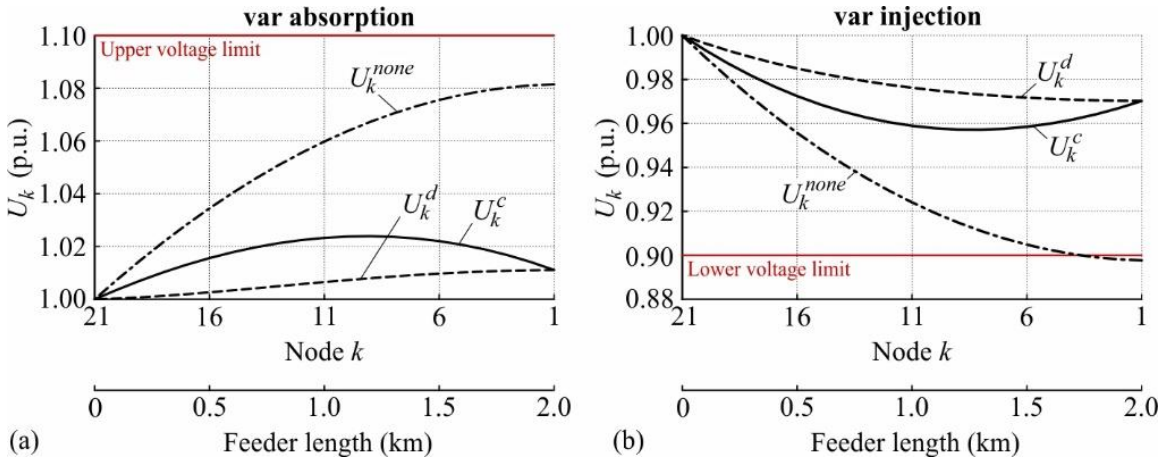

Fig. 3.37 The loaded feeder's voltage profile for no, distributed and concentrated var contributions: (a) Var absorption case; (b) Var injection case.

The curves describing the impact of the distributed and concentrated var contributions on the loaded feeder's voltage profile are quite similar to those of the unloaded feeder, Fig. 3.38.

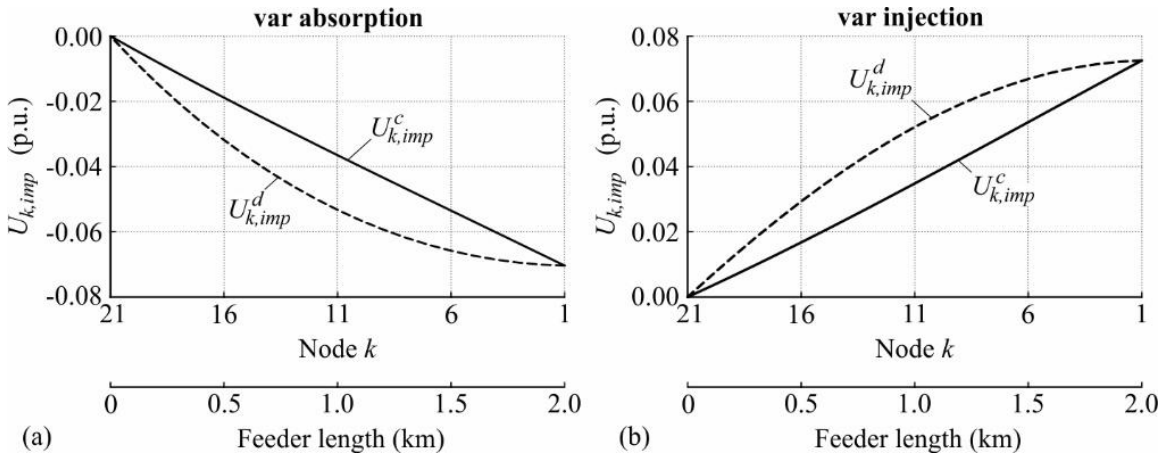

Fig. 3.38 Impact of the distributed and concentrated var contributions on the loaded feeder's voltage profile: (a) Var absorption case; (b) Var injection case.

The simulations of the loaded feeder have verified the conclusions drawn from the closed-form analysis of the unloaded feeder.

3.5.3.2 *X*(*U*)-control

The term '*X*(*U*)' refers to a voltage-dependent reactance that adjusts itself to inject or absorb the reactive power amount required to maintain acceptable voltages in LV level. In contrast to the *L*(*U*)-control (Ilo and Schultis 2019), which can only absorb reactive power, the *X*(*U*)-control is capable of absorbing and injecting reactive power to mitigate violations of the upper and lower voltage limits. Fig. 3.39 illustrates the concept of the *X*(*U*)-control: one controllable shunt-connected RPD is connected close to the end of each violating feeder, i.e. each feeder that may violate the BVLs of thereto connected elements (mainly customer plants). More than one RPD may be necessary when the feeder is branched.

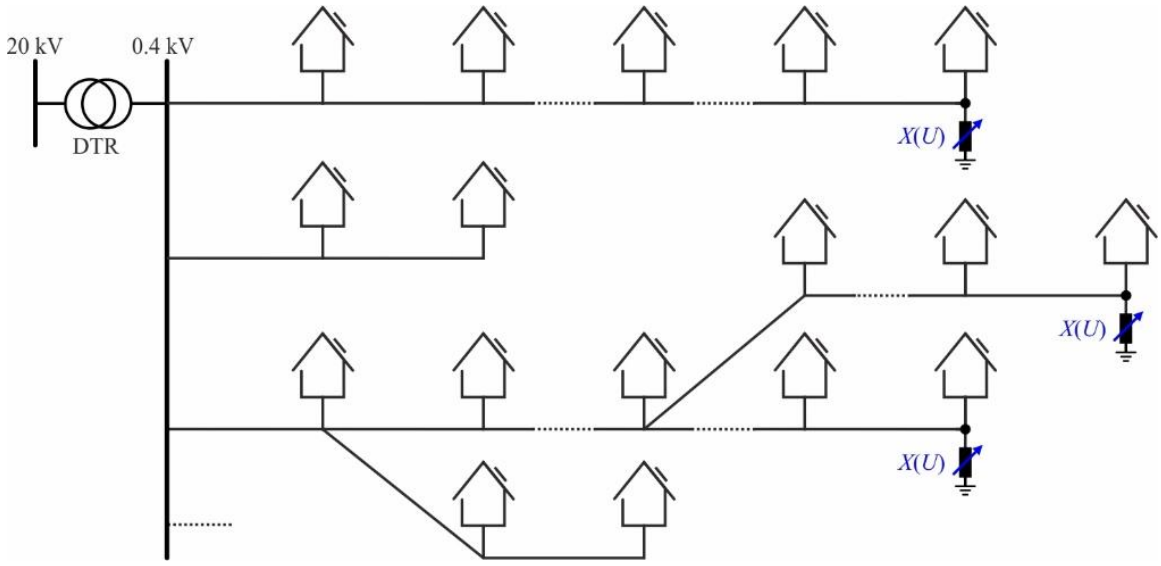

Fig. 3.39 Illustration of the *X*(*U*)-control strategy.

Mechanically switched capacitors and reactors, as well as static var compensators may be used for this shunt reactance insertion (see Table 3.2). As an alternative, the *X*(*U*)-control may also be realised by shunt current injections, e.g. by using STATCOMs. Two types of *X*(*U*)-control are generally distinguished: Primary and local (see §3.1.5). In any case, its use resolves the intertwining of the LV grid and CP operation provoked by the *Q*(*U*)-control (see §3.4 and (Ilo and Schultis 2019)).

X(*U*) primary control

Fig. 3.40 shows an overview of the Volt/var chain control in LV and CP level when the *X*(*U*) primary control is used. The $\boldsymbol{VvSC^{LV}}$ adapts the voltage set-points of the *X*(*U*)-control devices'

primary controls and the reactive power set-points to be respected by the $\boldsymbol{VvSC}^{CP}$ of the connected CPs. The $\boldsymbol{VvSC}^{CP}$ adapts the primary control settings of the PV inverter to meet the constraint at the BLiN$^{\text{LV-CP}}$.

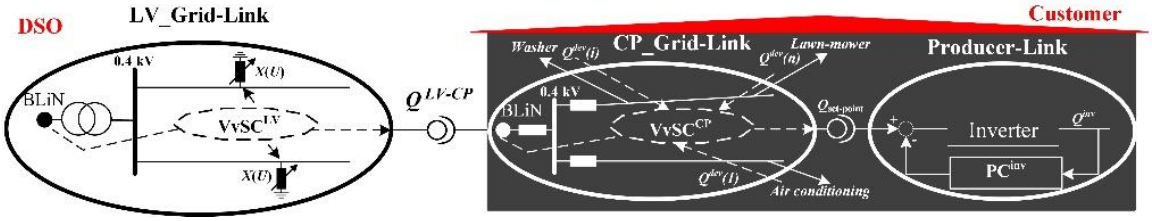

Fig. 3.40 Overview of the Volt/var chain control in LV and CP level when $X(U)$ primary control is used.

$X(U)$ local control

The $X(U)$ local control with fixed control parameters may be used as an alternative to the combination of primary and secondary controls in LV level. In this case, the RPDs inject or absorb reactive power to maintain their terminal voltages within a predefined band, e.g. between 0.91 and 1.09 p.u.

3.5.3.3 CP_Q-Autarky

CP_Q-Autarky is a special case of the $\boldsymbol{VvSC}$ realised at the CP level where the reactive power constraint between LV and CP level is set to zero. This means the concept of load compensation, which is traditionally used at the device level or in industrial CPs (see §3.1.3.1), is applied to all types of CPs, including residential ones. The reactive power needed for the functioning of rotating devices such as washing machines, lawnmowers, and air conditioning units is compensated directly at the CP level.

> ***Q*-Autarkic** or ***Q*-self-sufficient** customer plants produce the required reactive power within their own premises. Per definition, they do not exchange any reactive power with the LV_Grid-Link. In this case, the LV_Grid-Link serves prosumers and consumers by a factor of unity.

To realise CP_Q-Autarky, the $\boldsymbol{VvSC}^{CP}$ adapts the control settings of the RPDs, Producer- and Storage-Links connected at the CP level to eliminate the reactive power flow through the LV-CP boundary node at all times, Fig. 3.41. The compact representation of the control variables and dynamic constraints of Q-Autarkic CPs is given in Equation (3.39).

$$\boldsymbol{VvSC}^{CP}\left(\boldsymbol{PC}_{Pr}^{CP},\ \boldsymbol{PC}_{St}^{CP},\ \boldsymbol{PC}_{RPD}^{CP},\boldsymbol{DiC}_{RPD}^{CP};\ \boldsymbol{Cns}_{NgbLV}^{CP} = 0\ \text{kvar}\right) \tag{3.39}$$

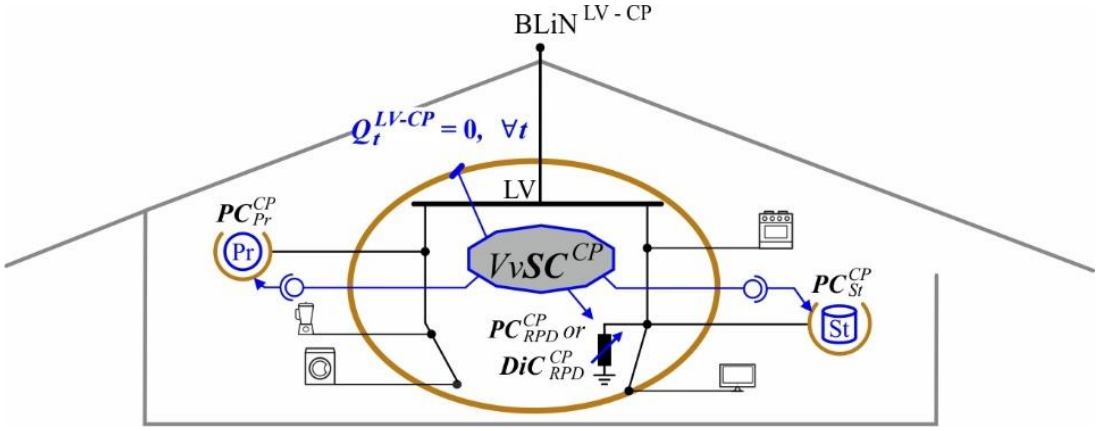

Fig. 3.41 Illustration of the CP_*Q*-Autarky.

3.5.3.4 *X*(*U*) and CP_*Q*-Autarky control ensemble

The presented Volt/var control strategies may be combined. Fig. 3.42 shows the reactive power flows through an LV feeder when no control is used and when *X*(*U*)-control and its combination with CP_*Q*-Autarky are applied.

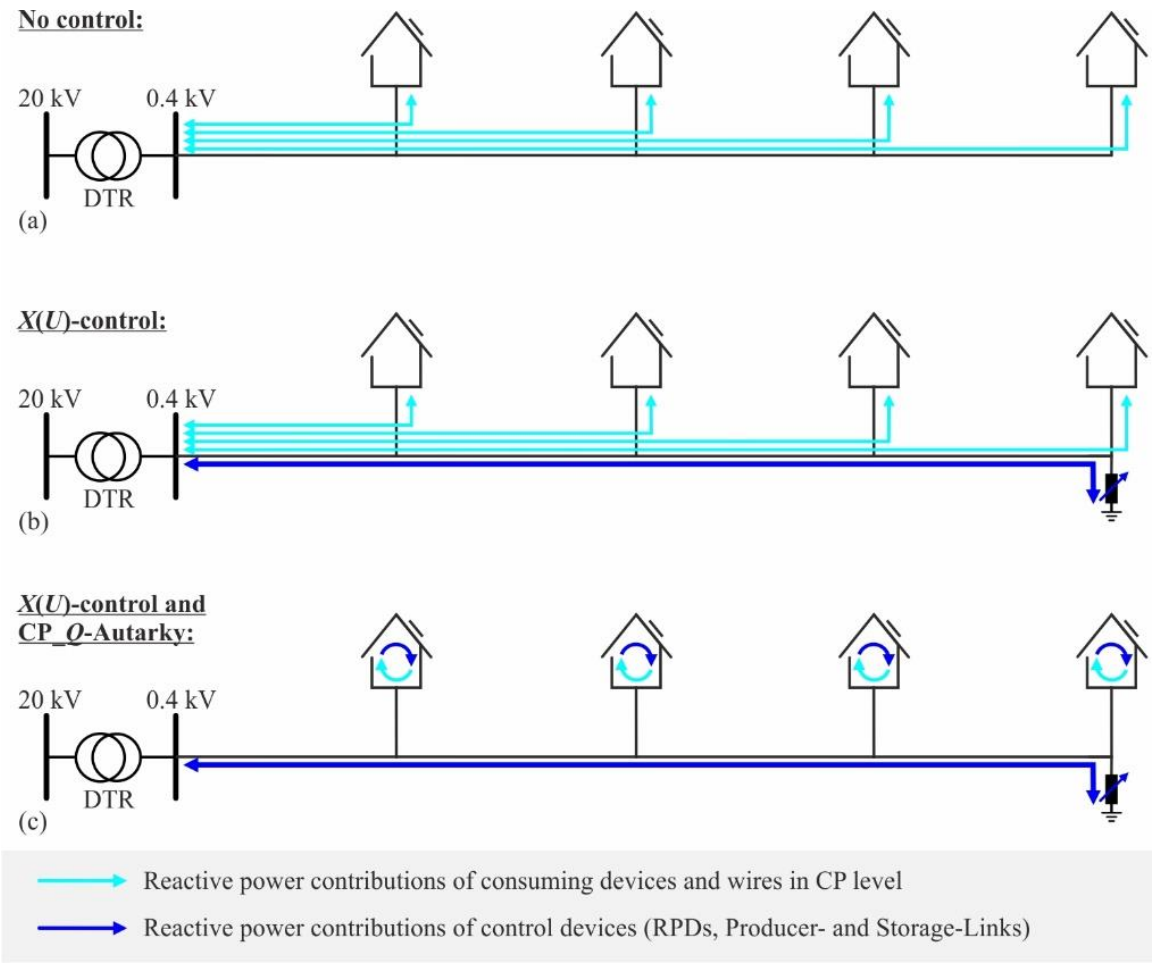

Fig. 3.42 Reactive power flows through an LV feeder for different Volt/var control arrangements: (a) No control; (b) *X*(*U*)-control; (c) *X*(*U*)-control and CP_*Q*-Autarky.

The cyan coloured arrows represent the reactive power contributions of the consuming devices and the wires at the CP level. While the consuming devices contribute reactive power when used, the wires produce and consume reactive power depending on the voltage and the power flowing through them. The reactive power contributions of the control devices are shown in blue colour.

When no control is applied, the CPs exchange reactive power with the LV_Link-Grid, provoking distributed reactive power contributions along the feeder, Fig. 3.42a. The use of $X(U)$-control provokes – in addition to the distributed CP contributions – one concentrated reactive power contribution close to the end of the LV feeder, Fig. 3.42b. The combination of $X(U)$-control with CP_Q-Autarky eliminates the distributed reactive power contributions, Fig. 3.42c.

3.6 Link-Grids' Volt/var behaviour using different control strategies

This section systematically analyses the MV, LV and CP_Link-Grids' behaviour using different Volt/var control strategies and for the case without any Volt/var control. Different real Link-Grids are calculated for the recently emerging strategies, i.e. cos$\varphi(P)$- and $Q(U)$-control of PV inverters and OLTC in distribution substation, and for the newly introduced ones, i.e. $X(U)$-control and its combination with CP_Q-Autarky. The combination of the OLTC in the distribution substation with CP_Q-Autarky is also considered. The focus of this analysis is set on Volt/var controls applied at the LV and CP levels; Volt/var controls of producers connected at the MV level are not considered.

3.6.1 Modelling on the vertical axis

The *LINK*-Architecture allows for the systematic analysis of the vertical power system axis. Each Link level may be separately simulated using the extended lumped grid model (see §3.5.1.3) for the neighbour elements. This approach is illustrated in Fig. 3.43 for the MV, LV, and CP levels. It follows a bottom-up approach with three steps:

1. The first step is to define the CP models, i.e. the structures of the CP_Link-Grids; The $P_t(U_t)$- and $Q_t(U_t)$-behaviour of the connected consuming devices, storages and producers; And the upper and lower LV-CP boundary voltage limits. These specifications allow analysing the CP level and calculating the extended lumped CP models according to the procedure described in §3.5.1.3;
2. The next step is to analyse the LV level by representing the connected CPs by their extended lumped models and by specifying the behaviour and boundary voltage limits

of producers and storages directly connected at the LV level. Again, the procedure described in §3.5.1.3 is used to calculate the extended lumped LV_Link-Grid models.

3. Finally, the MV level is analysed by representing the connected LV and CP_Link-Grids by their extended lumped models and by specifying the behaviour and boundary voltage limits of the producers and storages directly connected at the MV level. The extended lumped MV_Link-Grid model can be calculated and provided for the analysis of the HV level.

The daily behaviour of different Link-Grids is calculated for each system level. The following sections §3.6.2 to §3.6.4 describe the analysis of selected Link-Grids in detail, while the results of all Link-Grids are catalogued in §A.1.

3.6.2 Customer plant level

Customer plants comprise the CP_Link-Grid and all thereto connected consuming devices, producers and storages. They are typically unbalanced due to the connection of single-phase devices. The CP_Link-Grid consists of the underpinned wires connecting the house's boundary node to the switches and sockets. The latter ones are the connection points for all consuming devices, electricity producers and storages. CPs are commonly categorised into residential, commercial and industrial ones due to their similar consumption patterns. While residential CPs are always connected at the LV level, commercial and industrial CPs may also be connected at the MV level.

Traditionally, the modelling of single residential CPs was not of particular interest as load flow studies were performed only at the HV and MV level. Lumped models represented the LV grids. These lumped models are usually developed by estimating the average behaviour of many CPs without considering the grid at the LV and CP level (CIGRE 2014b). In recent years, the analysis of the LV level became more important due to the integration of distributed generation, electric vehicle chargers, etc. Since then, much effort was devoted to develop lumped models of single residential CPs based on load profiles (McKenna and Thomson 2016; Pflugradt and Muntwyler 2017) and ZIP models (Bokhari et al. 2014; Collin et al. 2014). The load profiles specify the time-dependency of the power contributions at nominal LV-CP boundary voltage. They mainly depend on the behaviour of occupants and thermostatic controls that switch on and off the consuming devices and on the weather conditions that determine the production of PV systems. Meanwhile, the ZIP models specify the voltage-dependency of the power contributions for each instant of time (see §3.1.2.4). They mainly depend on the load composition, which naturally varies over time.

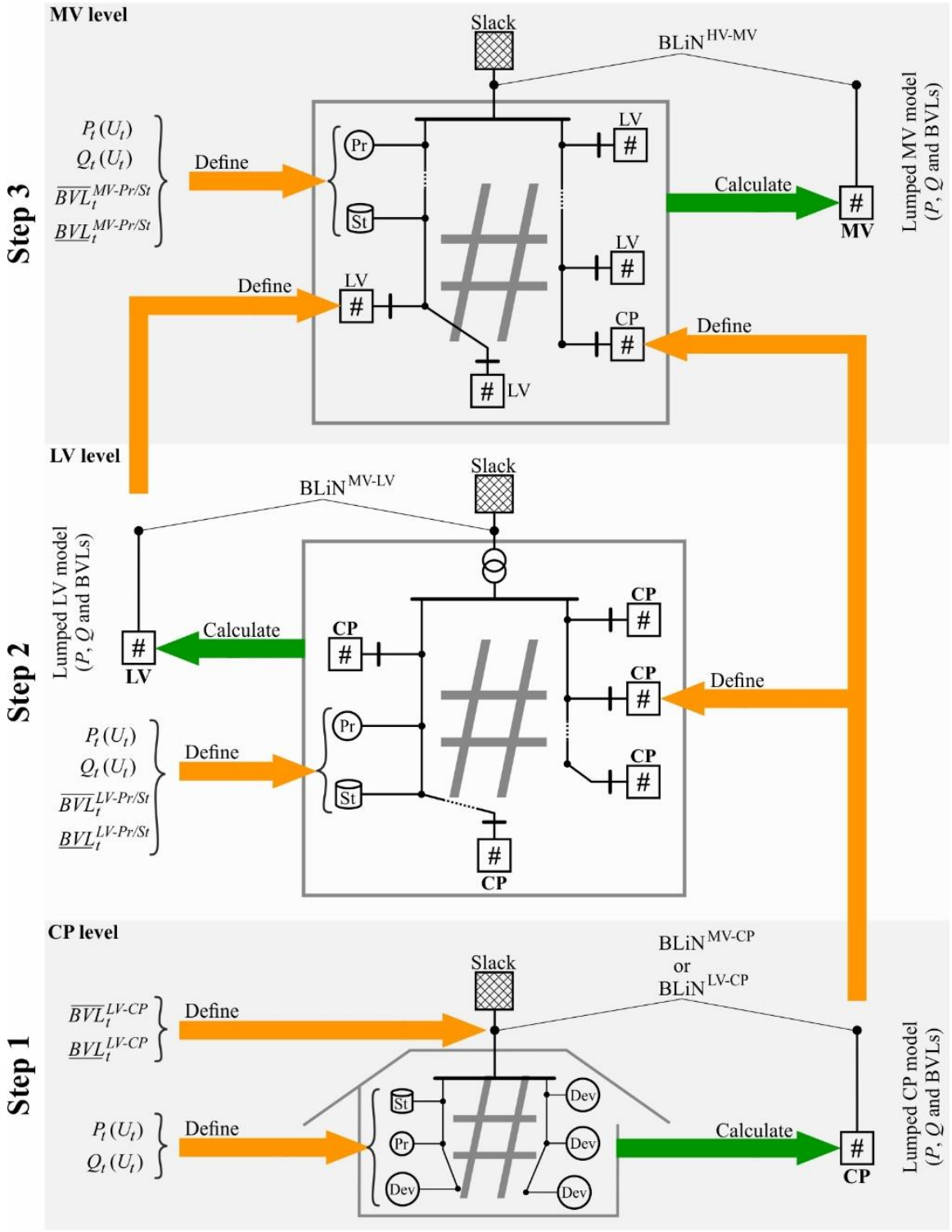

Fig. 3.43 Overview of the systematic modelling of the Link-Grids in the vertical axis.

3.6.2.1 Model specification

The model of residential CPs located in a rural region is specified for two different types of load profiles: Spiky and smoothed. The spiky one considers the impact of clouds on the PV production and reflects the discrete behaviour of the consuming devices and storages within a single CP. Meanwhile, the smoothed one represents the average behaviour of the consuming

devices and storages located in many CPs. In both cases, the unbalance and grid at the CP level are neglected, leading to the simplified CP structure shown in Fig. 3.44a. It consists of three components: The equivalent consuming device model (Dev.-model), the producer model (Pr.-model), and the storage model (St.-model), all directly connected to the LV-CP boundary node, $BLiN^{LV\text{-}CP}$. The behaviour of the residential CP is analysed for the spiky and smoothed load profiles in §3.6.2.2.

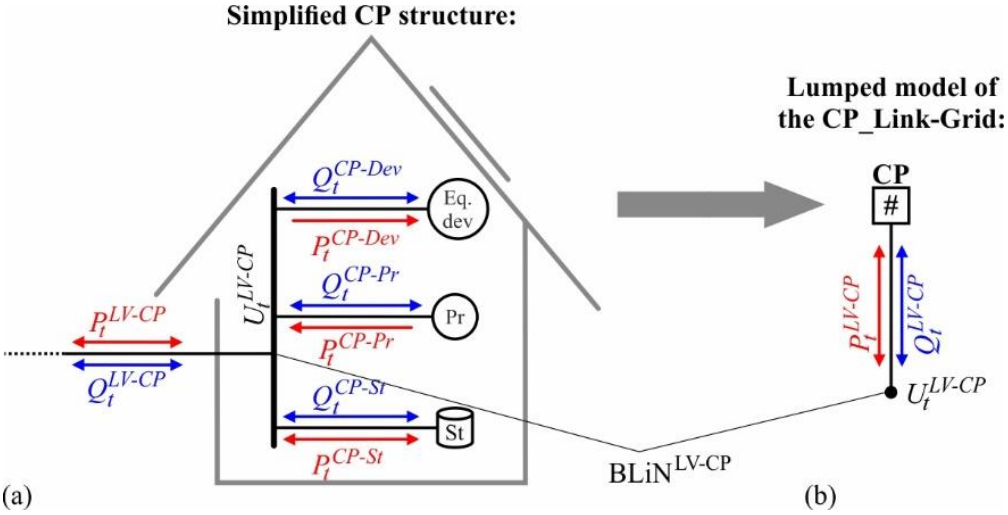

Fig. 3.44 Residential customer plants: (a) Simplified CP structure; (b) Lumped CP_Link-Grid model.

Model components

The model components are specified to represent rural residential CPs with a PV system, EV charger and modern consuming devices. The spiky load profiles of the Dev.- and St.-model are synthesised with the Load Profile Generator (LPG 2020), which models the behaviour of occupants and thermostatic controls.

Equivalent consuming device model

The Dev.-model represents all consuming devices simultaneously connected to the CP_Link-Grid, including Switch-Mode Power Supply (SMPS), resistive, and lighting devices as well as motors, Equation (3.40).

$$P_t^{CP-Dev}(U_t^{LV-CP}) = \sum_{\forall i} P_{i,t}^{CP-Dev}(U_t^{LV-CP}) \tag{3.40a}$$

$$Q_t^{CP-Dev}(U_t^{LV-CP}) = \sum_{\forall i} Q_{i,t}^{CP-Dev}(U_t^{LV-CP}) \tag{3.40b}$$

Where $P_{i,t}^{CP-Dev}$, $Q_{i,t}^{CP-Dev}$ are the power contributions of the consuming device i. The power contributions of the Dev.-model are specified using load profiles and ZIP coefficients for

modern residential CPs, Equation (3.41). While time-invariant ZIP coefficients from (Bokhari et al. 2014) are used for the case with spiky load profiles, time-variant ones from (Schultis 2019) are used for the case with smooth ones.

$$\frac{P_t^{CP-Dev}}{P_{nom,t}^{CP-Dev}} = C^{Z,P} \cdot \left(\frac{U_t^{LV-CP}}{U_{nom}^{LV}}\right)^2 + C^{I,P} \cdot \left(\frac{U_t^{LV-CP}}{U_{nom}^{LV}}\right) + C^{P,P} \tag{3.41a}$$

$$\frac{Q_t^{CP-Dev}}{Q_{nom,t}^{CP-Dev}} = C^{Z,Q} \cdot \left(\frac{U_t^{LV-CP}}{U_{nom}^{LV}}\right)^2 + C^{I,Q} \cdot \left(\frac{U_t^{LV-CP}}{U_{nom}^{LV}}\right) + C^{P,Q} \tag{3.41b}$$

Both the spiky and smoothed load profiles are shown in Fig. 3.45.

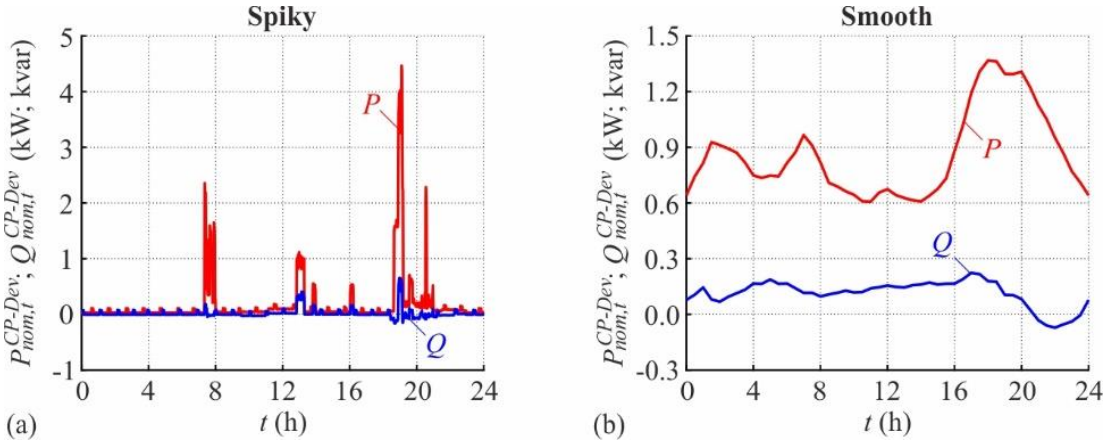

Fig. 3.45 Load profiles of the Dev.-model of the rural residential CP: (a) Spiky; (b) Smoothed.

The spiky profiles have higher peaks than the smoothed ones but provoke lower daily energy consumptions. While the spiky profiles have consumption peaks of 4.46 kW and 0.65 kvar, the smoothed ones reach maximum consumption values of 1.37 kW and 0.22 kvar. The result is a daily energy consumption of 4.25 and 20.75 kWh, respectively, for the spiky and smoothed load profiles. The maximal reactive power production amounts to 0.16 kvar in Fig. 3.45a and to 0.07 kvar in Fig. 3.45b. The capacitive behaviour in the evening results from the use of LED lamps and other modern appliances.

Producer model

The Pr.-model represents the PV system with a module rating of 5 kW and an inverter rating of 5.56 kVA. Its active power production is determined by the weather conditions and is independent of the LV-CP boundary voltage (Wang et al. 2008). Consequently, the production profile alone is sufficient to express the active power part of the Pr.-model, Equation (3.42). It is characterised by a peak around midday, Fig. 3.46. Clouds reduce the power production, leading to a spiky production profile.

$$P_t^{CP-Pr} = P_{nom,t}^{CP-Pr} \tag{3.42}$$

The spiky and smoothed load profiles implicate an energy production of 23.14 and 31.37 kWh, respectively. The reactive power contribution of the Pr.-model is determined by the applied Volt/var control strategy.

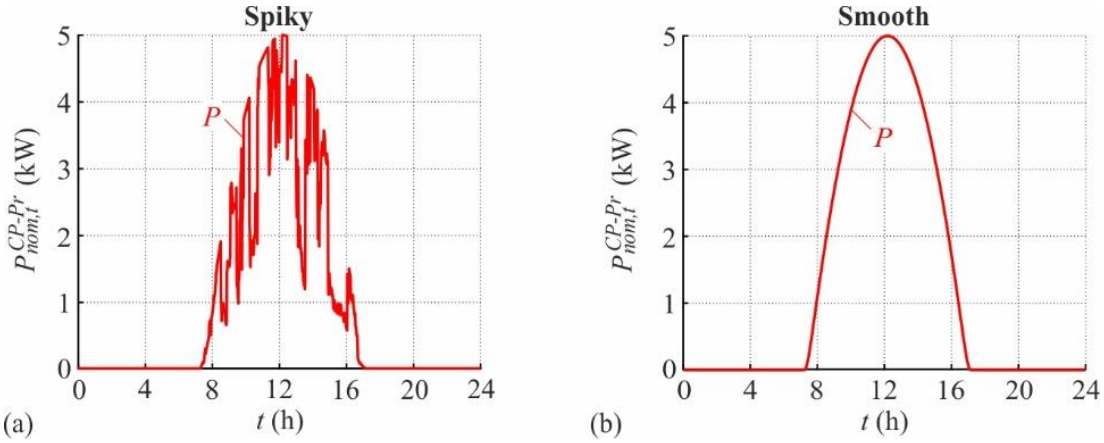

Fig. 3.46 Load profiles of the Pr.-model of the rural residential CP: (a) Time-discontinuous; (b) Time-continuous.

Fig. 3.47 shows the used cos$\varphi(P)$- and $Q(U)$-control characteristics. The impact of the $Q(U)$-parametrisation on the behaviour of low voltage grids is discussed in §A.2.1. The Pr.-model of a Q-Autarkic CP fully compensates the LV-CP reactive power exchange.

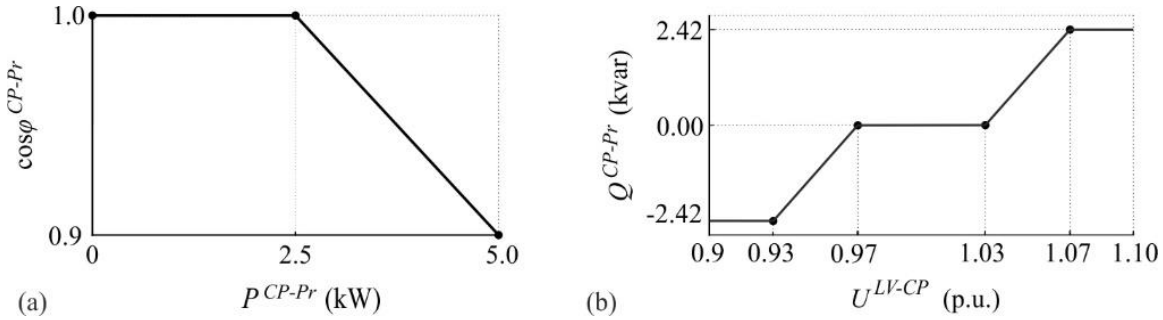

Fig. 3.47 Different control characteristics of the Pr.-model of the rural residential CP: (a) cos$\varphi(P)$; (b) $Q(U)$.

Storage model

The St.-model represents the battery of the EV that is connected through the EV charger.

$$\frac{P_t^{CP-St}}{P_{nom,t}^{CP-St}} = -0.02 \cdot \left(\frac{U_t^{LV-CP}}{U_{nom}^{LV}}\right)^2 + 0.03 \cdot \left(\frac{U_t^{LV-CP}}{U_{nom}^{LV}}\right) + 0.99 \tag{3.43a}$$

$$Q_t^{CP-St}(U_t) = 0 \tag{3.43b}$$

By analogy with the Dev.-model, the active power absorbed by the charger is specified using ZIP models from (Shukla et al. 2017) and load profiles from (Aunedi et al. 2015), Equation (3.43).

Fig. 3.48 shows the spiky and smoothed load profiles of the St.-model. Residential EV chargers typically draw 3.7 kW at nominal LV-CP boundary voltage, Fig. 3.48a. The charging process of EVs is initiated by the user and terminated when the battery is fully charged or the user unplugs the EV prematurely. Due to the short charging time in the given case, only 1.85 kWh are consumed. The smoothed load profile has a maximum value of 0.30 kW and leads to the daily energy consumption of 3.51 kWh, Fig. 3.48b.

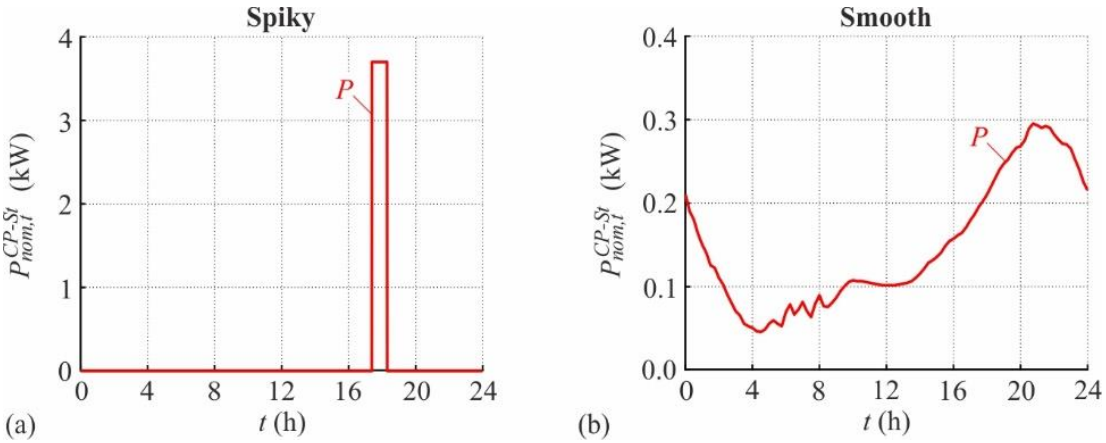

Fig. 3.48 Load profiles of the St.-model of the rural residential CP: (a) Spiky; (b) Smoothed.

Lumped model equations

The CP_Link-Grid modelling as a single node allows specifying its lumped model, which is shown in Fig. 3.44b, without involving numerical simulations. The corresponding model equations represent the aggregate behaviour of all model components, Equation (3.44).

$$P_t^{LV-CP} = P_t^{CP-Dev} + P_t^{CP-Pr} + P_t^{CP-St} \quad (3.44a)$$

$$Q_t^{LV-CP} = Q_t^{CP-Dev} + Q_t^{CP-Pr} + Q_t^{CP-St} \quad (3.44b)$$

The LV-CP boundary voltage limits are set to ±10% around the nominal value to reflect the Grid Code requirements (EN 50160:2010), Equation (3.45).

$$\overline{BVL}_t^{LV-CP} = 1.10 \text{ p.u.} \quad \forall t \quad (3.45a)$$

$$\underline{BVL}_t^{LV-CP} = 0.90 \text{ p.u.} \quad \forall t \quad (3.45b)$$

3.6.2.2 Behaviour of CP_Link-Grid

The CP_Link-Grid behaviour is discussed for the case without any Volt/var controlled PV system, for cos$\varphi(P)$- and $Q(U)$-control, and for CP_Q-Autarky. Both types of load profiles, i.e. spiky and smoothed, are considered separately.

Spiky load profiles

Without any Volt/var controlled PV system

Constant boundary voltage limits and a strong time-dependency and weak voltage-dependency of the LV-CP active and reactive power exchanges characterise the daily behaviour of the rural residential CP_Link-Grid with spiky load profiles and without any Volt/var control, Fig. 3.49.

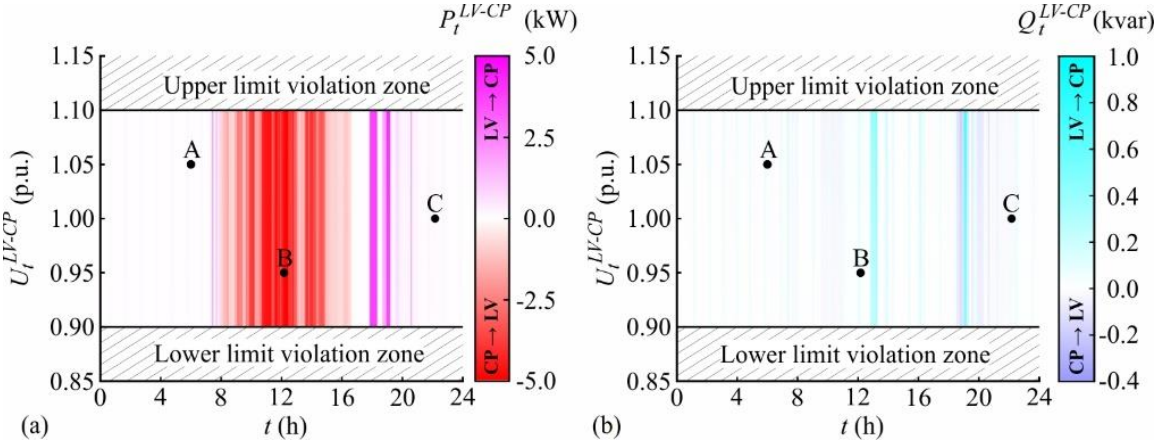

Fig. 3.49 Daily behaviour of the rural residential CP_Link-Grid with spiky load profiles and without any Volt/var control for various voltages at the LV-CP boundary node: (a) LV-CP active power exchange; (b) LV-CP reactive power exchange.

The CP mainly consumes active power before 8:00 and after 17:00 and produces it in between. Meanwhile, no clear trend is observed for the reactive power flow direction: It alternates during the day. Before 7:20 and after 21:00, the thermostatic controls that switch on and off the consuming devices dominate the CP power contributions. In cases A and C, the CP consumes 28.60 and 79.17 W and produces 4.37 and 13.07 var, respectively. The active power consumption increases considerably when the occupants actively use consuming devices, i.e. from 7:20 to 8:00 and 17:00 to 21:00. Two active power consumption peaks appear around 18:00 and 19:00. While the former results from EV charging, the latter is provoked by the use of household appliances. Between 8:00 and 17:00, the PV system produces electricity. It turns the consumer into a producer, leading to an active power injection of 4.90 kW and reactive power absorption of 0.02 kvar in case B.

With Volt/var controlled PV system

The Volt/var control strategies do not affect the LV-CP active power exchange because the losses of the PV inverter and the grid at the CP level are not modelled. Therefore, the investigation focus is set on the reactive power exchange. All control strategies significantly modify the customer plant's reactive power behaviour, while the boundary voltage limits are traditionally considered constant, Fig. 3.50.

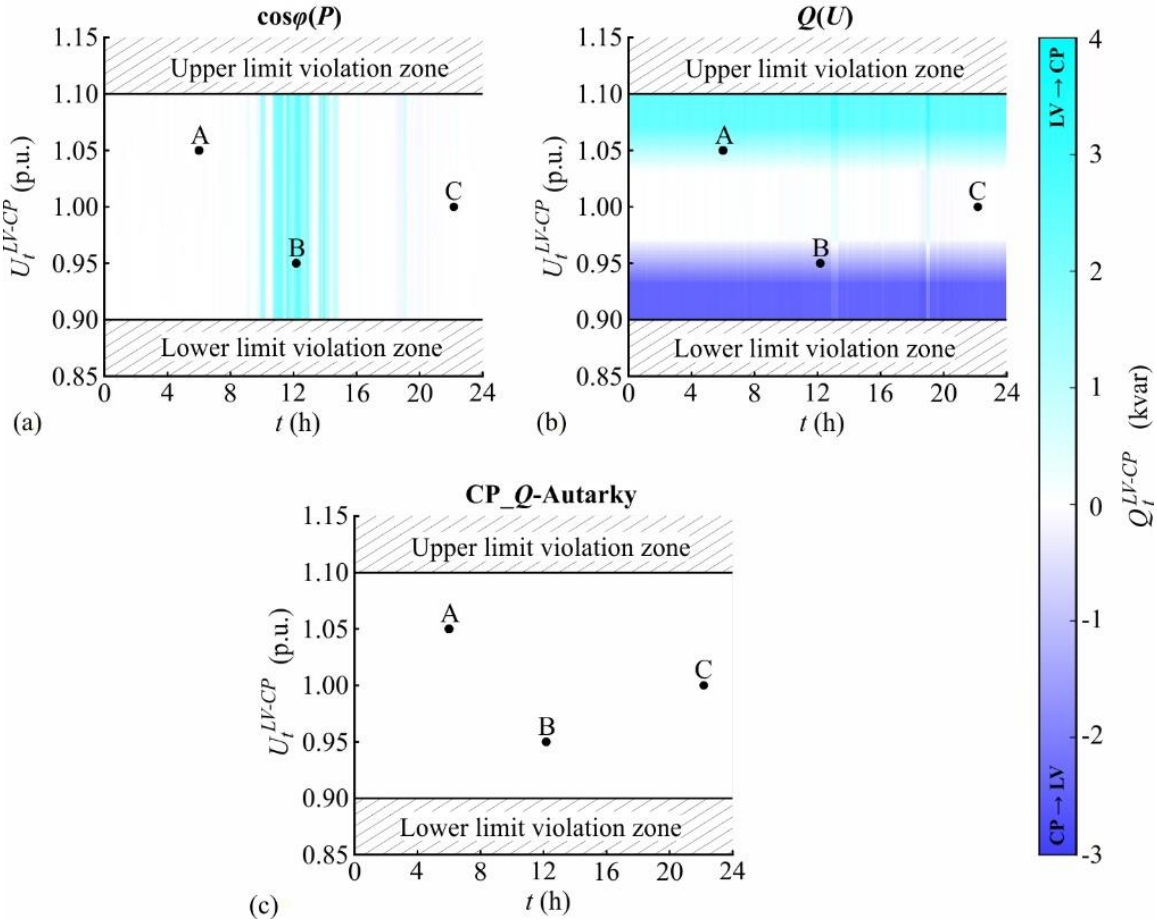

Fig. 3.50 Daily LV-CP reactive power exchange of the rural residential CP_Link-Grid with spiky load profiles for various voltages at the LV-CP boundary node and different control strategies: (a) cos$\varphi(P)$; (b) $Q(U)$; (c) CP_Q-Autarky.

The cos$\varphi(P)$-controlled PV system is shown in Fig. 3.50a.

The cos$\varphi(P)$ control strategy provokes a strong time-dependency of the reactive power exchange between the LV grid and CPs.

The fluctuating radiation leads to intermittent reactive power contributions. Independently of the boundary voltage, the PV inverter consumes reactive power conform the cos$\varphi(P)$ characteristic (Fig. 3.47a) when enough active power is produced, i.e. between 9:05 and 14:53.

This control strategy drastically increases the total reactive power consumption around noontime. In case B, the reactive power consumption increases from 0.02 kvar when no control is used to 2.44 kvar. Meanwhile, cases A and C remain unaffected.

Fig. 3.50b shows the case with $Q(U)$-controlled PV system. According to the $Q(U)$ characteristic (Fig. 3.47b), the PV inverter consumes reactive power for boundary voltages above 1.03 p.u. and produces one for boundary voltages below 0.97 p.u. This control strategy changes the var behaviour of the CP into a mainly voltage-dependent one.

The $Q(U)$ control strategy provokes a strong voltage-dependent of the reactive power exchange between the LV grid and CPs.

Compared to the setup without any Vol/var control, the use of $Q(U)$-control reverses the LV-CP reactive power flow direction in cases A and B. In the former, the reactive power injection of 4.37 var is changed into an absorption of 1.21 kvar; And in the latter, the absorption of 0.02 kvar is changed into an injection of 1.19 kvar. Case C remains unaffected because the boundary voltage lies within the $Q(U)$ characteristic's dead-band. The LV-CP reactive power exchange of the Q-Autarkic CP_Link-Grid is shown in Fig. 3.50c. Independent of the time and boundary voltage, the PV inverter locally supplies the reactive power demand of the consuming devices. As a consequence, no reactive power is exchanged between the CP_ and the LV_Link-Grid.

Link-Grid behaviour for different control strategies and the specific cases

The different Volt/var control strategies significantly affect the composition of the LV-CP reactive power exchange of the rural residential CP_Link-Grid with spiky load profiles in cases A, B, and C, Fig. 3.51. In general, this composition includes Q-amount of the CP_Link-Grid itself and all connected elements, i.e. consuming devices, producers and storages. However, in this study, the CP_Link-Grid is modelled as a single node that does not contribute any reactive power. The EV charger is specified to operate with a unity power factor. Therefore, only the consuming devices and producer contribute to the LV-CP reactive power exchange. When spiky load profiles are set, the consuming devices contribute very low amounts of reactive power in the specific cases A, B and C.

When no Volt/var control is applied, the PV system does not contribute any reactive power, so the consuming devices alone determine the LV-CP reactive power exchange. Relatively low Q-amounts result in cases A, B and C. The $\cos\varphi(P)$-controlled PV inverter strongly modifies the reactive power exchange by consuming 2.42 kvar in case B, which is the highest value of all control strategies. Using $Q(U)$-control makes the PV inverter consume and produce 1.21

kvar in cases A and B, respectively. The PV system of a *Q*-Autarkic CP eliminates the LV-CP reactive power exchange. In this case, the producer mirrors the *Q*-amount of the consuming devices.

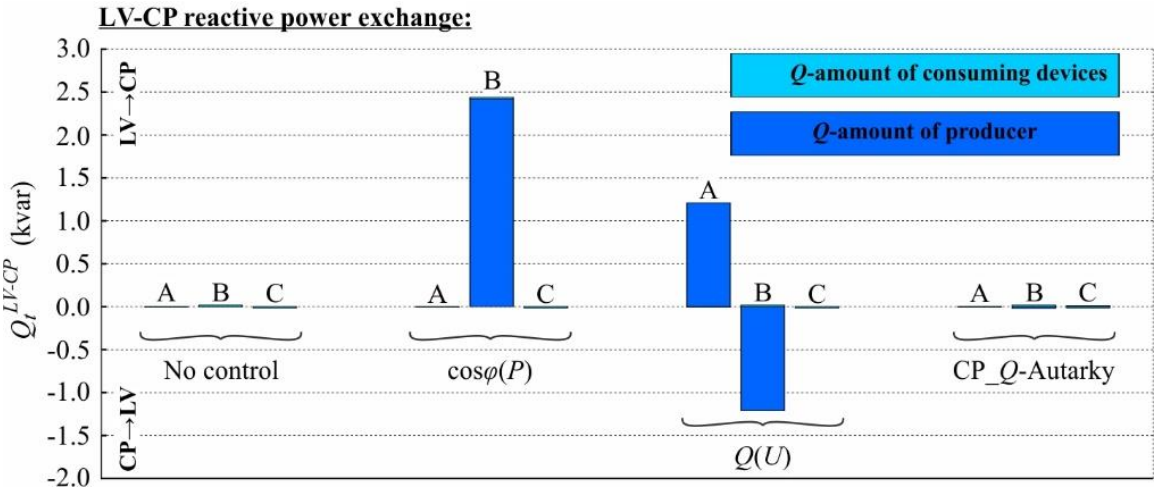

Fig. 3.51 Composition of the LV-CP reactive power exchange of the rural residential CP_Link-Grid with spiky load profiles for different cases, no control and various control strategies.

Smoothed load profiles

Without any Volt/var controlled PV system

Fig. 3.52 shows the daily behaviour of the rural residential CP_Link-Grid with smoothed load profiles and without any Volt/var control for various voltages at the LV-CP boundary node.

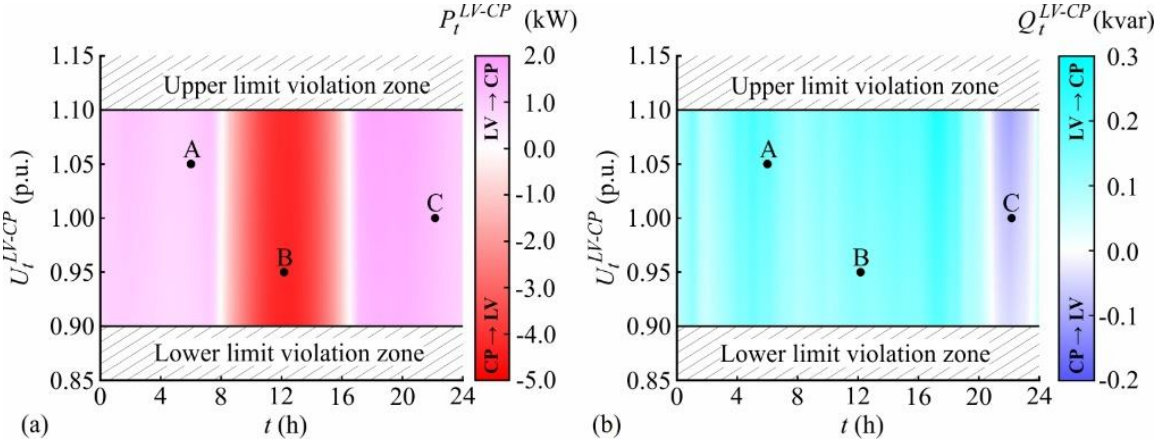

Fig. 3.52 Daily behaviour of the rural residential CP_Link-Grid with smoothed load profiles and without any Volt/var control for various voltages at the LV-CP boundary node: (a) LV-CP active power exchange; (b) LV-CP reactive power exchange.

As in the case with spiky load profiles, the LV-CP boundary voltage limits are fixed at 0.9 and 1.1 p.u. A significant time-dependency of the power contributions is observed, while the voltage-dependency is rather weak. The smooth character of the load profiles is reflected by smoothly blending colours. Both active and reactive power change their flow directions twice a day. The CP consumes active power between 0:00 and 7:40 and between 16:40 and 24:00, reaching values of 0.93 and 1.20 kW for cases A and C, respectively. The uninterrupted radiation leads to an active power production between 8:00 and 16:20. In case B, 4.27 kW are injected. The intervals in which the active power flow changes its direction, i.e. from 7:40 to 8:00 and from 16:20 to 16:40, are characterised by very low active power exchanges. Therein, the consumption is locally supplied by the PV production. The CP consumes reactive power all the time, except for the interval between 21:00 and 23:40, where the LED lamps and other modern appliances shift the inductive CP behaviour into a capacitive one. It consumes 0.18 and 0.14 kvar in cases A and B, respectively, and produces 0.07 kvar in case C.

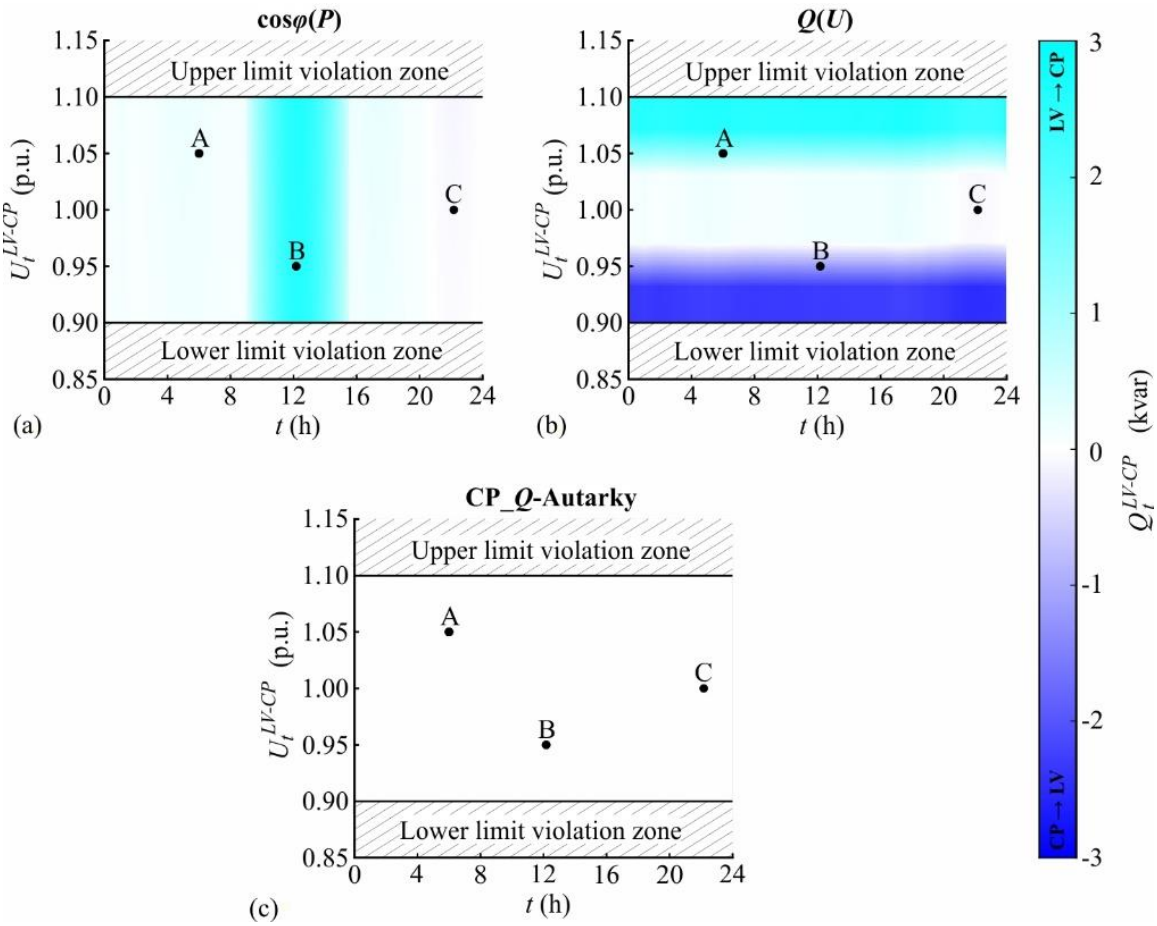

Fig. 3.53 Daily LV-CP reactive power exchange of the rural residential CP_Link-Grid with smoothed load profiles for various voltages at the LV-CP boundary node and different control strategies: (a) cos$\varphi(P)$; (b) $Q(U)$; (c) CP_Q-Autarky.

With Volt/var controlled PV system

Only the reactive power exchange is discussed, as the active power one is not affected by the Volt/var control strategies. Similarly to the case with spiky load profiles, the customer plant's reactive power behaviour is significantly modified by the control strategies. At the same time, the boundary voltage limits remain unaffected (as they are defined to be 0.9 and 1.1 p.u.), Fig. 3.53. Fundamentally, the control strategies have the same effects on the LV-CP reactive power exchange as in the case with spiky load profiles: The cos$\varphi(P)$-control intensifies its time-dependency, while the $Q(U)$-control changes the behaviour into a mainly voltage-dependent one. The former increases the CP's reactive power consumption between 8:53 and 15:28, reaching 2.56 kvar in case B. Meanwhile, the use of $Q(U)$-control provokes an absorption of 1.39 kvar in case A and a production of 0.07 kvar in case C. The CP_Q-Autarky eliminates the LV-CP reactive power exchange.

Link-Grid behaviour for different control strategies and the specific cases

Compared to the CP_Link-Grid with spiky load profiles, the consuming devices consume and produce more reactive power in the selected cases A, B and C, Fig. 3.54. However, the results clearly show the same trend for the control strategies' effect on the LV-CP reactive power exchange.

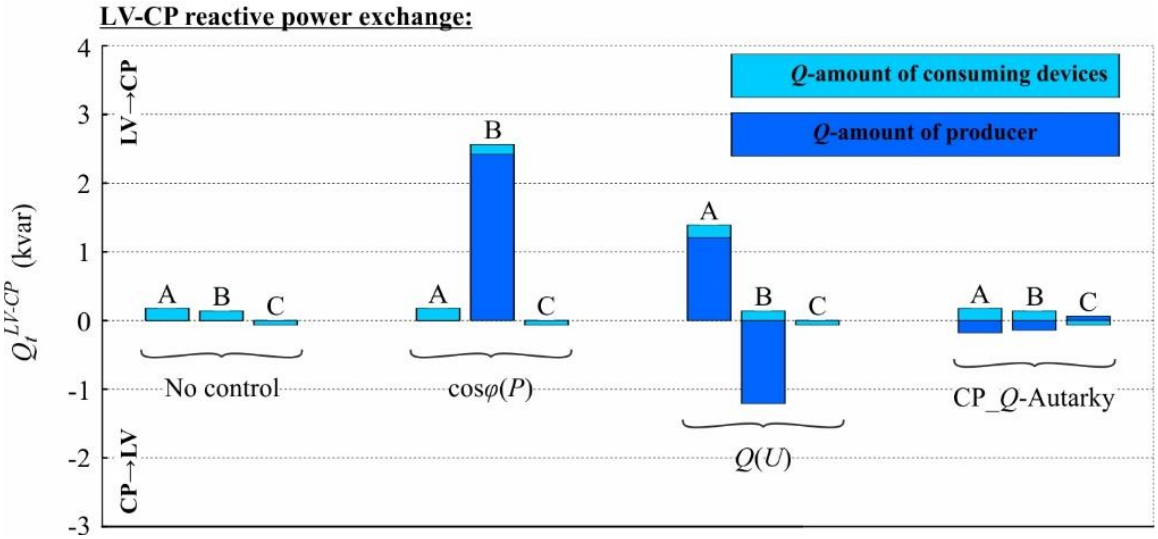

Fig. 3.54 Composition of the LV-CP reactive power exchange of the rural residential CP_Link-Grid with smoothed load profiles for different cases, no control and various control strategies.

The PV system without any Volt/var control contributes no reactive power. When cos$\varphi(P)$-control is applied, it consumes 2.42 kvar in case B. While the $Q(U)$-controlled PV system

consumes and produces 1.21 kvar in cases A and B, the one of the *Q*-Autarkic CP mirrors the reactive power contribution of the consuming devices.

3.6.3 Low voltage level

European low voltage grids are typically unbalanced and radial, and the CPs are connected anywhere along the feeders (CIGRE 2014a). On the European average, they have a cable share of 55 % (Eurelectric 2013). They are roughly categorised into rural and urban ones. While the rural LV_Link-Grids have relative long feeders and low load densities, the urban ones have short feeders and high load densities. Two real Austrian low voltage grids – a rural and an urban one – are analysed for all investigated Volt/var control strategies. Their exact model data is provided in a public data repository (Schultis and Ilo 2018). Unbalance is not considered as it is already neglected at the CP level.

3.6.3.1 Model specification

Fig. 3.55 shows the simplified one-line diagram of the rural LV_Link-Grid, wherein the RPDs used for *X*(*U*)-control and the OLTC are marked as optional elements. It includes four feeders with a total line length of 6.335 km and a cable share of 58.64 %. While the shortest feeder is 0,565 km in length, the longest one reaches 1.63 km. The feeders connect 61 rural residential CP_Link-Grids.

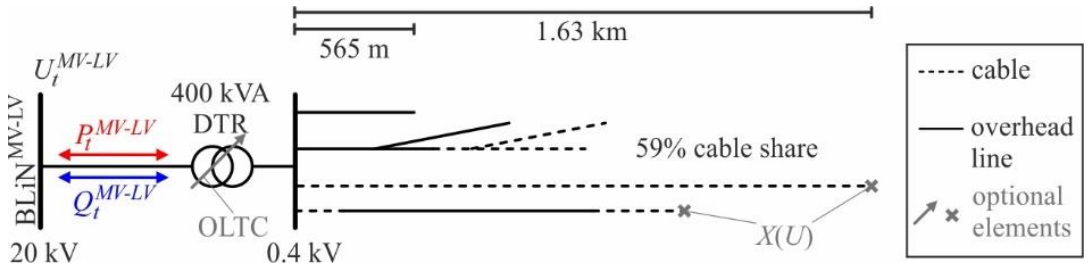

Fig. 3.55 Simplified one-line diagram of the rural LV_Link-Grid.

The 21 kV / 0.42 kV distribution transformer is 400 kVA with a total short circuit voltage of 3.7 % and a resistive part of 1 %. Its OLTC has five tap positions, i.e. 1 to 5, and adds 2.5 % of the nominal LV_Link-Grid voltage per tap. Tap position 3 is the mid position and sets the transmission ratio to its nominal value. When activated, the OLTC maintains the voltage at the secondary bus of the DTR between 0.95 and 0.99 p.u., which is identified as the appropriate setting (see §A.2.2). Otherwise, the tap changer is fixed in its mid position. The *X*(*U*)-controls are parametrized to maintain their terminal voltages between 0.91 and 1.09 p.u.

3.6.3.2 Behaviour of LV_Link-Grid

The behaviour of the LV_Link-Grid is discussed separately for both spiky and smoothed load profiles at the CP level. The MV-LV power exchanges, the LV active power loss, and the DTR loading are analysed in detail. They are calculated without applying any Volt/var control and for the different control strategies.

Spiky load profiles in CP level

While different load profiles are used for all Dev.- and St.-models, the same profile is used for all Pr.-models, reflecting the occupants' individual behaviour and the similar radiation in the region.

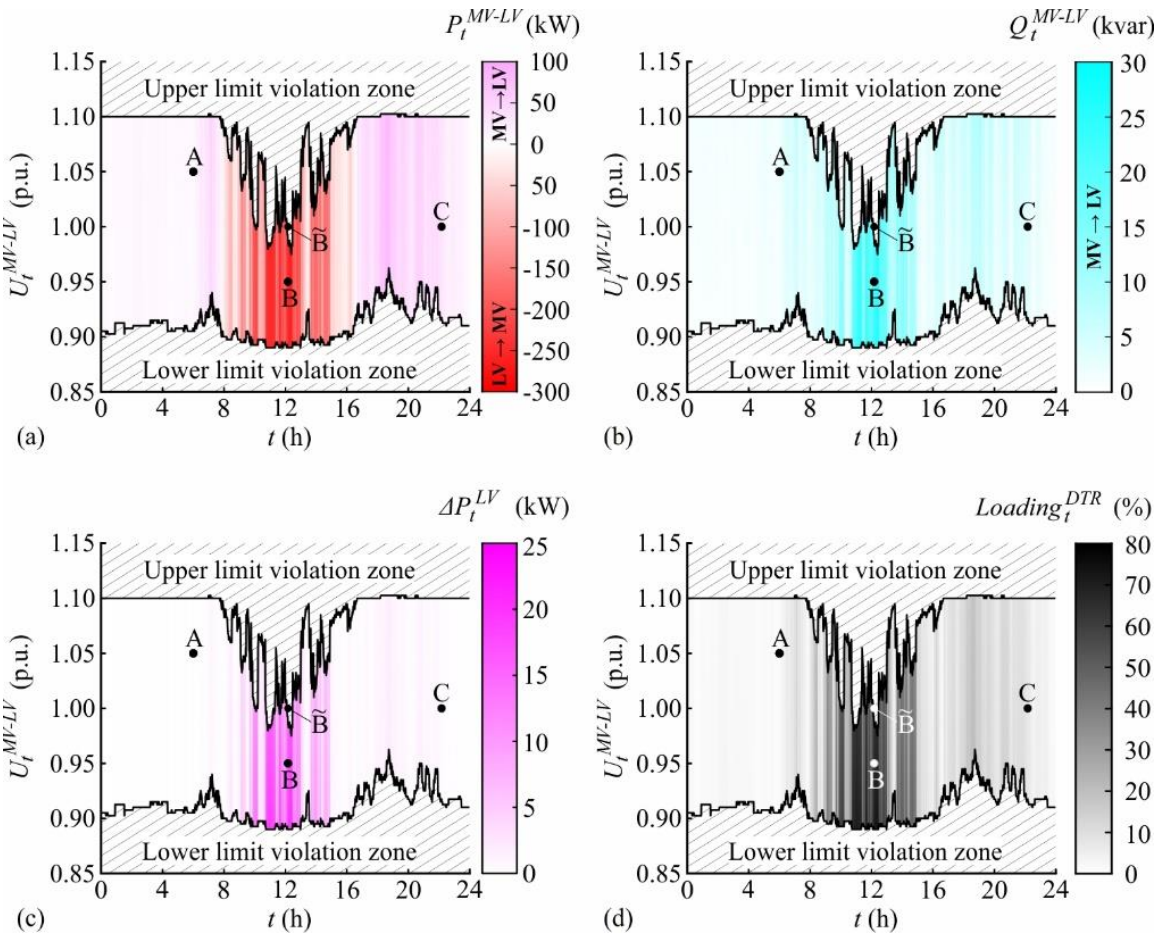

Fig. 3.56 Daily behaviour of the rural LV_Link-Grid without any Volt/var control for various voltages at the MV-LV boundary node and spiky load profiles at the CP level: (a) MV-LV active power exchange; (b) MV-LV reactive power exchange; (c) LV active power loss; (d) DTR loading.

Without any Volt/var control strategy

The spikiness of the load profiles at the CP level shapes the daily behaviour of the rural LV_Link-Grid without any Volt/var control, Fig. 3.56. The fluctuating power contributions of the connected CPs deform the upper and lower MV-LV boundary voltage limits into spiky shapes, reaching their minimum and maximum value of 0.9750 and 0.9625 p.u. at 12:23 and 18:44, respectively. No voltage limits are violated in cases A, B and C; But, case $\widetilde{\mathrm{B}}$ ($U_t^{MV-LV} =$ 1 p.u., $t =$ 12:10) lies within the upper voltage limit violation zone. The power contributions, the active power loss and the DTR loading intensively vary over time. Meanwhile, no distinct dependency on the MV-LV boundary voltage is observable.

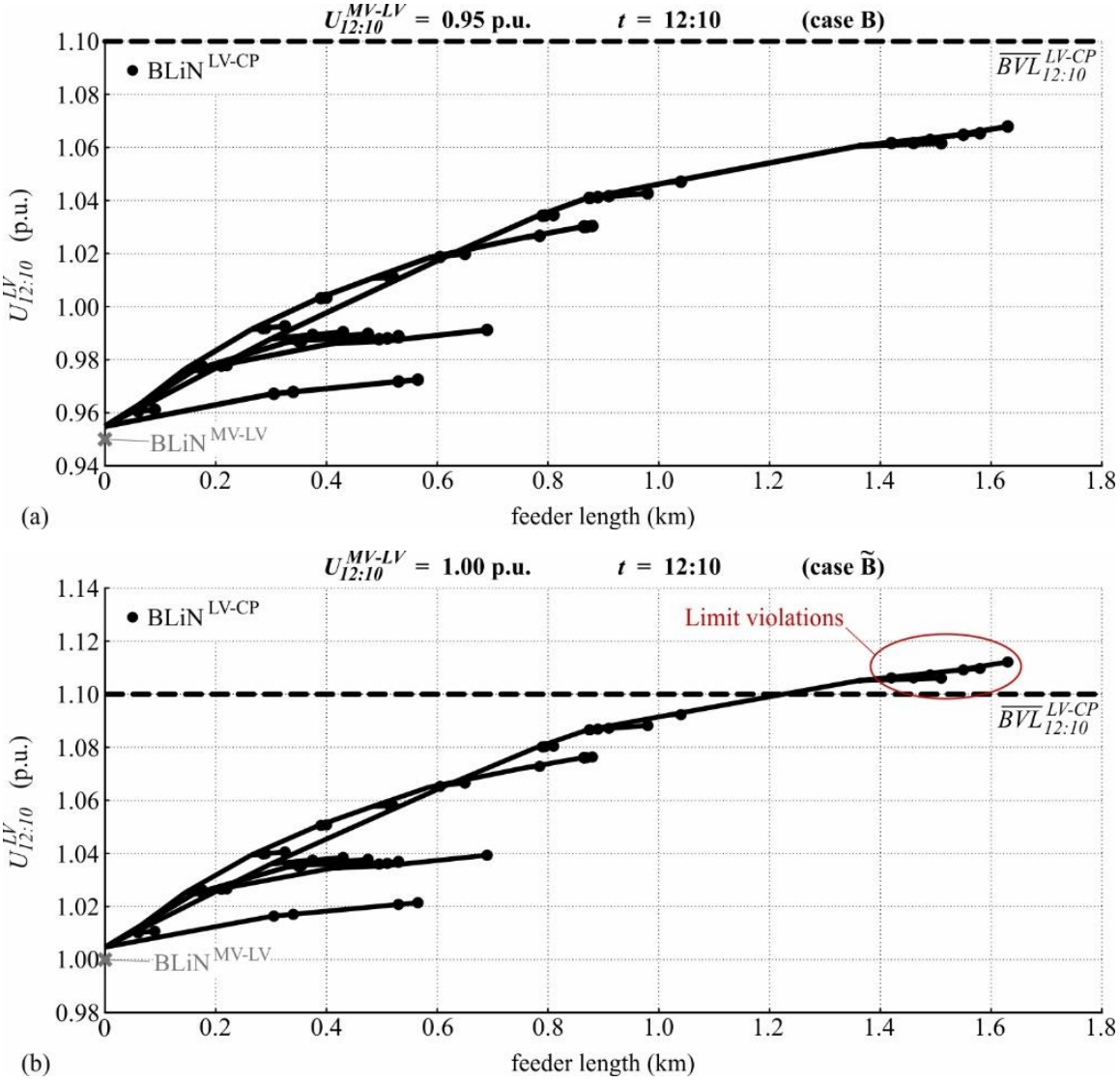

Fig. 3.57 Voltage profiles of the rural LV_Link-Grid's feeders without any Volt/var control at 12:10 for different MV-LV boundary voltages and spiky load profiles at the CP level: (a) 0.95 p.u. (case B); (b) 1.00 p.u. (case $\widetilde{\mathrm{B}}$).

Before 7:48 and after 16:32, the LV_Link-Grid absorbs active power from the MV level, while in between, it injects active power. It consumes 8.31 and 28.80 kW in cases A and C, respectively, and produces 257.54 kW in case B. Reactive power is flowing from MV to LV level over the whole day, reaching its highest values during noontime, and the values of 1.18, 23.79 and 3.76 kvar in cases A, B and C, respectively. A considerable active power loss and DTR loading occur during PV production, reaching values of 17.12 kW and 68.06 % in case B. In cases A and C, 0.03 and 0.24 kW are lost, respectively, while the DTR is loaded by 2.00 and 7.26 %.

The corresponding voltage profiles are shown in Fig. 3.57a and b for cases B and $\widetilde{\text{B}}$, respectively. While the grey cross marks the MV-LV boundary link node, the black bullets mark the LV-CP ones. Due to the PV injections, the voltages increase with an increasing distance from the distribution substation in both cases. In Fig. 3.57a, no $\text{BLiN}^{\text{LV-CP}}$ violates its voltage limits, and therefore, case B lies within the acceptable MV-LV voltage band (see Fig. 3.56). In contrast, Fig. 3.57b shows that violations of the upper voltage limit occur close to the end of the longest feeder in case $\widetilde{\text{B}}$.

With Volt/var control strategies

Fig. 3.58 shows the daily MV-LV reactive power exchange of the rural LV_Link-Grid for various voltages at the MV-LV boundary node, spiky load profiles at the CP level and different control strategies. The combinations of $X(U)$-control and OLTC in the distribution substation with CP_Q-Autarky are denoted as '$X(U)$+' and 'OLTC+'. All Volt/var control strategies strongly modify the MV-LV boundary voltage limits and the reactive power exchange when spiky load profiles are set at the CP level. While the var controls (PV inverter controls and $X(U)$) deform the limits, the Volt control (OLTC) shifts them in parallel. All strategies except the cos$\varphi(P)$ one compress both the upper and lower voltage limit violation zones. The spikiness of the upper $\text{BVL}^{\text{MV-LV}}$ is effectively mitigated only by the $X(U)$-control and its combination with CP_Q-Autarky. Meanwhile, all var controls have a considerable impact on the MV-LV reactive power exchange.

Fig. 3.58a shows the case with cos$\varphi(P)$-control. The LV_Link-Grid consumes large amounts of reactive power during high PV production periods, tightening the upper limit violation zone significantly and extending the lower one slightly. Although no limit violations occur in case B without any Volt/var control, the cos$\varphi(P)$-control increases the MV-LV reactive power exchange by 154.51 kvar. In total, 178.29 kvar flow from the MV into the LV level. Meanwhile, cases A and C are not affected by this control strategy.

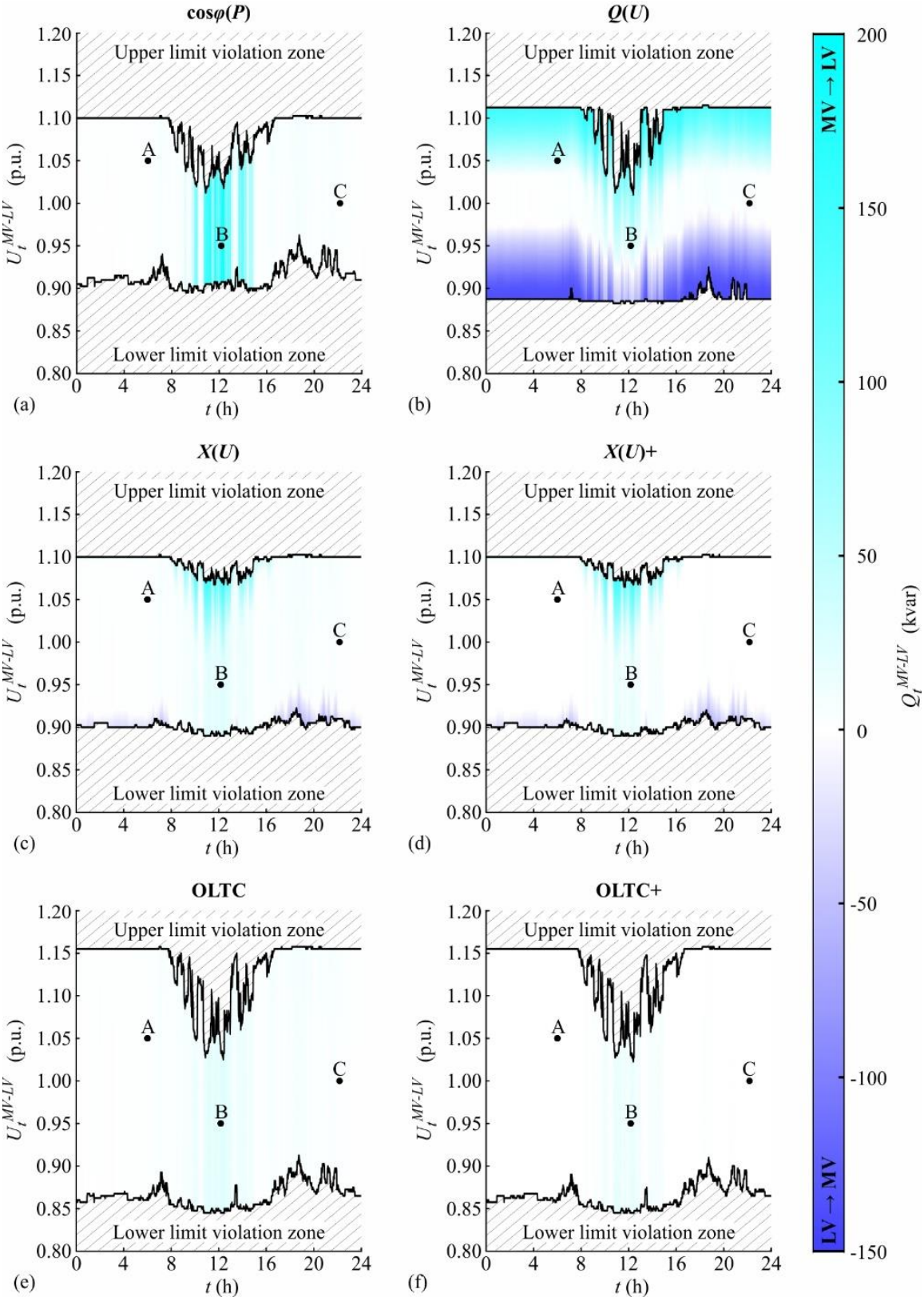

Fig. 3.58 Daily MV-LV reactive power exchange of the rural LV_Link-Grid for various voltages at the MV-LV boundary node, spiky load profiles at the CP level, and different control strategies: (a) cos$\varphi(P)$; (b) $Q(U)$; (c) $X(U)$; (d) $X(U)$ and CP_Q-Autarky; (e) OLTC; (f) OLTC and CP_Q-Autarky.

When $Q(U)$-control is applied, the LV grid exchanges large amounts of reactive power in a wide range of the MV-LV boundary voltage, Fig. 3.58b. The additional reactive power flows widen the permissible voltage range over the entire time horizon by compressing both the upper and lower limit violation zones. In cases A and B, the $Q(U)$-control unnecessarily increases the reactive power consumption of the LV-Link-Grid to 37.81 and 36.12 kvar, respectively, while in case C, it does not provoke any additional reactive power flows. The $X(U)$-control completely changes the shape of the limit violation zones, Fig. 3.58c. Both zones are straightened, allowing for the MV-LV boundary voltage almost the complete range of ± 10% around nominal voltage during the whole day. The MV-LV reactive power exchange is increased only when required to eliminate voltage limit violations. Therefore, cases A, B and C are not affected by the $X(U)$-control strategy. In combination with CP_Q-Autarky, it reduces the reactive power flow over the $BLiN^{MV\text{-}LV}$, Fig. 3.58d. In case A, 0.16 kvar flow from the LV into the MV level, while in cases B and C, the LV_Link-Grid draws 16.63 and 0.05 kvar from the MV level, respectively. Fig. 3.58e shows that the OLTC shifts the limit violation zones mainly in parallel; By about ± 5 %, which is the maximum range of the tap changer. It does not significantly modify the MV-LV reactive power exchange. 1.04, 23.41, and 3.58 kvar flow from the MV into the LV level in cases A, B and C, respectively. As shown in Fig. 3.58f, the application of CP_Q-Autarky reduces the reactive power exchange: In case A, the LV_Link-Grid injects 0.14 kvar into the MV level. In cases B, and C, it absorbs 16.63 and 0.07 kvar, respectively.

The different Volt/var control strategies also modify the daily active power loss within the rural LV_Link-Grid, Fig. 3.59. When the PV systems are injecting, the $\cos\varphi(P)$-control significantly intensifies the grid loss over the complete boundary voltage range: 24.98 kW are lost in case B. Meanwhile, the $Q(U)$-control increases the loss during the whole day but only in the edge regions of the permissible MV-LV boundary voltage range. The losses are increased to 0.29 and 17.68 kW in cases A and B, respectively. The $X(U)$-control significantly increases the grid loss only in regions where limit violations would occur without any Volt/var control. Therefore, it does not affect the losses in the selected cases. The OLTC increases the losses when it decreases the voltages at the LV level and vice versa. 25.4 and 247.5 W are lost in cases A and C, respectively, and 16.31 kW in case B. CP_Q-Autarky, whether combined with $X(U)$-control or OLTC, decreases the losses in the complete voltage-time-plane. In the former, losses of 24.5 W, 17.01 kW and 235.0 W occur in cases A, B, and C, respectively, while in the latter, the losses amount to 25.0 W, 17.01 kW and 242.6 W.

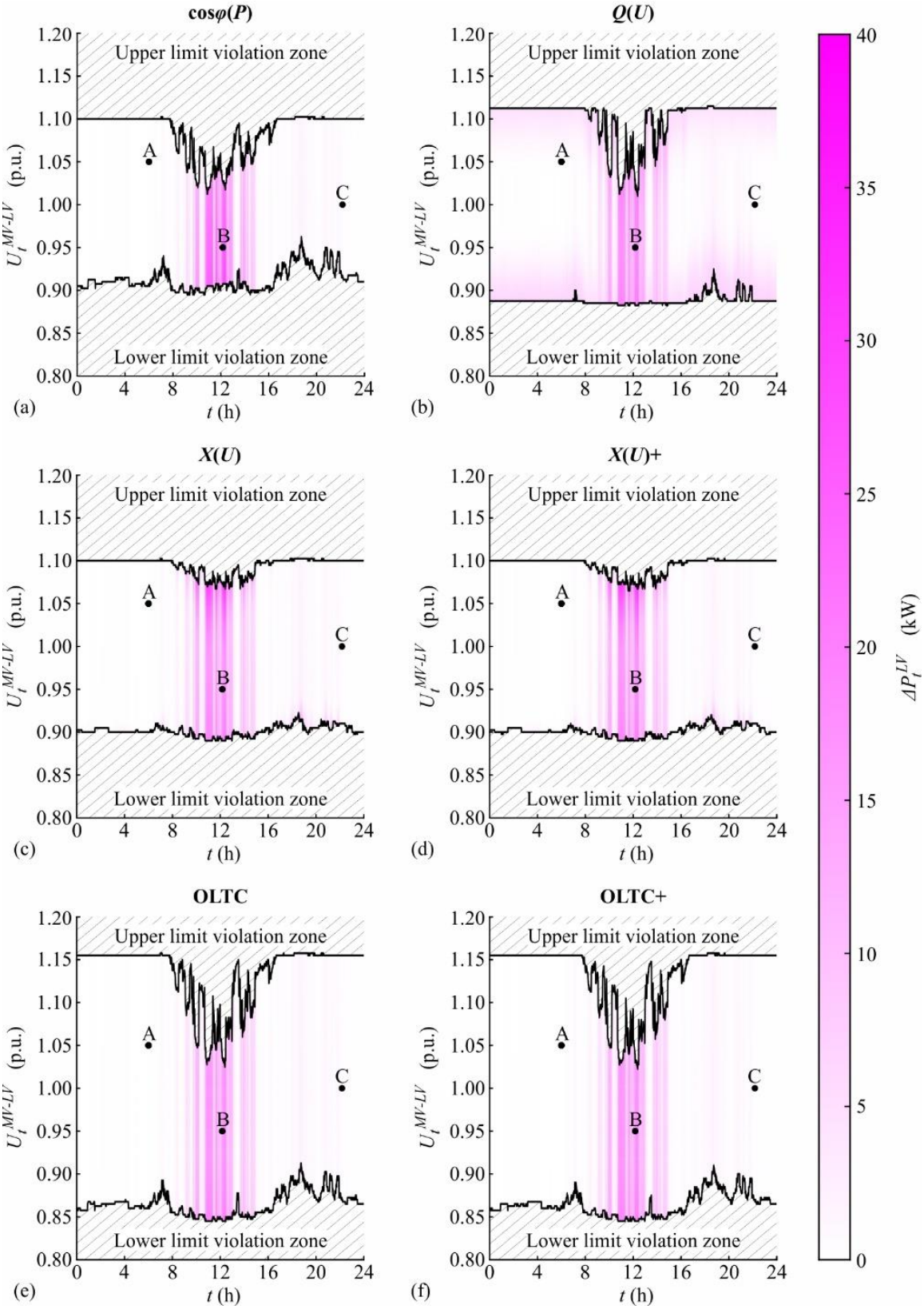

Fig. 3.59 Daily active power loss within the rural LV_Link-Grid for various voltages at the MV-LV boundary node, spiky load profiles at the CP level, and different control strategies: (a) cosφ(P); (b) Q(U); (c) X(U); (d) X(U) and CP_Q-Autarky; (e) OLTC; (f) OLTC and CP_Q-Autarky.

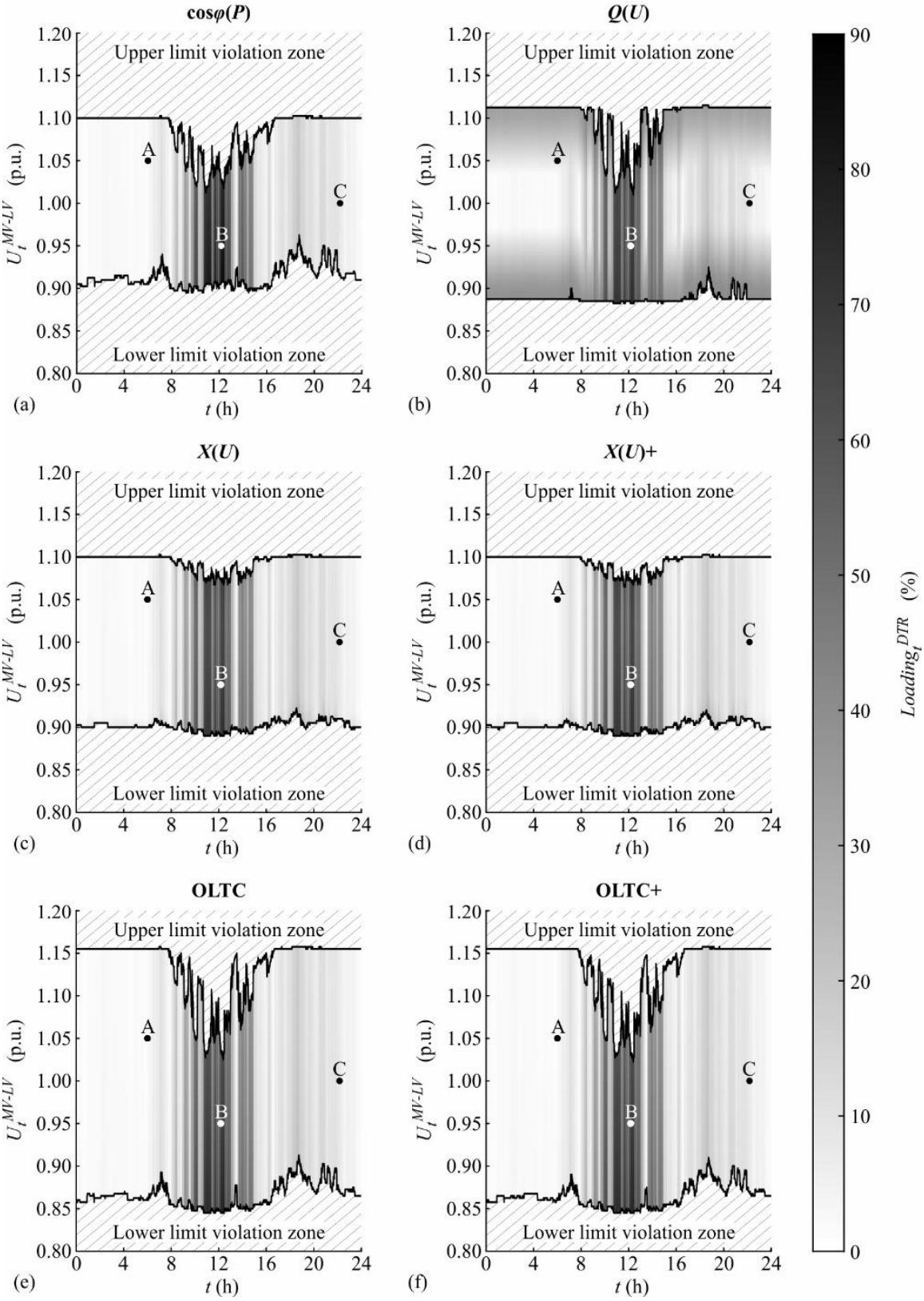

Fig. 3.60 Daily DTR loading within the rural LV_Link-Grid for various voltages at the MV-LV boundary node, spiky load profiles at the CP level, and different control strategies: (a) cosφ(P); (b) Q(U); (c) X(U); (d) X(U) and CP_Q-Autarky; (e) OLTC; (f) OLTC and CP_Q-Autarky.

Fig. 3.60 shows that the daily DTR loading follows the same trend as the MV-LV reactive power exchange for the different control strategies. The cos$\varphi(P)$-control provokes high DTR loadings when the PV systems are injecting. In case B, it amounts to 80.92 %. When $Q(U)$-control is used, high loadings appear in the edge regions of the relevant boundary voltage range, reaching 9.23 and 68.32 % in cases A and B, respectively. Due to its inactivity in cases A, B, and C, the $X(U)$-control does not affect the corresponding DTR loadings. Its combination with Q-Autarkic CPs slightly unloads the DTR: It is loaded by 1.98, 67.93, and 7.20 % in cases A, B and C, respectively. The OLTC reduces the DTR loading in cases A and C to 1.92 and 7.18 %, respectively, and increases it to 68.14 % in case B. When combined with CP_Q-Autarky, lower DTR loadings occur, i.e. 1.90, 67.93, and 7.13 % for cases A, B, and C, respectively.

Link-Grid behaviour for different control strategies and the specific cases

The composition of the MV-LV reactive power exchange differs for the different Volt/var control strategies, Fig. 3.61. It is determined exclusively by the Q-amounts of the connected CP_Link-Grids and the LV_Link-Grid itself, as no storages and producers are connected at the LV level. Independently of the applied control strategy, the LV lines and the DTR consume significant amounts of reactive power in case B. This reactive power loss results from the intensive active power transfer during PV peak production periods and the low MV-LV boundary voltage (see Equation 3.4b).

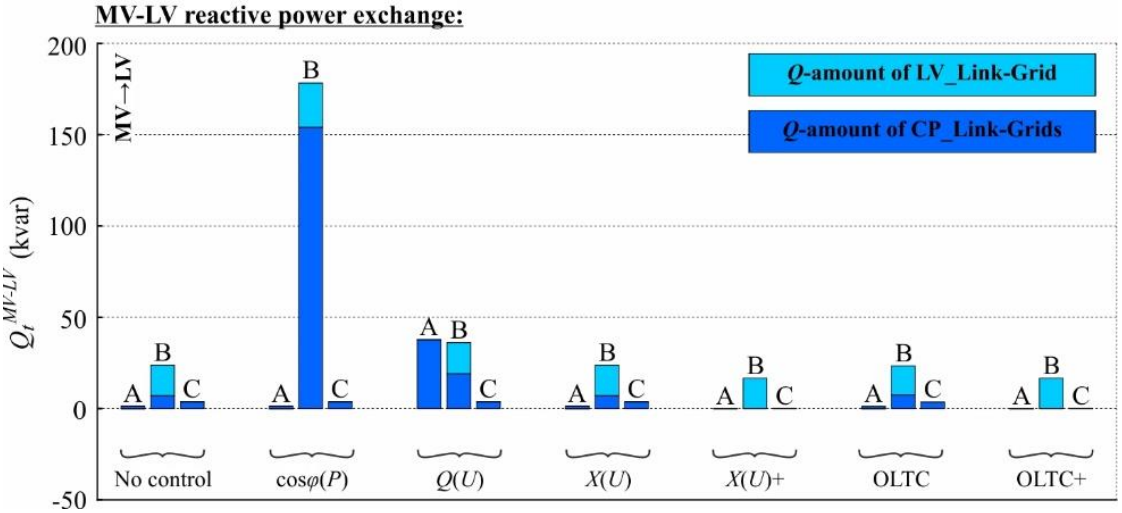

Fig. 3.61 Composition of the MV-LV reactive power exchange of the rural LV_Link-Grid for spiky load profiles at the CP level, different cases, no control and various control strategies.

When no control is applied, the Q-amounts of the CP_Link-Grids dominate the reactive power composition in cases A and C, while in case B, the reactive power losses in LV level constitute the major part. In the latter, the use of cos$\varphi(P)$-control increases the reactive power consumption

of the CPs substantially. The additional reactive power flow also increases the Q-losses in LV level considerably. The $Q(U)$-control intensifies the LV-CP reactive power exchanges in cases A and B, which slightly increases the Q-losses at the LV level. The $X(U)$-control is inactive in all cases, yielding the same reactive power composition as the setup without any Volt/var control. Its combination with CP_Q-Autarky eliminates the LV-CP reactive power exchanges and reduces the Q-consumption of the LV_Link-Grid marginally. The OLTC has a relatively low impact on the reactive power balance in LV level: In cases A and C, it slightly reduces the Q-amounts of the CPs by reducing the grid voltages. In further consequence, this increases the losses at the LV level. Meanwhile, in case B, the OLTC steps up the voltage, which increases the LV-CP reactive power exchanges and decreases the Q-losses. Its combination with CP_Q-Autarky eliminates the CPs' Q-contributions and the necessity to step up the voltage in case B, reducing the impact of the OLTC on the reactive power losses in all cases.

The distinct Volt/var control strategies differently affect the active power loss within the LV_Link-Grid, Fig. 3.62. In analogy with the reactive power loss, high LV active power losses occur in case B for each control strategy. Meanwhile, relative low losses appear in cases A and C.

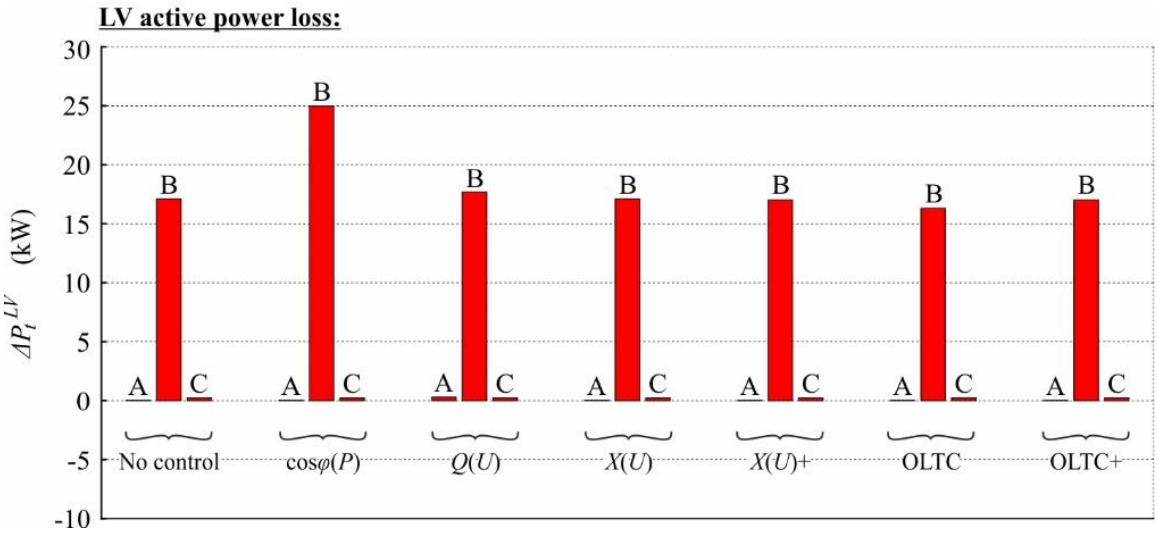

Fig. 3.62 Active power loss within the rural LV_Link-Grid for spiky load profiles at the CP level, different cases, no control and various control strategies.

Compared to the setup without any Volt/var control, the use of cos$\varphi(P)$-control considerably intensifies the grid losses in case B. The additional reactive power flows provoked by the $Q(U)$-control strategy slightly increase the active power loss in cases A and B. Due to its inactivity in the selected cases, the $X(U)$-control does not provoke any additional losses. In combination with CP_Q-Autarky, it even reduces the grid loss. The OLTC increases the grid loss in cases A

and C and decreases it in case C. This impact is reduced when the OLTC is combined with *Q*-Autarkic CPs.

The DTR loading is shown in Fig. 3.63 for the different control strategies and cases. The high active power transfer and low MV-LV boundary voltage excessively load the DTR in case B. The cos$\varphi(P)$-control-related reactive power flows additionally load the DTR in case B. Using $Q(U)$-control increases the DTR loading significantly in case A, and slightly in case B. While the $X(U)$-control does not affect the DTR loading in the selected cases, the OLTC reduces it in cases A and C and increases it in case B. Whether combined with $X(U)$-control or OLTC, the CP_*Q*-Autarky unloads the DTR in all cases.

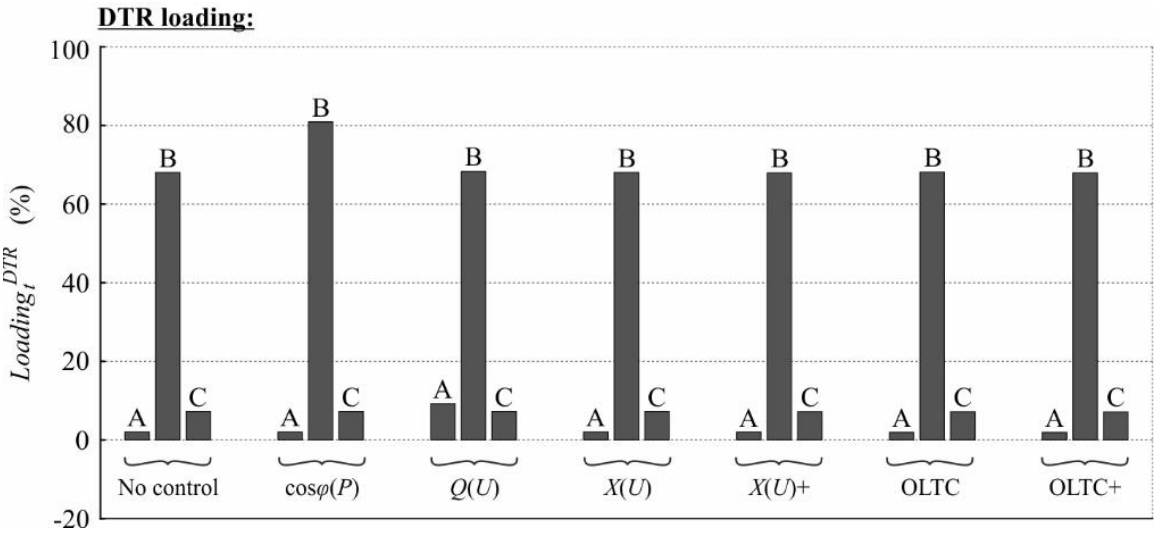

Fig. 3.63 DTR loading within the rural LV_Link-Grid for spiky load profiles at the CP level, different cases, no control and various control strategies.

Smoothed load profiles in CP level

The same smoothed load profiles are used for all CPs connected to the rural LV_Link-Grid.

Without any Volt/var control strategy

The smoothed power contributions of the connected CPs deform the boundary voltage limits of the rural LV_Link-Grid into curved shapes and blend the colours representing the power exchanges, the active power loss and the DTR loading continuously, Fig. 3.64. Due to the relatively high power factor at the BLiN$^{MV\text{-}LV}$, a strong coupling is observed between the MV-LV active power exchange and the limit curve deformation. In PV production times, the upper BVL is strongly tightened, reaching a very low value of 0.9875 p.u. around noontime. The lower limit is tightened almost during the complete time horizon, especially when the LV_Link-Grid consumes active power. This increases the lower boundary voltage limit up to the maximum value of 0.9525 p.u. in the evening hours. The limits are not violated in cases A, B

and C; But, case $\widetilde{B}$ lies within the upper limit violation zone. The power exchanges, active power loss and DTR loading are characterised by a strong time-dependency and weak voltage-dependency.

The colour shades representing the MV-LV active and reactive power exchanges basically replicate the CP power contributions (see Fig. 3.52). They are only slightly modified by the grid losses, resulting in an MV→LV active power transfer of 56.62 and 73.85 kW in cases A and C, respectively, and a reverse one of 241.99 kW in case B. Meanwhile, 11.21 and 24.78 kvar flow from the MV into the LV level in cases A and B, respectively. In case C, 2.53 kvar are injected into the MV level. The active power loss and the DTR loading are mainly determined by the active power flows, as the reactive power flows are relatively low.

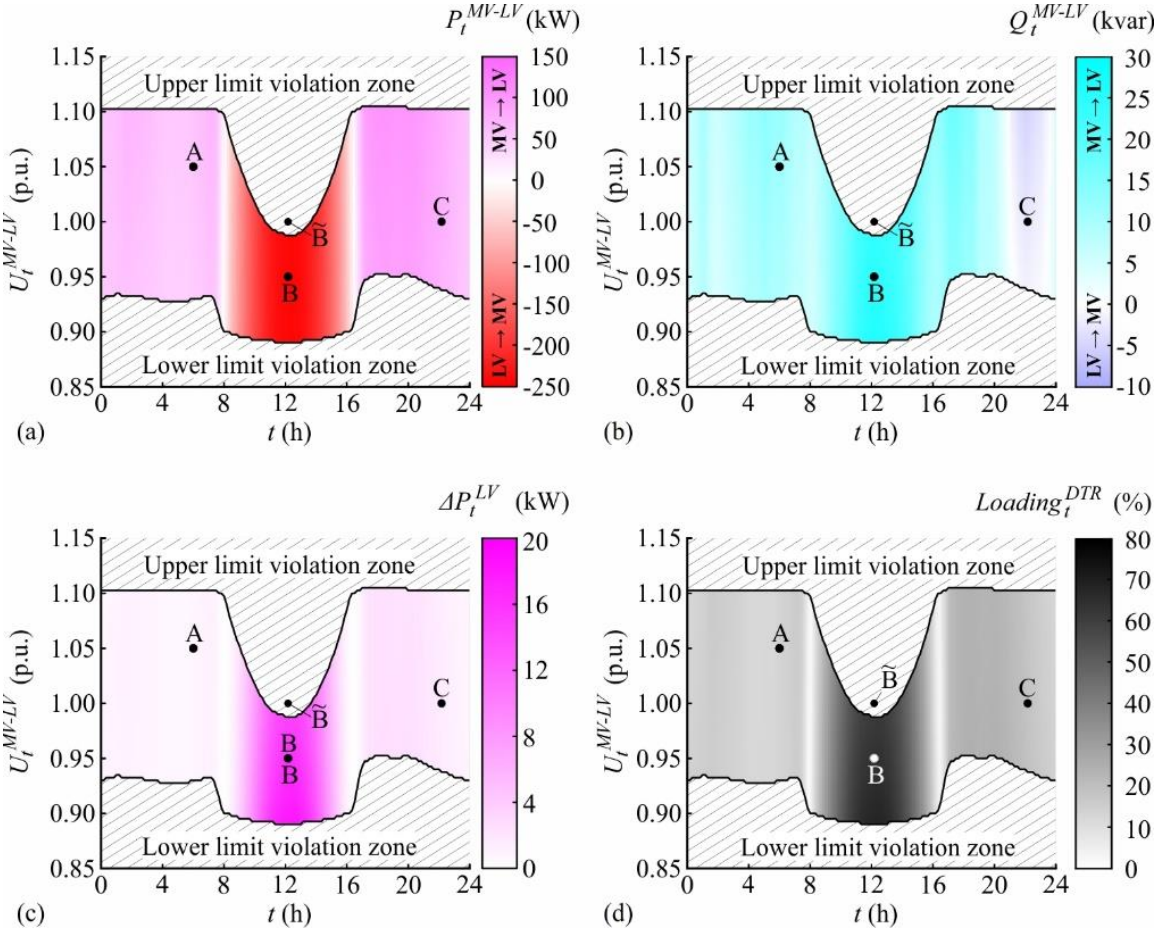

Fig. 3.64 Daily behaviour of the rural LV_Link-Grid without any Volt/var control for various voltages at the MV-LV boundary node and smoothed load profiles at the CP level: (a) MV-LV active power exchange; (b) MV-LV reactive power exchange; (c) LV active power loss; (d) DTR loading.

While the active power loss amounts to 0.76, 15.97 and 1.39 kW in cases A, B and C, respectively, the DTR is loaded by 13.74, 64.01 and 18.47 %.

The corresponding voltage profiles are shown in Fig. 3.65a and b for case B and $\widetilde{\text{B}}$, respectively. In Fig. 3.65a, no limit violations occur, although the PV injections significantly increase the feeder voltages. Meanwhile, the upper voltage limit is violated in case $\widetilde{\text{B}}$, Fig. 3.65b.

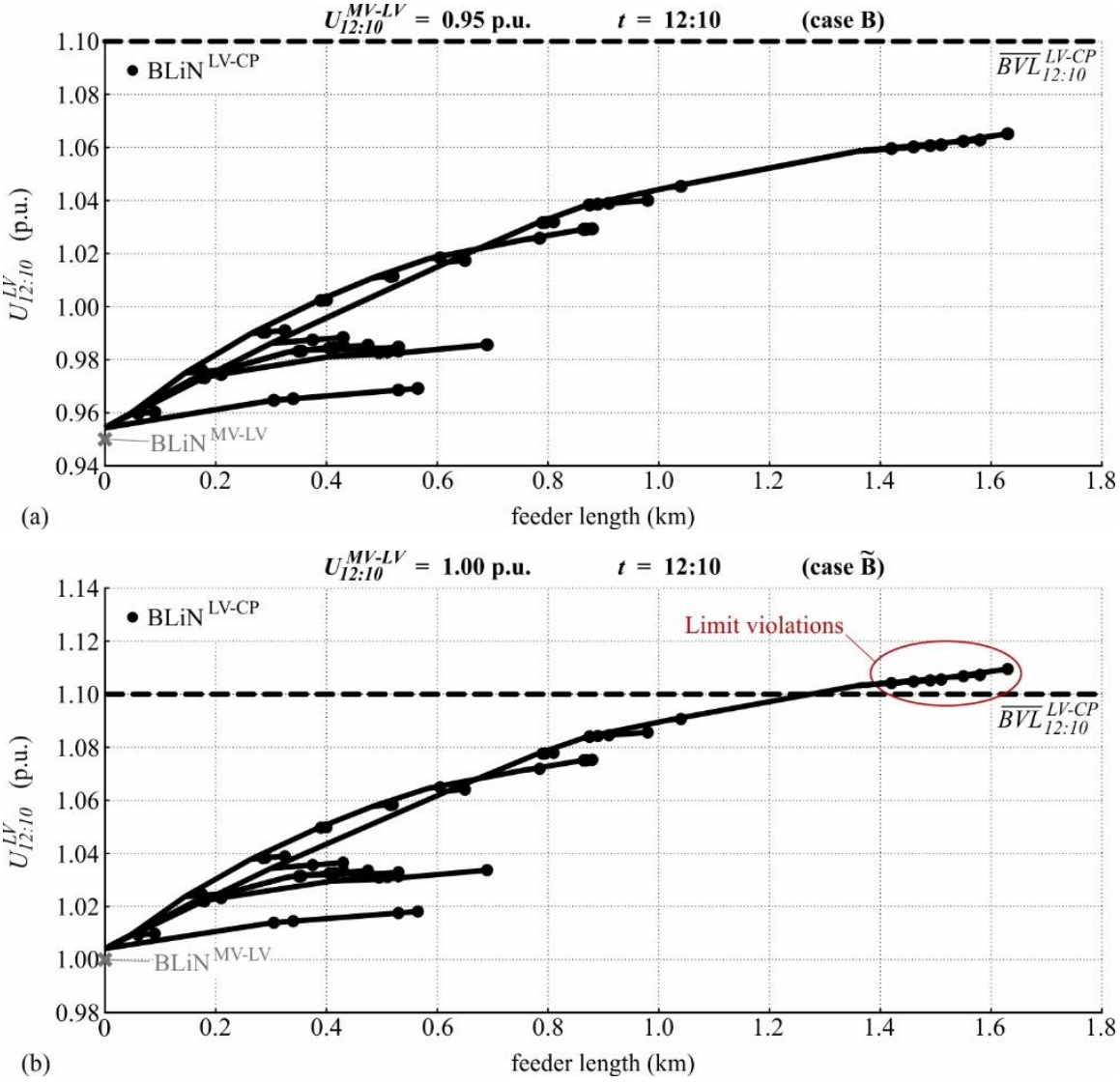

Fig. 3.65 Voltage profiles of the rural LV_Link-Grid's feeders without any Volt/var control at 12:10 for different MV-LV boundary voltages and smoothed load profiles at the CP level: (a) 0.95 p.u. (case B); (b) 1.00 p.u. (case $\widetilde{\text{B}}$).

With Volt/var control strategies

Fundamentally, the same effects of the different Volt/var control strategies on the MV-LV boundary voltage limits and the reactive power exchange are observed for smoothed load profiles in CP level as for the spiky ones, Fig. 3.66. The var controls deform the limits, and the Volt control shifts them in parallel. All strategies except the cos$\varphi(P)$ one compress both the

upper and lower voltage limit violation zones. In contrast to the Volt control, the var controls significantly affect the MV-LV reactive power exchange.

The cosφ(P)-control excessively increases the reactive power flow from the MV into the LV level between 8:53 and 15:28, reaching 179.62 kvar in case B. As a result, the upper boundary voltage limit is significantly tightened, and the lower one is slightly widened. In the remaining interval, neither the BVLs nor the reactive power exchange is affected. In contrast, the Q(U)-control compresses both limit violation zones all day through, allowing for boundary voltages above 1.1 and below 0.9 p.u. many hours a day. This considerably intensifies the MV-LV reactive power exchange in the edge regions of the permissible voltage range. Although no limit violations occur without any Volt/var control, the reactive power exchange is increased to 26.02, 35.30 and -4.08 kvar in cases A, B and C, respectively. X(U)-control, whether combined with CP_Q-Autarky or not, straightens the upper and lower BVLs, leaving only small protrusions during the noon and evening hours. It is inactive in the selected cases, as no reactive power support is necessary to maintain acceptable voltages. Therefore, when X(U)-control is combined with Q-Autarkic CPs, the MV-LV reactive power exchange is reduced to 0.52, 15.19 and 1.15 kvar in cases A, B and C, respectively. The OLTC shifts the BVLs by around ±5 % in parallel, conserving their original shape. This slightly reduces the MV-LV reactive power exchange to 10.46 and -2.06 kvar in cases A and C, respectively. It is further reduced when the CPs act Q-Autarkic: 0.54, 15.19 and 1.18 kvar flow from the MV level into the LV level.

For smoothed load profiles at the CP level, similar effects of the different control strategies on the LV active power loss are observed as for the spiky ones, Fig. 3.67. The cosφ(P)-control drastically increases the grid loss around noontime, reaching 23.92 kW in case B. Q(U)-control adds significant losses only in the edge regions of the permissible voltage range, provoking values of 0.83, 16.44 and 1.40 kW in cases A, B and C, respectively. The X(U)-control is active mainly in regions where limit violations would occur without any Volt/var control. Therefore, it does not affect the losses in the selected cases. Meanwhile, its combination with CP_Q-Autarky reduces the losses to 0.74, 15.86 and 1.39 kW in cases A, B and C, respectively. The OLTC steps down the voltage in cases A and C, reducing the loss to 0.76 kW in case A and increasing it to 1.418 kW in case C. The losses resulting from this setup are reduced to 0.74, 15.86 and 1.416 kW when the CPs act Q-Autarkic.

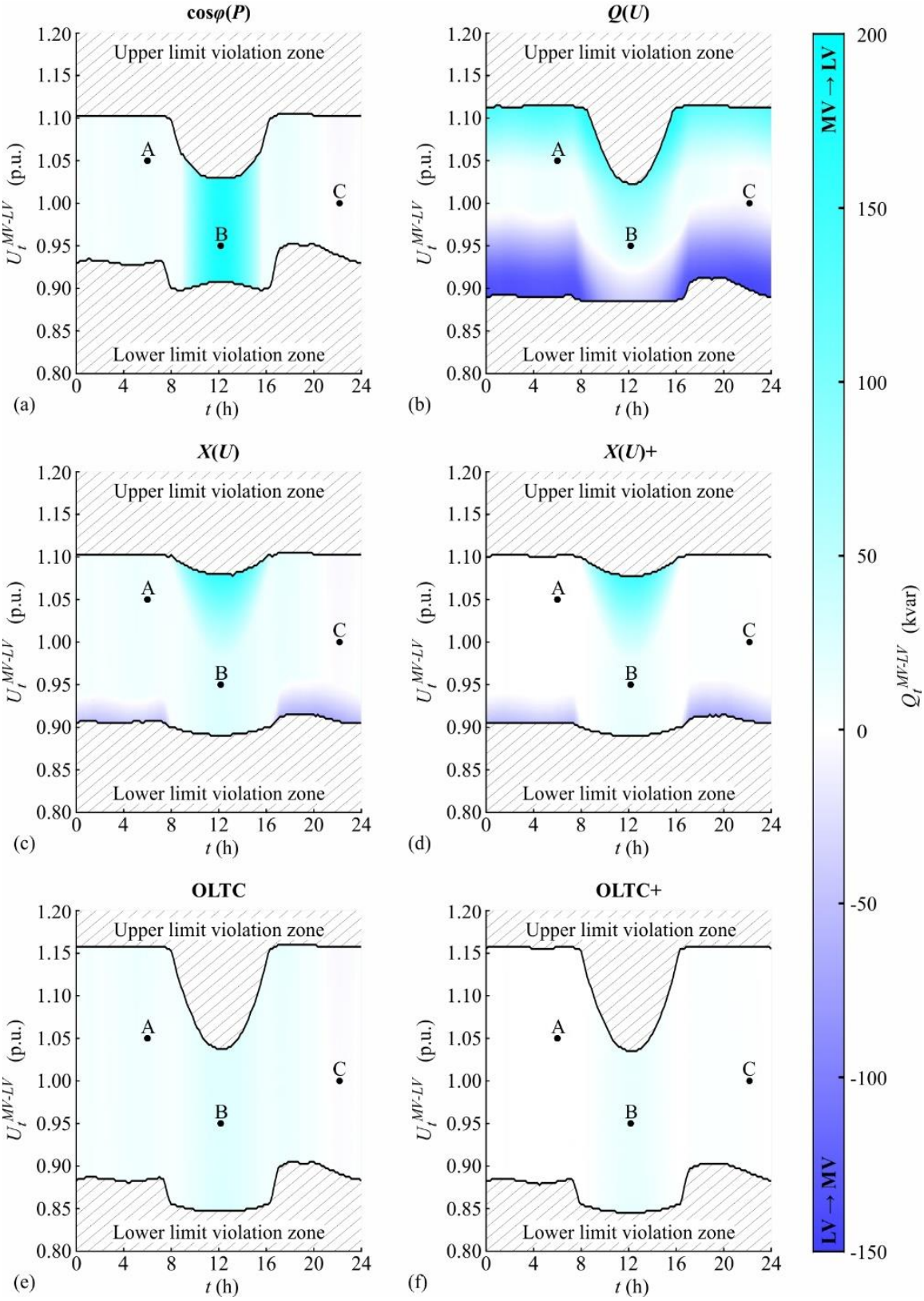

Fig. 3.66 Daily MV-LV reactive power exchange of the rural LV_Link-Grid for various voltages at the MV-LV boundary node, smoothed load profiles at the CP level and different control strategies: (a) cos$\varphi(P)$; (b) $Q(U)$; (c) $X(U)$; (d) $X(U)$ and CP_Q-Autarky; (e) OLTC; (f) OLTC and CP_Q-Autarky.

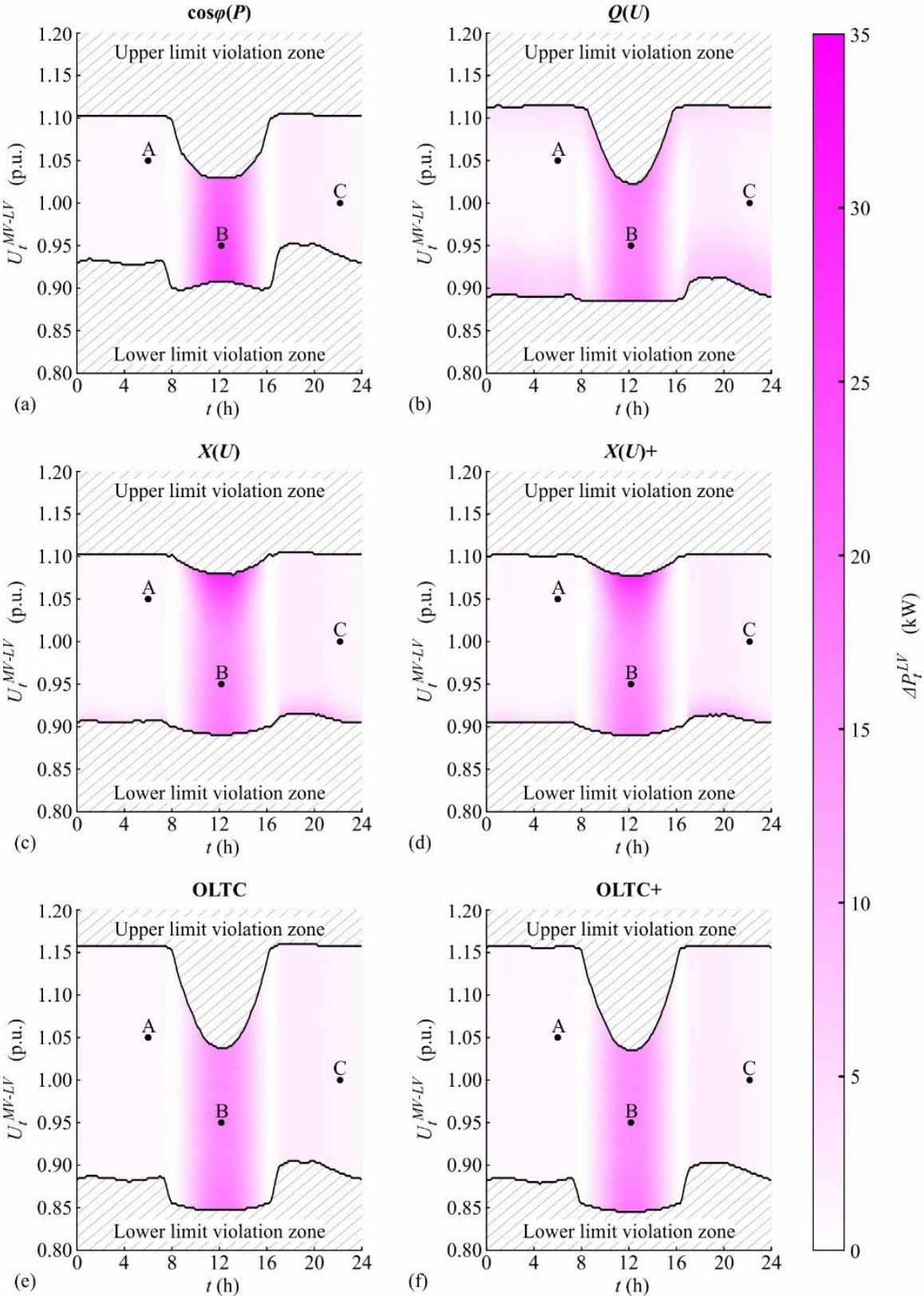

Fig. 3.67 Daily active power loss within the rural LV_Link-Grid for various voltages at the MV-LV boundary node, smoothed load profiles at the CP level and different control strategies: (a) cosφ(P); (b) Q(U); (c) X(U); (d) X(U) and CP_Q-Autarky; (e) OLTC; (f) OLTC and CP_Q-Autarky.

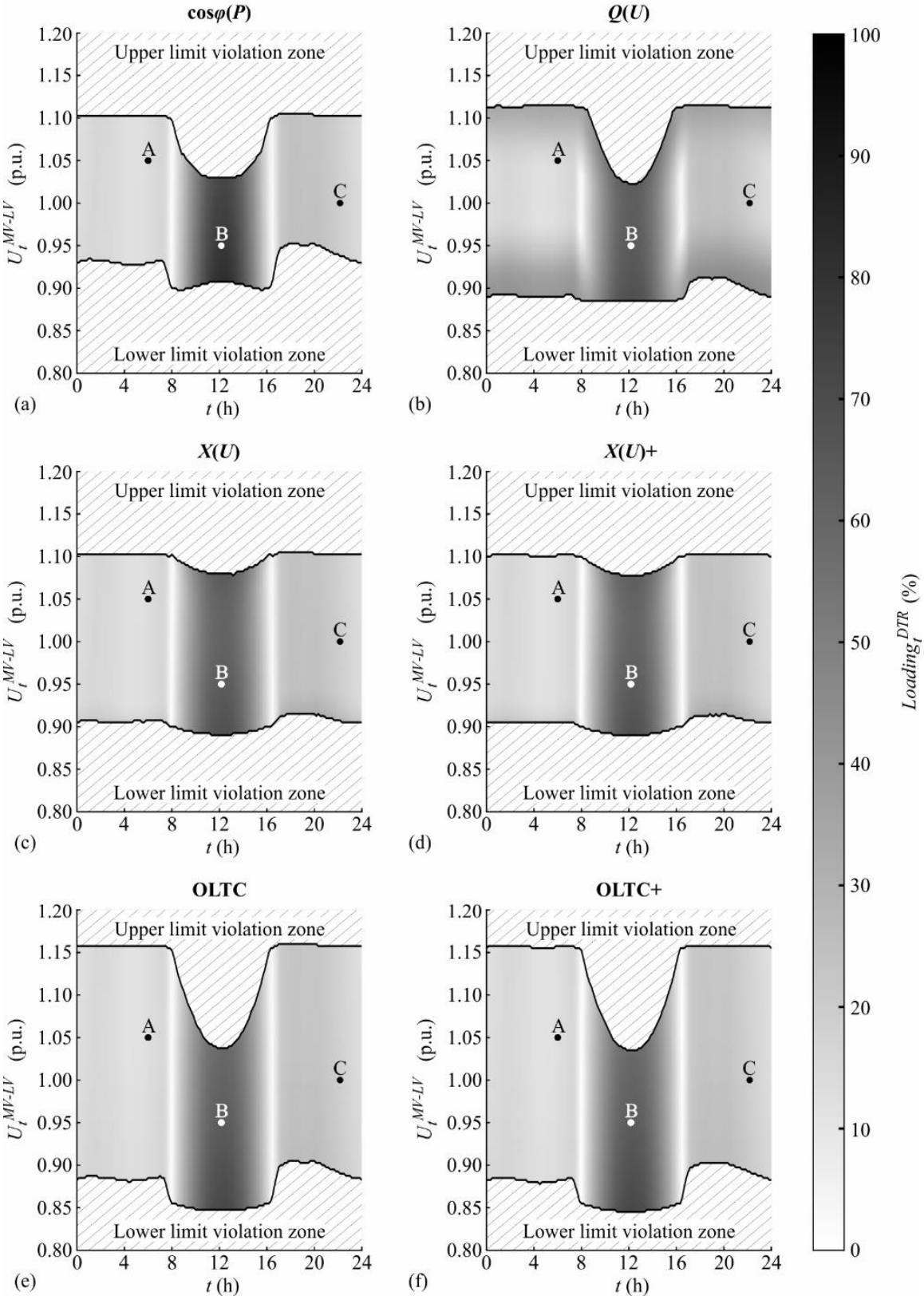

Fig. 3.68 Daily DTR loading within the rural LV_Link-Grid for various voltages at the MV-LV boundary node, smoothed load profiles at the CP level, and different control strategies: (a) cosφ(P); (b) Q(U); (c) X(U); (d) X(U) and CP_Q-Autarky; (e) OLTC; (f) OLTC and CP_Q-Autarky.

Also, for the DTR loading, analogous effects for smoothed and spiky load profiles at the CP level are observed, Fig. 3.68. The use of cos$\varphi(P)$-control highly loads the DTR when the PV systems produce significant amounts of active power, reaching 77.96 % in case B. The additional reactive power flows provoked by the $Q(U)$-control increase the DTR loading in the edge region of the permissible voltage range. In cases A, B and C, this loads the DTR by 14.82, 64.27 and 18.50 %, respectively. As not active in these cases, the $X(U)$-control does not affect the corresponding DTR loadings. Its combination with Q-Autarkic CPs slightly unloads the DTR to 13.51, 63.81 and 18.46 % in cases A, B and C, respectively. The DTR loading is decreased in cases A and C when the OLTC is used to control the voltage, obtaining values of 13.05 and 18.21 %, respectively. Its combination with CP_Q-Autarky further reduces it to 12.84, 63.81 and 18.20 % respective to cases A, B and C.

Link-Grid behaviour for different control strategies and the specific cases

Fig. 3.69 shows the composition of the reactive power exchanged between MV_ and LV_Link-Grid. Significant reactive power losses occur in case B for each control strategy.

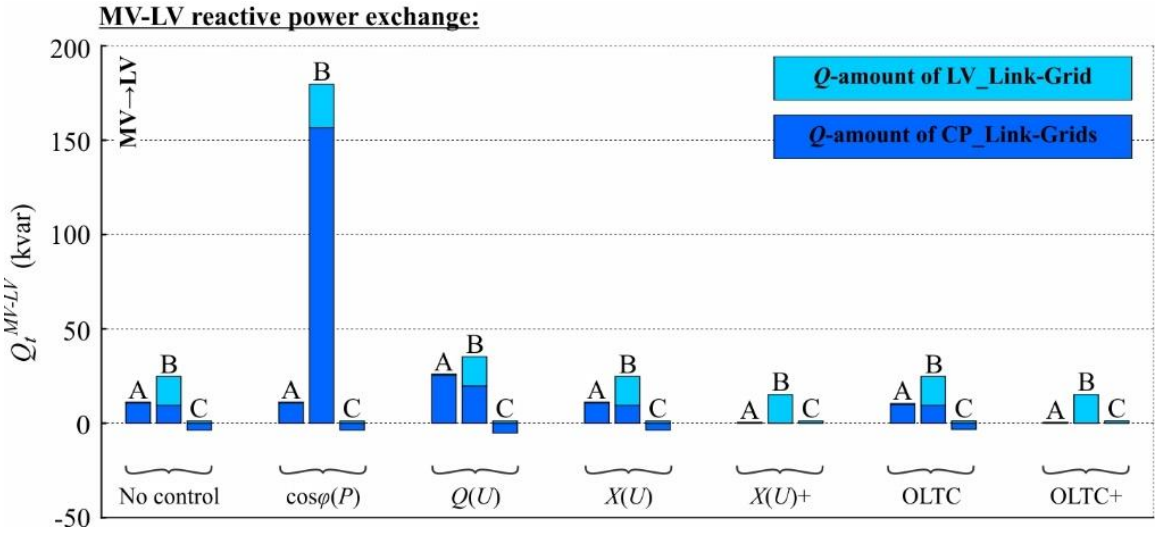

Fig. 3.69 Composition of the MV-LV reactive power exchange of the rural LV_Link-Grid for smoothed load profiles at the CP level, different cases, no control and various control strategies.

Without any Volt/var control, the Q-composition is dominated by the Q-amounts of the CPs in cases A and C and by the grid loss in case B. In the latter, cos$\varphi(P)$-controlled PV systems substantially increase the LV-CP reactive power exchanges, causing additional reactive power losses in further consequence. The $Q(U)$-control intensifies the LV reactive power loss and especially the LV-CP reactive power exchanges in all cases. Due to its inactivity in the selected

cases, the $X(U)$-control does not modify the corresponding reactive power compositions. In cases A and C, the OLTC reduces the reactive power Q-amounts of the CPs and increases the one of the LV_Link-Grid itself. Q-Autarkic customers do not exchange any reactive power with the grid, reducing the grid's reactive power loss in both combinations.

When smoothed load profiles are used at the CP level, the different Volt/var control strategies affect the composition of the MV-LV reactive power exchange in the same way as when spiky load profiles are used.

The active power loss in LV level behaves analogue to reactive power one, Fig. 3.70. While high losses occur in case B for each control strategy, relative low ones prevail in cases A and C. The cos$\varphi(P)$-control considerably intensifies the grid losses in case B. Meanwhile, the $Q(U)$-control slightly increases the losses in all cases. The $X(U)$-control does not affect the losses in the selected cases. When an OLTC is used, the losses are decreased in case A and increased in case C. The application of CP_Q-Autarky generally reduces the grid loss.

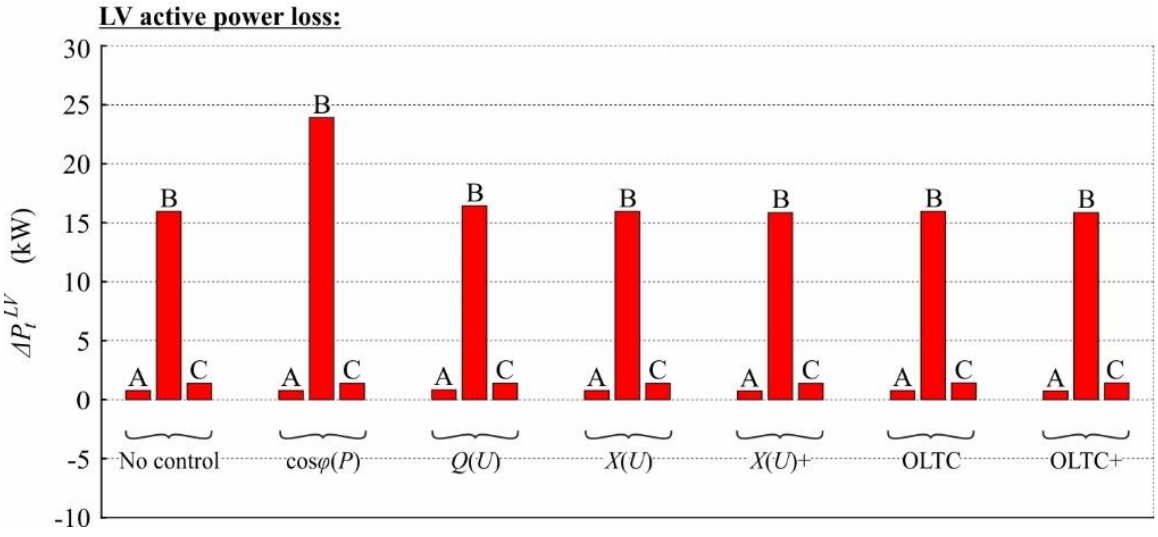

Fig. 3.70 Active power loss within the rural LV_Link-Grid for smoothed load profiles at the CP level, different cases, no control and various control strategies.

The impact of the different Volt/var control strategies on the DTR loading follows the same trend for smoothed as for spiky load profiles at the CP level. However, significantly higher values are observed for the former in cases A and C, Fig. 3.71. Compared to the cos$\varphi(P)$-control, which drastically increases the DTR loading in case B, the other control strategies have a marginal impact. In contrast to the $X(U)$-control, the $Q(U)$-control slightly increase the DTR

loading in all cases. Using an OLTC reduces the DTR loading in cases A and C. In any combination, *Q*-Autarkic CPs unload the DTR from their reactive power contributions.

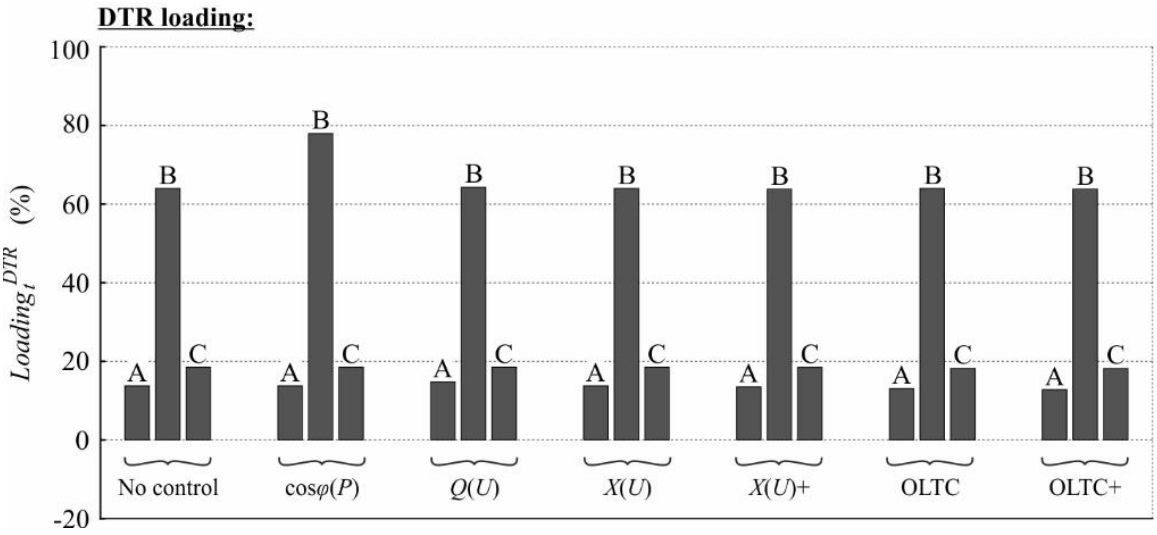

Fig. 3.71 DTR loading within the rural LV_Link-Grid for smoothed load profiles at the CP level, different cases, no control and various control strategies.

3.6.4 Medium voltage level

European medium voltage grids are three-phase and basically balanced. They are of meshed or radial structure, with the latter dominating rural installations. Each feeder includes numerous laterals with connected distribution substations (CIGRE 2014a). On the European average, they have a cable share of 41 % (Eurelectric 2013). Two real Austrian medium voltage grids – a large and a small one – are analysed for all investigated Volt/var control strategies.

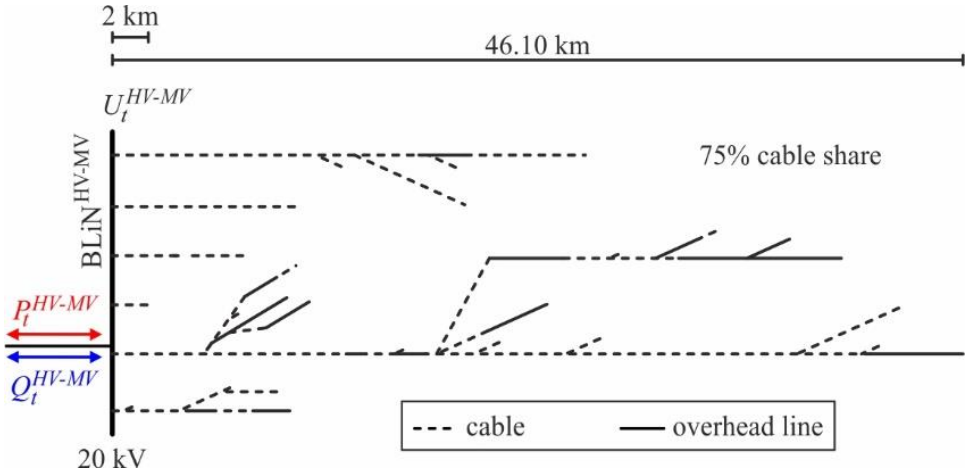

Fig. 3.72 Simplified one-line diagram of the large MV_Link-Grid.

3.6.4.1 Model specification

Fig. 3.72 shows a large MV_Link-Grid, which includes six feeders with a total line length of 267.151 km and a cable share of 74.66 %. While the shortest feeder is 2 km in length, the longest one reaches 46.10 km. It is operated with a nominal voltage of 20 kV. In total, the feeders connect 143 commercial and two big industrial CP_Link-Grids, as well as 45 rural and 11 urban LV_Link-Grids. Furthermore, 15 hydroelectric power plants with maximal production capacities between 60 and 400 kW are connected along the feeders. They are simply modelled as PQ node-elements that constantly inject 70 % of their maximal active power production with unity power factor. Their upper and lower BVLs are set to 1.1 and 0.9 p.u., respectively. The supplying transformer is not included in the model.

3.6.4.2 Behaviour of MV_Link-Grid

The analysis of the CP and LV level has revealed the same trends in the Volt/var behaviour for both types of load profiles: Spiky and smoothed. Therefore, the MV level is calculated only for the smoothed load profiles at the CP level. The HV-MV power exchanges and the MV active power loss are analysed in detail. They are calculated without applying any Volt/var control and for the different control strategies.

Without any Volt/var control strategy

The boundary voltage limits at the $BLiN^{HV\text{-}MV}$ of the large MV_Link-Grid are drastically deformed, leaving only a small corridor of permissible voltages during the day, Fig. 3.73. Each point within the limit violation zones corresponds to violations of the connected elements' BVLs, i.e. commercial and industrial CPs directly connected to the MV_Link-Grid, hydroelectric power plants, and urban and rural LV_Link-Grids. The colours representing the HV-MV power exchanges and the active power loss blend into each other continuously. Strong coupling is found between the active power exchange and the limit curve deformation. The injection of active power into the HV level lowers the upper BVL to 0.9175 p.u. at midday. As a consequence, case B lies far within the upper limit violation zone. When high amounts of active power flow into the MV level, the lower voltage limit increases, reaching 1.0175 p.u. at 18:00. A strong time-dependency and weak voltage-dependency are observed for the power exchanges and the active power loss. The results clearly show that MV_Link-Grids with high PV penetration can hardly be operated in the traditional way, i.e. with OLTC in supplying substation and without additional Volt/var control strategies applied in LV and/or CP level.

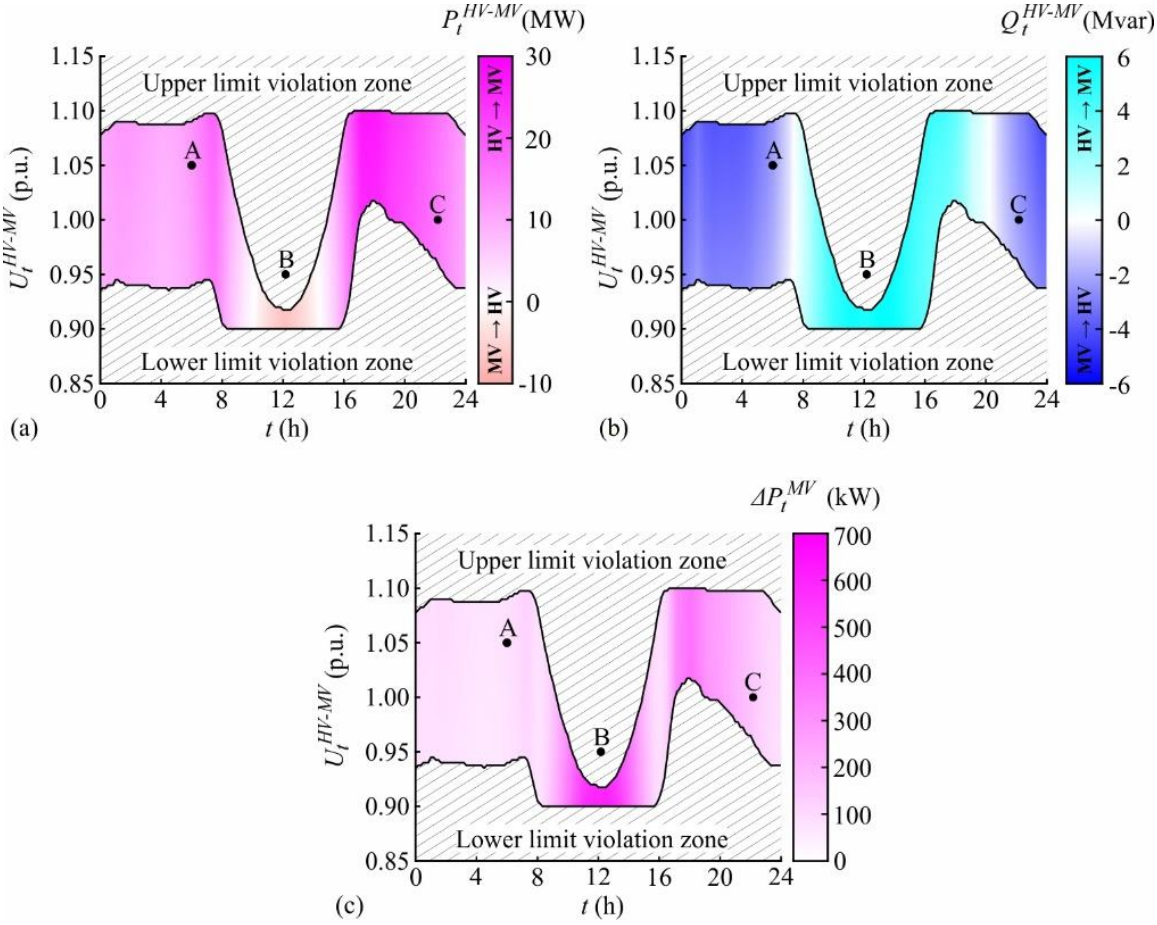

Fig. 3.73 Daily behaviour of the large MV_Link-Grid without any Volt/var control for various voltages at the HV-MV boundary node and smoothed load profiles at the CP level: (a) HV-MV active power exchange; (b) HV-MV reactive power exchange; (c) MV active power loss.

The MV_Link-Grid injects active power into the HV level from 10:15 to 13:59 and absorbs one before and after this interval. In case A and C, 12.22 and 15.21 MW flow from the HV into the MV level, respectively, while in case B, 6.22 MW flow reversely. Meanwhile, the reactive power flows into the HV level at night-time, i.e. before 7:19 and after 20:12, amounting to 2.18 and 2.29 Mvar respective to cases A and C. In case B, the MV_Link-Grid absorbs 5.32 Mvar from the HV level. Relative high active power losses occur around midday and around 18:00. 83.11, 536.98 and 144.18 kW are lost in cases A, B and C, respectively.

Fig. 3.74 shows the corresponding voltage profiles for case B. Therein, the boundary nodes to the connected elements are marked by different symbols and colours: While black bullets are used to represent the boundary link nodes to the commercial and industrial CPs, the ones to the rural and urban LV_Link-Grids are marked by yellow and violet asterisks, respectively.

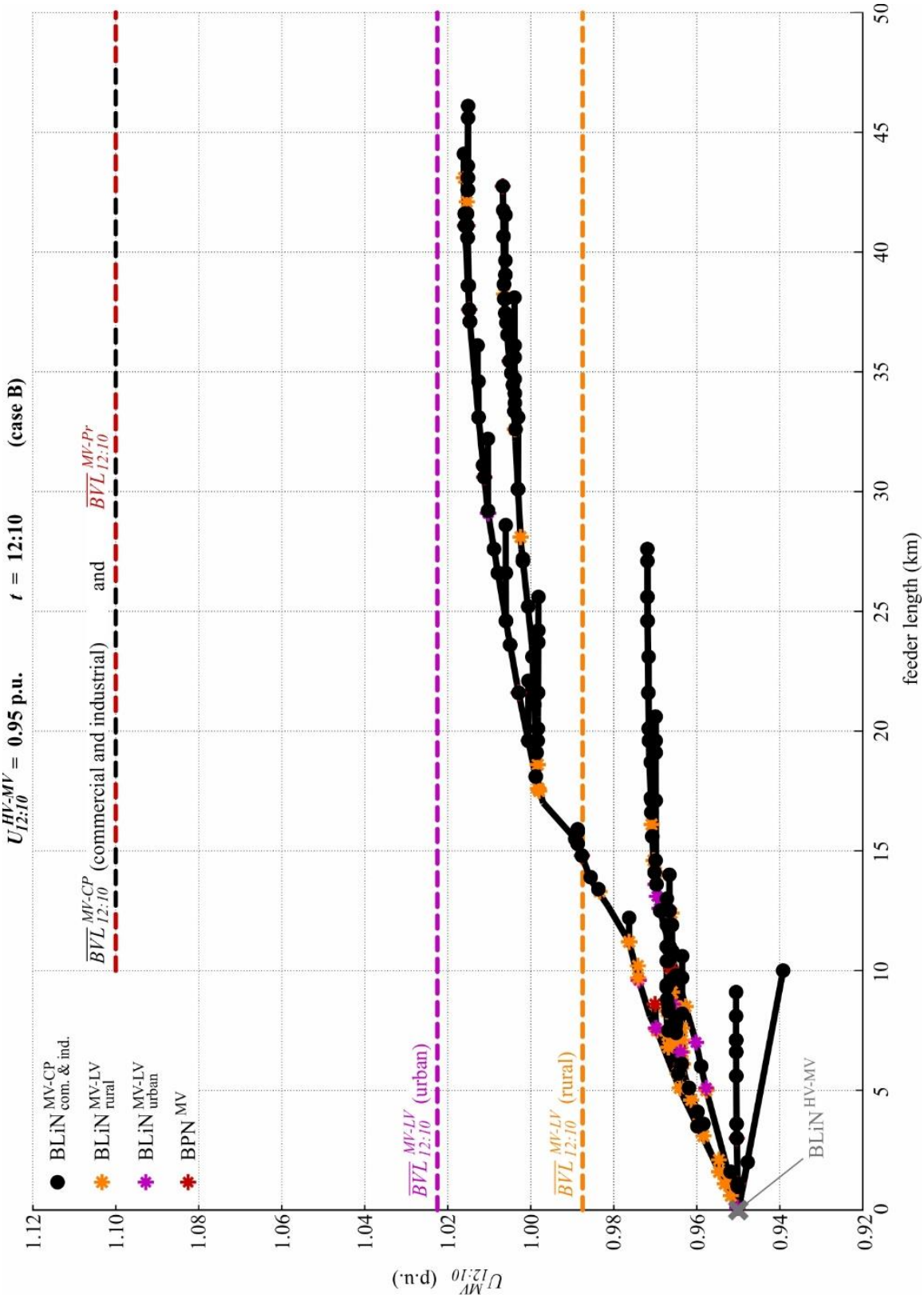

Fig. 3.74 Voltage profiles of the large MV_Link-Grid's feeders without any Volt/var control at 12:10 for an HV-MV boundary voltage of 0.95 p.u. (case B) and smoothed load profiles at the CP level.

The boundary producer nodes at which the hydroelectric power plants are connected are highlighted as red asterisks. Furthermore, the relevant boundary voltage limits are shown in the respective colours. The CPs and the hydroelectric power plants all have an upper boundary voltage limit of 1.1 p.u. throughout the complete time horizon. Meanwhile, the BVLs of the rural and urban LV_Link-Grids vary over time, restricting the maximal MV-LV boundary voltage to 0.9875 and 1.0225 p.u. at 12:10, respectively (see Fig. A.31 and Fig. A.40 in §A.1.2). The voltages increase along the feeders, reaching 1.0161 p.u. close to the end of the longest feeder. In these conditions, some of the $BLiN^{MV\text{-}LV}$ to the rural LV_Link-Grid violate their upper voltage limit. As a result, case B lies within the upper limit violation zone. Fig. 3.74 also shows that no LV_Link-Grids are connected to two relative short MV feeders. This should be kept in mind when comparing the different Volt/var control strategies: In contrast to the PV inverter based controls, the $X(U)$-control and the OLTC in distribution substation do not affect the voltage profiles of these MV feeders.

With Volt/var control strategies

The investigated Volt/var control strategies differently widen the permissible voltage band at the HV-MV boundary link node and differently affect the corresponding reactive power exchange, Fig. 3.75. Each control strategy eliminates the limit violations in case B. As observed at the LV level, the var controls deform the limits also at the MV level. Meanwhile, the parallel shifting effect of the Volt control is restricted by the fact that the commercial and industrial CPs and the hydroelectric power plants do not include transformers with OLTCs.

> All strategies except the $\cos\varphi(P)$ control compress both the upper and lower voltage limit violation zones. Only the var controls significantly modify the MV-LV reactive power exchange.

During the daytime, the $\cos\varphi(P)$-control provokes tremendous reactive power flows from HV into MV level, tightening the upper and widening the lower limit violation zone. It relaxes the upper voltage limit at midday to 1.0025 but does not ease the highly restricting lower BVL around 18:00. The reactive power flow amounts to 21.19 Mvar in case B. $Q(U)$-control affects the var exchange almost in the complete voltage-time-plane, compressing both the upper and lower violation zones significantly. At midday, the upper HV-MV boundary voltage limit of 0.965 p.u. remains relative restrictive. Meanwhile, the lower limit is considerably relaxed, reaching 0.9425 p.u. at 18:00. In cases A and B, the MV_Link-Grid draws 0.11 and 6.40 Mvar from the HV level, while in case C, it injects 2.59 Mvar.

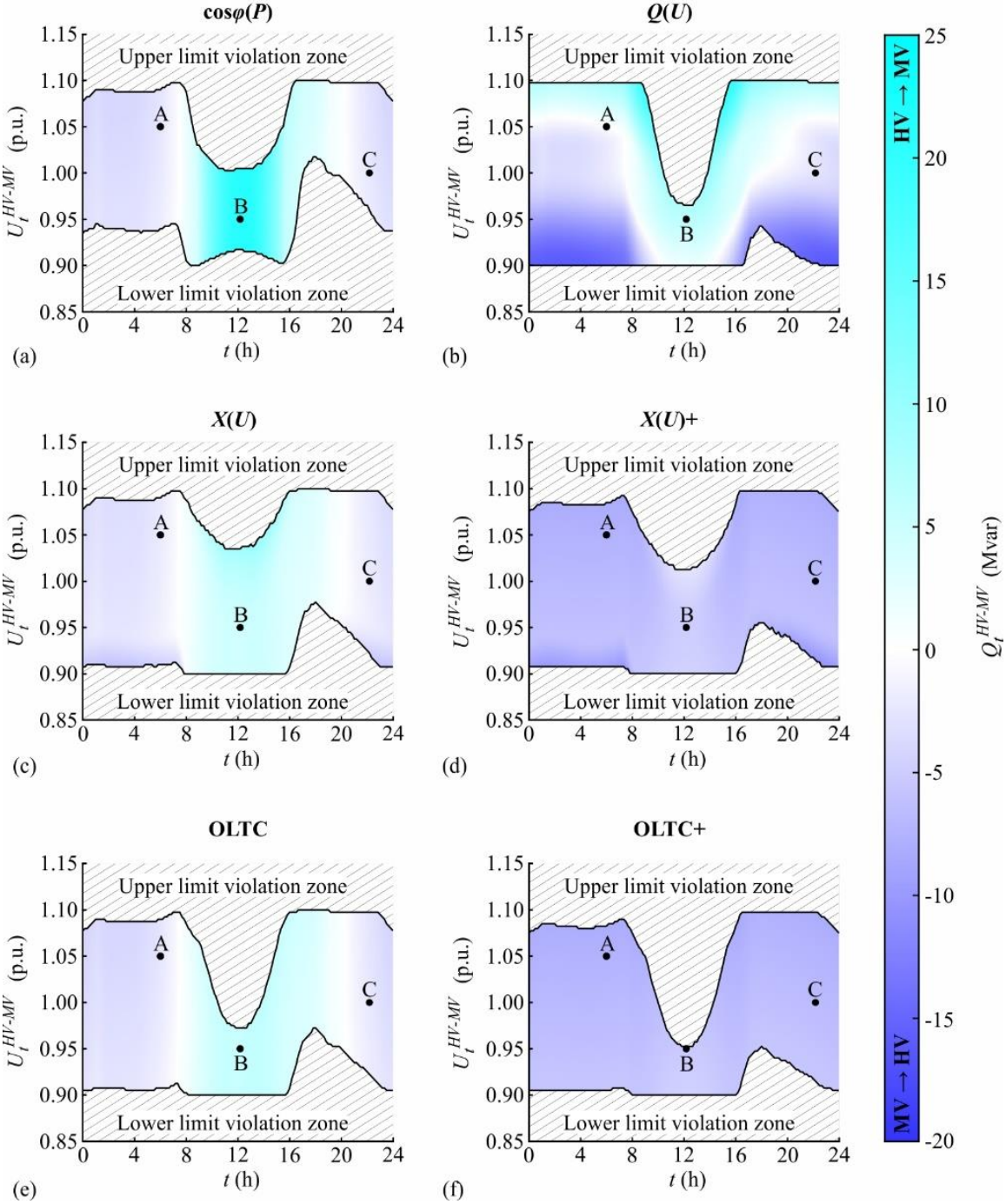

Fig. 3.75 Daily HV-MV reactive power exchange of the large MV_Link-Grid for various voltages at the HV-MV boundary node, smoothed load profiles at the CP level and different control strategies: (a) cosφ(P); (b) Q(U); (c) X(U); (d) X(U) and CP_Q-Autarky; (e) OLTC; (f) OLTC and CP_Q-Autarky.

The X(U)-control significantly widens the permissible voltage band at the HV-LV boundary link node during the complete time horizon by adding only small portions of reactive power. While the upper BVL is greatly relaxed around midday, the lower one remains relative

restrictive in the evening hours: Voltages up to 1.035 p.u. and down to 0.9775 p.u. are acceptable at midday and 18:00, respectively. The HV-MV reactive power exchange is insignificantly affected in cases A and C, while in case B, it is increased to 5.52 Mvar. The OLTC increases the upper and decreases the lower BVLs during the complete time horizon without changing the var behaviour considerably. However, both limits remain relative restrictive: Maximal and minimal HV-MV boundary voltages of 0.9725 p.u. are allowed at midday and 18:00, respectively. In cases A and C, 2.23 and 2.27 Mvar flow from the MV into the HV level. Meanwhile, 5.33 Mvar flow reversely in case B. Whether combined with $X(U)$-control or OLTC, the CP_Q-Autarky reduces the upper and lower BVLs. It intensifies the capacitive behaviour seen from the HV level in cases A and C and reverses the reactive power flow in case B. In the former combination, the MV_Link-Grid injects 7.48, 4.75 and 6.58 Mvar, respectively, while in the latter, it injects 7.48, 5.14 and 6.58 Mvar.

The Volt/var control strategies differ from each other in the active power loss they provoke in MV level, Fig. 3.76. Intensive losses result from the use of the $\cos\varphi(P)$-control around noontime, reaching 846.09 kW in case B. The $Q(U)$-control increases the active power loss for boundary voltages close to the lower limit and decreases it for boundary voltages close to the upper limit. This reduces the loss to 52.61 kW in case A and increases it to 538.54 and 149.24 kW cases B and C, respectively. While the $X(U)$-control does not significantly affect the losses in MV level, its combination with Q-Autarkic CPs increases them almost in the complete voltage-time plane. Losses of 121.45, 554.80 and 181.14 kW occur in cases A, B and C, respectively. The OLTC has a very low impact on the MV active power loss, provoking 81.92, 537.24 and 143.63 kW respective to cases A, B and C. When combined with CP_Q-Autarky, higher losses of 119.65, 572.32 and 180.34 kW occur in these cases.

Link-Grid behaviour for different control strategies and the specific cases

The MV_Link-Grid itself and the connected CP and LV_Link-Grids contribute reactive power, thus composing the HV-MV reactive power exchange. Meanwhile, the hydroelectric power plants do not produce and consume any reactive power. The compositions resulting in cases A, B and C strongly depend on the applied control strategy, Fig. 3.77. Due to its high cable share, the MV_Link-Grid generally produces significant amounts of reactive power. Especially in case B, this reactive power production is partly compensated by the reactive power losses in the MV lines' series impedances.

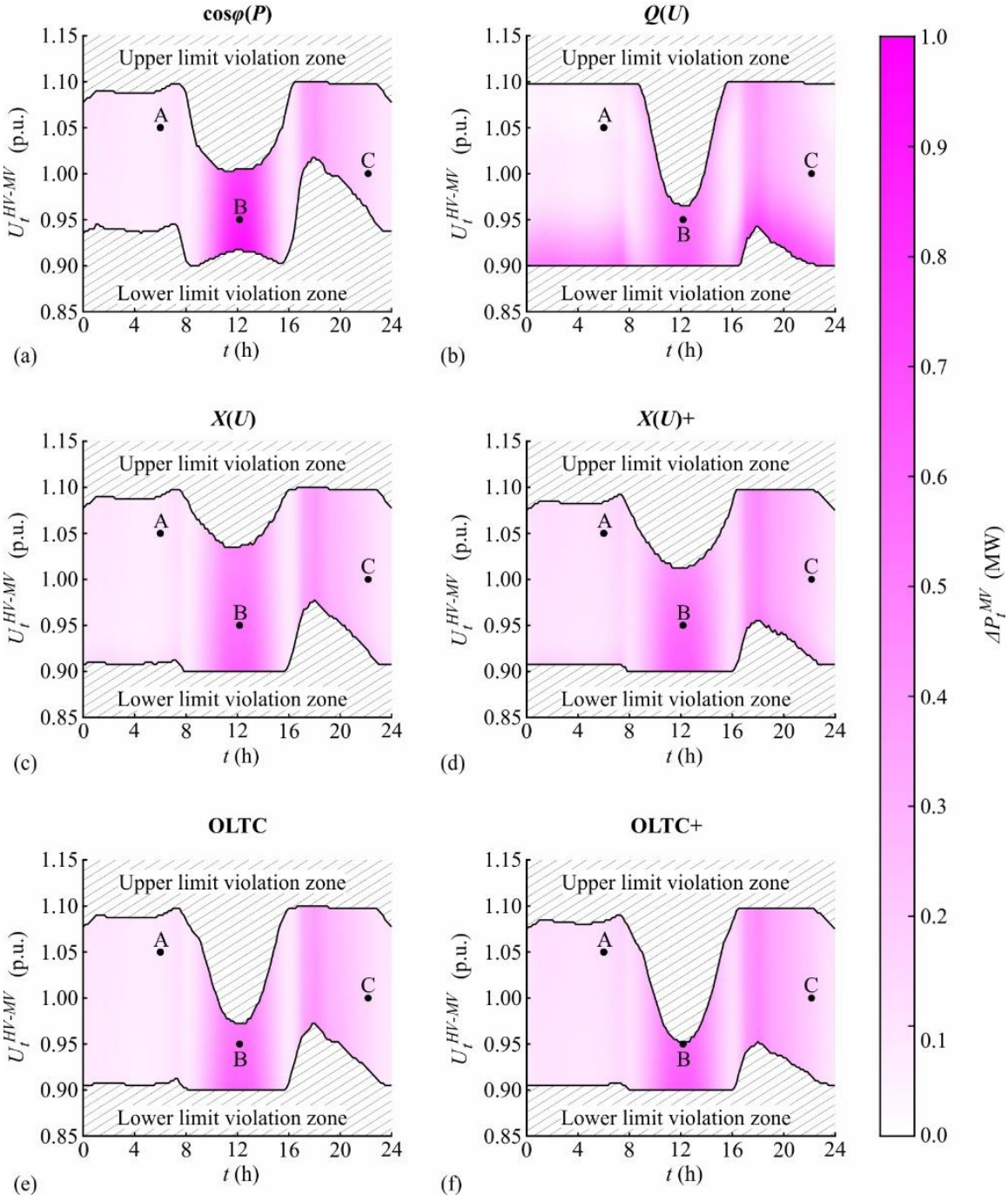

Fig. 3.76 Daily active power loss within the large MV_Link-Grid for various voltages at the HV-MV boundary node, smoothed load profiles at the CP level and different control strategies: (a) cosφ(P); (b) Q(U); (c) X(U); (d) X(U) and CP_Q-Autarky; (e) OLTC; (f) OLTC and CP_Q-Autarky.

When no Volt/var control is applied, the connected CPs draw reactive power from the MV level in any case. The LV_Link-Grids absorb relative low amounts of reactive power in cases A and B, while in case C, they behave slightly capacitive and inject reactive power. The reactive power consumption is overcompensated in cases A and C, leading to a capacitive behaviour of the

whole distribution grid at the HV-MV boundary node. This behaviour is changed into an inductive one by the large consumption of the CPs and LV_Link-Grids in case B. The use of cosφ(P)-control drastically increases the reactive power contributions of the CP and especially the LV_Link-Grids in case B. Tremendous amounts of reactive power are absorbed from the HV level. Q(U)-controlled PV inverters increase the reactive power consumption of the CPs in case A and decrease it in case B; No significant modification occurs in case C. Furthermore, they intensify the reactive power contribution of the LV_Link-Grids in all cases. The X(U)-control does not significantly affect the reactive power composition in cases A and C, while in case B, it slightly increases the reactive power absorption of LV_Link-Grids. This reduces the voltages in MV level and thus the reactive power consumption of the connected CPs. Meanwhile, the OLTC in the distribution substation has a very low impact on the Q-composition at the MV level. In both combinations, the Q-Autarky eliminates the relative large reactive power consumption of the commercial and industrial CPs, drastically changing the overall system behaviour. It also reduces the reactive power contributions of the LV_Link-Grids in all cases, reversing MV-LV reactive power exchange in case C in total.

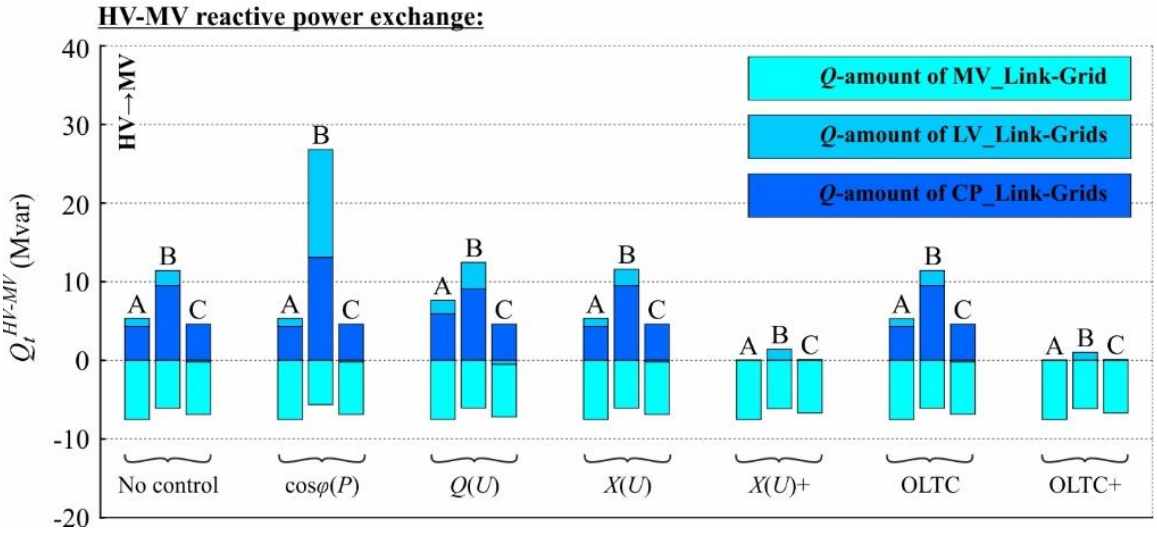

Fig. 3.77 Composition of the HV-MV reactive power exchange of the large MV_Link-Grid for smoothed load profiles at the CP level, different cases, no control and various control strategies.

The different Volt/var control strategies provoke different active power losses in MV level, Fig. 3.78. Due to the intensive power transfer, relatively high losses prevail in case B, while lower ones occur in case C and especially in case A.

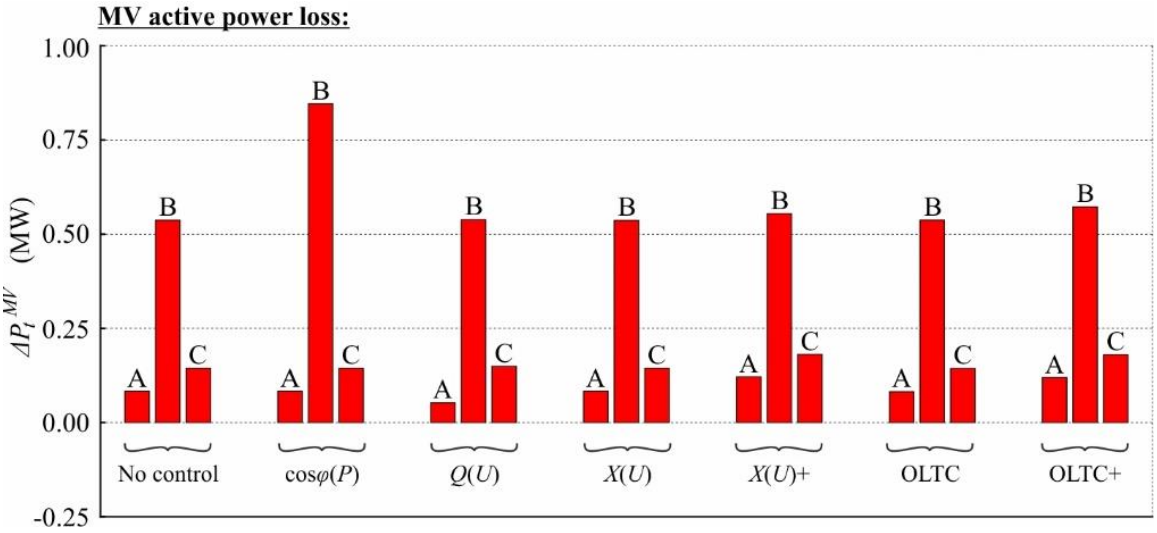

Fig. 3.78 Active power loss within the large MV_Link-Grid for smoothed load profiles at the CP level, different cases, no control and various control strategies.

The cosφ(P)-control considerably intensifies the loss in case B, as it drastically increases the reactive power flows through the MV lines. Meanwhile, the Q(U)-control partly compensates the reactive power production of the MV lines in case A, thus reducing the reactive power flows in MV level and the associated active power loss. Both the X(U)-control and the OLTC do not significantly affect the losses in all cases. Their combinations with CP_Q-Autarky increase the MV active power loss.

3.7 Evaluation of Volt/var control strategies

The comprehensive analysis conducted in §3.6 provides deep insights into the technical performance of the Volt/var control strategies applied at the LV and CP level. Volt/var control of producers connected in MV level is not investigated. However, the large number of simulation results makes it hard to recognise each control strategy's strengths and weaknesses at a glance. Social aspects, such as data privacy and discrimination, are not considered. This section provides a clear comparison of the Volt/var control strategies by evaluating them against various technical and social criteria. The evaluation results are visualised for both LV_Link-Grids, which are catalogued in §A.1.2, within separate evaluation hexagons.

3.7.1 Evaluation procedure

The compact comparison of the control strategies requires the specification of the relevant criteria and their visualisation within the hexagon. Both are roughly described in §3.7.1.1 and §3.7.1.2. The exact calculation formulas are given in §A.3.

3.7.1.1 Evaluation criteria

The performance of the different control strategies is assessed by means of technical and social criteria. While the technical ones are calculated based on the simulation results, the social ones are analysed qualitatively.

Technical criteria

- **Voltage limit violations**: The purpose of the investigated Volt/var control strategies is to mitigate violations of the stipulated voltage limits of ±10 % around the nominal value. This impact is assessed using the voltage limit Violation Index (VI), which penalises limit violations at the LV level by considering the number of violating nodes and the corresponding voltage values.
- **MV-LV reactive power exchange**: The impact of the control strategies on the reactive power flow through the MV-LV boundary node is assessed by means of the reactive energy exchange. The flow direction is not considered for the calculation.
- **Active power loss**: Each control strategy provokes distinct active power losses within the grid. This impact is evaluated based on the energy loss at the LV level.
- **DTR loading**: The control strategies modify the DTR loading. This impact is assessed by calculating the average loading of the DTR.

The technical criteria are calculated for the (U,t)-plane spanned by the simulated time horizon of 24 hours and by the MV-LV boundary voltages between 0.9 and 1.1 p.u. This plane is shown in Fig. 3.79 and is denoted as ‘Evaluation zone’.

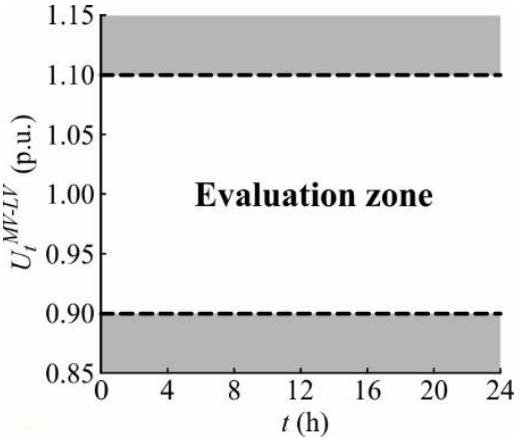

Fig. 3.79 Zone within the (U,t)-plane used to calculate the technical evaluation criteria for all simulations in LV level.

Social criteria

- **Discrimination**: Per definition, all individuals within a non-discriminatory society have an equal and fair prospect to access the available opportunities. In power system operation, an opportunity for customers, storage- and producer-operators is to provide reactive power as an ancillary service to support the grid operation. To promote freedom from discrimination in power system operation, (Directive EU 2019/944) directs DSOs to procure the non-frequency ancillary services needed for their systems according to transparent, non-discriminatory, and market-based procedures. In this sense, the applied control strategy should enable all stakeholders an equal and fair prospect to offer reactive power. The discrimination criterion is set to one when the reactive power contribution duty is divided unequally between the customers, and otherwise, it is set to zero.
- **Data privacy**: The privacy of each individual, customer and company is inviolable. The applied control strategy should enable the coordination of the underlying control variables with minimal data exchanges through external interfaces to protect data privacy. The data privacy criterion is set to one when data exchanges through the LV-CP interfaces are necessary to coordinate the control variables, and otherwise, it is set to zero.

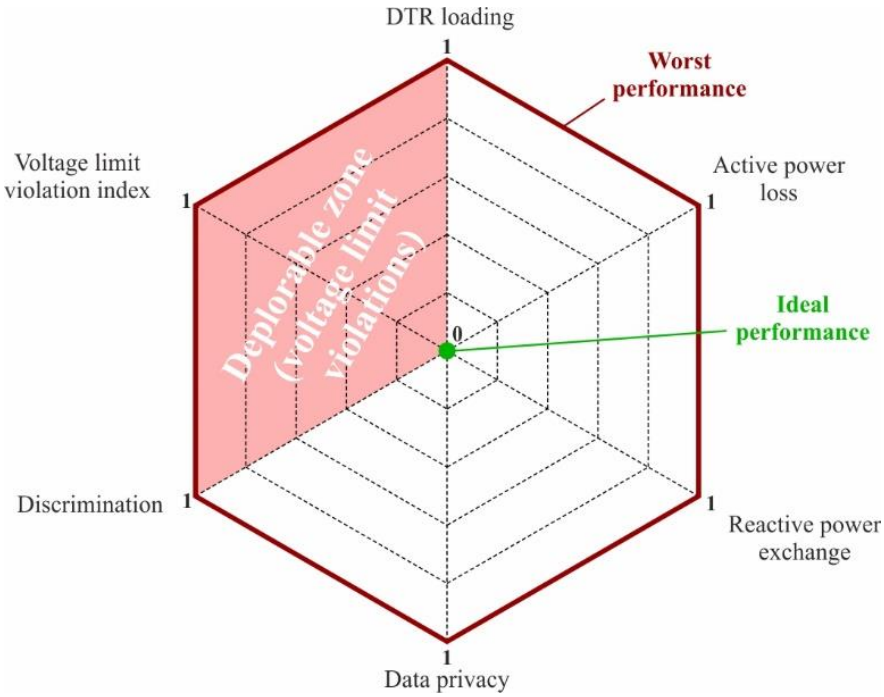

Fig. 3.80 Evaluation hexagon with the worst and ideal performance of the control strategies.

3.7.1.2 Result visualisation

The visualisation within the evaluation hexagon requires further processing of the calculated technical criteria (see §A.3.2). The calculated values of the evaluation criteria are normalised to eliminate their physical units and lie within the interval [0, 1].

Fig. 3.80 shows the evaluation hexagon with the worst and ideal performance of the control strategies. On its corners are set the evaluation criteria. A completely filled area indicates the worst performance, and the ideal one corresponds to a point in the middle of the chart. Violations of the voltage limits offend against the law. Thus, they are unacceptable. The corresponding zone within the evaluation hexagon is highlighted in red.

3.7.2 Evaluation results

The voltage limit violation index is the most critical technical evaluation criterion. It is shown in Fig. 3.81 for the rural and urban LV_Link-Grids and the investigated control strategies. The violation index is always higher in the rural LV_Link-Grid than in the urban one.

A clear trend is observed in both Link-Grids. All control strategies mitigate the excessive voltage limit violations that occur without any Volt/var control. However, relative high violation indices remain when cosφ(P)-control is used, which is mainly caused by its inability to mitigate the lower voltage limit violations. In comparison, lower but still significant violation indices result from $Q(U)$-control. The OLTC provokes relative low voltage limit violation indices compared to the cosφ(P)- and $Q(U)$-control, especially within the urban LV_Link-Grid. The lowest violation indices are reached in both LV_Link-Grids when $X(U)$-control is used. Combining the OLTC and the $X(U)$-control with the CP_Q-Autarky slightly increases the corresponding violation indices.

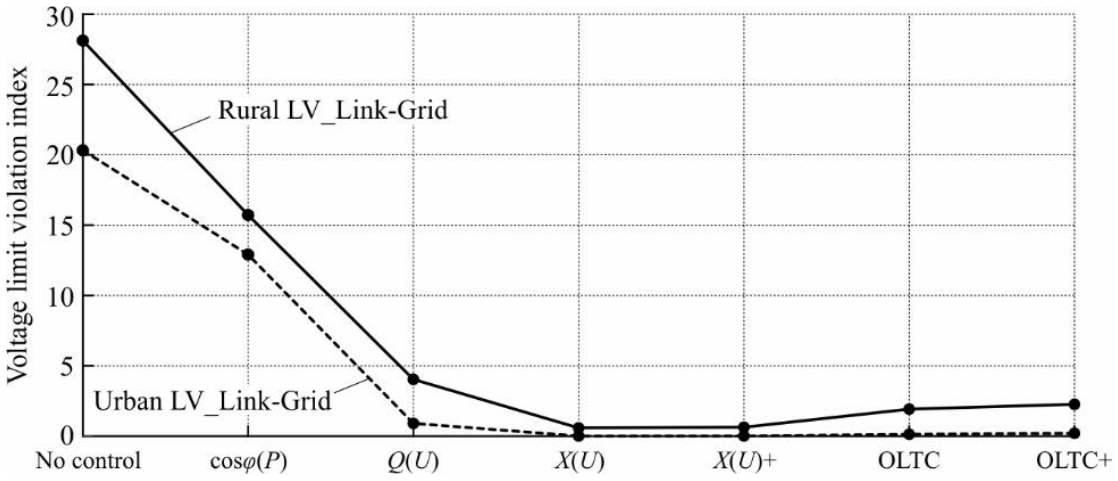

Fig. 3.81 Voltage limit violation index for the rural and urban LV_Link-Grids and different control strategies.

Fig. 3.82a and b show the evaluation hexagons for the rural and urban LV_Link-Grids separately. Different colours and line types present the control strategies: Solid lines in yellow, orange, green, purple and grey are used for cosφ(P), Q(U), X(U), OLTC in distribution substation, and for the setup without any Volt/var control, respectively. The combinations of X(U) and OLTC with Q-Autarkic CPs are shown by dashed lines in lighter shades of the corresponding colours. They are designated as 'X(U)+' and 'OLTC+', respectively.

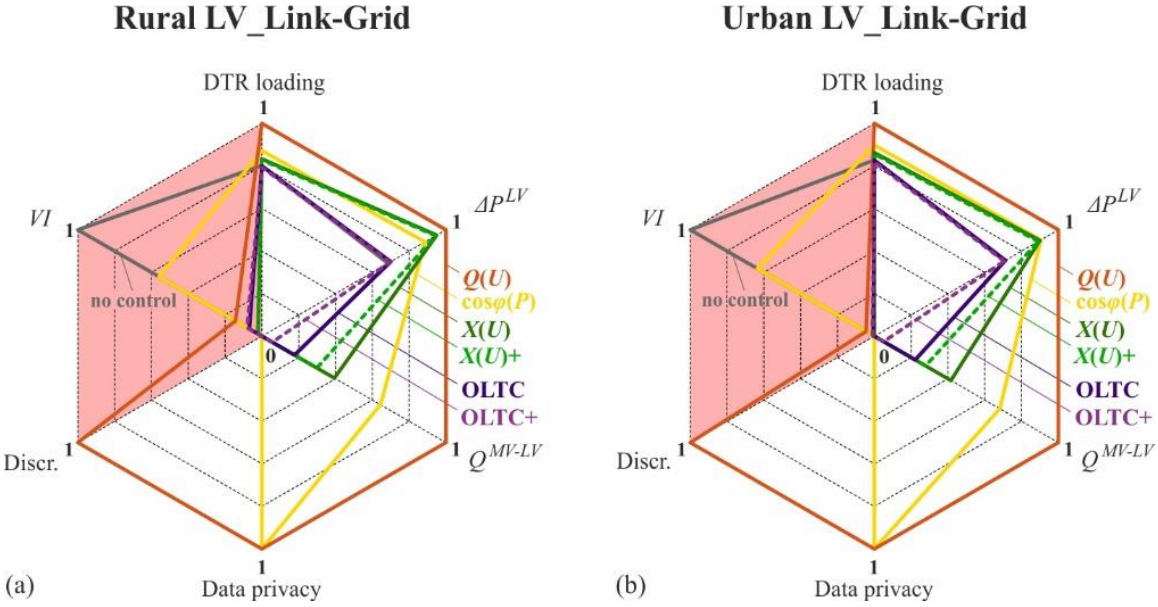

Fig. 3.82 Evaluation hexagons of Volt/var control strategies for different LV_Link-Grids: (a) Rural; (b) Urban.

While clear trends are observed in both LV_Link-Grids for the voltage limit violation index, the DTR loading and the MV-LV reactive power exchange, none is found for the active power loss. cosφ(P)-control provokes an unacceptably high voltage limit violation index. Furthermore, a relative high DTR loading, active power loss, and MV-LV reactive power exchange appear. It does not guarantee data privacy but avoids discriminatory ancillary service procurement. The highest DTR loading, active power loss and MV-LV reactive power exchange occur when Q(U)-control is used. It leaves significant violations of the voltage limits, and neither supports data privacy nor non-discriminatory ancillary service procurement. X(U)-control eliminates almost all voltage limit violations while increasing the DTR loading and MV-LV reactive power exchange to a moderate extent. It provokes a relative high active power loss while preserving data privacy and freedom of discrimination. Its combination with CP_Q-Autarky significantly reduces the MV-LV reactive power exchange. The active power loss and DTR loading are slightly reduced, and a few more violations of the voltage limits appear. The use of OLTCs in the distribution substations results in a considerable voltage limit violation index

within the rural LV_Link-Grid. Compared to the other control strategies, it modifies the DTR loading, the active power loss and the MV-LV reactive power exchange only insignificantly. Data privacy is preserved, and the customers are not discriminated. Its combination with *Q*-Autarkic CPs significantly decreases the MV-LV reactive power exchange and slightly increases the voltage limit violation index. Furthermore, the DTR loading and active power loss are marginally reduced.

Due to its inability to mitigate violations of the lower voltage limit, the cosφ(*P*)-control should not be used for voltage control at the LV level.

Fig. 3.83 shows the common evaluation hexagon of Volt/var control strategies. It is calculated by superimposing the results of both LV_Link-Grids (see §A.3.2). The cosφ(*P*)-control is excluded from the diagram as it is ineligible for voltage control at the LV level.

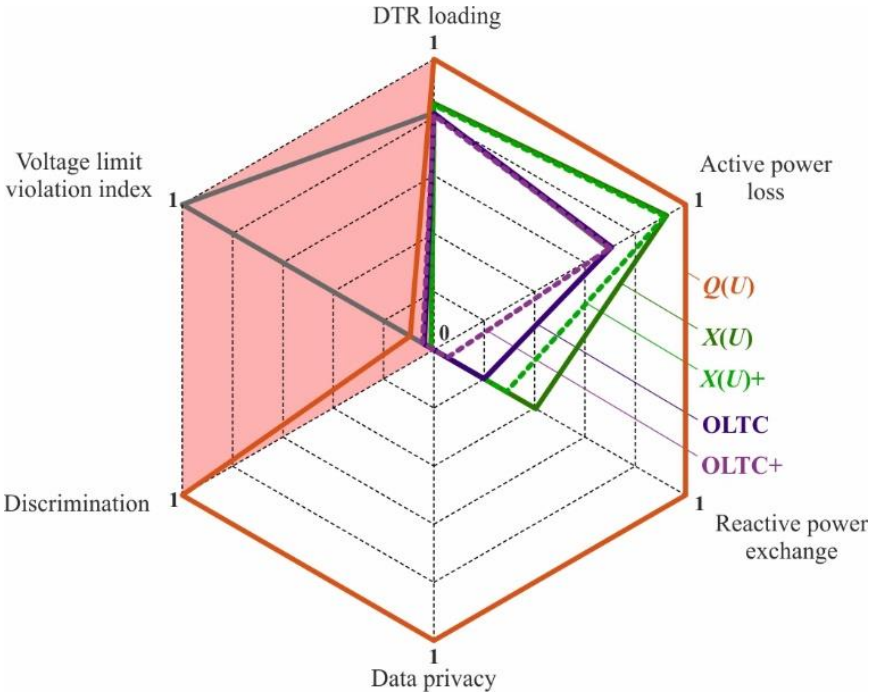

Fig. 3.83 Common evaluation hexagon of Volt/var control strategies.

The *Q*(*U*)-control leaves significant voltage limit violations and provokes excessive DTR loading, active power loss and MV-LV reactive power exchange. It does neither support data privacy nor non-discriminatory ancillary service procurement. Compared to *Q*(*U*), the OLTC and its combination with *Q*-Autarkic CPs have better voltage regulation ability. It provokes lower DTR loading, active power loss and MV-LV reactive power exchanges; And guarantees data privacy and freedom from discrimination. *X*(*U*)-control is the most reliable solution to maintain voltage limit compliance. It eliminates almost all limit violations while provoking

relative low DTR loadings, active power losses and MV-LV reactive power exchanges. Its combination with CP_*Q*-Autarky slightly impairs limit compliance while reducing the MV-LV reactive power exchange significantly.

3.8 Volt/var control chain setup in Y-axis

The design of the Volt/var chain control most suitable for a specific vertical power system axis is a complex topic that requires the close integration of planning and operation. Implementing automation and communication or installing new control devices increases the electrical infrastructure utilisation and causes additional costs. Depending on the prevalent conditions, this may increase or decrease the total system costs. Careful analysis must ensure an adequate trade-off between hardware-, automation- and communication-related expenditures already in the planning stage. Due to each vertical power system axis's distinct characteristics, design recommendations can only be made on a very general level. The general guideline on how to set the Volt/var chain control is given in §3.8.1. To facilitate the setting process, §3.8.2 analyses the impact of Compensating Device (CD) placement on the effectiveness of the Volt/var chain control in a theoretical distribution grid. §3.8.3 presents the Volt/var chain control setup procedure for the vertical axis, including MV, LV, CP, and consuming device level.

3.8.1 General guideline

Vertical power system axes are very complex in nature as they include the complete fractal set of smart grids (Ilo 2019). Their ramified structures interconnect millions of customer plants and numerous producers and storages owned and operated by different stakeholders. Meanwhile, compliance to the operational limits and the optimal use of the existing infrastructures is of utmost importance for utilities. These conditions give rise to several basic requirements on the Volt/var chain control design:

- **Reliability**: The solution shall guarantee voltage limit compliance during normal system operation
- **Efficiency**: The solution shall provide energy efficiency by dynamic optimisation.
- **Social compatibility**: The solution shall preserve the interests of all involved stakeholders, including non-discriminatory market access and data privacy.
- **Economy**: The solution shall represent an appropriate trade-off between hardware-, automation- and communication-related expenditures.

The Volt/var chain control is derived from the generalised form described in §3.5.2. The following should be considered:

- **Control the reactive power flow through external boundary nodes**
  LINK-Smart Grids consists of numerous Links that are owned and operated by different stakeholders. They are interconnected via external boundary nodes and interfaces. Each Grid-Link operator should maintain voltage limit compliance in its Grid-Link or Grid-Link-bundle by controlling the reactive power exchanges with the neighbouring external Links.
- **Minimisation of the number of control units**
  The reduction of capital and operational expenditures of the Volt/var chain control is directly related to the number of control units. Based on the fractal dimension analyses (Ilo 2019), the Smart Grids' realisation requires the highest global resources in CP and LV levels. The focus is minimising the number of control units in those levels by using an appropriate Volt/var control chain strategy.
- **Selection of the appropriate Volt/var control strategy in the Grid-Link chain**
  The selection of an appropriate Volt/var control strategy for each Grid-Link is possible through a holistic analysis of the control chain. The general description of the Volt/var control chain creates the basis for its analyses and design (see §3.5.2).

3.8.2 Reactive power compensation in the vertical axis

Generally, the var contributions of shunt-connected RPDs, producers and storages are controlled for two distinct purposes: Voltage support and load compensation. Both aspects must be considered to design the effective control ensemble, which maintains voltages with minimal reactive power flows. Distributed and concentrated var contributions are used to maintain voltage limit compliance throughout the grid (see §3.5.3.1). They provoke reactive power flows that are compensated by elements connected somewhere within the grid. Both the choice between distributed and concentrated var contributions and the placement of the compensating devices significantly affect the resulting effectiveness of the control ensemble.

From a physical point of view, the total reactive power contribution of all elements within an isolated power system is always balanced. As a consequence, the reactive power used to maintain voltages at the LV level must be compensated by other elements connected somewhere within the system. Distinct operators often manage the different grids, so the controllability of the corresponding *Q*-exchanges is of great interest. The standardised structure of the *LINK*-Architecture allows applying load compensation, which is traditionally used at the device level or in industrial CPs (see §3.1.3.1), to any Grid-Link within the vertical power system axis, i.e. HV, MV, LV and CP_Grid-Link. The latter case is described in §3.5.3.3. The

impact of load compensation at the MV and LV level on the effectiveness of the resulting Volt/var control ensemble is analysed in this section.

The setups used to study this impact are shown in Fig. 3.84 and Fig. 3.85. They include detailed models of an 18.5 MVA STR with its tap changer fixed in mid-position, a 24 km MV cable feeder, and 32 equal LV_Link-Grids, each connecting 61 Q-Autarkic residential Customer Plants (CP). The LV grid is a real rural grid with four feeders where local $X(U)$-control (see §3.5.3.2) is applied at the two longest feeders. The $X(U)$ local controls provoke the concentrated var contributions required to maintain the voltage at their connection points between 0.91 and 1.09 p.u. The HV grid is modelled as an ideal voltage source (slack) with nominal voltage. All CPs contribute the same active power P^{CP} and no reactive power.

In Fig. 3.84a, no compensating devices are installed at the LV and MV level that compensate for the reactive power flows. Reactive power is exchanged between HV, MV and LV level. In the other cases, compensating devices are applied that compensate for the reactive power exchanges between the different grid levels. In Fig. 3.84b, the device is connected to the secondary bus of the STR, compensating the reactive power flow at the STR primary side. The compensation of the reactive power exchange between LV and MV level is also investigated. Therefore, in each of the 32 distribution substations, the compensating device is connected to the primary (Fig. 3.85a) and secondary bus (Fig. 3.85b) of the DTR, respectively. In both cases, they compensate for the reactive power flow at the DTR primary side.

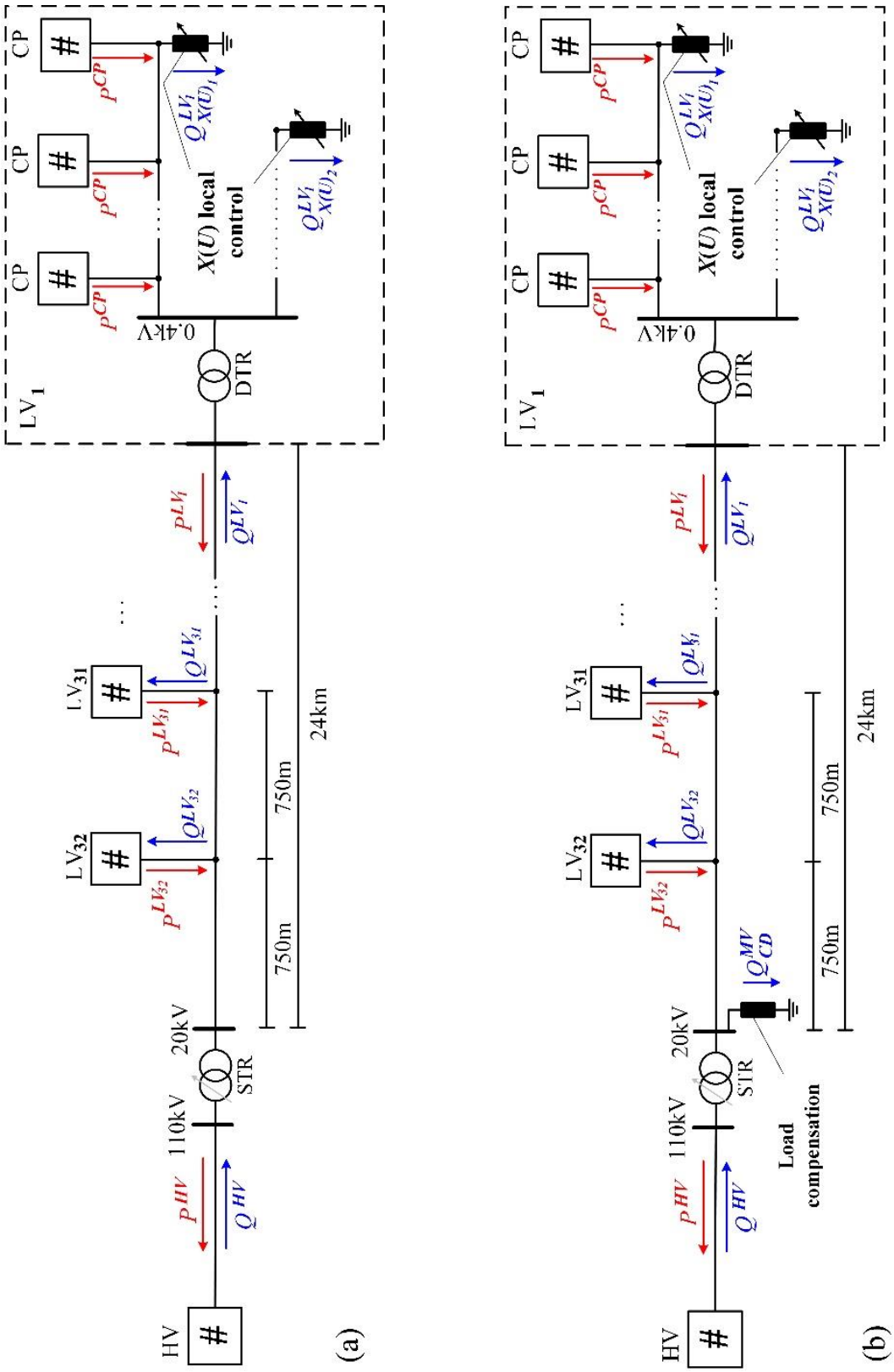

Fig. 3.84 Setups used to analyse the impact of CD placement on the effectiveness of the Volt/var control ensemble: (a) No CDs; (b) CD at STR secondary bus.

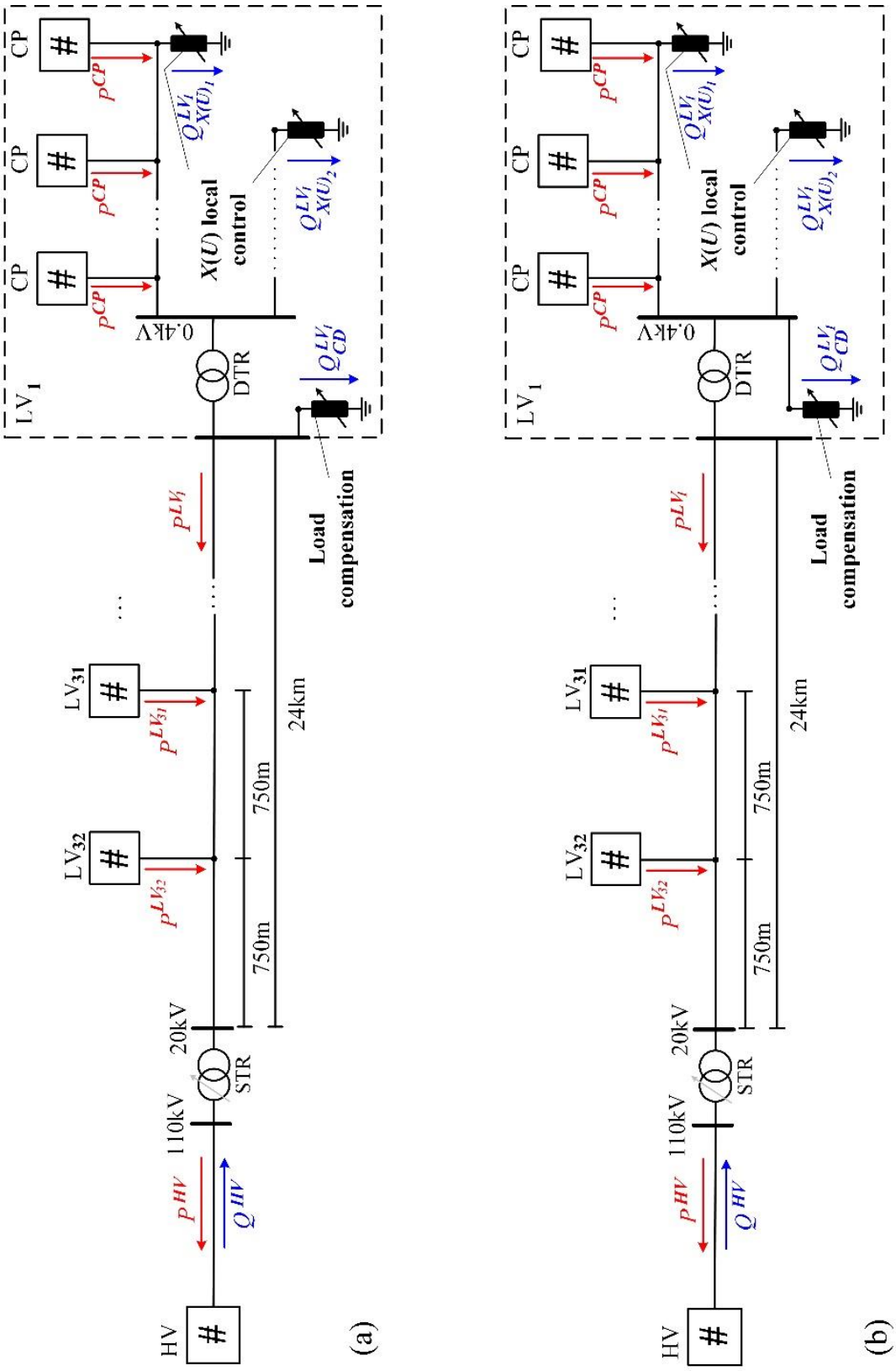

Fig. 3.85 Setups used to analyse the impact of CD placement on the effectiveness of the Volt/var control ensemble: (a) CDs at DTR primary buses; (b) CDs at DTR secondary buses.

Load flow simulations are conducted in each setup for gradually increasing values of P^{CP}. The effectiveness of the resulting Volt/var control ensemble is assessed for the different setups based on three criteria:

- The total reactive power contribution $Q^{\Sigma}_{X(U)}$ of all X(U) local controls, calculated according to Equation (3.46).

$$Q^{\Sigma}_{X(U)} = \sum_{i=1}^{32} \left(Q^{LV_i}_{X(U)_1} + Q^{LV_i}_{X(U)_2} \right) \tag{3.46}$$

- The total reactive power contribution Q^{Σ}_{CD} of all compensating devices, calculated according to Equations (3.47a), (3.47b) and (3.47c), for the setups without CDs, with one CD at the STR secondary bus, and with one CD in each distribution substation, respectively.

$$Q^{\Sigma}_{CD} = 0 \tag{3.47a}$$

$$Q^{\Sigma}_{CD} = Q^{MV}_{CD} \tag{3.47b}$$

$$Q^{\Sigma}_{CD} = \sum_{i=1}^{32} Q^{LV_i}_{CD} \tag{3.47c}$$

- The voltage profiles of the MV and LV feeders.

Fig. 3.86a shows the total reactive power contributions of all compensating devices as functions of P^{CP}.

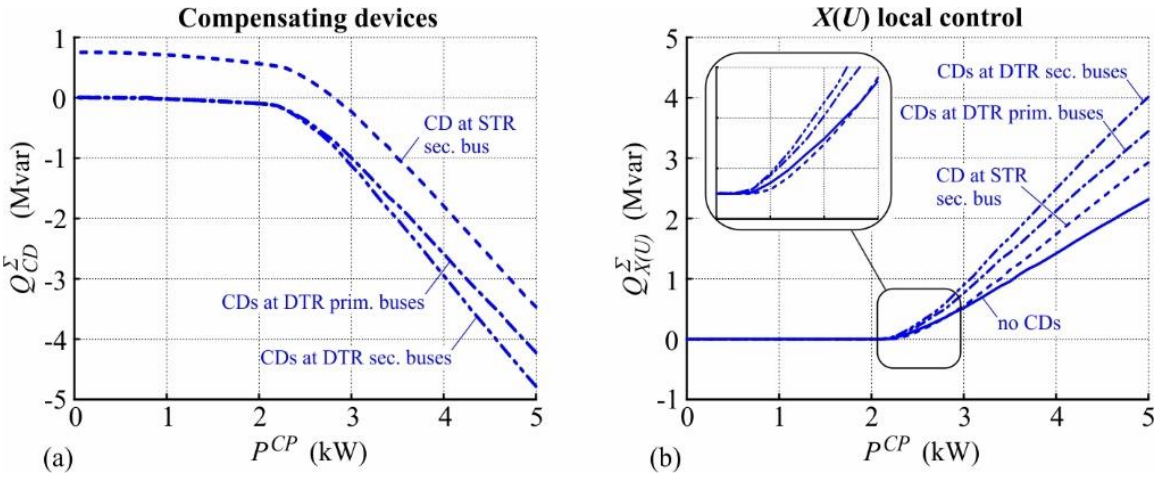

Fig. 3.86 Total reactive power contribution of different control devices: (a) Compensating devices; (b) Voltage maintaining devices.

For active power injections below 2.81 kW per CP, the CD connected at the STR secondary bus consumes reactive power to compensate for the *Q*-production of the MV cables. For higher *P*-injections, it produces reactive power to meet the remaining demand of the connected LV

grids. The CDs located in the distribution substation produce insignificant amounts of reactive power for $P^{CP} < 2.2$ kW to compensate for the losses at the LV level. Their Q-production drastically increases for greater P-injections, especially if they are connected at the DTR secondary side. The $X(U)$ local controls consume reactive power to push down the voltages when the active power injection per CP exceeds 2.1 kW, Fig. 3.86b. For P-injections above 2.81 kW, the Q-production of the CDs increases the amount of reactive power required to maintain acceptable voltages, especially if they are placed close to the $X(U)$s. For P-injections between 2.1 and 2.81 kW, the reactive power consumption of the CD located in supplying substation slightly reduces the consumption of the corresponding $X(U)$s.

The voltage profiles of the MV and LV feeders are shown in Fig. 3.87 and Fig. 3.88 for the different CD placements and active power injections of 5 kW per CP. A clear trend is observable at first glance: The closer the compensating devices and $X(U)$s are placed together, the lower is the resulting margin to the upper voltage limit. In Fig. 3.87 and Fig. 3.88a, the voltage drop over the DTR appears as a discontinuity in the profile, as the DTRs are associate with zero length. When the CDs are located at the DTR secondary buses, the reactive power flows through the DTRs are almost compensated, reducing the corresponding voltage drops significantly. As a result, maintaining acceptable voltages is aggravated. All in all, the following trend is observed:

> The closer the compensating devices and $X(U)$s are placed together, the less effective is the resulting Volt/var control ensemble.

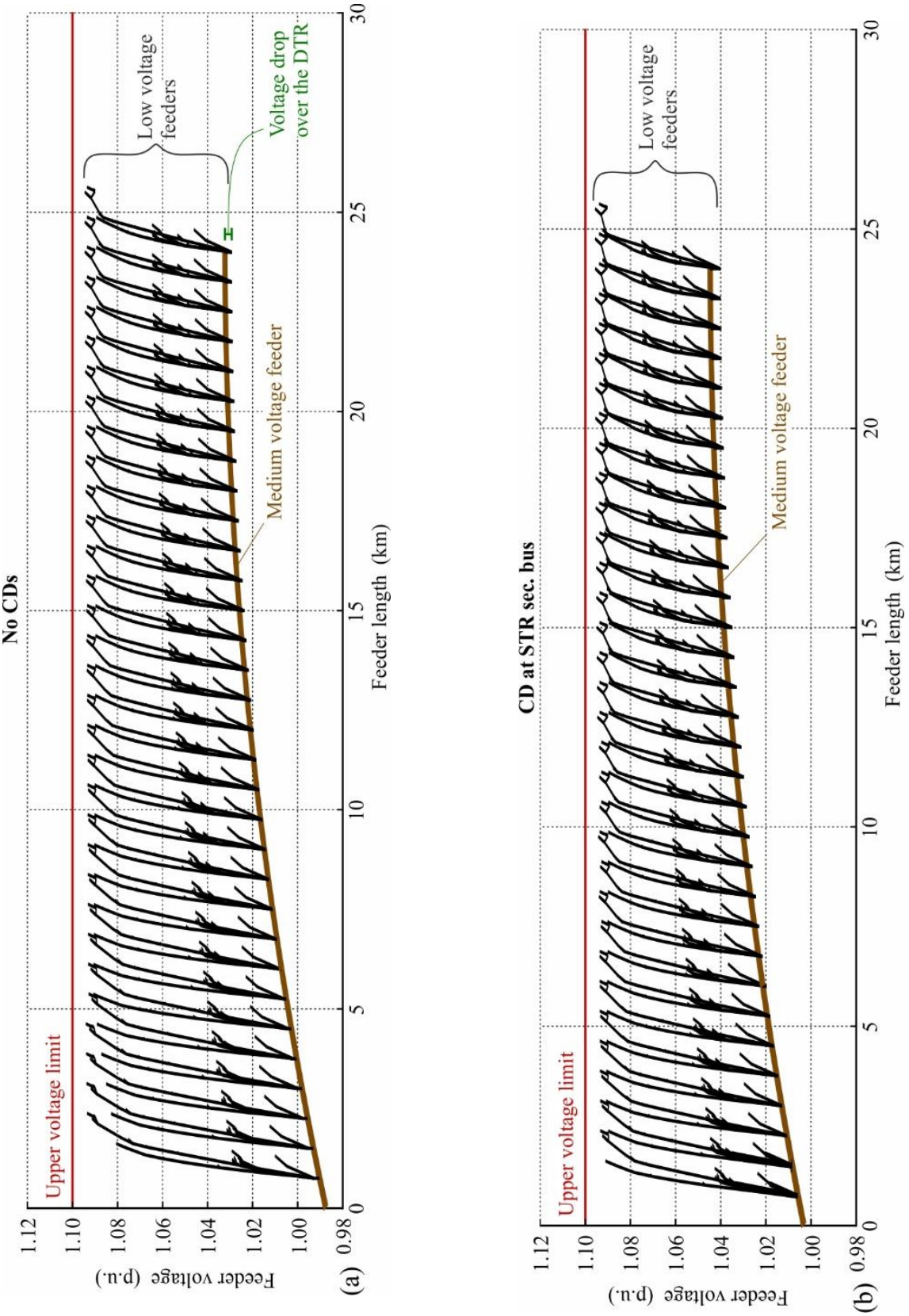

Fig. 3.87 Voltage profiles of MV and LV feeders for P^{CP} = 5 kW and different CD placements: (a) No CDs; (b) CD at STR secondary bus.

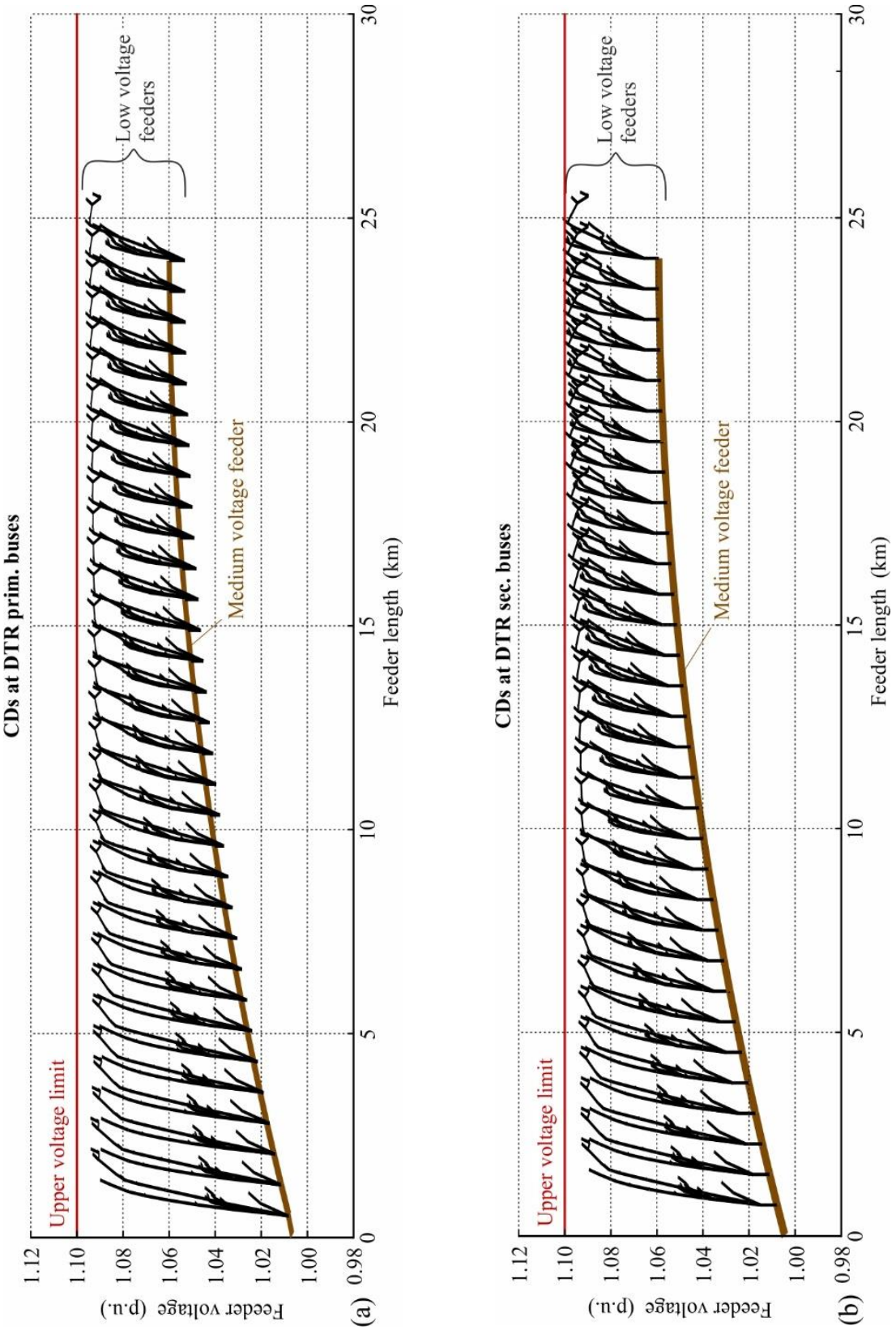

Fig. 3.88 Voltage profiles of MV and LV feeders for P^{CP} = 5 kW and different CD placements: (a) CDs at DTR primary buses; (b) CDs at DTR secondary buses.

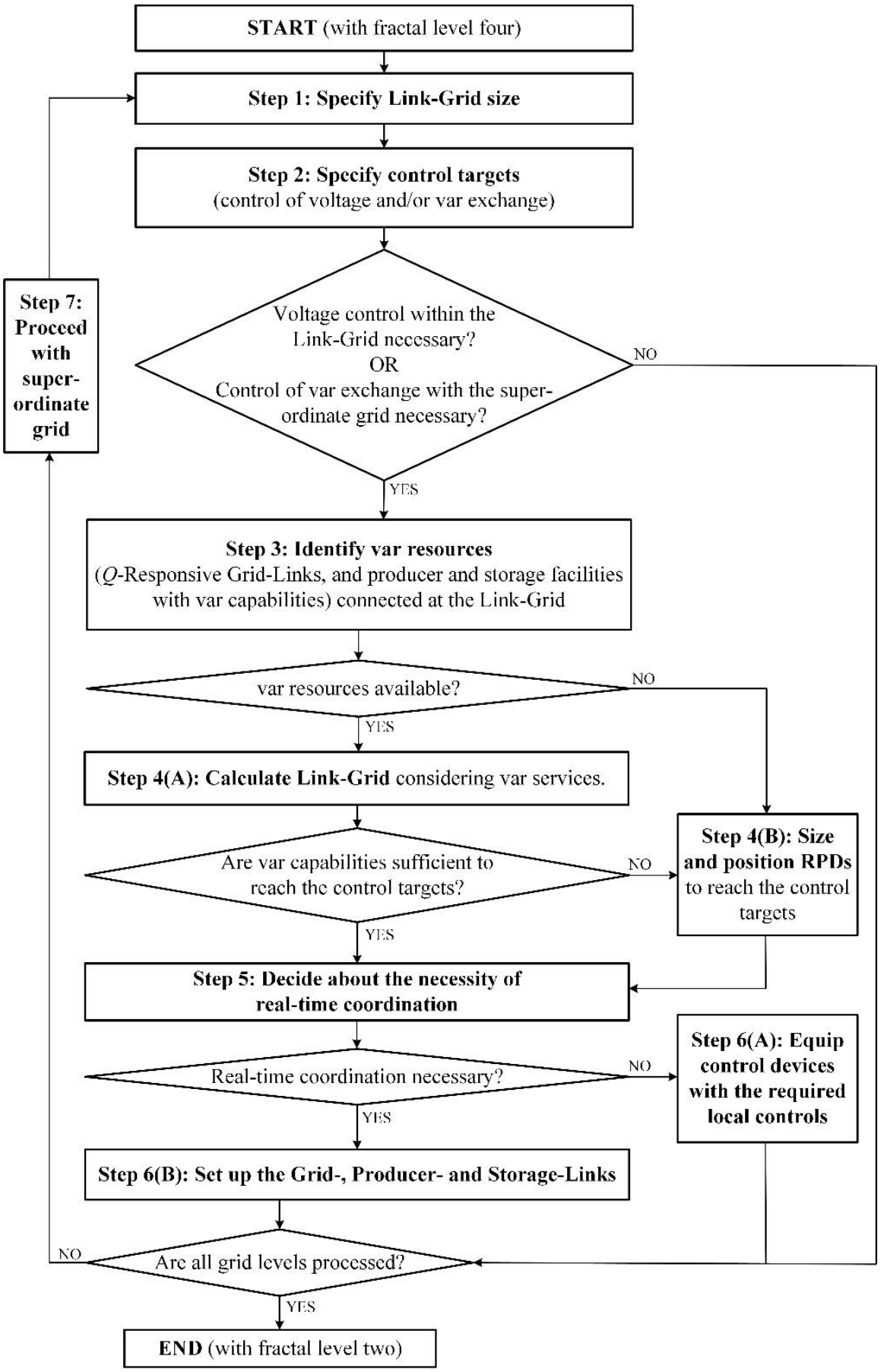

Fig. 3.89 Generalised setup procedure of the Volt/var chain control in the MV-LV-CP chain.

3.8.3 Setup procedure of the Volt/var chain control's structure

The generalised chain setup procedure is designed to meet the basic requirements presented in §3.8.1. Due to the major disadvantages of the distributed cos$\varphi(P)$ and $Q(U)$ controls and the OLTC at the distribution substation identified in §3.5.3.1, §3.6 and §3.7, only the $X(U)$ control is considered for setting up the Volt/var chain control. The chain setup procedure is used to set up the Volt/var chain control in an exemplary MV-LV-CP chain to clarify its application.

3.8.3.1 Generalised chain setup procedure

The *LINK*-based holistic architecture supports the systematic setup of the vertical Volt/var chain control as it relies on the fractal feature of power systems. Fig. 3.89 shows the generalised setup procedure for the MV-LV-CP-Device chain. It allows specifying the Volt/var control structure of each grid part according to a bottom-up approach: it starts at the fractal level four of Smart Grids (CP level) and ends at the fractal level two (medium voltage level). Due to the central position of the distribution grids (between transmission grid and customer plants), the DSO has a strategic role in setting up the vertical Volt/var chain control. Therefore, the DSO may use the generalised setup procedure shown in Fig. 3.89 to determine the chain control's structure in the MV-LV-CP chain in accordance with all involved stakeholders, i.e. the TSO, the customers, and the producer and storage operators. It includes seven steps as follows.

1. **Specify Link-Grid size**

   The first step is to determine the size of the Link-Grid, which is variable and defined from the area where the corresponding secondary control is set up (see §2.2.1). The Link-Grid size is crucial to maintain data privacy, as it defines the position of the interfaces between the different grid parts.

   The involved stakeholders may wish to define individual objective functions for the $\boldsymbol{VvSC}$ of each Link-Grid. For example, environmentalists may set the objective function of their $\boldsymbol{VvSC}^{CP}$ to minimise CO_2 emissions or maximise the PV self-consumption, while money-saving people may prefer to minimise costs or maximise revenues, etc.

   Fig. 3.90 shows different Link-Grid arrangements in the vertical axis resulting from the generalised setup procedure. In Fig. 3.90a, the Link-Grids are set upon the classical power system levels, i.e. MV, LV and CP. This setup may be suitable when different companies operate the MV and LV grids. Meanwhile, one Link-Grid may be set upon the MV and LV levels when both are operated by the same company, Fig. 3.90b. Fig.

3.90c shows the Link-Grid arrangement in an apartment building. Separate Link-Grids are set upon each flat and the housing area (ETIP SNET 2019), or depending on the circumstances, it can be applied to a housing area.

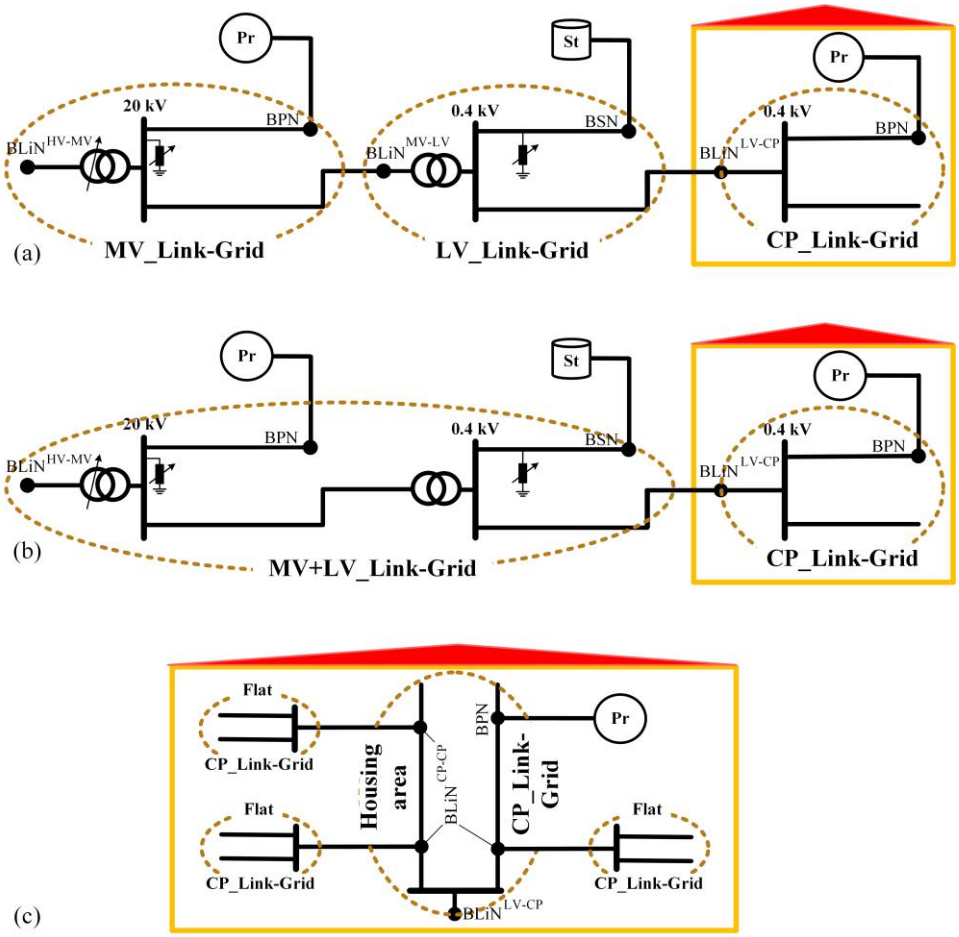

Fig. 3.90 Different Link-Grid arrangements in the vertical axis: (a) Link-Grids are set upon the MV, LV and CP levels; (b) One Link-Grid is set upon the MV and LV levels; (c) Link-Grids are set upon each flat and the housing area of an apartment building.

2. Specify control targets

This step dedicates the specification of the Volt/var secondary control targets of the Link-Grid. The potential targets of Volt/var control are:

- Voltage control within the own Link-Grid;
- And control of the var exchange with the superordinate grid.

The Grid Codes typically specify voltage limits at the connection points of customer plants. In these conditions, voltage control may be necessary at the HV, MV and LV level but not at the CP and consuming device level. The operators of Link-Grids must

agree upon the controllability of their var exchange. *LINK*-Solution offers different control modes:

- ***Q*-Responsive** Grid-Link that respect set-points received from superordinate Grid-Links in real-time. Data exchange between both involved Grid-Links is necessary;
- ***Q*-Autarkic** Grid-Link does not exchange any reactive power with the superordinate Link-Grid (see §3.5.3.3 for the CP level). No data exchange is needed; and
- ***Q*-Uncontrolled** Link-Grid that provokes uncontrolled reactive power exchanges with the superordinate Link-Grid.

3. **Identify var resources**

   This step identifies the available var resources. From the Link-Grid's point of view, var resources include:

   - Producer facilities with var capabilities;
   - Storage facilities with var capabilities;
   - And subordinate *Q*-Responsive Grid-Links.

   The identified var resources may provide var services to reach the specified control targets.

4. **(A) Calculate Link-Grid**

   If var resources are available, calculate the Link-Grid under the consideration of var services to check whether the available var resources are sufficient to reach the specified control targets. Consider var services procured by non-discriminatory, market-based and transparent procedures to comply with (Directive EU 2019/944). If no var resources are available, proceed with step 4 (B).

   (B) Size and position RPDs

   When no var resources are available, or their var capabilities are insufficient to reach the control targets, RPDs must be sized and positioned within the Link-Grid. The identification of the appropriate size, position and number of RPDs requires careful analysis of the Link-Grid.

5. **Decide about the necessity of real-time coordination**

   The real-time coordination of the available var resources allows optimising the grid operation but requires distributed data collection, central data processing and

communication infrastructure. Analyse the costs and benefits of coordination and decide about its implementation.

6. **(A) Equip control devices with the required local controls**

   If coordination is not necessary, equip the RPDs and the producer and storage facilities with the local Volt/var controls required to reach the control targets.

   (B) Set up the Grid, Producer- and Storage-Links

   If coordination is necessary, upgrade the Link-Grid with secondary control and interfaces and each producer and storage facility that possesses var capabilities with primary control and interface.

7. **Proceed with superordinate grid**

   If not all grid levels are processed, repeat the generalised setup procedure for the superordinate grid. Otherwise, terminate the procedure.

An exemplary setup of the Volt/var chain control in the MV-LV-CP levels illustrates the setup procedure in the following.

3.8.3.2 Setup example

The considered MV-LV-CP chain consists of one MV grid that includes solely one voltage level (e.g. 20 kV), several LV grids, and numerous single-family houses connected at the LV level. One DSO operates the MV and all LV grids. Producer and storage facilities are connected to the MV and CP grids but not to the LV grids. While the STR possesses an OLTC, the DTRs do not.

Application of the setup procedure

Fig. 3.91 shows the procedure used to determine the Volt/var chain control's structure for the regarded MV-LV-CP chain. It is directly derived from the generalised one by starting at fractal level four (CP level) and ending at fractal level two (MV level) (Ilo 2019).

Determination of the control structure at the CP level

The first step is to determine the Link-Grid size of all CPs included in the MV-LV-CP chain. In the considered example, all CPs are single-family houses. Therefore, one Link-Grid is set upon each CP; the $BLiN^{LV\text{-}CP}$s are the CPs' connection points to the LV grids. Voltage control at the CP level is not required since the distances between the $BLiN^{LV\text{-}CP}$s and the connection points of various devices (CP's sockets) are minimal; A significant voltage drop is usually not detectable. However, the customers and the DSO agree to eliminate the uncontrolled LV-CP

var exchange by setting the CP_Grid-Link with the parametrisation: *Q*-Autarky. Each CP has one PV and one battery system with var capabilities that are used to achieve the CP_*Q*-Autarky.

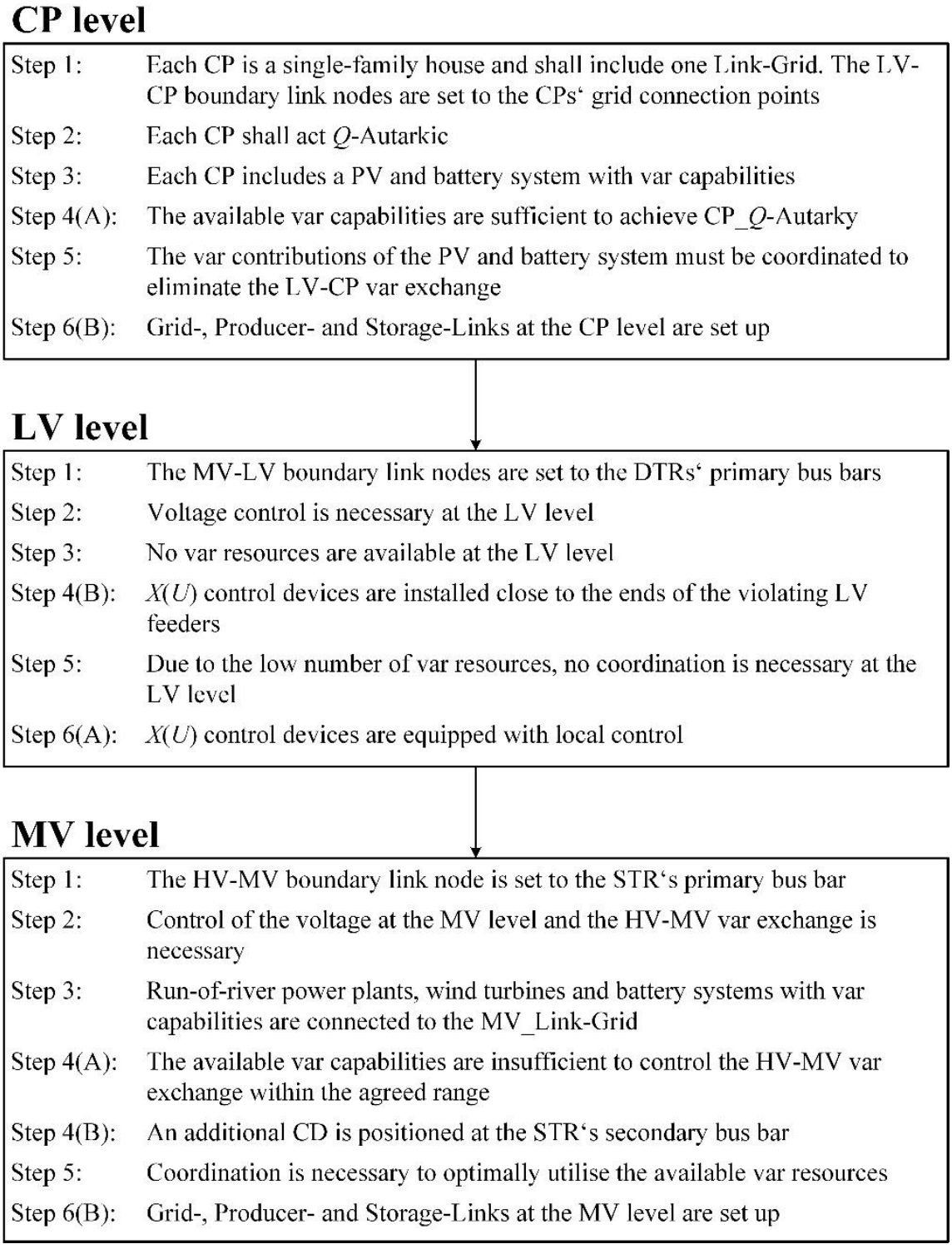

Fig. 3.91 Procedure used to determine the Volt/var chain control’s structure for an exemplary MV-LV-CP chain.

The calculation of the CP_Link-Grids shows that the var capabilities of the PV and battery systems are sufficient to compensate the var requirements within the CP fully and, as a result, to eliminate the LV-CP var exchange of each CP. Coordination of the PV and battery systems' var contributions is necessary for each CP to realise *Q*-Autarky. Both the PV and battery systems are upgraded with primary controls and interfaces, and the CP_Link-Grids are upgraded with secondary controls and interfaces to the corresponding Producer- and Storage-Links. No LV-CP interfaces are implemented as no LV-CP data exchange is necessary for the *Q*-Autarkic operation mode of CPs.

The resulting Volt/var control structure at the CP level is shown in Fig. 3.92. While the power flow path is shown in black, the automation and communication path is blue-coloured. Golden ellipses indicate Grid-, Producer- and Storage-Links. The $\boldsymbol{VvSC^{CP}}$ calculates real-time var set-points for the primary controls of the Producer- ($\boldsymbol{PC_{Pr}^{CP}}$) and Storage-Link ($\boldsymbol{PC_{St}^{CP}}$) to respect the fixed var constraint ($\boldsymbol{Cns_{NgbLV}^{CP}} = 0$ kvar) at the BLiN$^{\text{LV-CP}}$. Neither reactive power nor any related data is exchanged between the LV grid and the CPs.

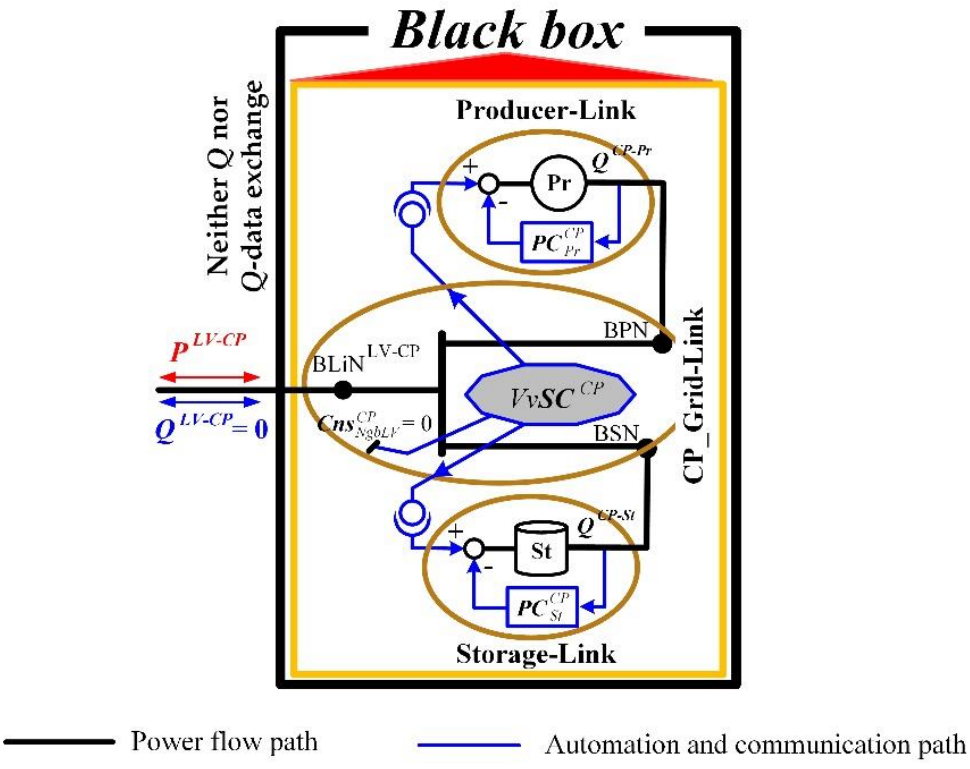

Fig. 3.92 Volt/var control structure at the CP level of the exemplary MV-LV-CP chain (*Q*-Autarkic CP_Grid-Link).

Determination of the control structure at the LV level

Each LV_Link-Grid's size is specified by setting the $BLiN^{MV\text{-}LV}$ to the primary busbar of the DTR. Due to the high PV penetration in the CP level, voltage control is necessary at the LV level. Meanwhile, the DSO does not intend to control the MV-LV var exchange for the following reasons:

- The DSO operates both the MV and LV grids. Therefore, all $BLiN^{MV\text{-}LV}$ are internal boundary nodes.
- The analysis conducted in §3.8.2 indicates that compensating for the reactive power flow through the DTR increases the reactive power consumption of the $X(U)$ local controls needed to maintain voltage limit compliance at the LV level.

No var resources are available from the viewpoint of the LV_Link-Grids as no producer and storage facilities are directly connected, and all CPs act Q-Autarkic. Therefore, $X(U)$ control devices are installed close to the ends of the limit violating LV feeders, and their rating is determined based on load flow calculations and worst-case assumptions. Due to the low number of var resources in each LV_Link-Grid and the reliability and effectiveness of $X(U)$ local control, coordination at the LV level is not necessary. Instead, the $X(U)$ control devices are equipped with local control.

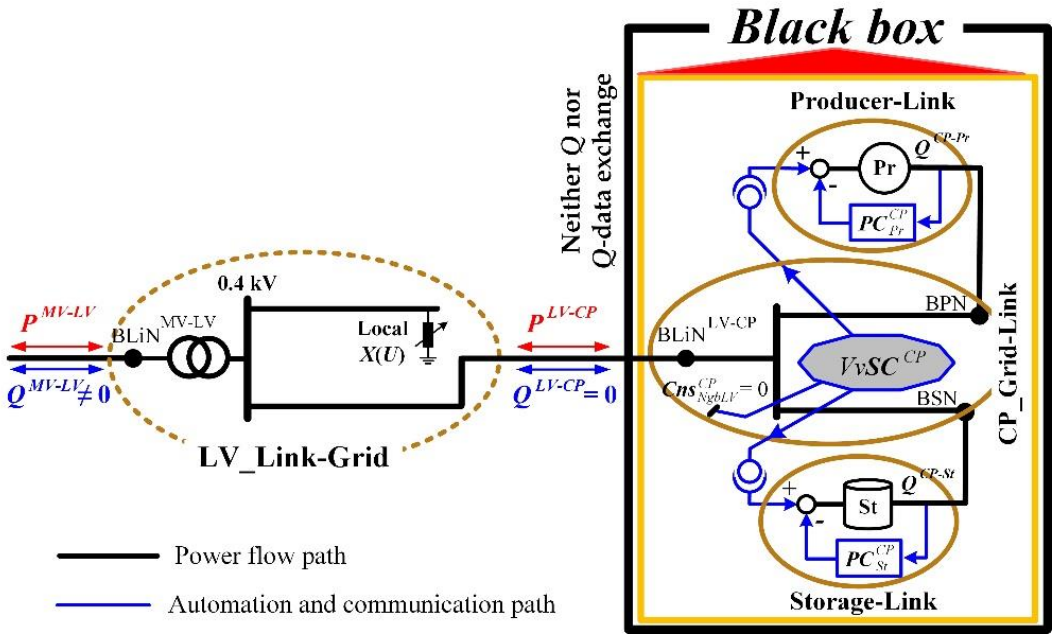

Fig. 3.93 Volt/var control structure at the exemplary LV-CP chain (LV_Link-Grid with $X(U)$ local control and Q-Autarkic CP_Grid-Link).

The resulting Volt/var control structure at the LV-CP chain is shown in Fig. 3.93. Gold-coloured dashed ellipses indicate Link-Grids. $X(U)$ local controls maintain voltage limit

compliance at the LV level by provoking minimal uncontrolled reactive power exchanges between the MV and the LV_Link-Grids. No communication infrastructure is necessary at the LV level as no data is exchanged between the MV and LV and the LV and CP level.

Determination of the control structure at the MV level

The MV_Link-Grid size is specified by setting the $BLiN^{HV\text{-}MV}$ to the STR primary busbar and the above determined $BLiN^{MV\text{-}LV}$s. Voltage control within the MV_Link-Grid is necessary to maintain voltage limits compliance. Furthermore, the DSO may agree with TSO to provide reactive power as an ancillary service by controlling the HV-MV var exchange within a specific range. Run-of-river power plants, wind turbines and battery systems with var capabilities are connected to the MV_Link-Grid. However, the calculation of the MV_Link-Grid shows that procuring var services from these resources is insufficient to control the agreed HV-MV reactive power exchange; additional CD within the MV_Link-Grid are necessary. In analogy with the conclusion drawn in §3.8.2, the analysis of the MV_Link-Grid showed that positioning the CD at the secondary busbar of the STR maximises the effectiveness of the resulting Volt/var control chain; the appropriate CD rating is calculated. In agreement with the relevant stakeholders (for example, producer operators, etc.), the DSO implements MV_Link-Grid at the MV level to optimise the operational grid performance and enable the non-discriminatory, market-based, and transparent procurement of var services. Therefore, the necessary automation and communication are implemented as follows:

- The OLTC of the STR, which already possesses primary control;
- The CD is upgraded with primary control;
- The producer and storage facilities are upgraded with primary controls and interfaces; and
- The MV_Link-Grid is upgraded with Volt/var secondary control and interfaces to the Producer- and Storage-Links and to the HV grid.

The resulting Volt/var control structure at the MV-LV-CP chain is shown in Fig. 3.94. $\boldsymbol{VvSC^{MV}}$ coordinates the var contributions of the CD and the Producer- and Storage-Links with the OLTC of the STR by:

- Calculating real-time var set-points for the CDs and the Producer- and Storage-Links connected to the MV_Grid-Link;
- Calculating real-time voltage set-points for the OLTC of the STR;
- While respecting the internal voltage limits and the dynamic var constraint at the $BLiN^{HV\text{-}MV}$.

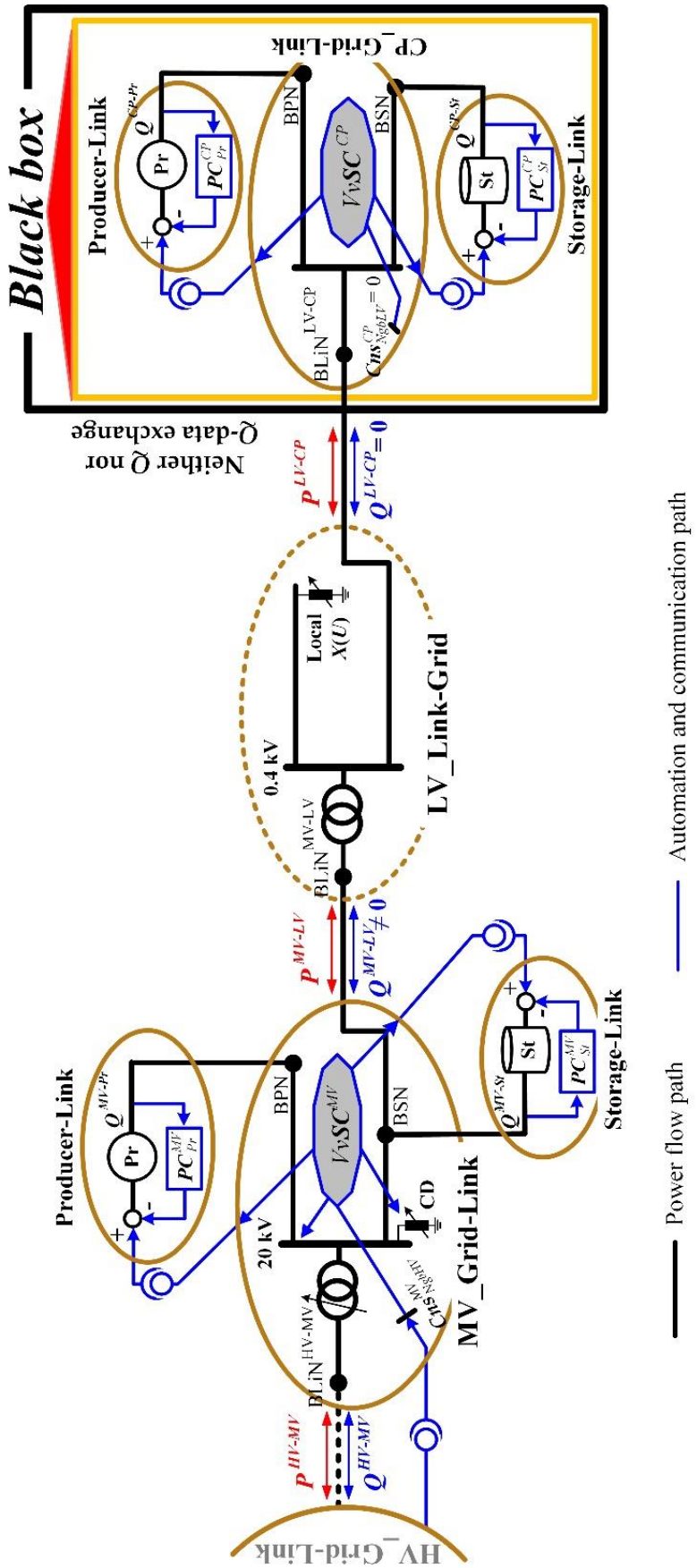

Fig. 3.94 Volt/var control structure at the exemplary MV-LV-CP chain (MV_Grid-Link with additional CD, LV_Link-Grid with $X(U)$ local control and Q-Autarkic CP_Grid-Link).

Setup overview

The Volt/var chain control setup shown in Fig. 3.94 is designed to meet the basic requirements by following the general guideline (see §3.8.1). The necessity of the $\boldsymbol{VvSC}^{LV}$ is eliminated by combining the $X(U)$ local control with the Q-Autarky of customer plants. This control ensemble maintains voltage limit compliance at the LV level effectively (see §3.5.3.1) without requiring any data exchanges between the DSO and the customers. The uncontrolled reactive power flows are reduced to their practical minimum. The $\boldsymbol{VvSC}^{MV}$ coordinates the var resources at the MV level with the OLTC of the STR to control the voltage at the MV level and respect var constraints at the BLiN$^{\text{HV-MV}}$. Equation (3.48) compactly represents the control variables and dynamic constraints of the designed vertical Volt/var chain control.

$$\begin{aligned}&\boldsymbol{VvSC}^{MV-LV-CP}_{Chain} = \{\\&\boldsymbol{VvSC}^{MV}\left(\boldsymbol{PC}^{MV}_{OLTC}, \boldsymbol{PC}^{MV}_{Pr}, \boldsymbol{PC}^{MV}_{St}, \boldsymbol{PC}^{MV}_{CD};\ \boldsymbol{Cns}^{MV}_{NgbHV}\right),\\&\boldsymbol{LC}^{LV}_{X(U)},\\&\boldsymbol{VvSC}^{CP}\left(\boldsymbol{PC}^{CP}_{Pr}, \boldsymbol{PC}^{CP}_{St};\ \boldsymbol{Cns}^{CP}_{NgbLV} = 0\ \text{kvar}\right)\}\end{aligned} \tag{3.48}$$

MV level

The $\boldsymbol{VvSC}^{MV}$ calculates in real-time:

- The voltage set-points for the primary controls $\boldsymbol{PC}^{MV}_{OLTC}$ of the supplying transformers and other transformers included in the MV_Grid-Link that have OLTC;
- The voltage and reactive power set-points for the primary controls $\boldsymbol{PC}^{MV}_{Pr}$ of the Producer-Links connected to the MV_Grid-Link;
- The voltage and reactive power set-points for the primary controls $\boldsymbol{PC}^{MV}_{St}$ of the Storage-Links connected to the MV_Grid-Link;
- And the voltage, reactive power and switch position set-points for the primary $\boldsymbol{PC}^{MV}_{RPD}$ and direct controls $\boldsymbol{DiC}^{MV}_{RPD}$ of the RPDs included in the MV_Grid-Link;

While respecting:

- The reactive power constraints $\boldsymbol{Cns}^{MV}_{NgbHV}$ at the boundary node to the neighbouring HV_Grid-Link.

LV level

No $\boldsymbol{VvSC}^{LV}$ is used. The voltage at the LV level is controlled by $X(U)$ local control (see §3.5.3.2).

CP level

The $\boldsymbol{VvSC}^{CP}$ realises CP_Q-Autarky (see §3.5.3.3) by calculating in real-time:

- The voltage and reactive power set-points for the primary controls $\boldsymbol{PC}_{Pr}^{CP}$ of the Producer-Links connected to the CP_Grid-Link;
- And the voltage and reactive power set-points for the primary controls $\boldsymbol{PC}_{St}^{CP}$ of the Storage-Links connected to the CP_Grid-Link;

While respecting:

- The fixed reactive power constraint $\boldsymbol{Cns}_{NgbLV}^{CP} = 0$ kvar at the boundary node to the neighbouring LV_Grid-Link.

4 Conclusion

The increasing share of distributed energy resources provoke violations of the voltage limits at the low voltage level, upsetting the traditional Volt/var control schemes.

The recently emerging local control strategies, such as cos$\varphi(P)$- and $Q(U)$-control of photovoltaic inverters and on-load tap changers in distribution substations, are insufficient to meet the social and technical requirements of future Smart Grids. Implementing cos$\varphi(P)$- and $Q(U)$-control leads to non-market-based and – in the case of the latter – discriminatory ancillary service procurement, fundamentally contradicting the political intent of the European Parliament. Due to their distributed nature, the inverter-based local controls are ineffective in maintaining voltage limit compliance, causing excessive uncontrolled reactive power flows in superordinate grids. The cos$\varphi(P)$-control of photovoltaic inverters does not support the increase of the electricity demand as it is incapable of mitigating violations of the lower voltage limit. Meanwhile, on-load tap changers in distribution substation do not impose social issues and do not modify the uncontrolled reactive power flows significantly. However, they are insufficient to mitigate violations of the upper voltage limit in times of high photovoltaic production. In contrast, the proposed control strategies, i.e. $X(U)$ local control at the low voltage and Q-Autarky at the customer plant level, overcome the disadvantages of the recently introduced ones. Social compatibility is achieved by excluding the customer plants from voltage control and voltage limit violations are effectively mitigated by reducing the uncontrolled reactive power flows to the technically necessary minimum.

The voltage limits in radial structures (e.g. medium voltage) are deformed by the voltage drops in the subordinate grids (e.g. low voltage). The deformation degree depends on the low voltage feeders' properties: the greater the feeder impedance and the number of connected customer plants, the more intensive is the deformation. The lumped grid models are extended by a new parameter, the "boundary voltage limits", allowing to verify voltage limit compliance at the low voltage level by conducting load flow analysis at the medium voltage level.

However, the optimal operation of the power system requires the closed-loop coordination of the control variables distributed throughout the entire Smart Grid. The *LINK*-based holistic architecture supports the execution of this coordination by chain controls that reduce the necessary data transfer and increase the system's resiliency by design. The extension of the conventional lumped grid model by variable boundary voltage limits allows increasing the operational efficiency of *LINK*-based Smart Grids.

List of References

Alassi A, Bañales S, Ellabban O, Adam G, MacIver C (2019) HVDC Transmission: Technology Review, Market Trends and Future Outlook. Renewable and Sustainable Energy Reviews, vol 112, pp 530-554

Albarracín R, Alonso M (2013) Photovoltaic reactive power limits. 12th International Conference on Environment and Electrical Engineering, Wroclaw, Poland, 5-8 May, pp 13-18, doi:10.1109/EEEIC.2013.6549630

Alla M, Guzman A, Finney D, Fischer N (2018) Capability Curve-Based Generator Protection Minimizes Generator Stress and Maintains Power System Stability. 45th Annual Western Protective Relay Conference, Spokane, WA, USA, 16-18 October, pp 1-16

Arif A, Wang Z, Wang J, Mather B, Bashualdo H, Zhao D (2018) Load Modeling—A Review. IEEE Transactions on Smart Grid, vol 9/6, pp 5986-5999. doi:10.1109/TSG.2017.2700436

Arrillaga J, Yonghe HL, Neville RW, Nicholas JM (2009) Self-Commutated Converters for high power applications. John Wiley & Sons, New Jersey

Aunedi M, Woolf M, Strbac G, Babalola O, Clark M (2015). Characteristic Demand Profiles of Residential and Commercial EV Users and Opportunities for Smart Charging. 23rd International Conference on Electricity Distribution, Lyon, France, 15-18 June, 1088.

Belvin RC, Short TA (2012) Voltage reduction results on a 24-kV circuit. IEEE PES Transmission and Distribution Conference and Exposition, Orlando, FL, USA, 7-10 May, pp 1-4. doi:10.1109/TDC.2012.6281592

Binder A (2012) Elektrische Maschinen und Antriebe: Grundlagen, Betriebsverhalten. Springer, Heidelberg

Bletterie B, Goršek A, Uljanić B, Blazic B, Woyte A, Vu Van T, Truyens F, Jahn J (2010) Enhancement of the Network Hosting Capacity—Clearing Space for/with PV. 25th European Photovoltaic Solar Energy Conference and Exhibition / 5th World Conference on Photovoltaic Energy Conversion, Valencia, Spain, 6-10 September, pp 4828-4834. doi:10.4229/25thEUPVSEC2010-5AO.7.3

Bokhari A, Alkan A, Dogan R, Diaz-Aguiló M, de León F, Czarkowski D, Zabar Z, Birenbaum L, Noel A, Uosef RE (2014) Experimental Determination of the ZIP Coefficients for Modern Residential, Commercial, and Industrial Loads. Transactions on Power Delivery, vol 29/3, pp 1372-1381. doi:10.1109/TPWRD.2013.2285096

Bollen MHJ, Sannino A (2005) Voltage control with inverter-based distributed generation. IEEE Transactions on Power Delivery, vol 20/1, pp 519-520. doi:10.1109/TPWRD.2004.834679

Carden J, Popovic D (2018) Closed-Loop Volt\/Var Optimization: Addressing Peak Load Reduction. IEEE Power and Energy Magazine, vol 16/2, pp 67-75. doi:10.1109/MPE.2017.2780962

Chen H, Cong TN, Yang W, Tan C, Li Y, Ding Y (2009) Progress in electrical energy storage system: A critical review. Progress in Natural Science, vol 19/3, pp 291-312. doi:10.1016/j.pnsc.2008.07.014

Choi J, Moon S (2009) The Dead Band Control of LTC Transformer at Distribution Substation. IEEE Transactions on Power Systems, vol 24/1, pp 319-326.

doi:10.1109/TPWRS.2008.2005706

Choi W, Wu Y, Han D, Gorman J, Palavicino PC, Lee W, Sarlioglu B (2017) Reviews on grid-connected inverter, utility-scaled battery energy storage system, and vehicle-to-grid application - challenges and opportunities. 2017 IEEE Transportation Electrification Conference and Expo (ITEC), Chicago, IL, USA, 22-24 June, pp 203-210

CIGRE Task Force C6.04 (2014a) Benchmark Systems for Network Integration of Renewable and Distributed Energy Resources.

CIGRE Working Group C4.605 (2014b) Modelling and Aggregation of Loads in Flexible Power Networks.

Collin AJ, Tsagarakis G, Kiprakis AE, McLaughlin S (2014) Development of Low-Voltage Load Models for the Residential Load Sector. IEEE Transactions on Power Systems, vol 29/5, pp 2180-2188. doi:10.1109/TPWRS.2014.2301949

Corsi S, Pozzi M, Sabelli C, Serrani A (2004) The coordinated automatic voltage control of the Italian transmission Grid-part I: reasons of the choice and overview of the consolidated hierarchical system. IEEE Transactions on Power Systems, vol 19/4, pp 1723-1732. doi:10.1109/TPWRS.2004.836185

Dabic V, Atanackovic D (2015) Voltage VAR optimisation real time closed loop deployment - BC Hydro challenges and opportunities. 2015 IEEE PES General Meeting, Denver, CO, USA, 26-30 July, pp 1-5. doi:10.1109/PESGM.2015.7286313

Demirok E, González PC, Frederiksen KHB, Sera D, Rodriguez P, Teodorescu R (2011) Local Reactive Power Control Methods for Overvoltage Prevention of Distributed Solar Inverters in Low-Voltage Grids. IEEE Journal of Photovoltaics, vol 1/2, pp 174-182. doi:10.1109/JPHOTOV.2011.2174821

Directive (EU) 2019/944 of the European Parliament and of the Council of 5 June 2019 on common rules for the internal market for electricity and amending Directive 2012/27/EU (Text with EEA relevance.) http://data.europa.eu/eli/dir/2019/944/oj Accessed 13 April 2021

Dixon J, Moran L, Rodriguez J, Domke R (2005) Reactive Power Compensation Technologies: State-of-the-Art Review. Proceedings of the IEEE, vol 93/12, pp 2144-2164. doi:10.1109/JPROC.2005.859937

EN 50160:2010 - Voltage characteristics of electricity supplied by public electricity networks

Engelhardt S, Erlich I, Feltes C, Kretschmann J, Shewarega F (2011) Reactive Power Capability of Wind Turbines Based on Doubly Fed Induction Generators. IEEE Transactions on Energy Conversion, vol 26/1, pp 364-372

ENTSO-E (2019) HVDC Links in System Operations. https://eepublicdownloads.entsoe.eu/clean-documents/SOC%20documents/20191203_HVDC%20links%20in%20system%20operations.pdf Accessed 13 April 2021

ETIP SNET (2019) White Paper Holistic architectures for future power systems. https://www.etip-snet.eu/white-paper-holistic-architectures-future-power-systems Accessed 13 April 2021

Eurelectric (2013) Power Distribution in Europe: Facts and Figures. https://cdn.eurelectric.org/media/1835/dso_report-web_final-2013-030-0764-01-e-h-D66B0486.pdf Accessed 13 April 2021

Farivar M, Zho X, Chen L (2015) Local voltage control in distribution systems: An incremental control algorithm. IEEE International Conference on Smart Grid Communications, Miami, FL, USA, 2-5 November, pp 732-737. doi:10.1109/SmartGridComm.2015.7436388

Hingorani NG, Gyugyi L (2000) Understanding FACTS, Concepts and Technology of Flexible AC Transmission Systems. IEEE Press

Hossain MI, Yan R, Saha TK (2016) Investigation of the interaction between step voltage regulators and large-scale photovoltaic systems regarding voltage regulation and unbalance. IET Renewable Power Generation, vol 10/3, pp 299-309. doi:10.1049/iet-rpg.2015.0086

IEA - International Energy Agency (2020) Electricity generation by source, Europe 1990-2018. https://www.iea.org/data-and-statistics?country=WEOEUR&fuel=Energy%20supply&indicator=ElecGenByFuel Accessed 13 April 2021

Ilo A (2013) The Energy Supply Chain Net. Energy and Power Engineering, vol 5, pp 384-390. doi:10.4236/epe.2013.55040

Ilo A (2016a) "Link" – The smart grid paradigm for a secure decentralised operation architecture. Electric Power Systems Research, vol 131, pp 116-125. doi:10.1016/j.epsr.2015.10.001

Ilo A (2016b) Effects of the Reactive Power Injection on the Grid - The Rise of the Volt/var Interaction Chain. Smart Grid and Renewable Energy, vol 7, pp 217-232

Ilo A (2017) Demand response process in context of the unified LINK-based architecture. Bessède, Jean-Luc. Eco-Design in Electrical Engineering Eco-Friendly Methodologies, Solutions and Example for Application to Electrical Engineering. Springer, Heidelberg.

Ilo A (2019) Design of the Smart Grid Architecture According to Fractal Principles and the Basics of Corresponding Market Structure. Energies 2019, vol 12, 4153

Ilo A (2020) Use cases in sector coupling as part of the LINK-based holistic architecture to increase the grid flexibility. CIRED 2020 Berlin Workshop, Berlin, 22-23 September, 394

Ilo A, Prata R, Iliceto A, Strbac G (2019) Embedding of Energy Communities in the Unified *LINK*-Based Holistic Architecture. 25th International Conference on Electricity Distribution, Madrid, Spain, 3-6 June, pp 1-5.

Ilo A, Schultis DL (2019) Low-voltage grid behaviour in the presence of concentrated var-sinks and var-compensated customers. Electric Power Systems Research, vol 171, pp 54-65. doi:10.1016/j.epsr.2019.01.031

Ilo A, Schultis DL, Schirmer C (2018) Effectiveness of Distributed vs. Concentrated Volt/Var Local Control Strategies in Low-Voltage Grids. Applied Sciences, vol 8/8, 1382. doi:10.3390/app8081382

Kundur P (1994) Power System Stability and Control. EPRI, McGraw-Hill, New York

Li Q, Zhang YJ, Ji T, Lin X, Cai Z (2018). Volt/var Control for Power Grids with Connections of Large-scale Wind Farms: A Review. IEEE Access, vol 6, pp 26675-26692. doi:10.1109/ACCESS.2018.2832175

LPF (2020) Load profile generator. https://www.loadprofilegenerator.de/ Accessed 13 April 2021

Marggraf O, Laudahn S, Engel B, Lindner M, Aigner C, Witzmann R, Schoeneberger M,

Patzack S, Vennegeerts H, Cremer M, Meyer M, Schnettler A, Berber I, Bülo T, Brantl J, Wirtz F, Frings R, Pizzutto F (2017) U-Control - Analysis of Distributed and Automated Voltage Control in current and future Distribution Grids. International ETG Congress 2017, Bonn, Germany, 28-29 November, pp 567-572

McKenna E, Thomson M (2016) High-resolution stochastic integrated thermal–electrical domestic demand model. Applied Energy, vol 165, pp 445-461. doi:10.1016/j.apenergy.2015.12.089

McKenna E, Thomson M, Barton J (2015) CREST Demand Model. Loughborough University. https://repository.lboro.ac.uk/articles/dataset/CREST_Demand_Model_v2_0/2001129/5 Accessed 13 April 2021

Neal R (2010) The use of AMI meters and solar PV inverters in an advanced Volt/VAr control system on a distribution circuit. IEEE PES Transmission and Distribution Conference and Exposition, New Orleans, LA, USA, 19-22 April, pp 1-4. doi:10.1109/TDC.2010.5484402

Nowak S, Wang L, Metcalfe MS (2020) Two-level centralized and local voltage control in distribution systems mitigating effects of highly intermittent renewable generation. International Journal of Electrical Power & Energy Systems, vol 119, 105858. doi:10.1016/j.ijepes.2020.105858

Oeding D, Oswald BR (2011) Elektrische Kraftwerke und Netze. Springer, Heidelberg. doi:10.1007/978-3-642-19246-3

Peskin MA, Powell PW, Hall EJ (2012) Conservation Voltage Reduction with feedback from Advanced Metering Infrastructure. IEEE PES Transmission and Distribution Conference and Exposition, Orlando, FL, USA, 7-10 May, pp 1-8. doi:10.1109/TDC.2012.6281644

Pflugradt N, Muntwyler U (2017) Synthesizing residential load profiles using behavior simulation. Energy Procedia, vol 122, pp 655-660. doi:10.1016/j.egypro.2017.07.365.

Poliseno MC, Mastromauro RA and Liserre M (2012) Transformer-less photovoltaic (PV) inverters: A critical comparison. 2012 IEEE Energy Conversion Congress and Exposition, Raleigh, NC, USA, 15-20 September, pp 3438-3445

Preiss RF, Warnock VJ (1978) Impact of Voltage Reduction on Energy and Demand. IEEE Transactions on Power Apparatus and Systems, vol PAS-97/5, pp 1665-1671. doi:10.1109/TPAS.1978.354658

Price WW, Chiang HD, Clark HK, Concordia C, Lee DC, Hsu JC, Ihara S, King CA, Lin CJ, Mansour Y, Srinivasan K, Taylor CW, Vaahedi E (1993) Load representation for dynamic performance analysis (of power systems). IEEE Transactions on Power Systems, vol 8/2, pp 472-482. doi:10.1109/59.260837

Riese P (2012) Handbuch der Blindstrom-Kompensation. https://www.frako.com/fileadmin/pdf/Downloads/Handbuch/95-00135_11_13_9066_handbuch_blk.pdf Accessed 20 May 2021

Rohjans S, Dänekas C, Uslar M (2012) Requirements for Smart Grid ICT-architectures. 3rd IEEE PES Innovative Smart Grid Technologies Europe, Berlin, Germany, 14-17 October, pp 1-8. doi:10.1109/ISGTEurope.2012.6465617

Roytelman I, Ganesan V (1999) Modeling of local controllers in distribution network applications. 21st International Conference on Power Industry Computer Applications. Connecting Utilities. PICA 99. To the Millennium and Beyond (Cat. No.99CH36351), Santa

Clara, CA, USA, 21 May, pp 161-166. doi:10.1109/PICA.1999.779399

Roytelman I, Ganesan V (2000) Coordinated local and centralized control in distribution management systems. IEEE Transactions on Power Delivery, vol 15/2, pp 718-724. doi:10.1109/61.853010

Sarkar MNI, Meegahapola LG, Datta M (2018) Reactive Power Management in Renewable Rich Power Grids: A Review of Grid-Codes, Renewable Generators, Support Devices, Control Strategies and Optimization Algorithms. IEEE Access, vol 6, pp 41458-41489

Schultis DL (2019) Daily load profiles and ZIP models of current and new residential customers. Mendeley Data. doi: 10.17632/7gp7dpvw6b.1

Schultis DL, Ilo A (2018) TUWien_LV_TestGrids. Mendeley Data. doi:10.17632/hgh8c99tnx.1

Schultis DL, Ilo A (2019a) Adaption of the Current Load Model to Consider Residential Customers Having Turned to LED Lighting. 11th IEEE PES Asia-Pacific Power & Energy Engineering Conference, Macao, China, 1-4 December, pp 1-5. doi:10.1109/APPEEC45492.2019.8994535

Schultis DL, Ilo A (2019b) Behaviour of Distribution Grids with the Highest PV Share Using the Volt/Var Control Chain Strategy. Energies, vol 12/20, 3865. doi:10.3390/en12203865

Schultis DL, Ilo A (2021) "Boundary Voltage Limits" – an instrument to increase the utilization of the existing infrastructures. CIRED 2021 Conference, Geneva, Switzerland, 20-23 September, 910. (accepted for publication)

Schürhuber R (2018) Ausgewählte Aspekte des Netzanschlusses von Erzeugungsanlagen. Impulsvortrag am Treffen der CIRED, Vienna, Austria, 30 January. https://cired.at/fileadmin//user_upload/Ausgewaehlte_Aspekte_Netzanschluss_Impulsvortrag_Wien_Prof_Schuerhuber.pdf Accessed 13 April 2021

Schweiger G, Eckerstorfer LV, Hafner I, Fleischhacker A, Radl J, Glock B, Wastian M, Rößler M, Lettner G, Popper N, Corcoran K (2020) Active consumer participation in smart energy systems. Energy and Buildings, vol 227, 110359. doi:10.1016/j.enbuild.2020.110359

Shukla A, Verma K, Kumar R (2017) Multi-stage voltage dependent load modelling of fast charging electric vehicle. 6th International Conference on Computer Applications in Electrical Engineering - Recent Advances, Roorkee, India, 5-7 October, pp 86-91. doi:10.1109/CERA.2017.8343306

Smith JW, Sunderman W, Dugan R, Seal B (2011) Smart inverter volt/var control functions for high penetration of PV on distribution systems. IEEE PES Power Systems Conference and Exposition, Phoenix, AZ, USA, 20-23 March, pp 1-6. doi:10.1109/PSCE.2011.5772598

Sun H, Guo Q, Qi J, Ajjarapu V, Bravo R, Chow J, Li Z, Moghe R, Nasr-Azadani E, Tamrakar U, Taranto GN, Tonkoski R, Valverde G, Wu Q, Yang G (2019) Review of Challenges and Research Opportunities for Voltage Control in Smart Grids. IEEE Transactions on Power Systems, vol 34/4, pp 2790-2801. doi:10.1109/TPWRS.2019.2897948

Teodorescu R, Liserre M, Rodríguez P (2007) Grid Converters for Photovoltaic and Wind Power Sytems. Wiley-IEEE Press

Tian J, Su C, Chen Z (2013) Reactive power capability of the wind turbine with Doubly Fed Induction Generator. 39th Annual Conference of the IEEE Industrial Electronics Society, Vienna, Austria, 10-13 November, pp 5312-5317. doi:10.1109/IECON.2013.6699999

Tonkoski R, Lopes LAC (2011) Impact of active power curtailment on overvoltage prevention and energy production of PV inverters connected to low voltage residential feeders. Renewable Energy, vol 36/12, pp 3566-3574. doi:10.1016/j.renene.2011.05.031

Turitsyn K, Sulc P, Backhaus S, Chertkov M (2011) Options for Control of Reactive Power by Distributed Photovoltaic Generators. Proceedings of the IEEE, vol 99/6, pp 1063-1073. doi:10.1109/JPROC.2011.2116750

Vaahedi E (2014) Practical power system operation. John Wiley & Sons, New Jersey

Vittal V, McCalley JD, Anderson PM, Fouad AA (2019) Power System Control and Stability. John Wiley & Sons Incorporated, New Jersey

Walker JH (1953) Operating characteristics of salient-pole machines. IEE - Part II: Power Engineering, vol 100/73, pp 13-24. doi:10.1049/pi-2.1953.0004

Wang W, Lu Z (2013) Cyber security in the Smart Grid: Survey and challenges. Computer Networks, vol 57/5, pp 1344–1371. doi:10.1016/j.comnet.2012.12.017

Wang YB, Wu CS, Liao H, Xu HH (2008) Steady-state model and power flow analysis of grid-connected photovoltaic power system. IEEE International Conference on Industrial Technology, Chengdu, China, 21-24 April, pp 1-6. doi:10.1109/ICIT.2008.4608553

Wilson TL, Bell DG (2004) Energy conservation and demand control using distribution automation technologies. Rural Electric Power Conference, Scottsdale, AZ, USA, 25 May, pp C4-1. doi:10.1109/REPCON.2004.1307059

Xu H, Liu W, Wang L, Li M, Zhang J (2015) Optimal sizing of small hydro power plants in consideration of voltage control. International Symposium on Smart Electric Distribution Systems and Technologies, Vienna, Austria, 8-11 September, pp 165-172. doi:10.1109/SEDST.2015.7315201

Xu S, Wang S, Zuo G, Davidson C, Oliveira M, Memisevic R, Pilz G, Donmez B, Andersen B (2019) Application Examples of STATCOM. In: Andersen B, Nilsson SL (eds) Flexible AC Transmission Systems. CIGRE Green Books. Springer, Cham. doi:10.1007/978-3-319-71926-9_13-1

Zeadally S, Pathan ASK, Alcaraz C, Badra M (2013) Towards Privacy Protection in Smart Grid. Wireless Personal Communications, vol 73/1, pp 1-22. doi:10.1007/s11277-012-0939-1

Zhang F, Guo X, Chang X, Fan G, Chen L, Wang Q, Tang Y, Dai J (2017) The reactive power voltage control strategy of PV systems in low-voltage string lines. IEEE Manchester PowerTech, Manchester, UK, 18-22 June, pp 1-6. doi:10.1109/PTC.2017.7980995

Zhang XP, Rehtanz C, Pal B (2006) Flexible AC Transmission Systems: Modelling and Control. Springer, Heidelberg

Zhou X, Farivar M, Liu Z, Chen L, Low SH (2021) Reverse and Forward Engineering of Local Voltage Control in Distribution Networks. IEEE Transactions on Automatic Control, vol 66/3, pp 1116-1128. doi:10.1109/TAC.2020.2994184

List of Abbreviations

AC ..... Alternating current
BLiN ..... Boundary link node
BPN ..... Boundary producer node
BSN ..... Boundary storage node
BVL ..... Boundary voltage limit
CD ..... Compensating device
CP ..... Customer plant
DC ..... Direct current
DER ..... Distributed energy resource
DFIG ..... Doubly-fed induction generator
DiC ..... Direct control
DMS ..... Distribution management system
DSO ..... Distribution system operator
DTR ..... Distribution transformer
ElA ..... Electrical appliance
EMS ..... Energy management system
EV ..... Electric vehicle
FACTS ..... Flexible alternating current transmission systems
FCWG ..... Full-converter wind generator
HV ..... High voltage
HVDC ..... High voltage direct current
HzW**SC** ..... Hertz/Watt secondary control
LC ..... Local control
LCC ..... Line-commutated converter
LV ..... Low voltage
LVR ..... Line voltage regulator
MC ..... Manual control
MSC ..... Mechanically switched capacitor
MSR ..... Mechanically switched reactor
MV ..... Medium voltage
OLTC ..... On-load tap changer
PC ..... Primary control
PhST ..... Phase-shifting transformer
PV ..... Photovoltaic
RPD ..... Reactive power device
SC ..... Secondary control

SCADA ..... Supervisory control and data acquisition
SM ..... Synchronous machine
SMPS ..... Switch-mode power supply
SO ..... System operator
SSSC ..... Static synchronous series compensator
STATCOM ..... Static synchronous compensator
STR ..... Supplying transformer
SVC ..... Static var compensator
SyC ..... Synchronous condenser
TCSC ..... Thyristor-controlled series capacitor
TCSR ..... Thyristor-controlled series reactor
TSO ..... Transmission system operator
TSSC ..... Thyristor-switched series capacitor
TSSR ..... Thyristor-switched series reactor
VI ..... Violation index
VSC ..... Voltage source converter
Vv**SC** ..... Volt/var secondary control
WT ..... Wind turbine

List of Figures

List of Tables

Affidavit

In lieu of oath, I declare that I wrote this thesis and performed the associated research myself, using only literature cited in this volume. If text passages from sources are used literally, they are marked as such.

I confirm that this work is original and has not been submitted elsewhere for any examination, nor is it currently under consideration for a thesis elsewhere.

I acknowledge that the submitted work will be checked electronically-technically using suitable and state-of-the-art means (plagiarism detection software). On the one hand, this ensures that the submitted work was prepared according to the high-quality standards within the applicable rules to ensure good scientific practice "Code of Conduct" at the TU Wien. On the other hand, a comparison with other student theses avoids violations of my personal copyright.

Vienna, 18 June 2021

City and Date

Signature

Appendix

A.1 Behaviour of different Link-Grids

This appendix catalogues the simulated behaviour of all Link-Grids listed in Table A.1 under different Volt/var control strategies and for the case without any Volt/var control. The rural residential CP_Link-Grid and the rural LV_Link-Grid are calculated for both spiky and smooth load profiles at the CP level. Meanwhile, all other Link-Grids are simulated only for the smoothed load profiles.

Table A.1 Overview of the simulated Link-Grids.

Level	**Link-Grid**	**Load profiles at the CP level**
CP	Rural residential	Spiky
		Smooth
	Urban residential	Smooth
LV	Rural	Spiky
		Smooth
	Urban	Smooth
MV	Small	Smooth
	Large	Smooth

A.1.1 Spiky load profiles

A.1.1.1 CP level

Rural residential CP_Link-Grid connected to LV level

Model specification:

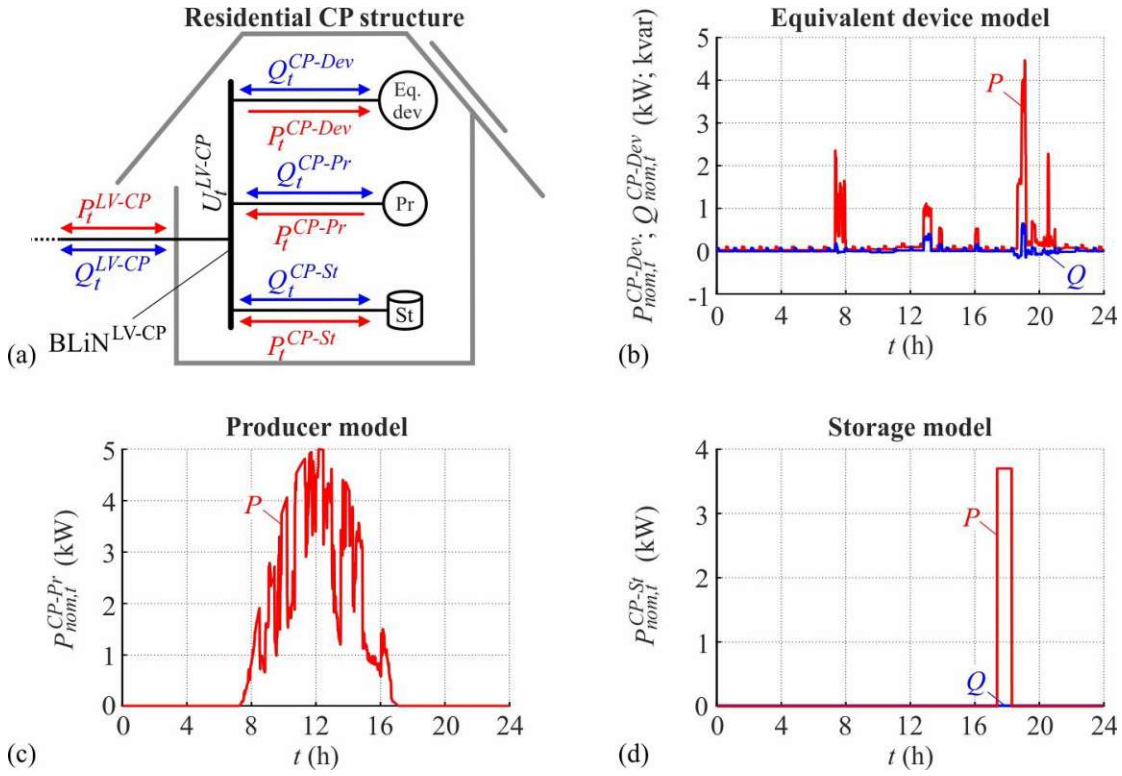

Fig. A.1 Rural residential CP_Link-Grid: (a) Structure; (b) Spiky load profiles of the Eq. dev.-model; (c) Spiky load profile of the Pr.-model; (d) Spiky load profiles of the St.-model.

Table A.2 Model data of the rural residential CP_Link-Grid with spiky load profiles.

CP structure	Equivalent device model	SMPS, motors, resistive, lighting
	Producer model	One photovoltaic system
	Storage model	One electric vehicle charger
Equivalent device model	Daily energy consumption	4.25 kWh
	Max. active power consumption	4.46 kW
	Max. reactive power consumption	0.65 kvar
	Max. reactive power production	0.16 kvar
	ZIP coefficients	Time-invariant
	References	(Bokhari et al. 2014; LPF 2020)
Producer model	Daily energy production	23.14 kWh
	Max. active power production	5.00 kW
	Reactive power contribution	According to Volt/var control strategy
	References	(McKenna et al. 2015)
Storage model	Daily energy consumption	1.85 kWh
	Max. active power consumption	3.7 kW
	ZIP coefficients	Time-invariant
	References	(Shukla et al. 2017; LPF 2020)

Behaviour of Link-Grid without any Volt/var controls:

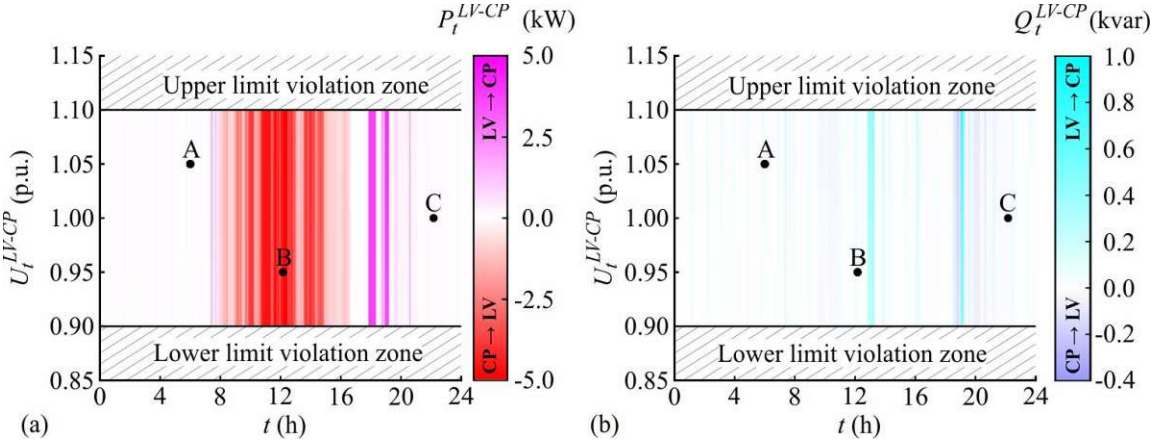

Fig. A.2 Daily behaviour of the rural residential CP_Link-Grid with spiky load profiles and without any Volt/var control for various voltages at the LV-CP boundary node: (a) LV-CP active power exchange; (b) LV-CP reactive power exchange.

LV-CP reactive power exchange for different Volt/var controls:

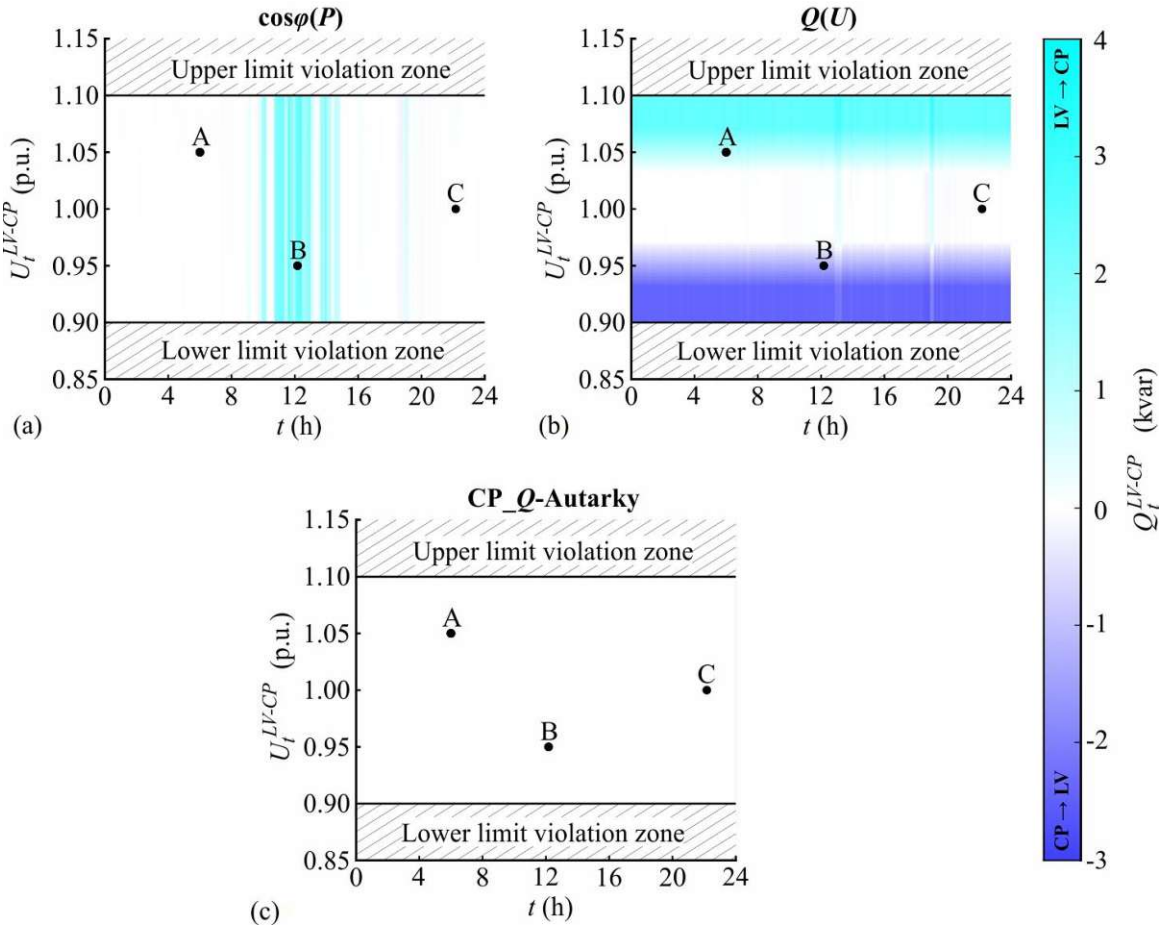

Fig. A.3 Daily LV-CP reactive power exchange of the rural residential CP_Link-Grid with spiky load profiles for various voltages at the LV-CP boundary node and different control strategies: (a) cosφ(P); (b) Q(U); (c) CP_Q-Autarky.

Behaviour of Link-Grid in cases A, B and C:

Table A.3 LV-CP reactive power exchange of the rural residential CP_Link-Grid with spiky load profiles for different cases, no control and various control strategies.

Control strategy	Q_t^{LV-CP} (kvar)		
	Case A	Case B	Case C
None	-0.0044	0.0182	-0.0131
cos$\varphi(P)$	-0.0044	2.4395	-0.0131
$Q(U)$	1.2056	-1.1918	-0.0131
CP_Q-Autarky	0.0000	0.0000	0.0000

Table A.4 Reactive power contribution of consuming devices connected to the rural residential CP_Link-Grid with spiky load profiles for different cases, no control and various control strategies.

Control strategy	Q_t^{CP-Dev} (kvar)		
	Case A	Case B	Case C
None	-0.0044	0.0182	-0.0131
cos$\varphi(P)$	-0.0044	0.0182	-0.0131
$Q(U)$	-0.0044	0.0182	-0.0131
CP_Q-Autarky	-0.0044	0.0182	-0.0131

Table A.5 Reactive power contribution of the producer connected to the rural residential CP_Link-Grid with spiky load profiles for different cases, no control and various control strategies.

Control strategy	Q_t^{CP-Pr} (kvar)		
	Case A	Case B	Case C
None	0.0000	0.0000	0.0000
cos$\varphi(P)$	0.0000	2.4213	0.0000
$Q(U)$	1.2100	-1.2100	0.0000
CP_Q-Autarky	0.0044	-0.0182	0.0131

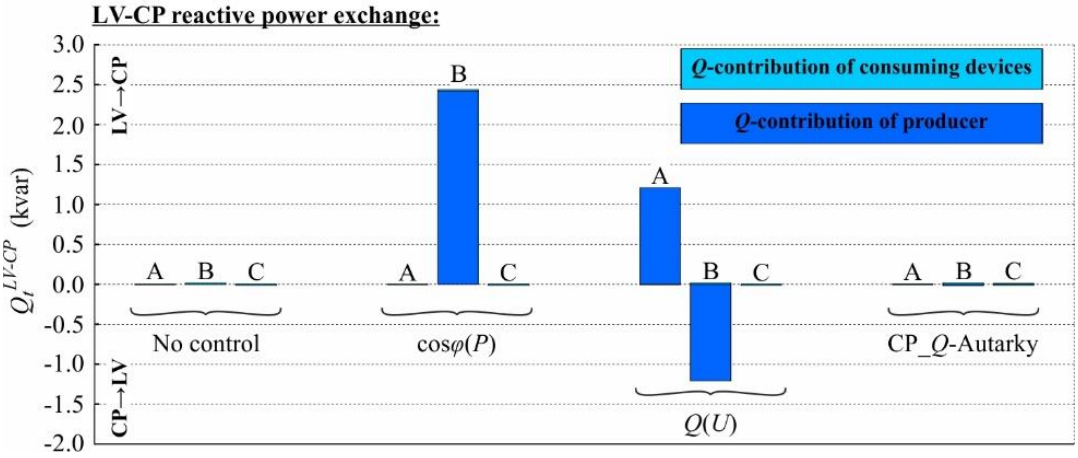

Fig. A.4 Composition of the LV-CP reactive power exchange of the rural residential CP_Link-Grid with spiky load profiles for different cases, no control and various control strategies.

A.1.1.2 LV level

Rural LV_Link-Grid

Model specification:

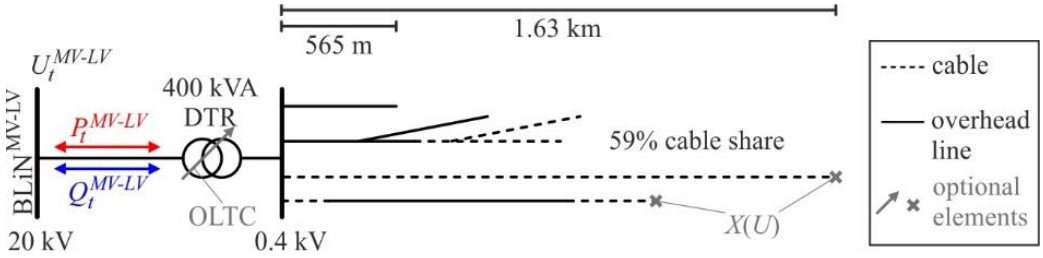

Fig. A.5 Simplified one-line diagram of the rural LV_Link-Grid (real Austrian grid).

Table A.6 Model data of the rural LV_Link-Grid for spiky load profiles at the CP level.

DTR	Rating:		400 kVA
	Nominal voltage	Primary Secondary	21.0 kV 0.42 kV
	Short circuit voltage	Total Resistive part	3.7 % 1.0 %
Feeders	Nominal voltage		0.4 kV
	Number of feeders		4
	Total line length		6.335 km
	Total cable share		58.64 %
	Feeder length	Maximal Minimal	1.630 km 0.565 km
Control parameters	OLTC	Upper voltage limit Lower voltage limit Min./mid/max. tap positions Additional voltage per tap	0.990 p.u. 0.950 p.u. 1/3/5 2.5 %
	$X(U)$	Upper voltage limit Lower voltage limit	1.09 p.u. 0.91 p.u.
Connected lumped models	Link-Grids CP	Residential with spiky load profiles	61

Behaviour of Link-Grid without any Volt/var controls:

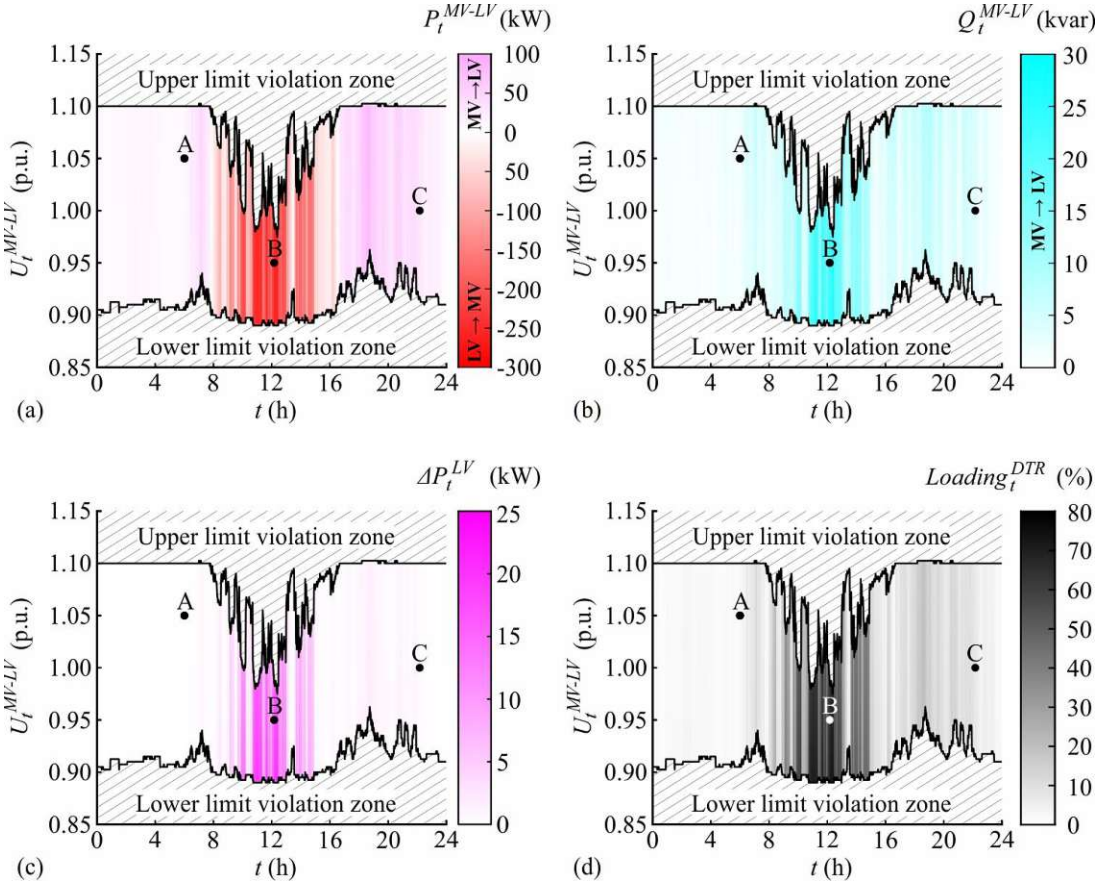

Fig. A.6 Daily behaviour of the rural LV_Link-Grid without any Volt/var control for various voltages at the MV-LV boundary node and spiky load profiles at the CP level: (a) MV-LV active power exchange; (b) MV-LV reactive power exchange; (c) LV active power loss; (d) DTR loading.

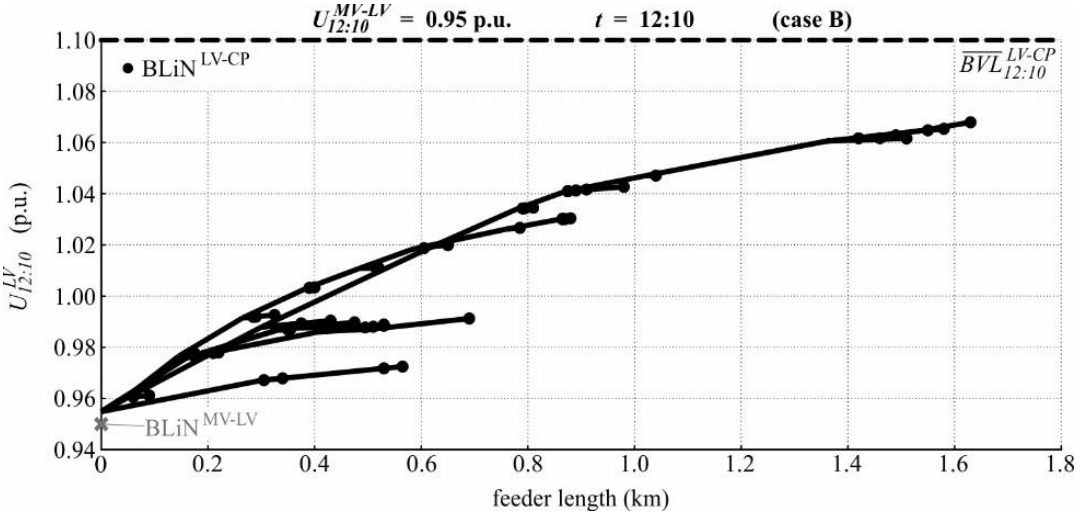

Fig. A.7 Voltage profiles of the rural LV_Link-Grid's feeders without any Volt/var control at 12:10 for an MV-LV boundary voltage of 0.95 p.u. (case B) and spiky load profiles at the CP level.

MV-LV reactive power exchange for different Volt/var controls:

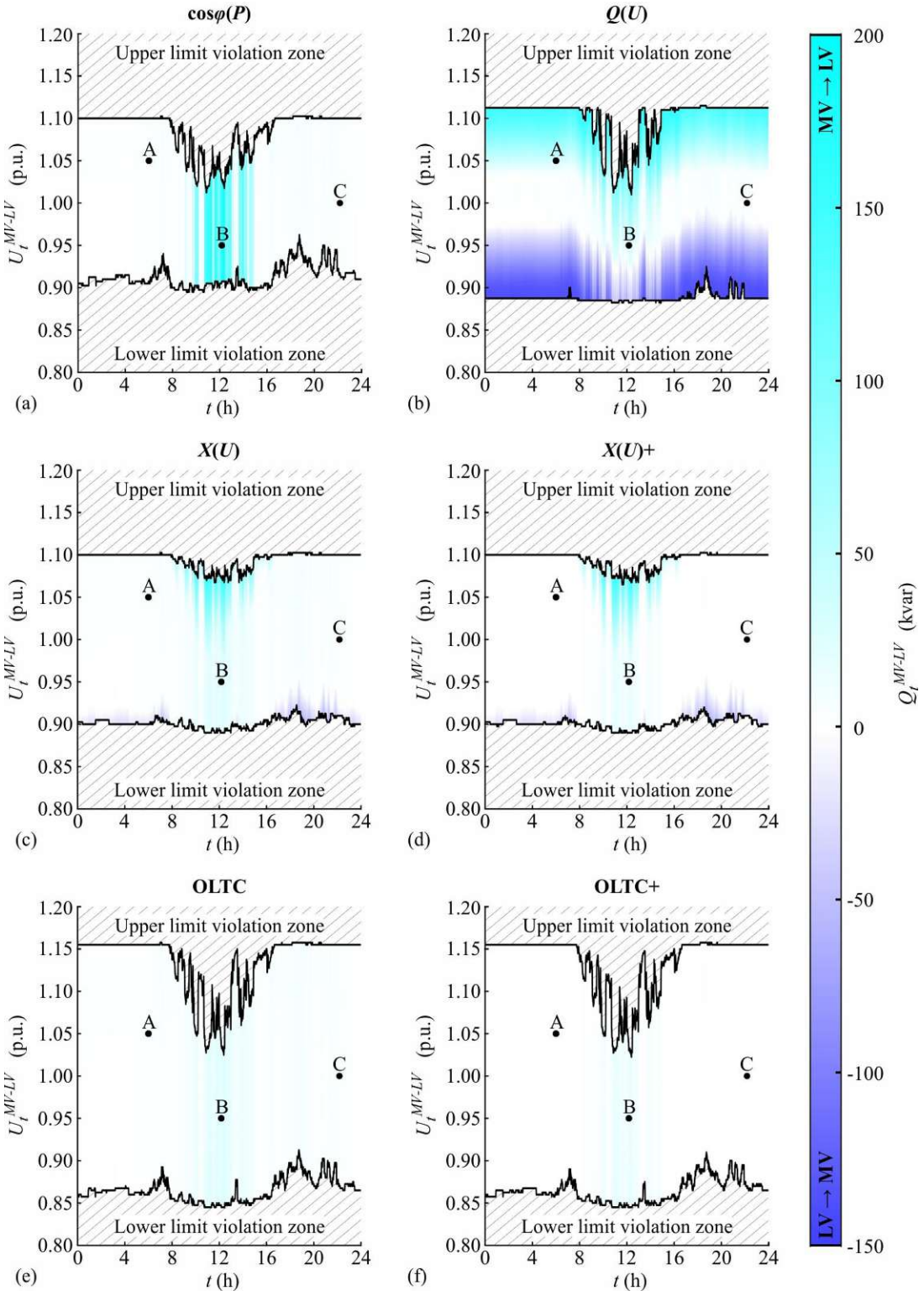

Fig. A.8 Daily MV-LV reactive power exchange of the rural LV_Link-Grid for various voltages at the MV-LV boundary node, spiky load profiles at the CP level, and different control strategies: (a) cos$\varphi(P)$; (b) $Q(U)$; (c) $X(U)$; (d) $X(U)$ and CP_Q-Autarky; (e) OLTC; (f) OLTC and CP_Q-Autarky.

LV active power loss for different Volt/var controls:

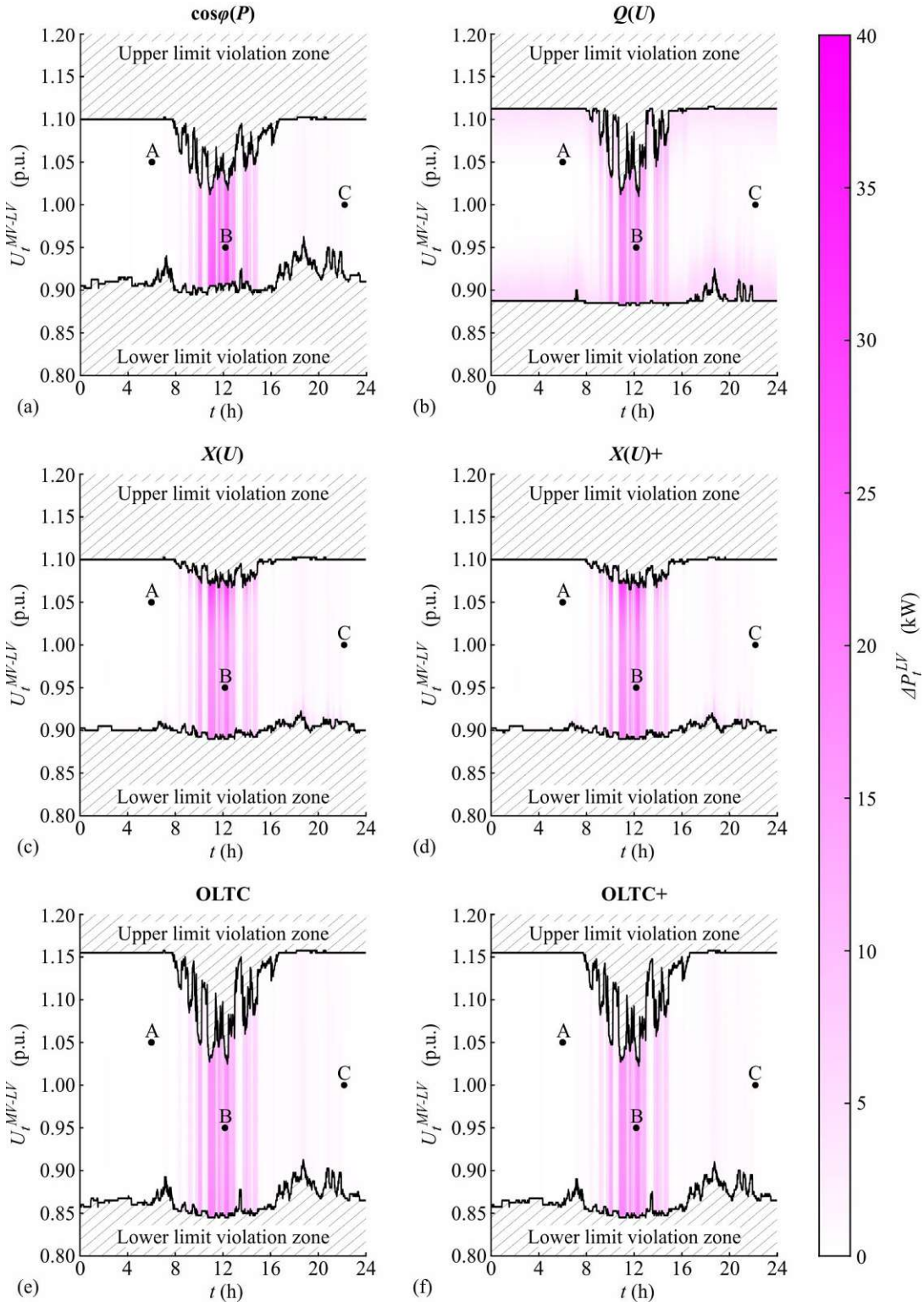

Fig. A.9 Daily active power loss within the rural LV_Link-Grid for various voltages at the MV-LV boundary node, spiky load profiles at the CP level, and different control strategies: (a) cos$\varphi(P)$; (b) $Q(U)$; (c) $X(U)$; (d) $X(U)$ and CP_Q-Autarky; (e) OLTC; (f) OLTC and CP_Q-Autarky.

DTR loading for different Volt/var controls:

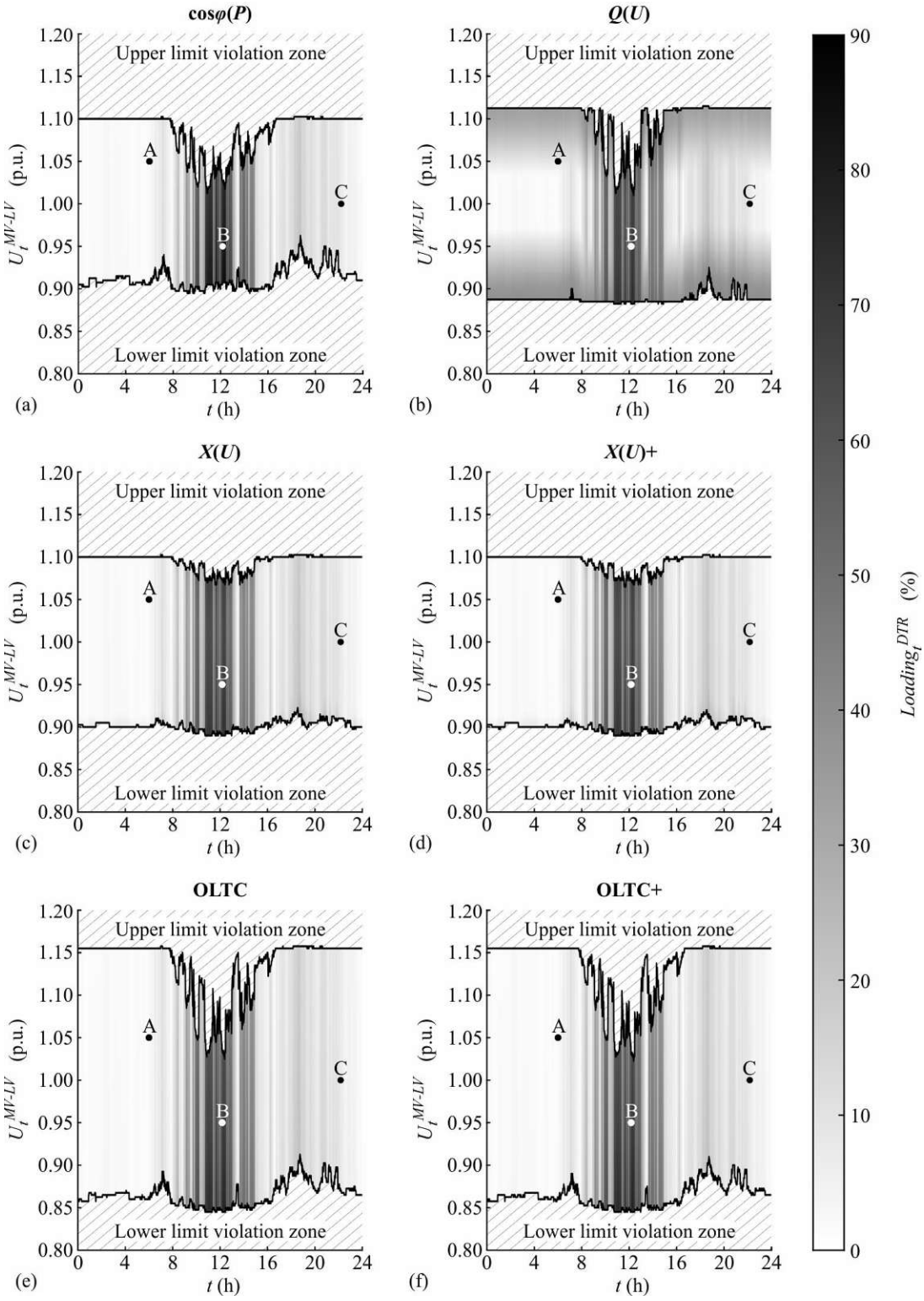

Fig. A.10 Daily DTR loading within the rural LV_Link-Grid for various voltages at the MV-LV boundary node, spiky load profiles at the CP level, and different control strategies: (a) cosφ(P); (b) Q(U); (c) X(U); (d) X(U) and CP_Q-Autarky; (e) OLTC; (f) OLTC and CP_Q-Autarky.

Behaviour of Link-Grid in cases A, B and C:

Table A.7 MV-LV reactive power exchange of the rural LV_Link-Grid for spiky load profiles at the CP level, different cases, no control and various control strategies.

Control strategy	Q_t^{MV-LV} (kvar)		
	Case A	Case B	Case C
None	1.1849	23.7847	3.7581
cos$\varphi(P)$	1.1849	178.2922	3.7581
$Q(U)$	37.8057	36.1168	3.7581
$X(U)$	1.1849	23.7847	3.7583
$X(U)$+	-0.1576	16.6295	0.0536
OLTC	1.0427	23.4057	3.5752
OLTC+	-0.1403	16.6295	0.0682

Table A.8 Reactive power contribution of the CP_Link-Grids connected to the rural LV_Link-Grid for spiky load profiles at the CP level, different cases, no control and various control strategies.

Control strategy	$Q_{\Sigma,t}^{LV-CP}$ (kvar)		
	Case A	Case B	Case C
None	1.3421	7.0678	3.6998
cos$\varphi(P)$	1.3421	154.0554	3.6998
$Q(U)$	37.6942	19.1260	3.6998
$X(U)$	1.3421	7.0678	3.6998
$X(U)$+	0.0000	0.0000	0.0000
OLTC	1.1826	7.4946	3.5024
OLTC+	0.0000	0.0000	0.0000

Table A.9 Reactive power contribution of the rural LV_Link-Grid for spiky load profiles at the CP level, different cases, no control and various control strategies.

Control strategy	$Q_{\Sigma,t}^{LV}$ (kvar)		
	Case A	Case B	Case C
None	-0.1572	16.7169	0.0585
cos$\varphi(P)$	-0.1572	24.2372	0.0585
$Q(U)$	0.1115	16.9907	0.0585
$X(U)$	-0.1572	16.7169	0.0585
$X(U)$+	-0.1576	16.6295	0.0536
OLTC	-0.1399	15.9111	0.0729
OLTC+	-0.1403	16.6295	0.0682

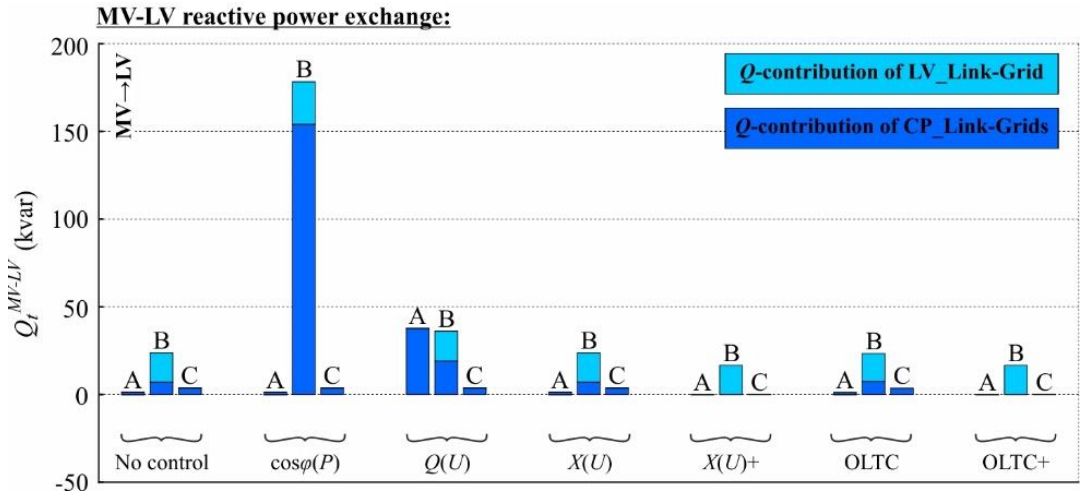

Fig. A.11 Composition of the MV-LV reactive power exchange of the rural LV_Link-Grid for spiky load profiles at the CP level, different cases, no control and various control strategies.

Table A.10 Active power loss within the rural LV_Link-Grid for spiky load profiles at the CP level, different cases, no control and various control strategies.

Control strategy	ΔP_t^{LV} (kW)		
	Case A	Case B	Case C
None	0.0250	17.1154	0.2402
cos$\varphi(P)$	0.0250	24.9791	0.2402
$Q(U)$	0.2931	17.6844	0.2402
$X(U)$	0.0250	17.1154	0.2402
$X(U)$+	0.0245	17.0116	0.2350
OLTC	0.0254	16.3134	0.2475
OLTC+	0.0250	17.0116	0.2426

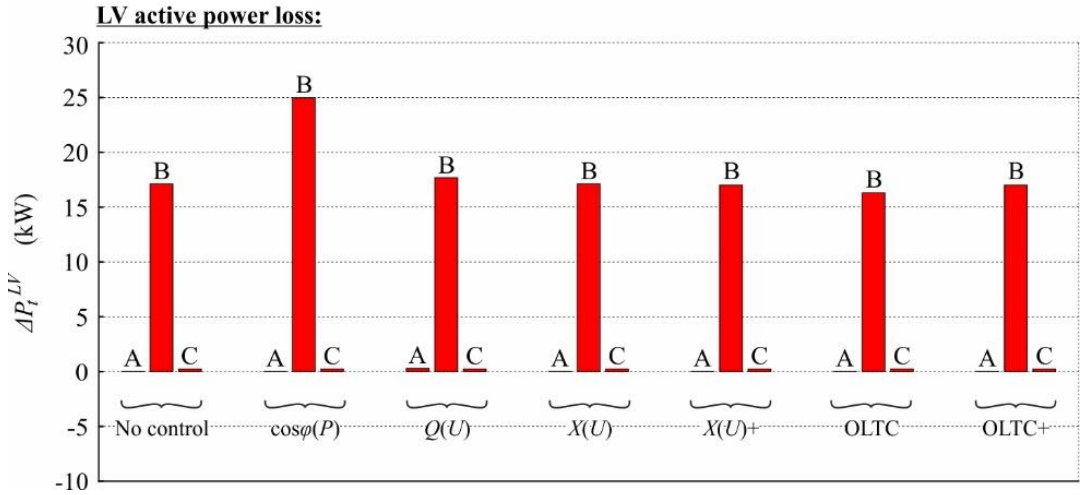

Fig. A.12 Active power loss within the rural LV_Link-Grid for spiky load profiles at the CP level, different cases, no control and various control strategies.

Table A.11 DTR loading within the rural LV_Link-Grid for spiky load profiles at the CP level, different cases, no control and various control strategies.

Control strategy	$Loading_t^{DTR}$ (%)		
	Case A	Case B	Case C
None	1.9979	68.0621	7.2600
cos$\varphi(P)$	1.9979	80.9169	7.2600
$Q(U)$	9.2271	68.3151	7.2600
$X(U)$	1.9979	68.0621	7.2600
$X(U)$+	1.9786	67.9281	7.2011
OLTC	1.9188	68.1371	7.1809
OLTC+	1.9033	67.9281	7.1269

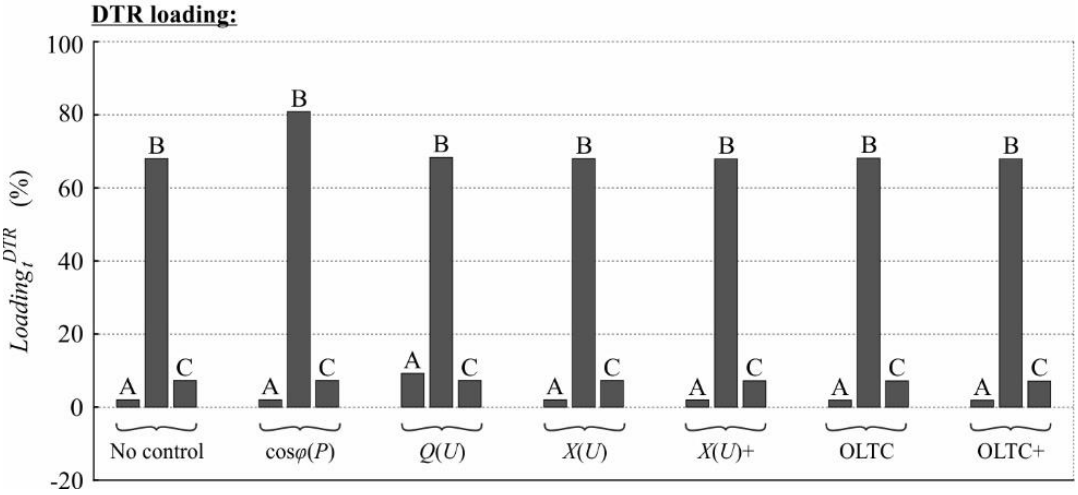

Fig. A.13 DTR loading within the rural LV_Link-Grid for spiky load profiles at the CP level, different cases, no control and various control strategies.

A.1.2 Smoothed load profiles

A.1.2.1 CP level

Rural residential CP_Link-Grid connected to LV level

Model specification:

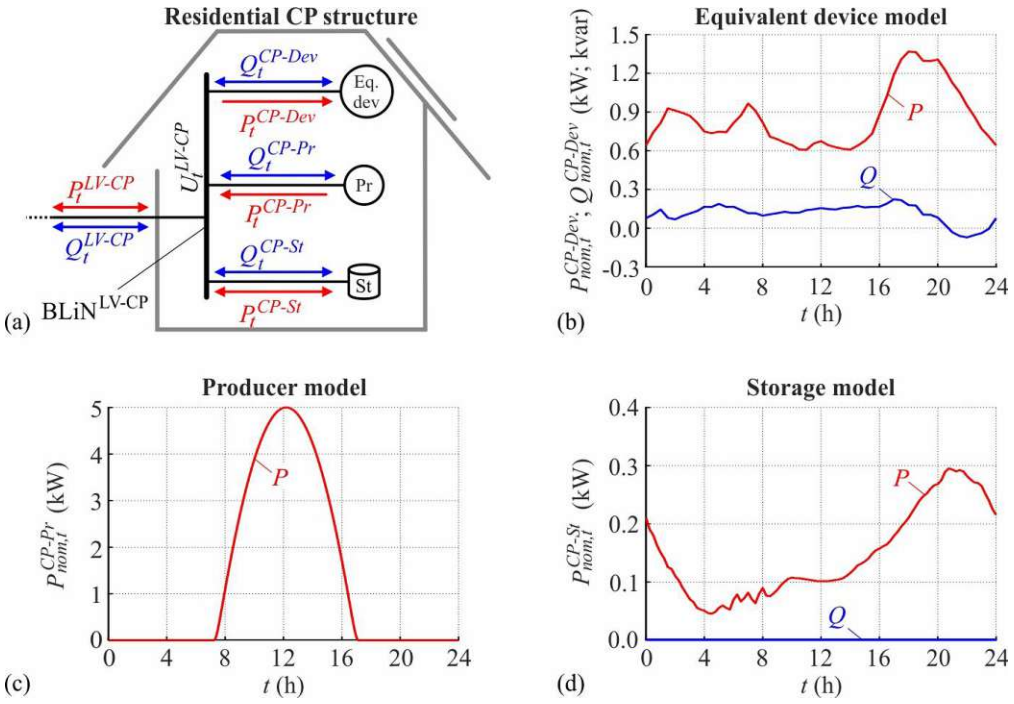

Fig. A.14 Rural residential CP_Link-Grid: (a) Structure; (b) Smoothed load profiles of the Eq. dev.-model; (c) Smoothed load profile of the Pr.-model; (d) Smoothed load profiles of the St.-model.

Table A.12 Model data of the rural residential CP_Link-Grid with smoothed load profiles.

CP structure	Equivalent device model	SMPS, motors, resistive, lighting
	Producer model	One photovoltaic system
	Storage model	One electric vehicle charger
Equivalent device model	Daily energy consumption	20.75 kWh
	Max. active power consumption*	1.37 kW
	Max. reactive power consumption	0.22 kvar
	Max. reactive power production	0.07 kvar
	ZIP coefficients	Time-variant
	References	(Schultis and Ilo 2019a)
Producer model	Daily energy production	31.37 kWh
	Max. active power production	5.00 kW
	Reactive power contribution	According to Volt/var control strategy
	References	(McKenna et al. 2015)
Storage model	Daily energy consumption	3.51 kWh
	Max. active power consumption	0.30 kW
	ZIP coefficients	Time-invariant
	References	(Shukla et al. 2017; Aunedi et al. 2015)

* This value is derived from the maximal active power flow through the DTR of the rural LV_Link-Grid measured throughout 2016.

Behaviour of Link-Grid without any Volt/var controls:

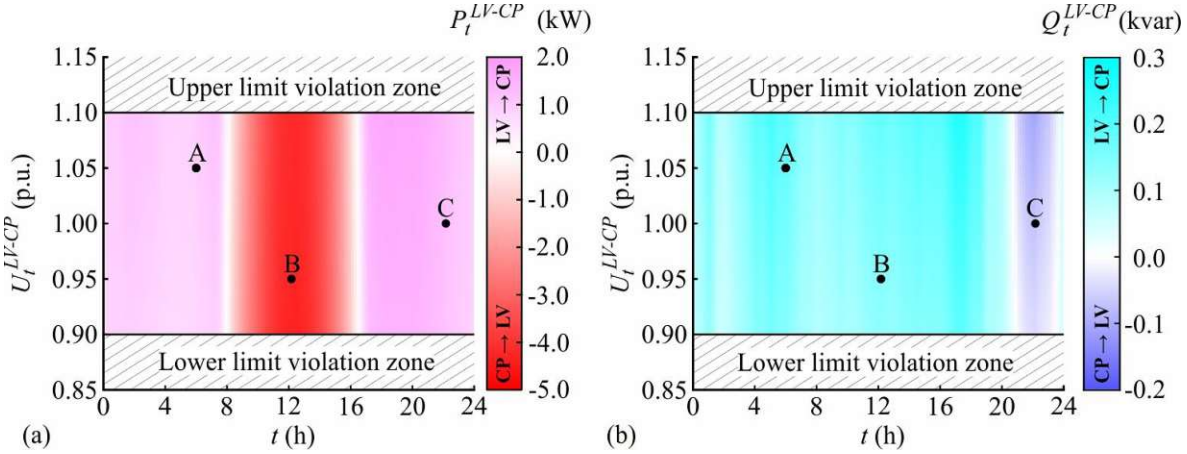

Fig. A.15 Daily behaviour of the rural residential CP_Link-Grid with smoothed load profiles and without any Volt/var control for various voltages at the LV-CP boundary node: (a) LV-CP active power exchange; (b) LV-CP reactive power exchange.

LV-CP reactive power exchange for different Volt/var controls:

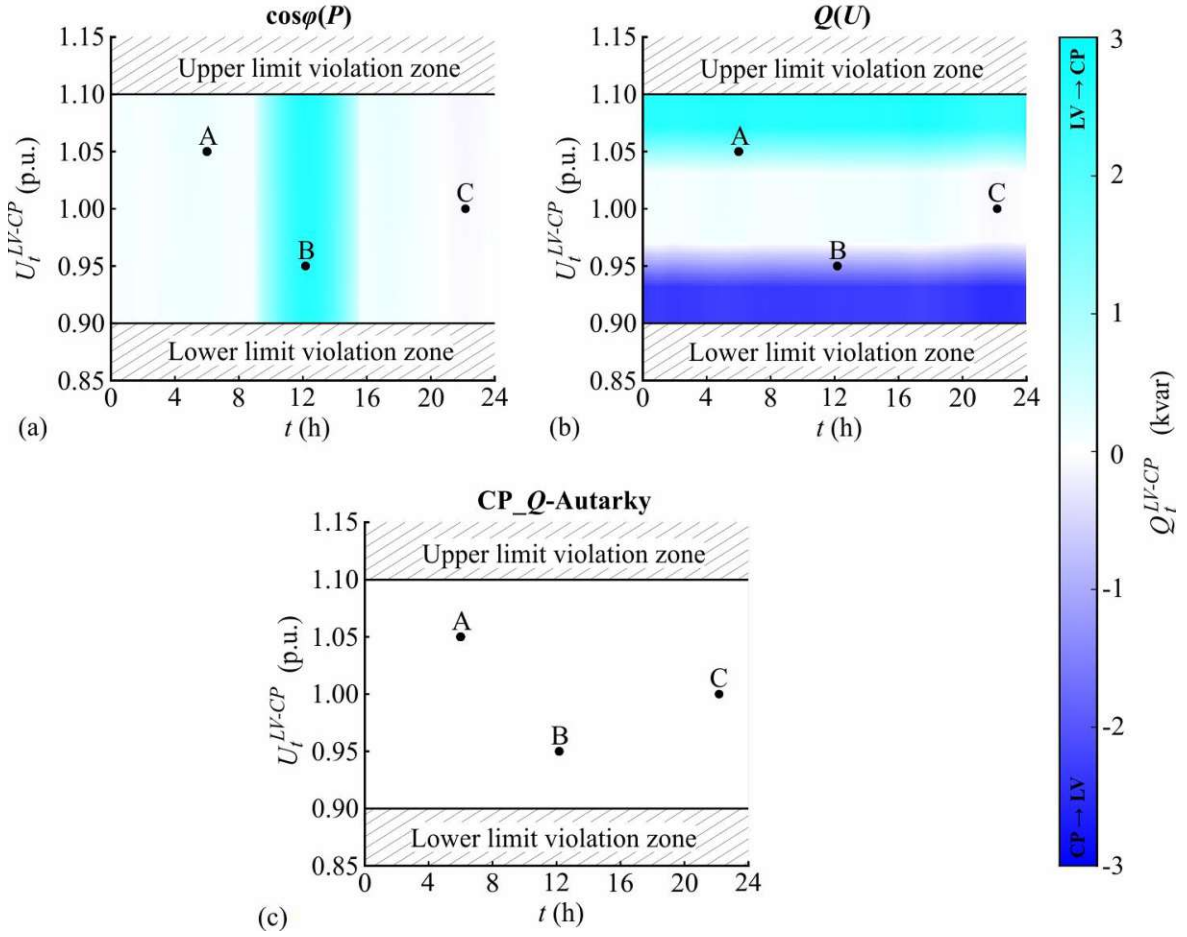

Fig. A.16 Daily LV-CP reactive power exchange of the rural residential CP_Link-Grid with smoothed load profiles for various voltages at the LV-CP boundary node and different control strategies: (a) cos$\varphi(P)$; (b) $Q(U)$; (c) CP_Q-Autarky.

Behaviour of Link-Grid in cases A, B and C:

Table A.13LV-CP reactive power exchange of the rural residential CP_Link-Grid for smoothed load profiles at the CP level, different cases, no control and various control strategies.

Control strategy	Q_t^{LV-CP} (kvar)		
	Case A	Case B	Case C
None	0.1791	0.1406	-0.0656
cos$\varphi(P)$	0.1791	2.5622	-0.0656
$Q(U)$	1.3891	-1.0694	-0.0656
CP_Q-Autarky	0.0000	0.0000	0.0000

Table A.14 Reactive power contribution of consuming devices connected to the rural residential CP_Link-Grid with smoothed load profiles for different cases, no control and various control strategies.

Control strategy	Q_t^{CP-Dev} (kvar)		
	Case A	Case B	Case C
None	0.1791	0.1406	-0.0656
cos$\varphi(P)$	0.1791	0.1406	-0.0656
$Q(U)$	0.1791	0.1406	-0.0656
CP_Q-Autarky	0.1791	0.1406	-0.0656

Table A.15 Reactive power contribution of the producer connected to the rural residential CP_Link-Grid with smoothed load profiles for different cases, no control and various control strategies.

Control strategy	Q_t^{CP-Pr} (kvar)		
	Case A	Case B	Case C
None	0.0000	0.0000	0.0000
cos$\varphi(P)$	0.0000	2.4215	0.0000
$Q(U)$	1.2100	-1.2100	0.0000
CP_Q-Autarky	-0.1791	-0.1406	0.0656

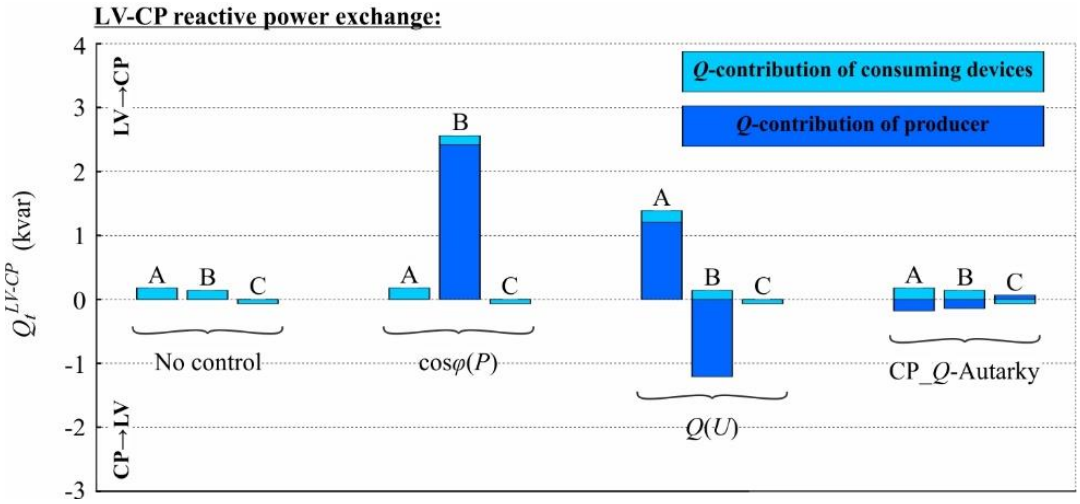

Fig. A.17 Composition of the LV-CP reactive power exchange of the rural residential CP_Link-Grid with smoothed load profiles for different cases, no control and various control strategies.

Urban residential CP_Link-Grid connected to LV level

Model specification:

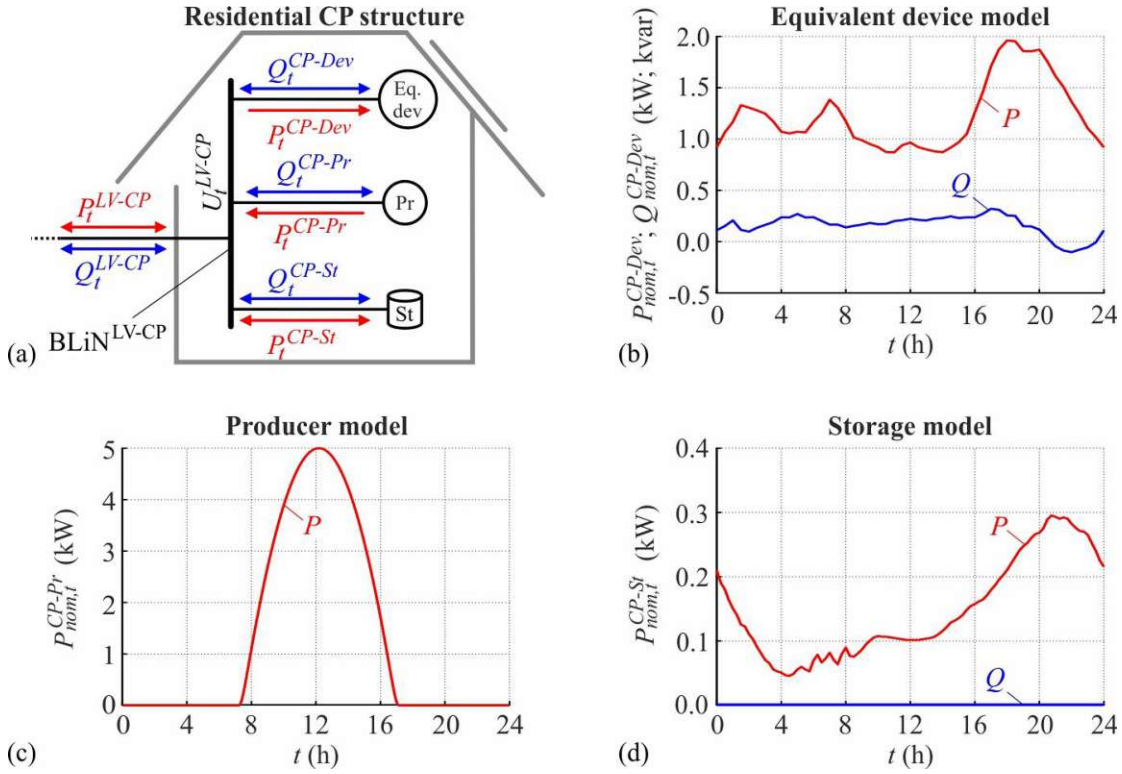

Fig. A.18 Urban residential CP_Link-Grid: (a) Structure; (b) Smoothed load profiles of the Eq. dev.-model; (c) Smoothed load profile of the Pr.-model; (d) Smoothed load profiles of the St.-model.

Table A.16 Model data of the urban residential CP_Link-Grid with smoothed load profiles.

CP structure	Equivalent device model	SMPS, motors, resistive, lighting
	Producer model	One photovoltaic system
	Storage model	One electric vehicle charger
Equivalent device model	Daily energy consumption	29.73 kWh
	Max. active power consumption*	1.96 kW
	Max. reactive power consumption	0.32 kvar
	Max. reactive power production	0.10 kvar
	ZIP coefficients	Time-variant
	References	(Schultis and Ilo 2019a)
Producer model	Daily energy production	31.37 kWh
	Max. active power production	5.00 kW
	Reactive power contribution	According to Volt/var control strategy
	References	(McKenna et al. 2015)
Storage model	Daily energy consumption	3.51 kWh
	Max. active power consumption	0.30 kW
	ZIP coefficients	Time-invariant
	References	(Shukla et al. 2017; Aunedi et al. 2015)

* This value is derived from the maximal active power flow through the DTR of the urban LV_Link-Grid measured throughout 2016.

Behaviour of Link-Grid without any Volt/var controls:

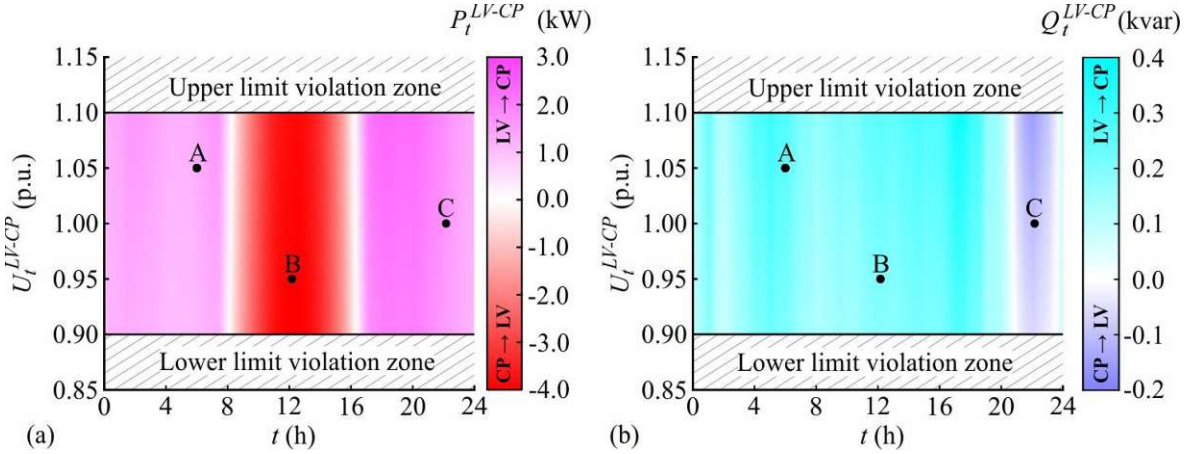

Fig. A.19 Daily behaviour of the urban residential CP_Link-Grid with smoothed load profiles and without any Volt/var control for various voltages at the LV-CP boundary node: (a) LV-CP active power exchange; (b) LV-CP reactive power exchange.

LV-CP reactive power exchange for different Volt/var controls:

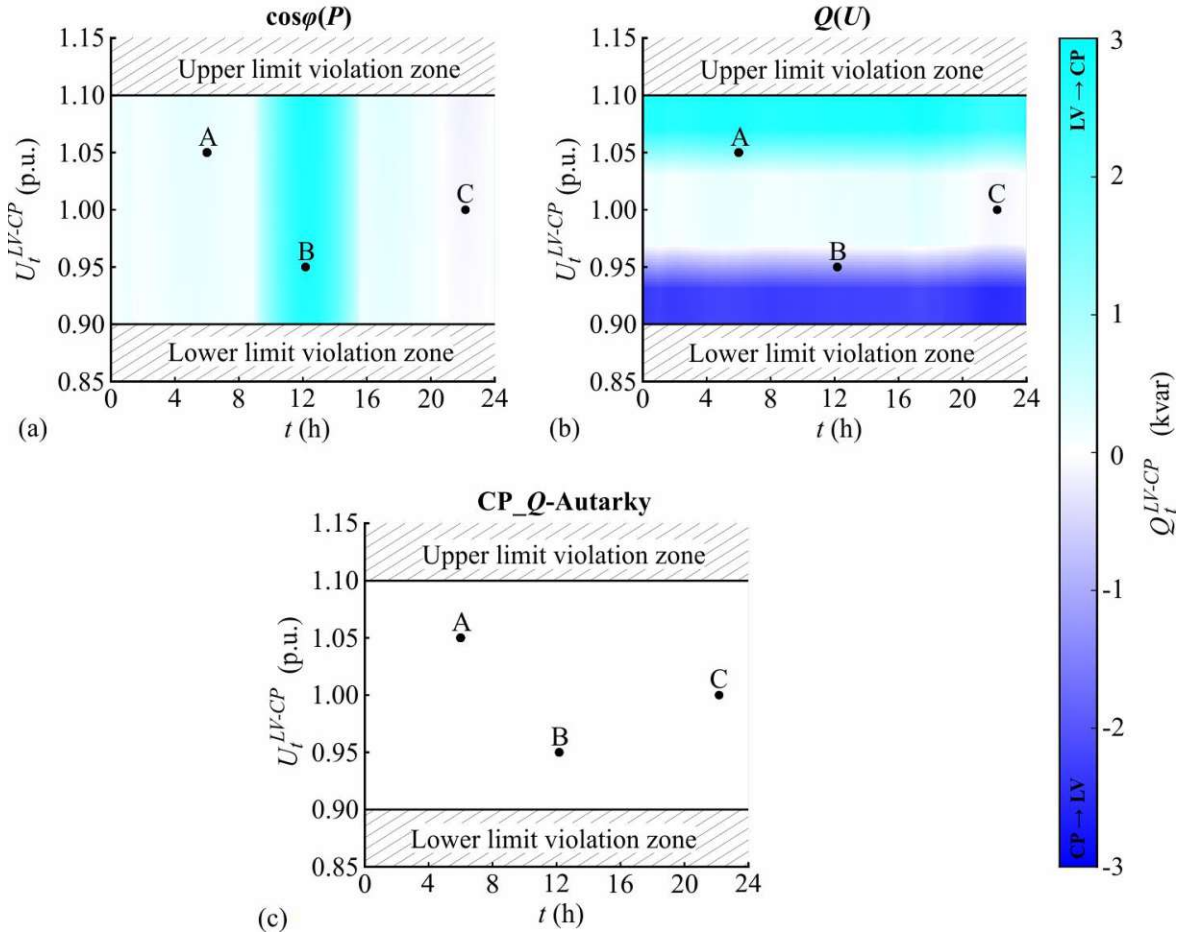

Fig. A.20 Daily LV-CP reactive power exchange of the urban residential CP_Link-Grid with smoothed load profiles for various voltages at the LV-CP boundary node and different control strategies: (a) cos$\varphi(P)$; (b) $Q(U)$; (c) CP_Q-Autarky.

Behaviour of Link-Grid in cases A, B and C:

Table A.17LV-CP reactive power exchange of the urban residential CP_Link-Grid for smoothed load profiles at the CP level, different cases, no control and various control strategies.

Control strategy	Q_t^{LV-CP} (kvar)		
	Case A	Case B	Case C
None	0.2566	0.2015	-0.0940
cos$\varphi(P)$	0.2566	2.6230	-0.0940
$Q(U)$	1.4666	-1.0085	-0.0940
CP_Q-Autarky	0.0000	0.0000	0.0000

Table A.18 Reactive power contribution of consuming devices connected to the urban residential CP_Link-Grid with smoothed load profiles for different cases, no control and various control strategies.

Control strategy	Q_t^{CP-Dev} (kvar)		
	Case A	Case B	Case C
None	0.2566	0.2015	-0.0940
cos$\varphi(P)$	0.2566	0.2015	-0.0940
$Q(U)$	0.2566	0.2015	-0.0940
CP_Q-Autarky	0.2566	0.2015	-0.0940

Table A.19 Reactive power contribution of the producer connected to the urban residential CP_Link-Grid with smoothed load profiles for different cases, no control and various control strategies.

Control strategy	Q_t^{CP-Pr} (kvar)		
	Case A	Case B	Case C
None	0.0000	0.0000	0.0000
cos$\varphi(P)$	0.0000	2.4215	0.0000
$Q(U)$	1.2100	-1.2100	0.0000
CP_Q-Autarky	-0.2566	-0.2015	0.0940

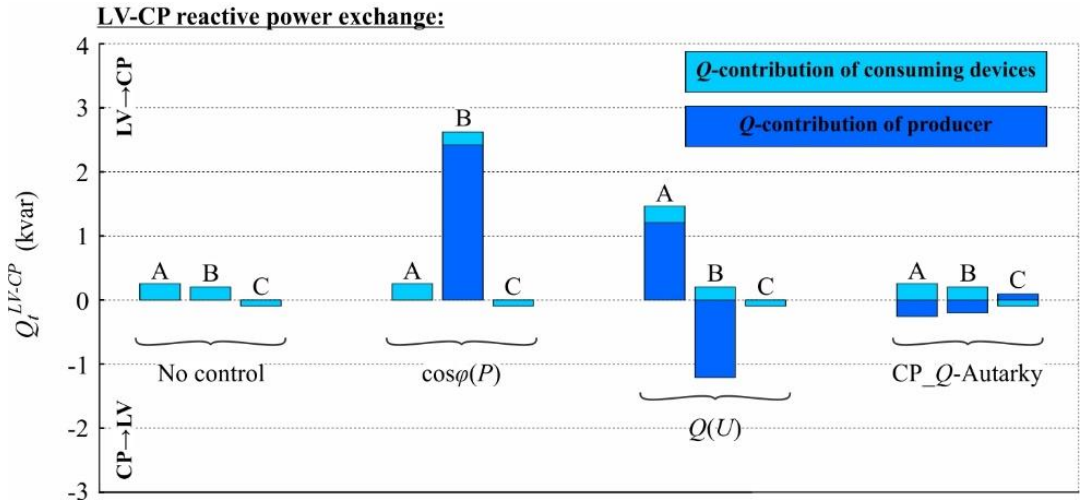

Fig. A.21 Composition of the LV-CP reactive power exchange of the urban residential CP_Link-Grid with smoothed load profiles for different cases, no control and various control strategies.

Commercial CP_Link-Grid connected to MV level

Model specification:

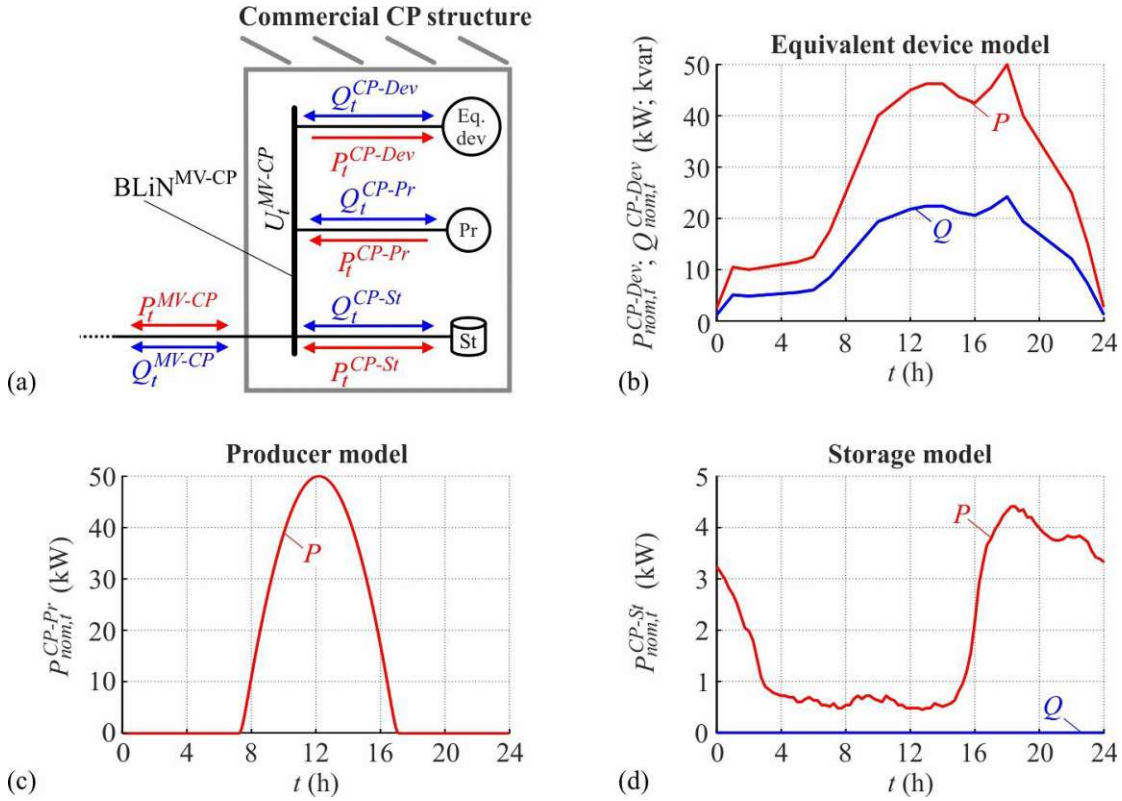

Fig. A.22 Commercial CP_Link-Grid: (a) Structure; (b) Smoothed load profiles of the Eq. dev.-model; (c) Smoothed load profile of the Pr.-model; (d) Smoothed load profiles of the St.-model.

Table A.20 Model data of the commercial CP_Link-Grid with smoothed load profiles.

CP structure	Equivalent device model	SMPS, motors, resistive, lighting
	Producer model	One photovoltaic system
	Storage model	Three electric vehicle chargers
Equivalent device model	Daily energy consumption	690.25 kWh
	Max. active power consumption	50 kW
	Power factor	0.90 inductive
	ZIP coefficients	Time-invariant
	References	(CIGRE 2014a; Bokhari et al. 2014)
Producer model	Daily energy production	313.65 kWh
	Max. active power production	50 kW
	Reactive power contribution	According to Volt/var control strategy
	References	(McKenna et al. 2015)
Storage model	Daily energy consumption	46.03 kWh
	Max. active power consumption	4.41 kW
	ZIP coefficients	Time-invariant
	References	(Shukla et al. 2017; Aunedi et al. 2015)

Behaviour of Link-Grid without any Volt/var controls:

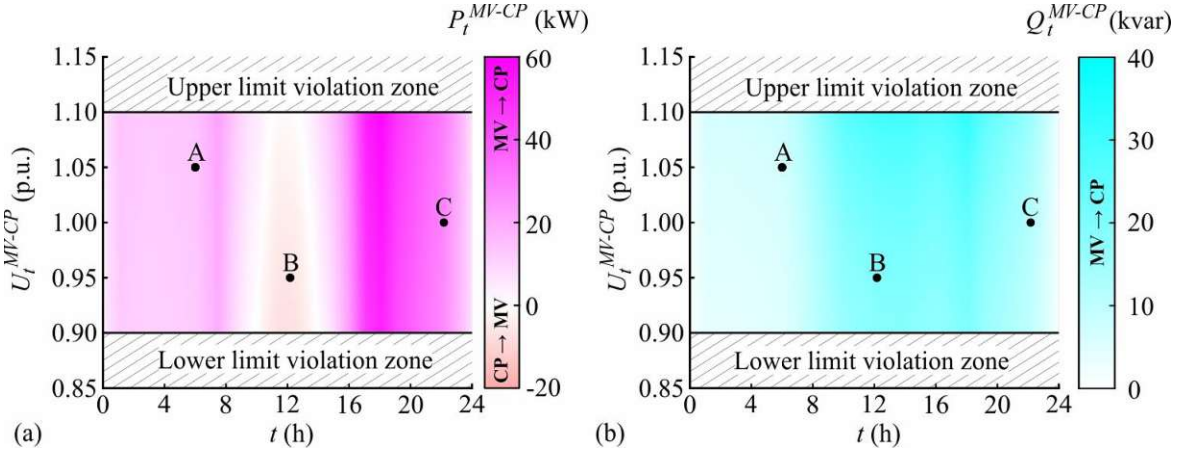

Fig. A.23 Daily behaviour of the commercial CP_Link-Grid with smoothed load profiles and without any Volt/var control for various voltages at the MV-CP boundary node: (a) MV-CP active power exchange; (b) MV-CP reactive power exchange.

MV-CP reactive power exchange for different Volt/var controls:

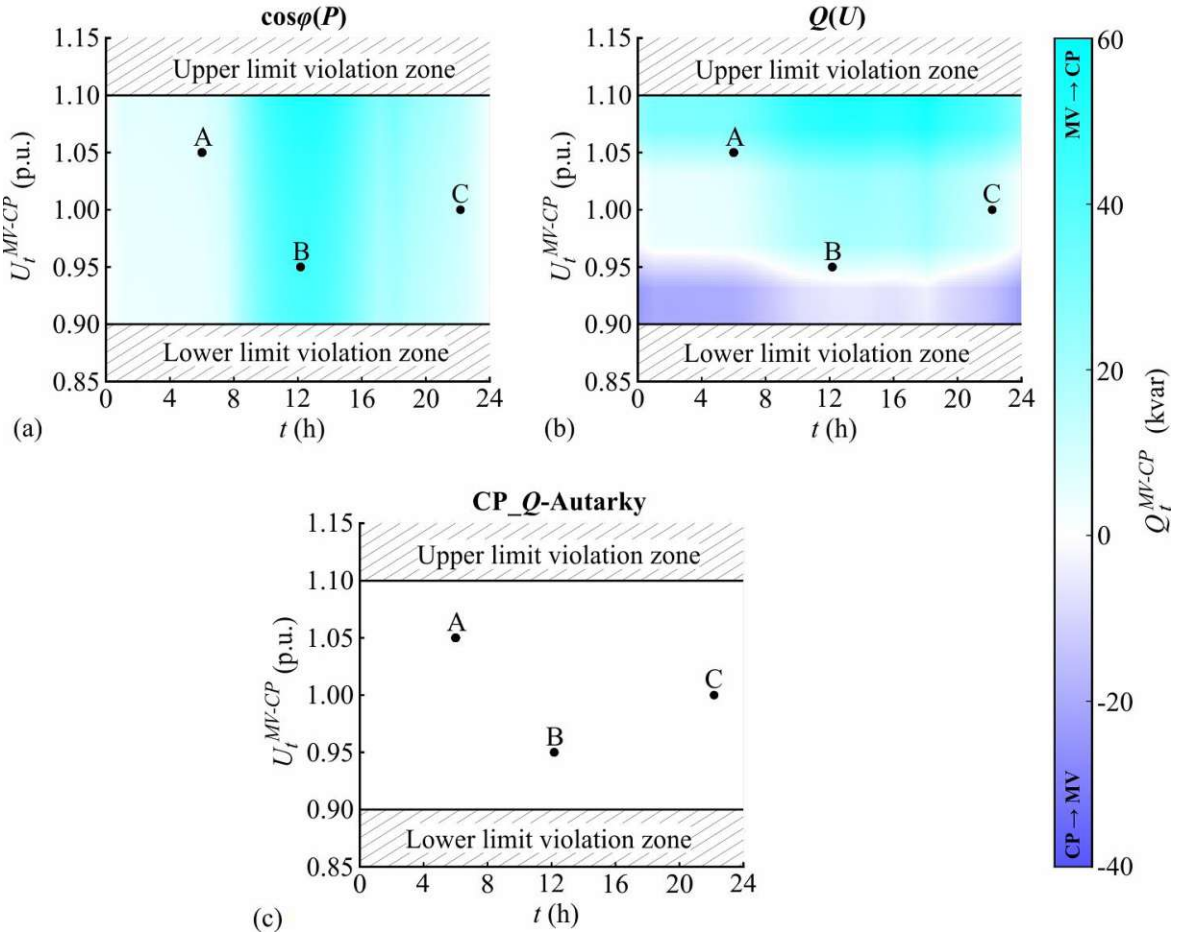

Fig. A.24 Daily MV-CP reactive power exchange of the commercial CP_Link-Grid with smoothed load profiles for various voltages at the MV-CP boundary node and different control strategies: (a) cos$\varphi(P)$; (b) $Q(U)$; (c) CP_Q-Autarky.

Behaviour of Link-Grid in cases A, B and C:

Table A.21 LV-CP reactive power exchange of the commercial CP_Link-Grid for smoothed load profiles at the CP level, different cases, no control and various control strategies.

Control strategy	Q_t^{MV-CP} (kvar)		
	Case A	Case B	Case C
None	6.9423	19.5685	11.3008
cos$\varphi(P)$	6.9423	43.7842	11.3008
$Q(U)$	19.0423	7.4685	11.3008
CP_Q-Autarky	0.0000	0.0000	0.0000

Table A.22 Reactive power contribution of consuming devices connected to the commercial CP_Link-Grid with smoothed load profiles for different cases, no control and various control strategies.

Control strategy	Q_t^{CP-Dev} (kvar)		
	Case A	Case B	Case C
None	6.9423	19.5685	11.3008
cos$\varphi(P)$	6.9423	19.5685	11.3008
$Q(U)$	6.9423	19.5685	11.3008
CP_Q-Autarky	6.9423	19.5685	11.3008

Table A.23 Reactive power contribution of the producer connected to the commercial CP_Link-Grid with smoothed load profiles for different cases, no control and various control strategies.

Control strategy	Q_t^{CP-Pr} (kvar)		
	Case A	Case B	Case C
None	0.0000	0.0000	0.0000
cos$\varphi(P)$	0.0000	24.2158	0.0000
$Q(U)$	12.1000	-12.1000	0.0000
CP_Q-Autarky	-6.9423	-19.5685	-11.3008

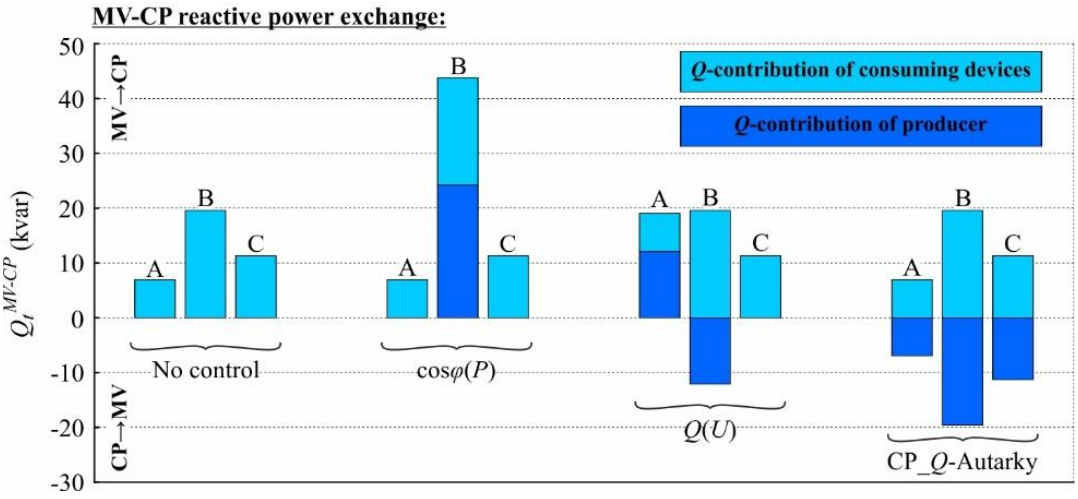

Fig. A.25 Composition of the MV-CP reactive power exchange of the commercial CP_Link-Grid with smoothed load profiles for different cases, no control and various control strategies.

Industrial CP_Link-Grid connected to MV level

Model specification:

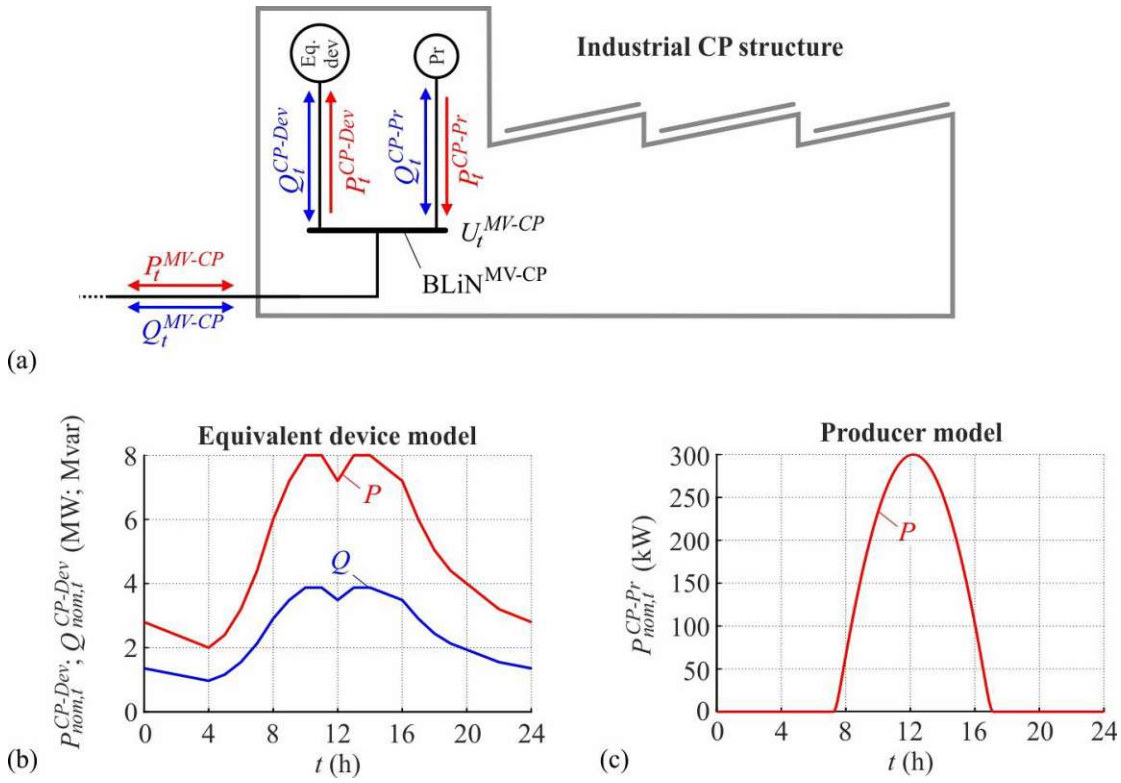

Fig. A.26 Industrial CP_Link-Grid: (a) Structure; (b) Smoothed load profiles of the Eq. dev.-model; (c) Smoothed load profile of the Pr.-model.

Table A.24 Model data of the industrial CP_Link-Grid with smoothed load profiles.

CP structure	Equivalent device model	SMPS, motors, resistive, lighting
	Producer model	One photovoltaic system
Equivalent device model	Daily energy consumption	118.44 MWh
	Max. active power consumption*	8 MW
	Power factor	0.90 inductive
	ZIP coefficients	Time-invariant
	References	(CIGRE 2014a; Bokhari et al. 2014)
Producer model	Daily energy production	1.88 MWh
	Max. active power production	300 kW
	Reactive power contribution	According to Volt/var control strategy
	References	(McKenna et al. 2015)

* This value corresponds to the billing demand of the two industrial customers connected to the large MV_Link-Grid.

Behaviour of Link-Grid without any Volt/var controls:

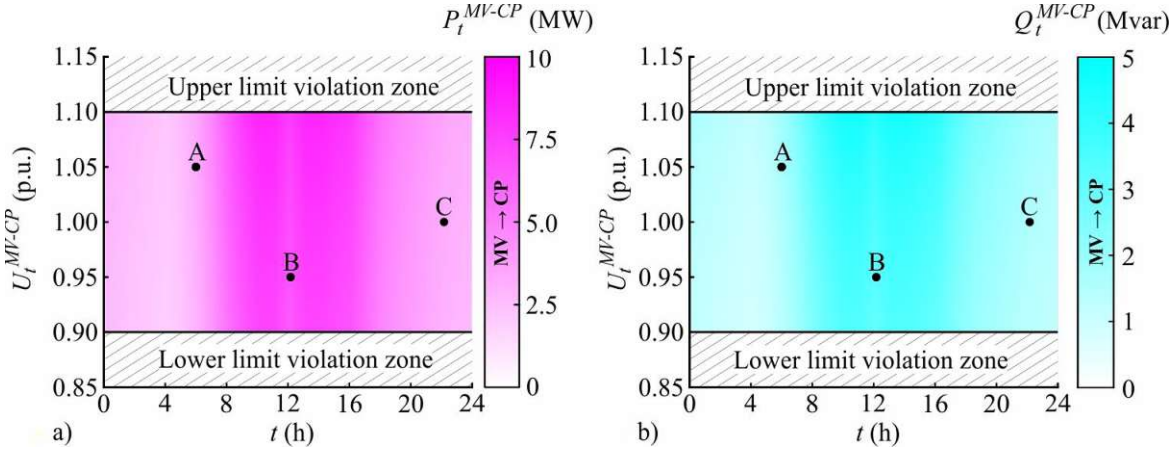

Fig. A.27 Daily behaviour of the industrial CP_Link-Grid with smoothed load profiles and without any Volt/var control for various voltages at the MV-CP boundary node: (a) MV-CP active power exchange; (b) MV-CP reactive power exchange.

MV-CP reactive power exchange for different Volt/var controls:

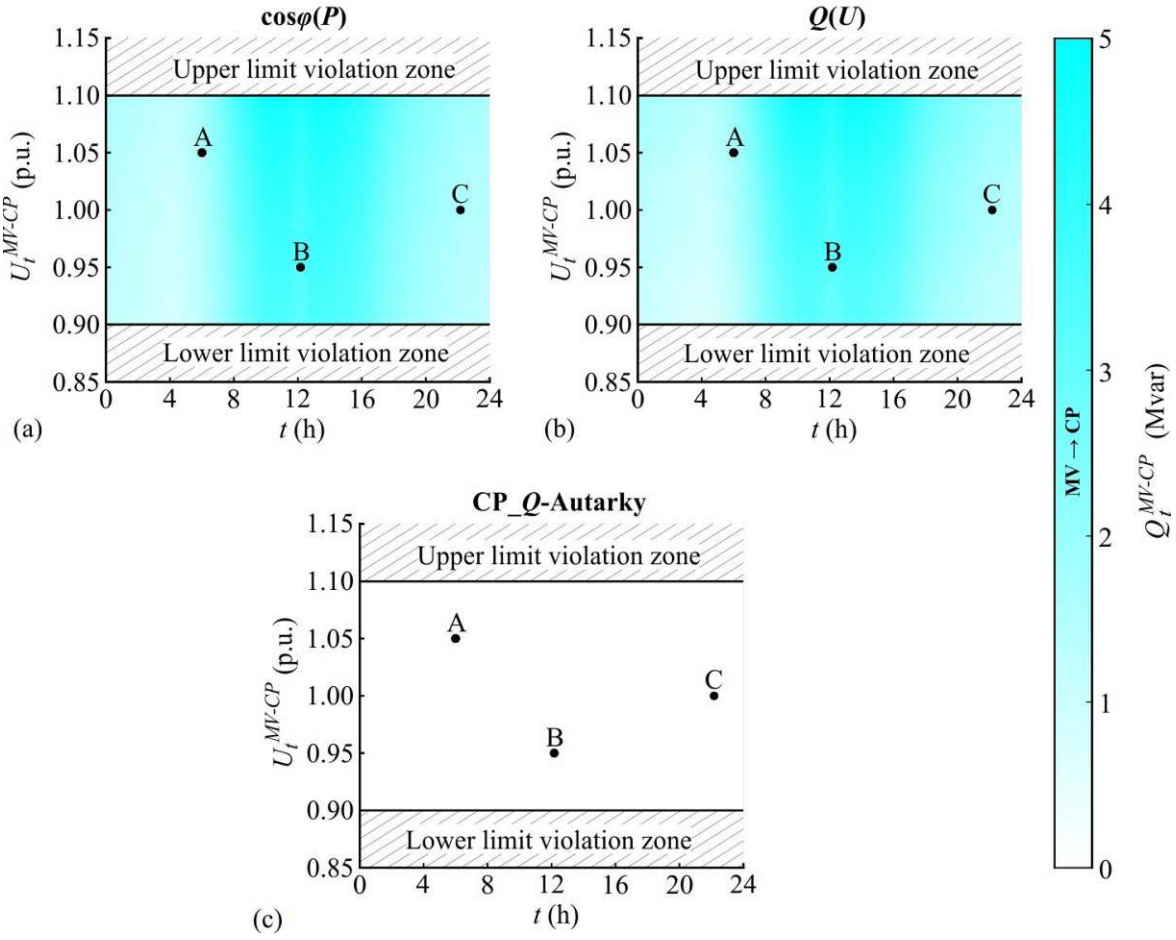

Fig. A.28 Daily MV-CP reactive power exchange of the industrial CP_Link-Grid with smoothed load profiles for various voltages at the MV-CP boundary node and different control strategies: (a) cos$\varphi(P)$; (b) $Q(U)$; (c) CP_Q-Autarky.

Behaviour of Link-Grid in cases A, B and C:

Table A.25 LV-CP reactive power exchange of the commercial CP_Link-Grid for smoothed load profiles at the CP level, different cases, no control and various control strategies.

Control strategy	Q_t^{MV-CP} (kvar)		
	Case A	Case B	Case C
None	1676.7231	3267.1158	1518.3498
cos$\varphi(P)$	1676.7231	3412.4081	1518.3498
$Q(U)$	1749.3231	3194.5158	1518.3498
CP_Q-Autarky	0.0000	0.0000	0.0000

Table A.26 Reactive power contribution of consuming devices connected to the industrial CP_Link-Grid with smoothed load profiles for different cases, no control and various control strategies.

Control strategy	Q_t^{CP-Dev} (kvar)		
	Case A	Case B	Case C
None	1676.7231	3267.1158	1518.3498
cos$\varphi(P)$	1676.7231	3267.1158	1518.3498
$Q(U)$	1676.7231	3267.1158	1518.3498
CP_Q-Autarky	1676.7231	3267.1158	1518.3498

Table A.27 Reactive power contribution of the producer connected to the industrial CP_Link-Grid with smoothed load profiles for different cases, no control and various control strategies.

Control strategy	Q_t^{CP-Pr} (kvar)		
	Case A	Case B	Case C
None	0.0000	0.0000	0.0000
cos$\varphi(P)$	0.0000	145.2922	0.0000
$Q(U)$	72.6000	-72.6000	0.0000
CP_Q-Autarky	-1676.7231	-3267.1158	-1518.3498

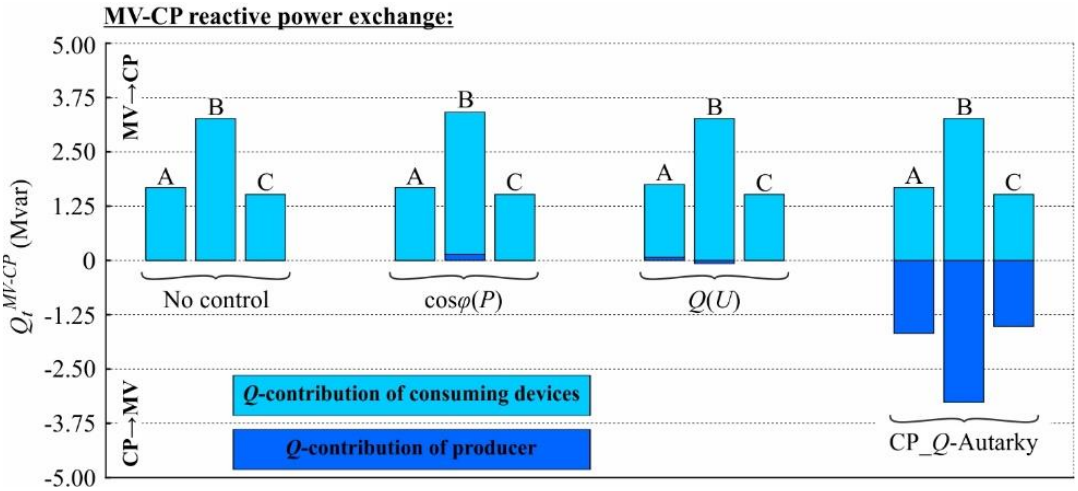

Fig. A.29 Composition of the MV-CP reactive power exchange of the industrial CP_Link-Grid with smoothed load profiles for different cases, no control and various control strategies.

A.1.2.2 LV level

Rural LV_Link-Grid

Model specification:

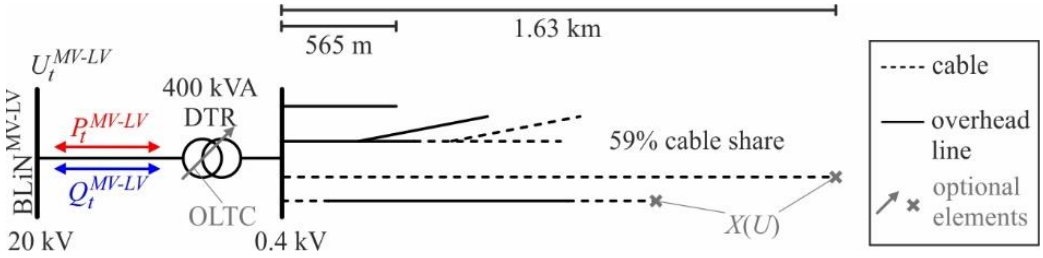

Fig. A.30 Simplified one-line diagram of the rural LV_Link-Grid (real Austrian grid).

Table A.28 Model data of the rural LV_Link-Grid for smoothed load profiles at the CP level.

DTR	Rating:			400 kVA
	Nominal voltage		Primary Secondary	21.0 kV 0.42 kV
	Short circuit voltage		Total Resistive part	3.7 % 1.0 %
Feeders	Nominal voltage			0.4 kV
	Number of feeders			4
	Total line length			6.335 km
	Total cable share			58.64 %
	Feeder length		Maximal Minimal	1.630 km 0.565 km
Control parameters	OLTC		Upper voltage limit Lower voltage limit Min./mid/max. tap positions Additional voltage per tap	0.990 p.u. 0.950 p.u. 1/3/5 2.5 %
	$X(U)$		Upper voltage limit Lower voltage limit	1.09 p.u. 0.91 p.u.
Connected lumped models	Link-Grids	CP	Rural residential with smoothed load profiles	61

Behaviour of Link-Grid without any Volt/var controls:

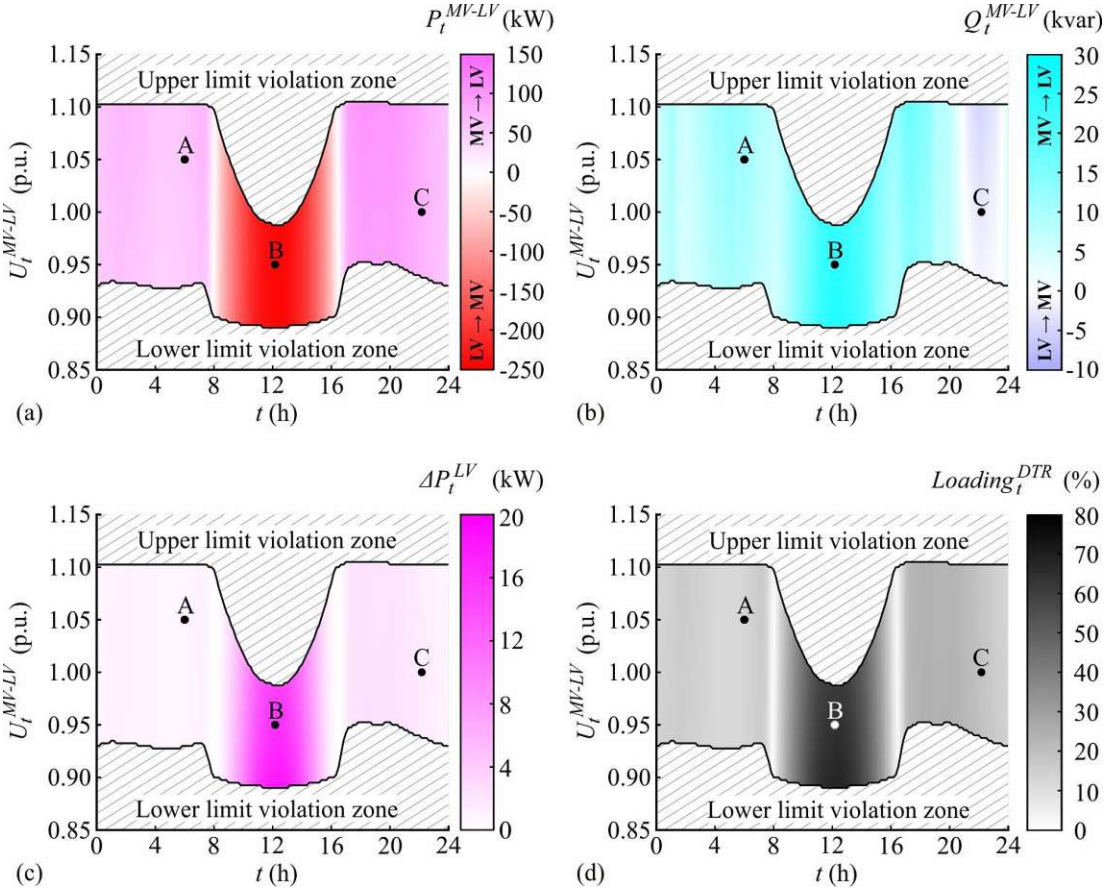

Fig. A.31 Daily behaviour of the rural LV_Link-Grid without any Volt/var control for various voltages at the MV-LV boundary node and smoothed load profiles at the CP level: (a) MV-LV active power exchange; (b) MV-LV reactive power exchange; (c) LV active power loss; (d) DTR loading.

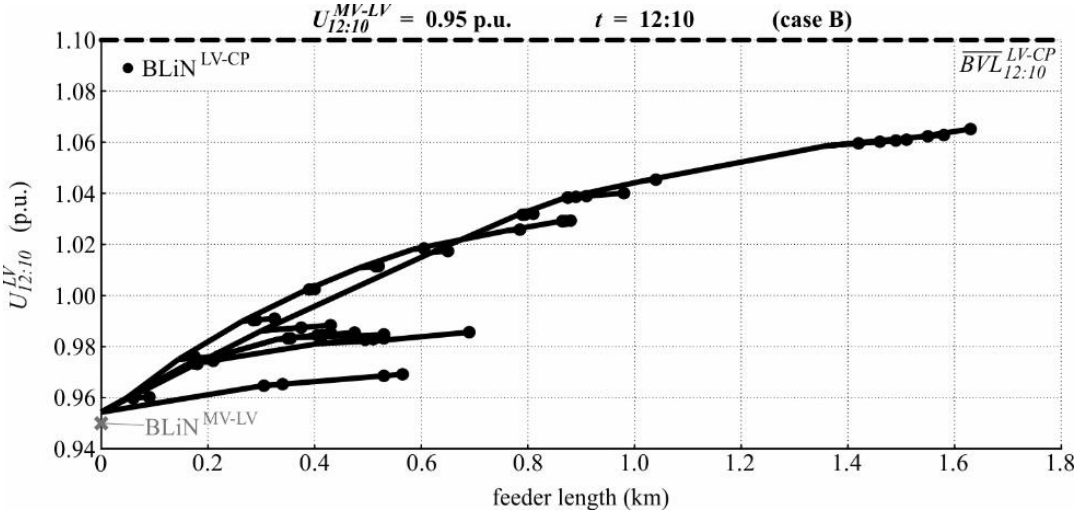

Fig. A.32 Voltage profiles of the rural LV_Link-Grid's feeders without any Volt/var control at 12:10 for an MV-LV boundary voltage of 0.95 p.u. (case B) and smoothed load profiles at the CP level.

MV-LV reactive power exchange for different Volt/var controls:

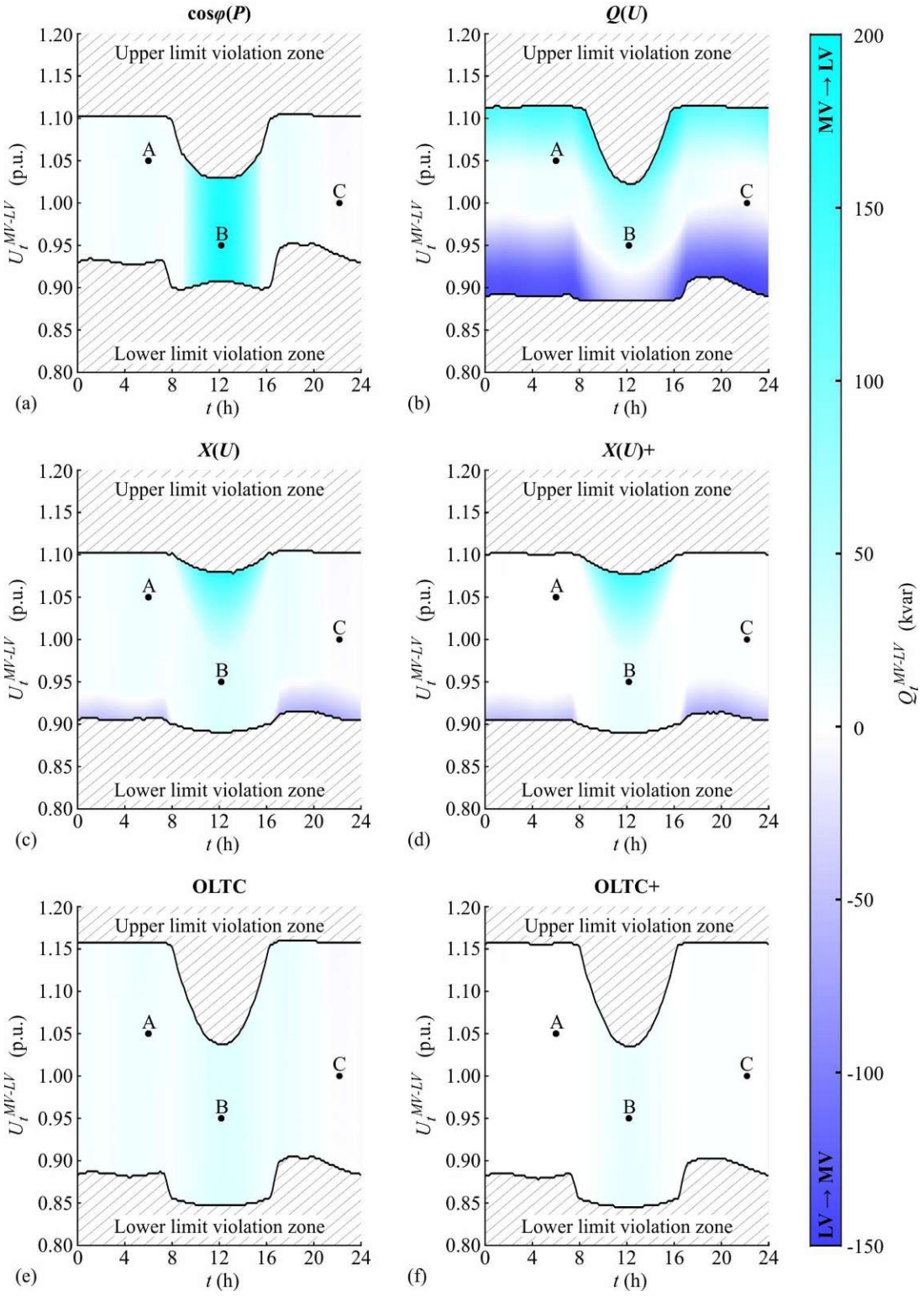

Fig. A.33 Daily MV-LV reactive power exchange of the rural LV_Link-Grid for various voltages at the MV-LV boundary node, smoothed load profiles at the CP level, and different control strategies: (a) cosφ(P); (b) Q(U); (c) X(U); (d) X(U) and CP_Q-Autarky; (e) OLTC; (f) OLTC and CP_Q-Autarky.

LV active power loss for different Volt/var controls:

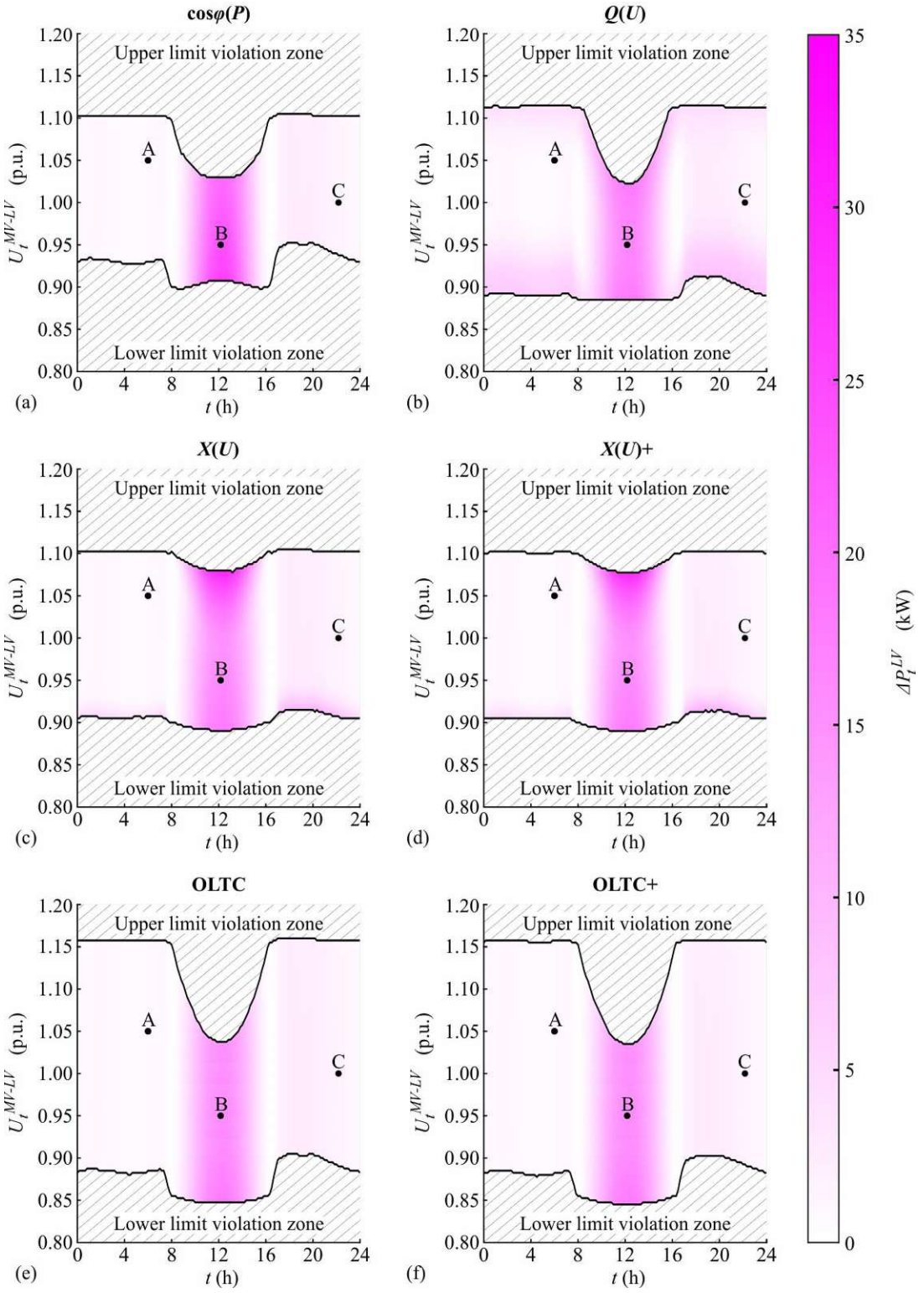

Fig. A.34 Daily active power loss within the rural LV_Link-Grid for various voltages at the MV-LV boundary node, smoothed load profiles at the CP level, and different control strategies: (a) cos$\varphi(P)$; (b) $Q(U)$; (c) $X(U)$; (d) $X(U)$ and CP_Q-Autarky; (e) OLTC; (f) OLTC and CP_Q-Autarky.

DTR loading for different Volt/var controls:

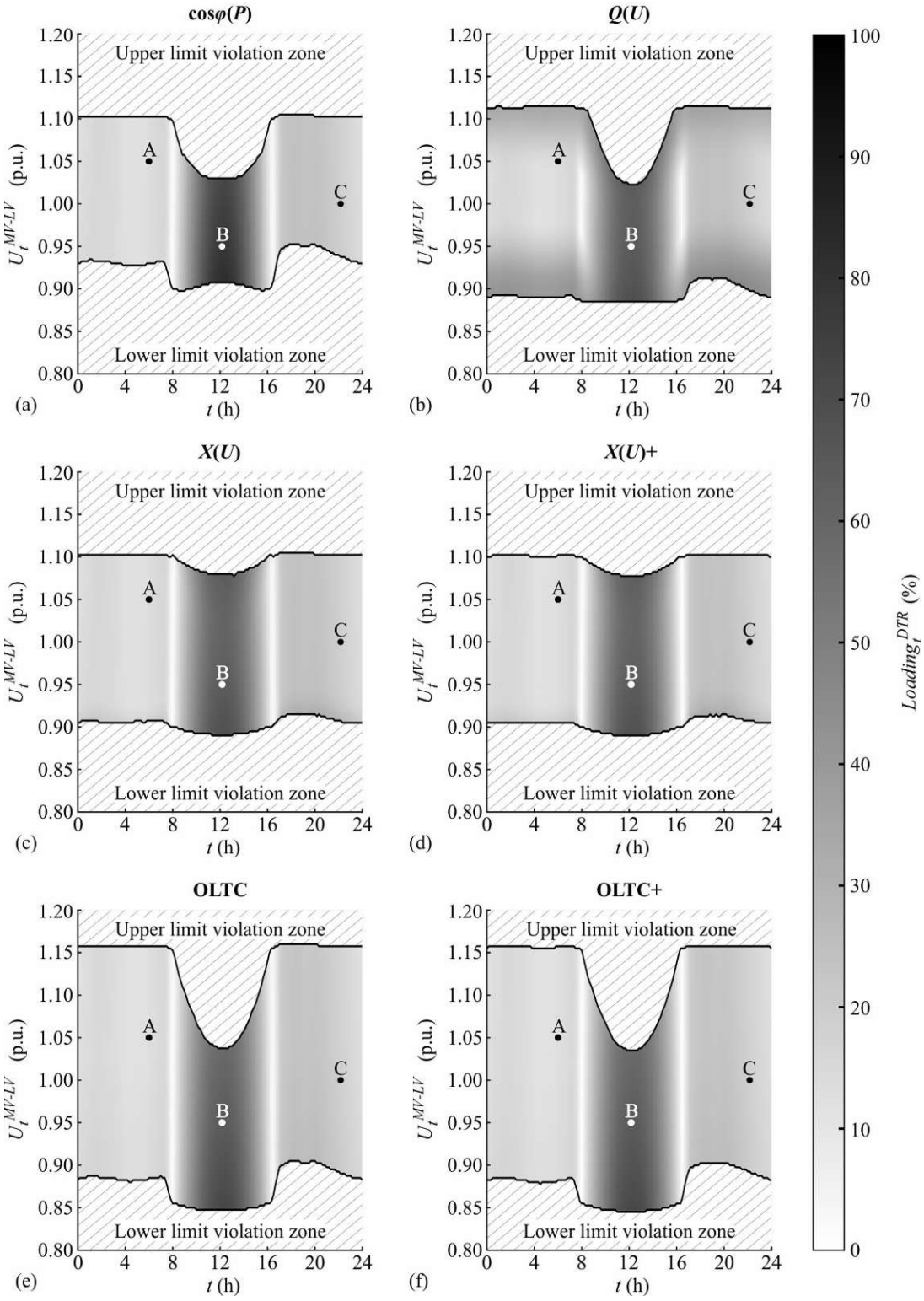

Fig. A.35 Daily DTR loading within the rural LV_Link-Grid for various voltages at the MV-LV boundary node, smoothed load profiles at the CP level, and different control strategies: (a) cosφ(P); (b) Q(U); (c) X(U); (d) X(U) and CP_Q-Autarky; (e) OLTC; (f) OLTC and CP_Q-Autarky.

Behaviour of Link-Grid in cases A, B and C:

Table A.29 MV-LV reactive power exchange of the rural LV_Link-Grid for smoothed load profiles at the CP level, different cases, no control and various control strategies.

Control strategy	Q_t^{MV-LV} (kvar)		
	Case A	Case B	Case C
None	11.2117	24.7847	-2.5265
cos$\varphi(P)$	11.2117	179.6204	-2.5265
$Q(U)$	26.0203	35.2988	-4.0817
$X(U)$	11.2117	24.7847	-2.5265
$X(U)$+	0.5220	15.1919	1.1476
OLTC	10.4582	24.7847	-2.0585
OLTC+	0.5354	15.1919	1.1833

Table A.30 Reactive power contribution of the CP_Link-Grids connected to the rural LV_Link-Grid for smoothed load profiles at the CP level, different cases, no control and various control strategies.

Control strategy	$Q_{\Sigma,t}^{LV-CP}$ (kvar)		
	Case A	Case B	Case C
None	10.6646	9.4851	-3.6763
cos$\varphi(P)$	10.6646	156.6212	-3.6763
$Q(U)$	25.3810	19.7681	-5.2365
$X(U)$	10.6646	9.4851	-3.6763
$X(U)$+	0.0000	0.0000	0.0000
OLTC	9.8987	9.4851	-3.2434
OLTC+	0.0000	0.0000	0.0000

Table A.31 Reactive power contribution of the rural LV_Link-Grid for smoothed load profiles at the CP level, different cases, no control and various control strategies.

Control strategy	$Q_{\Sigma,t}^{LV}$ (kvar)		
	Case A	Case B	Case C
None	0.5471	15.2995	1.1498
cos$\varphi(P)$	0.5471	22.9992	1.1498
$Q(U)$	0.6393	15.5307	1.1547
$X(U)$	0.5471	15.2995	1.1498
$X(U)$+	0.5220	15.1919	1.1476
OLTC	0.5595	15.2995	1.1850
OLTC+	0.5354	15.1919	1.1833

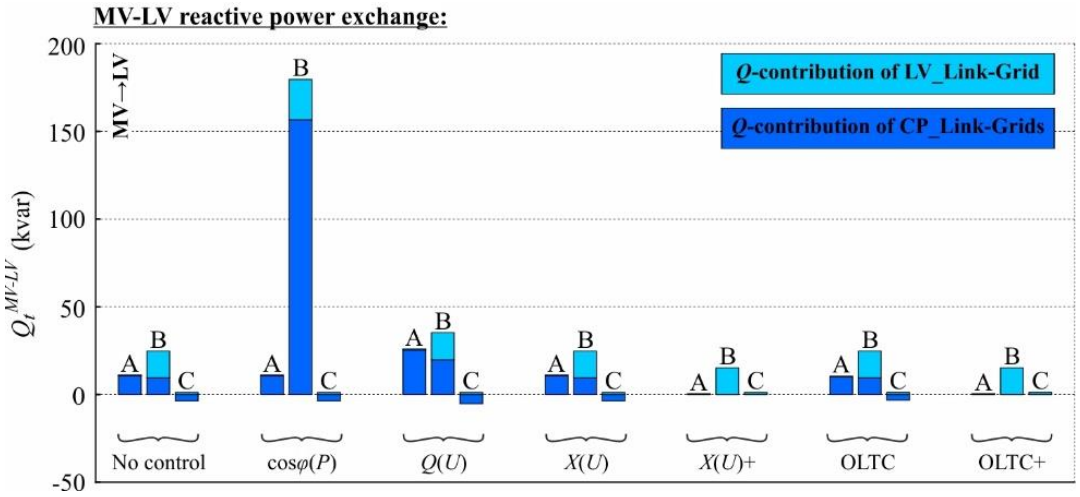

Fig. A.36 Composition of the MV-LV reactive power exchange of the rural LV_Link-Grid for smoothed load profiles at the CP level, different cases, no control and various control strategies.

Table A.32 Active power loss within the rural LV_Link-Grid for smoothed load profiles at the CP level, different cases, no control and various control strategies.

Control strategy	ΔP_t^{LV} (kW)		
	Case A	Case B	Case C
None	0.7643	15.9688	1.3885
cos$\varphi(P)$	0.7643	23.9166	1.3885
$Q(U)$	0.8266	16.4398	1.3990
$X(U)$	0.7643	15.9688	1.3885
$X(U)$+	0.7388	15.8581	1.3859
OLTC	0.7601	15.9688	1.4179
OLTC+	0.7356	15.8581	1.4159

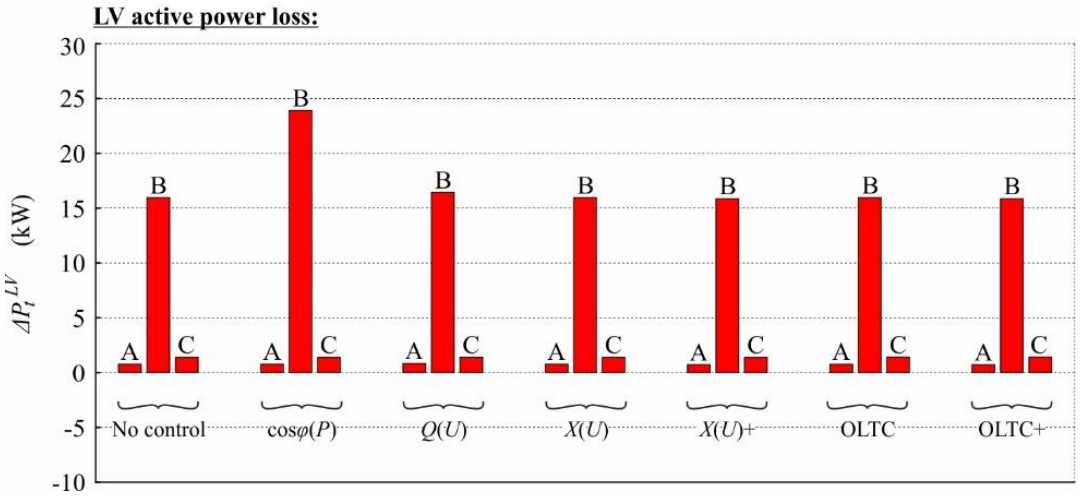

Fig. A.37 Active power loss within the rural LV_Link-Grid for smoothed load profiles at the CP level, different cases, no control and various control strategies.

Table A.33 DTR loading within the rural LV_Link-Grid for smoothed load profiles at the CP level, different cases, no control and various control strategies.

Control strategy	$Loading_t^{DTR}$ (%)		
	Case A	Case B	Case C
None	13.7426	64.0142	18.4742
cos$\varphi(P)$	13.7426	77.9572	18.4742
$Q(U)$	14.8192	64.2656	18.4987
$X(U)$	13.7426	64.0142	18.4742
$X(U)$+	13.5088	63.8105	18.4553
OLTC	13.0492	64.0142	18.2095
OLTC+	12.8352	63.8105	18.1956

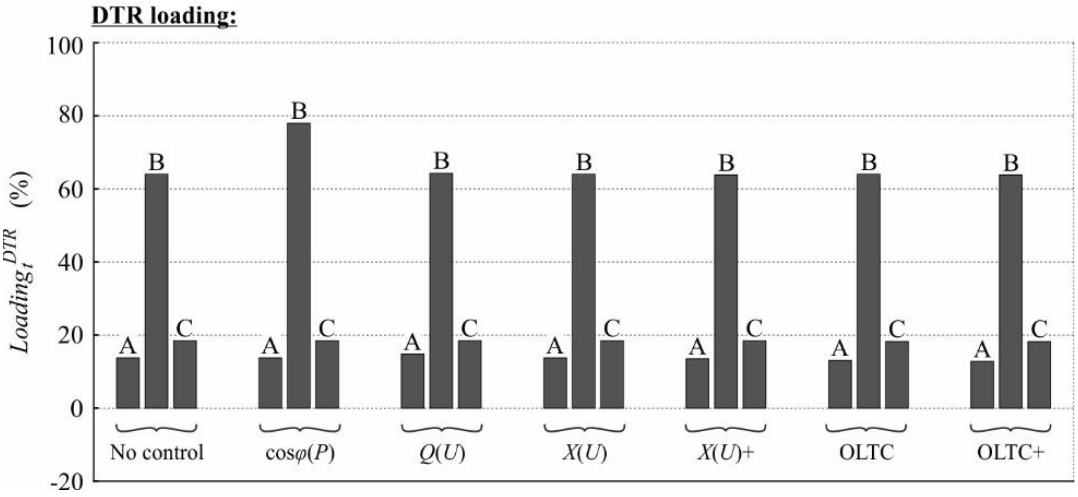

Fig. A.38 DTR loading within the rural LV_Link-Grid for smoothed load profiles at the CP level, different cases, no control and various control strategies.

Urban LV_Link-Grid

Model specification:

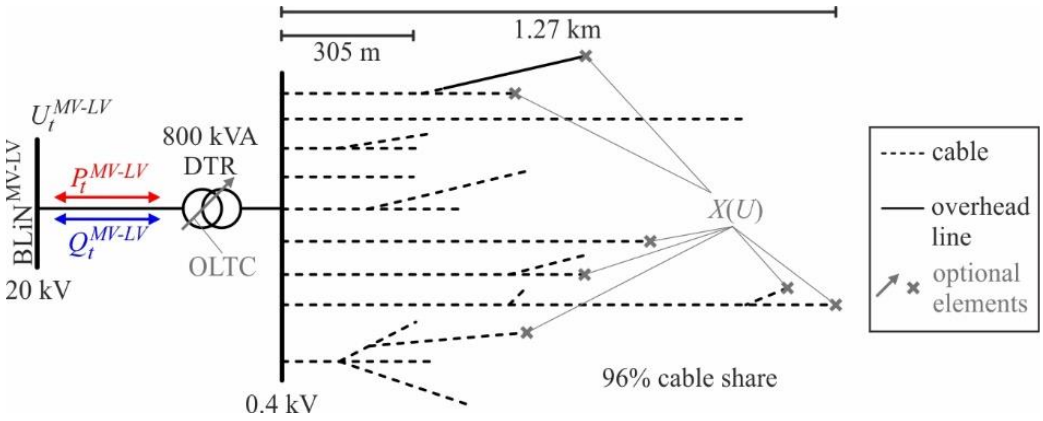

Fig. A.39 Simplified one-line diagram of the urban LV_Link-Grid (real Austrian grid).

Table A.34 Model data of the urban LV_Link-Grid for smoothed load profiles at the CP level.

DTR	Rating:			800 kVA
	Nominal voltage		Primary Secondary	20.0 kV 0.4 kV
	Short circuit voltage		Total Resistive part	4.0 % 1.0 %
Feeders	Nominal voltage			0.4 kV
	Number of feeders			9
	Total line length			12.815 km
	Total cable share			96.14 %
	Feeder length		Maximal Minimal	1.270 km 0.305 km
Control parameters	OLTC		Upper voltage limit Lower voltage limit Min./mid/max. tap positions Additional voltage per tap	1.025 p.u. 0.950 p.u. 1/3/5 2.5 %
	$X(U)$		Upper voltage limit Lower voltage limit	1.09 p.u. 0.91 p.u.
Connected lumped models	Link-Grids	CP	Urban residential with smoothed load profiles	175

Behaviour of Link-Grid without any Volt/var controls:

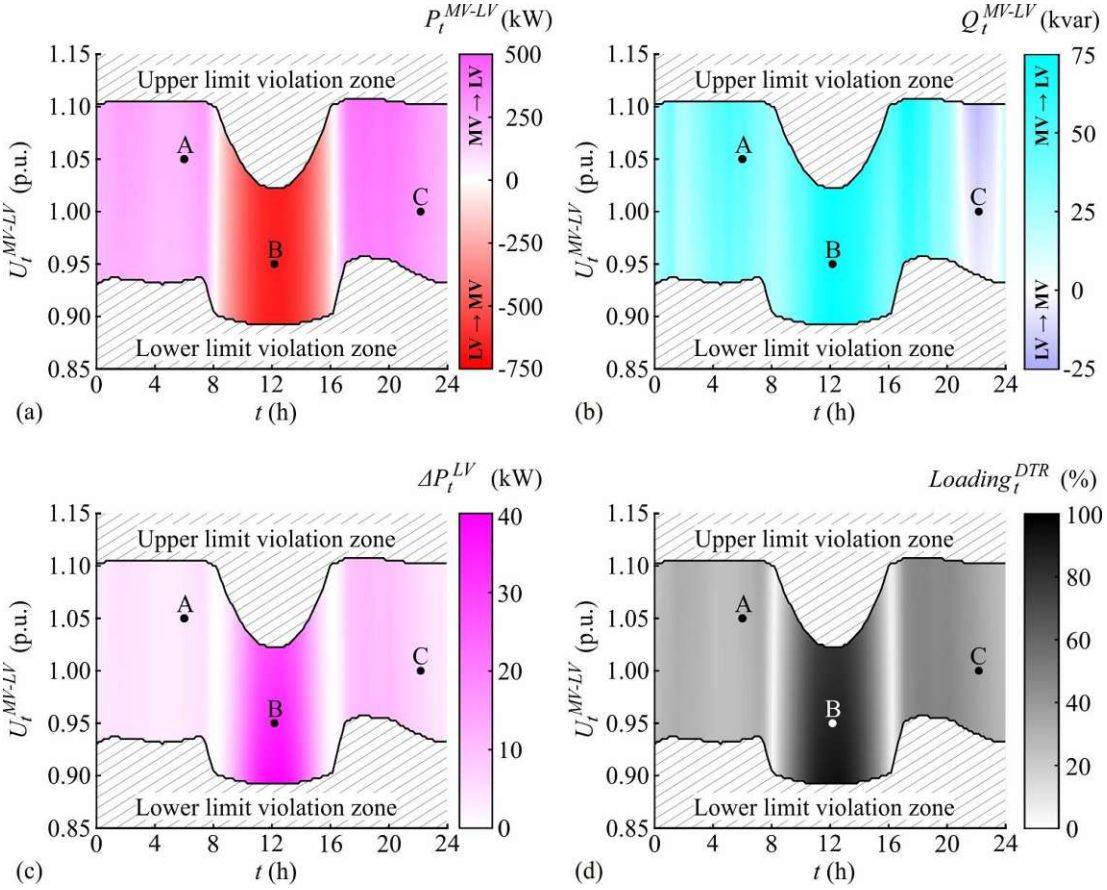

Fig. A.40 Daily behaviour of the urban LV_Link-Grid without any Volt/var control for various voltages at the MV-LV boundary node and smoothed load profiles at the CP level: (a) MV-LV active power exchange; (b) MV-LV reactive power exchange; (c) LV active power loss; (d) DTR loading.

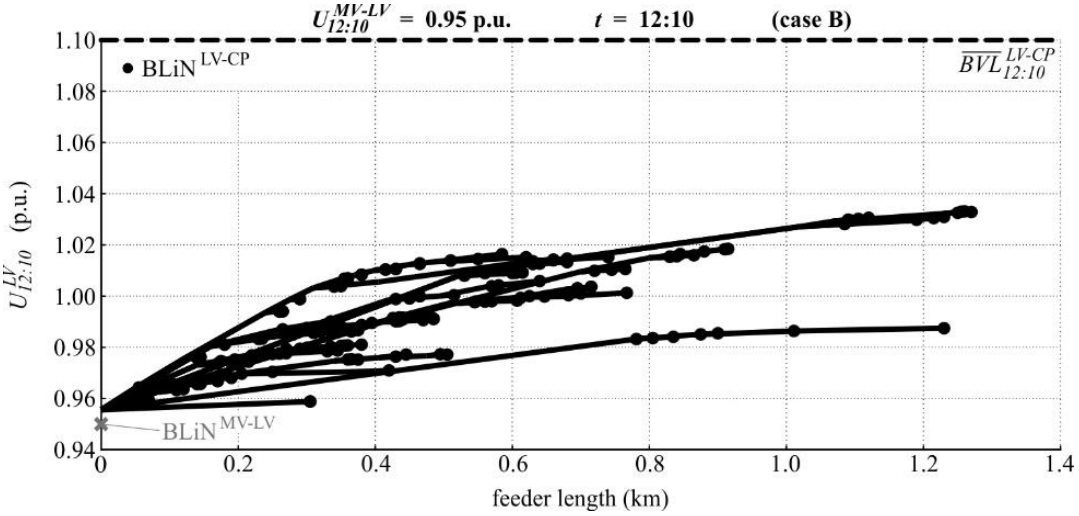

Fig. A.41 Voltage profiles of the urban LV_Link-Grid's feeders without any Volt/var control at 12:10 for an MV-LV boundary voltage of 0.95 p.u. (case B) and smoothed load profiles at the CP level.

MV-LV reactive power exchange for different Volt/var controls:

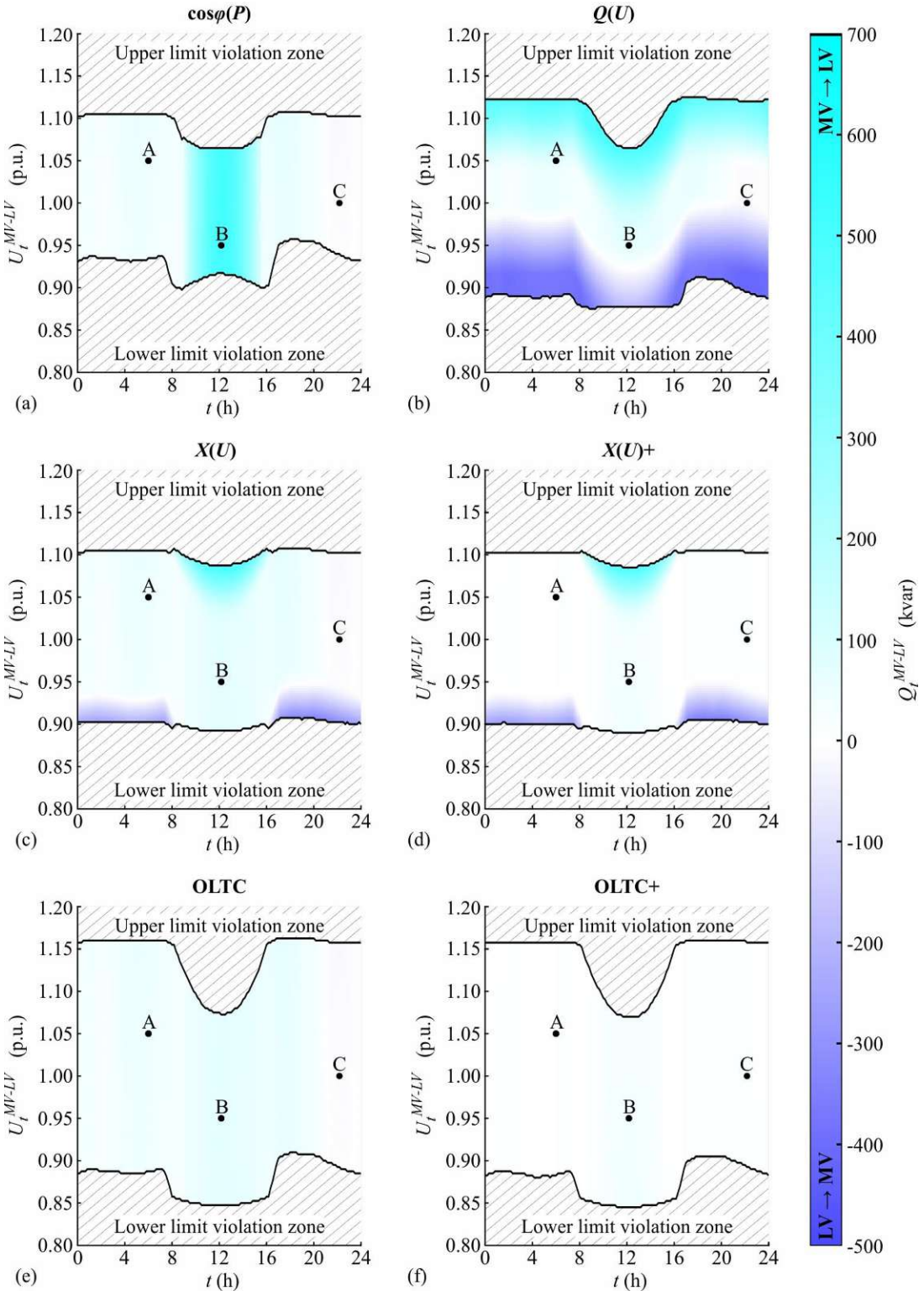

Fig. A.42 Daily MV-LV reactive power exchange of the urban LV_Link-Grid for various voltages at the MV-LV boundary node, smoothed load profiles at the CP level, and different control strategies: (a) cosφ(P); (b) Q(U); (c) X(U); (d) X(U) and CP_Q-Autarky; (e) OLTC; (f) OLTC and CP_Q-Autarky.

LV active power loss for different Volt/var controls:

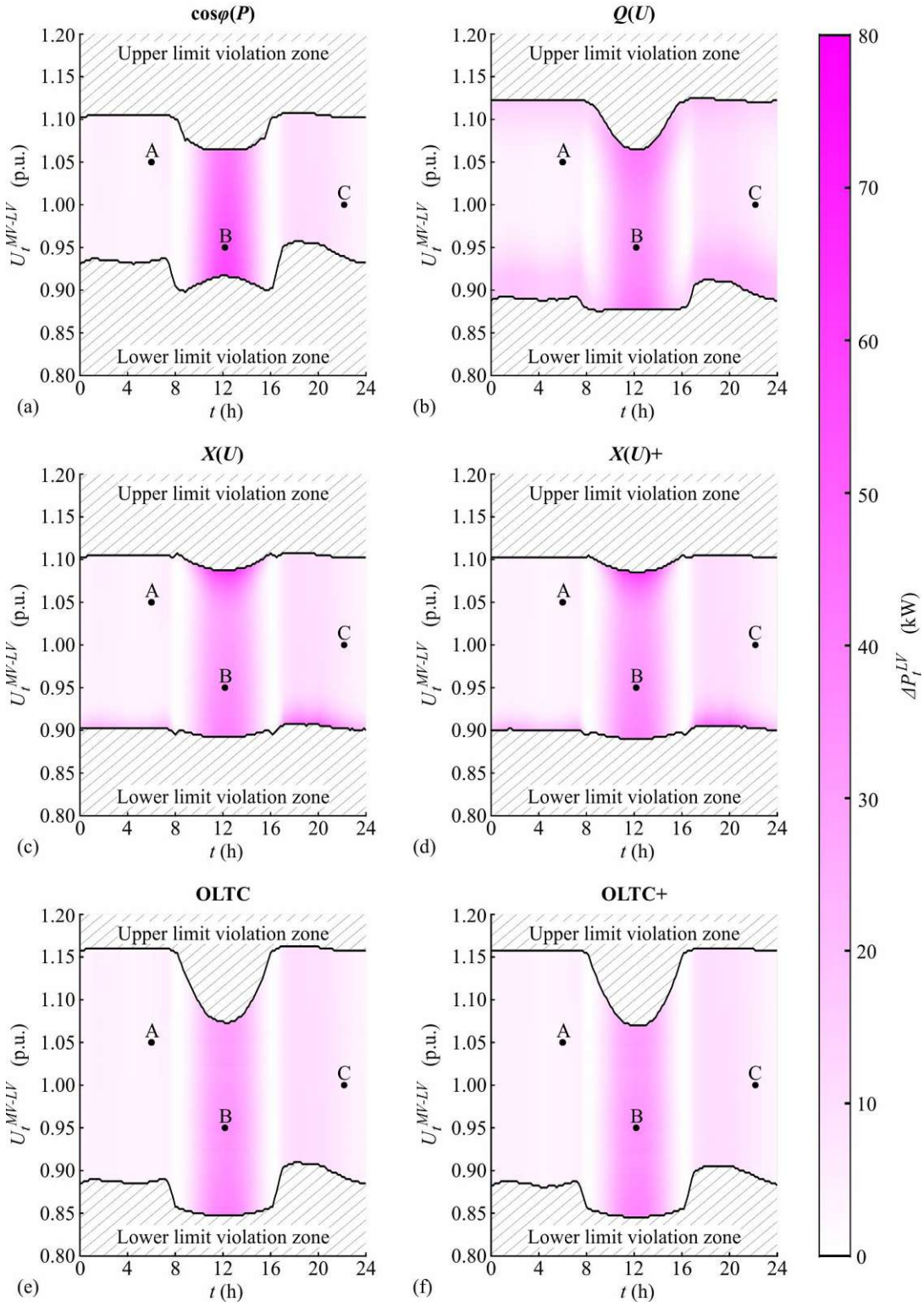

Fig. A.43 Daily active power loss within the urban LV_Link-Grid for various voltages at the MV-LV boundary node, smoothed load profiles at the CP level, and different control strategies: (a) cosφ(P); (b) Q(U); (c) X(U); (d) X(U) and CP_Q-Autarky; (e) OLTC; (f) OLTC and CP_Q-Autarky.

DTR loading for different Volt/var controls:

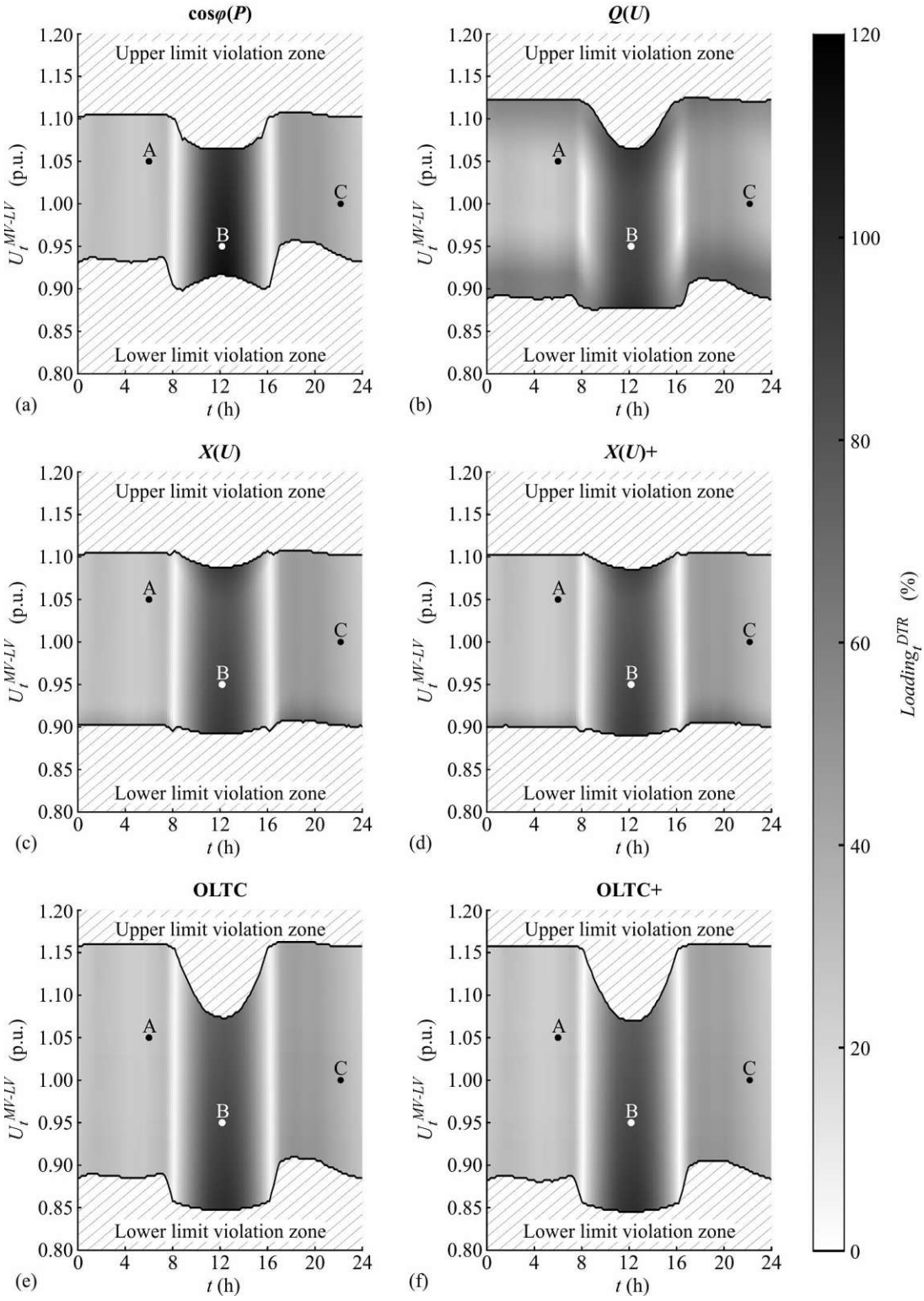

Fig. A.44 Daily DTR loading within the urban LV_Link-Grid for various voltages at the MV-LV boundary node, smoothed load profiles at the CP level, and different control strategies: (a) cosφ(P); (b) Q(U); (c) X(U); (d) X(U) and CP_Q-Autarky; (e) OLTC; (f) OLTC and CP_Q-Autarky.

Behaviour of Link-Grid in cases A, B and C:

Table A.35 MV-LV reactive power exchange of the urban LV_Link-Grid for smoothed load profiles at the CP level, different cases, no control and various control strategies.

Control strategy	Q_t^{MV-LV} (kvar)		
	Case A	Case B	Case C
None	46.5923	72.0637	-9.8095
cos$\varphi(P)$	46.5923	512.9641	-9.8095
$Q(U)$	75.7565	66.6676	-12.6388
$X(U)$	46.5923	72.0638	-9.8093
$X(U)$+	2.7900	33.6598	5.1902
OLTC	44.9710	72.0637	-9.8095
OLTC+	2.8048	33.6598	5.1902

Table A.36 Reactive power contribution of the CP_Link-Grids connected to the urban LV_Link-Grid for smoothed load profiles at the CP level, different cases, no control and various control strategies.

Control strategy	$Q_{\Sigma,t}^{LV-CP}$ (kvar)		
	Case A	Case B	Case C
None	43.6756	38.0601	-15.0114
cos$\varphi(P)$	43.6756	459.8271	-15.0114
$Q(U)$	72.6505	32.7091	-17.8544
$X(U)$	43.6756	38.0601	-15.0114
$X(U)$+	0.0000	0.0000	0.0000
OLTC	42.0423	38.0601	-15.0114
OLTC+	0.0000	0.0000	0.0000

Table A.37 Reactive power contribution of the urban LV_Link-Grid for smoothed load profiles at the CP level, different cases, no control and various control strategies.

Control strategy	$Q_{\Sigma,t}^{LV}$ (kvar)		
	Case A	Case B	Case C
None	2.9167	34.0037	5.2021
cos$\varphi(P)$	2.9167	53.1370	5.2021
$Q(U)$	3.1061	33.9585	5.2156
$X(U)$	2.9167	34.0037	5.2021
$X(U)$+	2.7900	33.6598	5.1902
OLTC	2.9287	34.0037	5.2021
OLTC+	2.8048	33.6598	5.1902

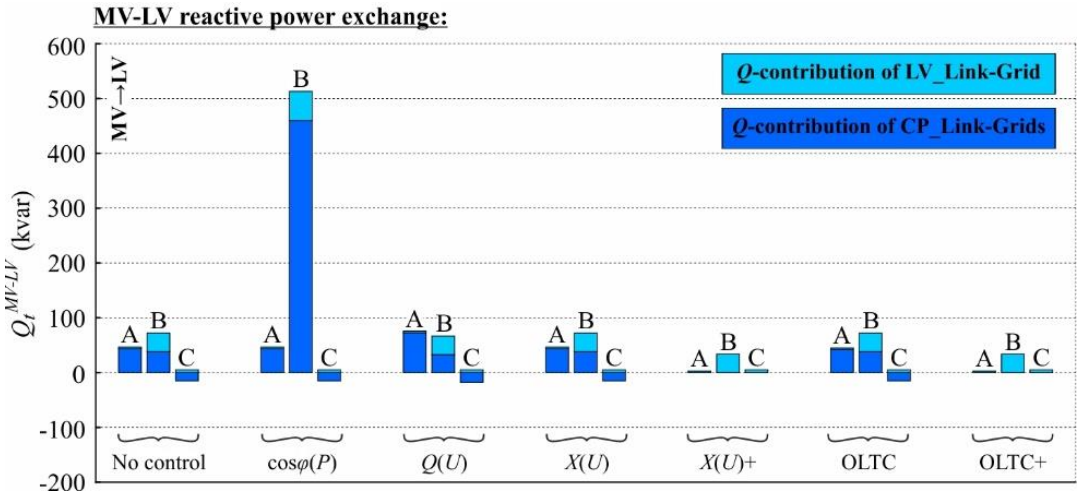

Fig. A.45 Composition of the MV-LV reactive power exchange of the urban LV_Link-Grid for smoothed load profiles in CP level, and for different cases, no control and various control strategies.

Table A.38 Active power loss within the urban LV_Link-Grid for smoothed load profiles at the CP level, different cases, no control and various control strategies.

Control strategy	ΔP_t^{LV} (kW)		
	Case A	Case B	Case C
None	3.4914	34.0481	5.7219
cos$\varphi(P)$	3.4914	53.0728	5.7219
$Q(U)$	3.6255	34.0269	5.7424
$X(U)$	3.4914	34.0481	5.7219
$X(U)$+	3.3684	33.7011	5.7095
OLTC	3.4750	34.0481	5.7219
OLTC+	3.3547	33.7011	5.7095

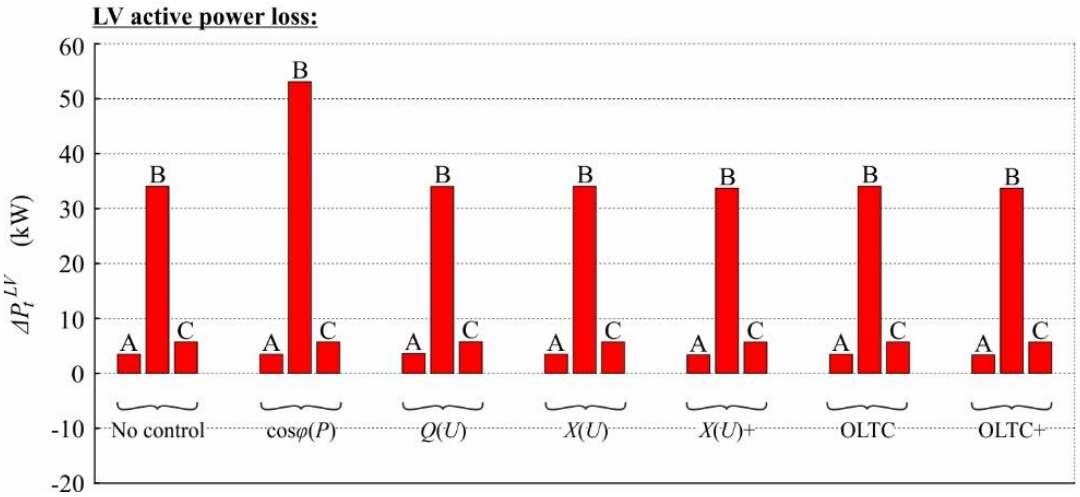

Fig. A.46 Active power loss within the urban LV_Link-Grid for smoothed load profiles at the CP level, different cases, no control and various control strategies.

Table A.39 DTR loading within the urban LV_Link-Grid for smoothed load profiles at the CP level, different cases, no control and various control strategies.

Control strategy	$Loading_t^{DTR}$ (%)		
	Case A	Case B	Case C
None	27.6187	87.0541	35.3063
cos$\varphi(P)$	27.6187	108.3297	35.3063
$Q(U)$	28.4914	86.9772	35.3293
$X(U)$	27.6188	87.0541	35.3063
$X(U)$+	27.1280	86.6339	35.2651
OLTC	26.8802	87.0541	35.3063
OLTC+	26.4107	86.6339	35.2651

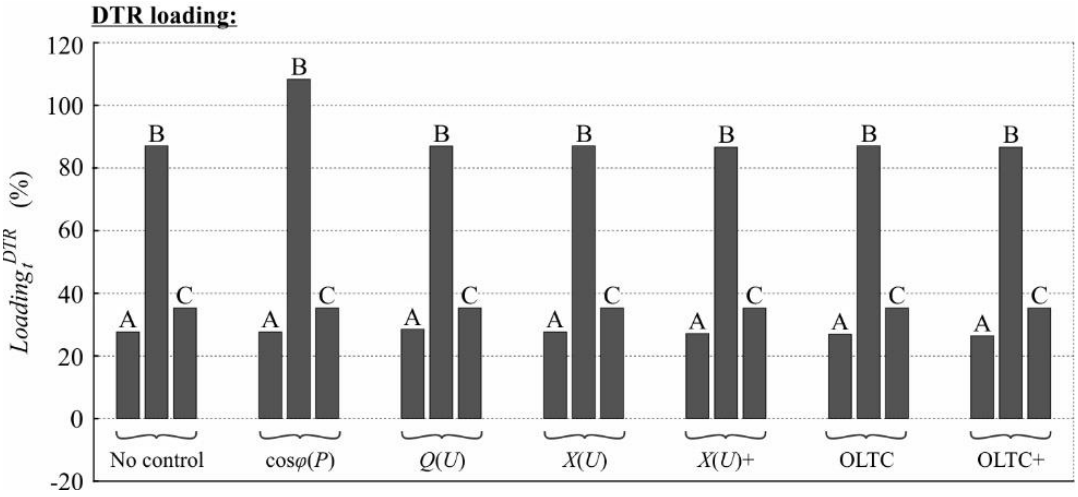

Fig. A.47 DTR loading within the urban LV_Link-Grid for smoothed load profiles at the CP level, different cases, no control and various control strategies.

A.1.2.3 MV level

Small MV_Link-Grid

Model specification:

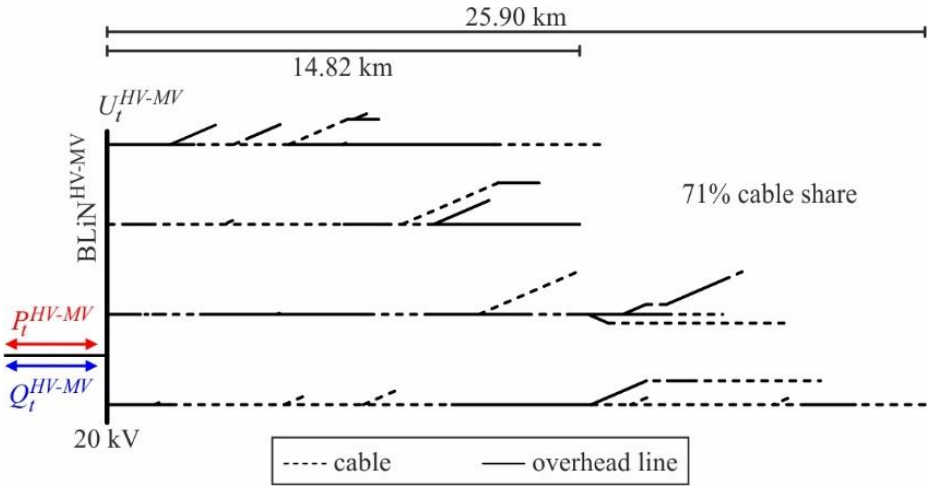

Fig. A.48 Simplified one-line diagram of the small MV_Link-Grid (real Austrian grid).

Table A.40 Model data of the small MV_Link-Grid for smoothed load profiles at the CP level.

Feeders	Nominal voltage			20 kV
	Number of feeders			4
	Total line length			158.46 km
	Total cable share			70.62 %
	Feeder length		Maximal Minimal	25.90 km 14.82 km
Connected lumped models	Link-Grids	CP	Commercial with smoothed load profiles	90
		LV	Rural for smoothed load profiles in CP level	49
			Urban for smoothed load profiles in CP level	4

Behaviour of Link-Grid without any Volt/var controls:

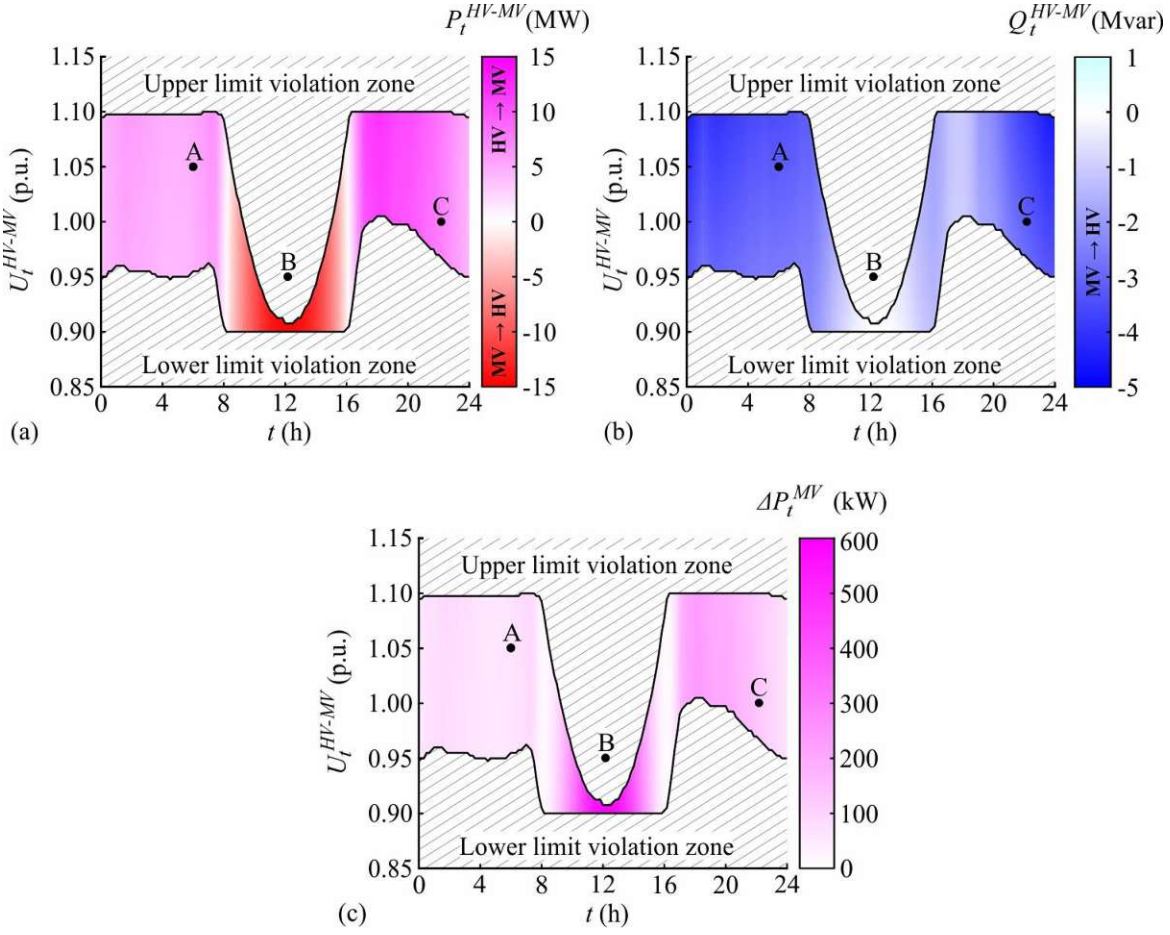

Fig. A.49 Daily behaviour of the small MV_Link-Grid without any Volt/var control for various voltages at the HV-MV boundary node and smoothed load profiles at the CP level: (a) HV-MV active power exchange; (b) HV-MV reactive power exchange; (c) MV active power loss.

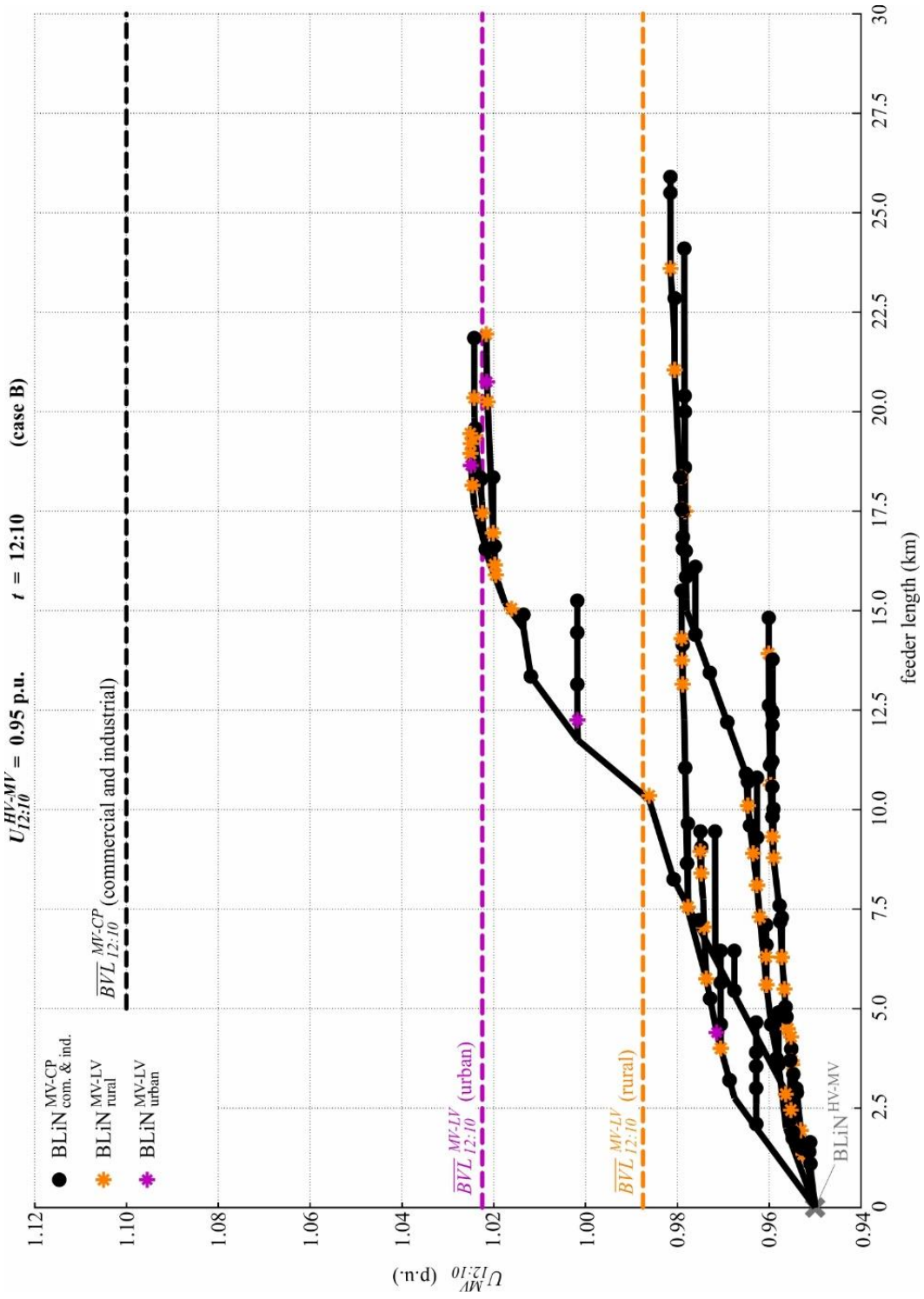

Fig. A.50 Voltage profiles of the small MV_Link-Grid's feeders without any Volt/var control at 12:10 for an HV-MV boundary voltage of 0.95 p.u. (case B) and smoothed load profiles at the CP level.

HV-MV reactive power exchange for different Volt/var controls:

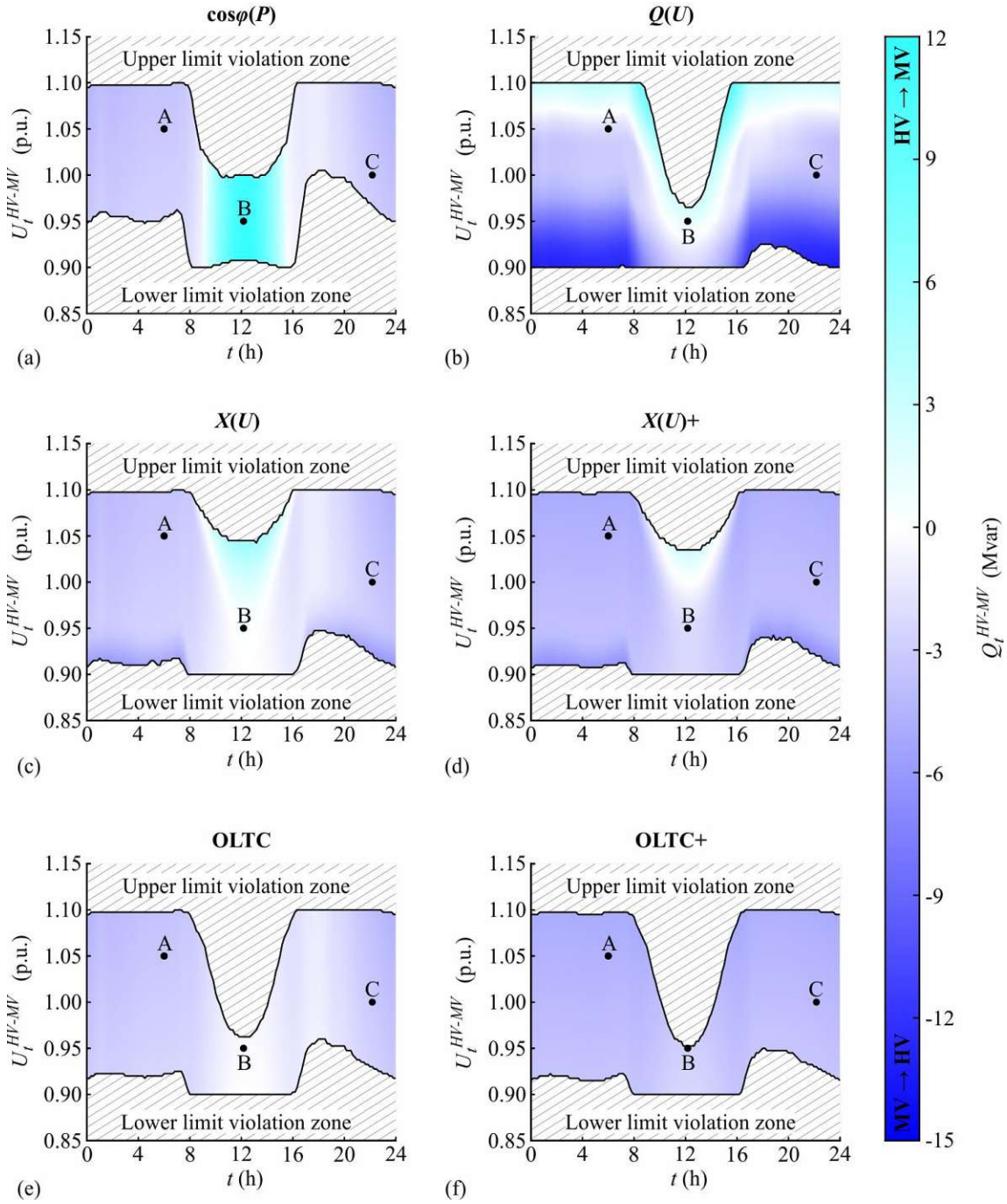

Fig. A.51 Daily HV-MV reactive power exchange of the small MV_Link-Grid for various voltages at the HV-MV boundary node, smoothed load profiles at the CP level, and different control strategies: (a) cosφ(P); (b) Q(U); (c) X(U); (d) X(U) and CP_Q-Autarky; (e) OLTC; (f) OLTC and CP_Q-Autarky.

MV active power loss for different Volt/var controls:

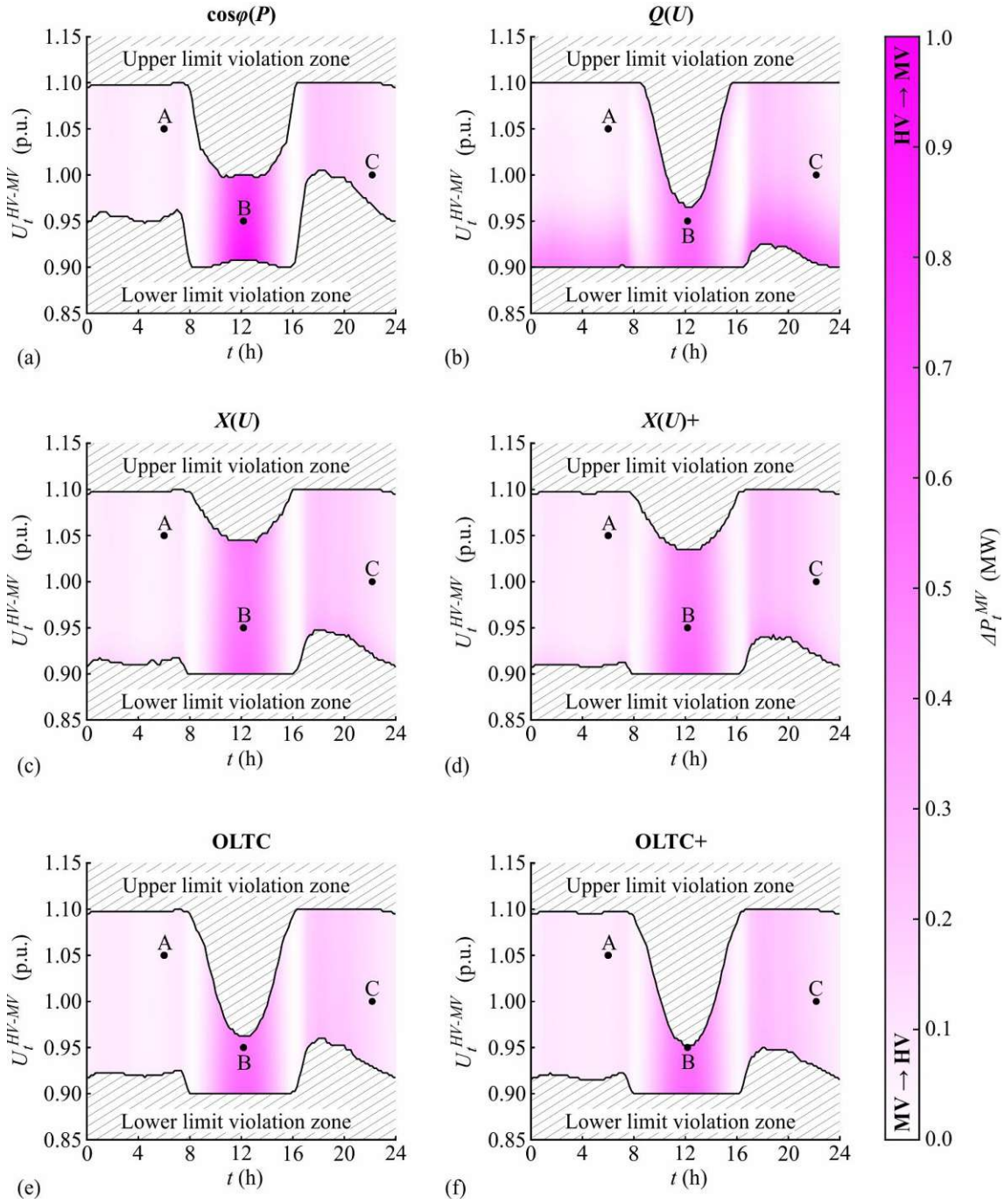

Fig. A.52 Daily active power loss within the small MV_Link-Grid for various voltages at the HV-MV boundary node, smoothed load profiles at the CP level, and different control strategies: (a) cosφ(P); (b) Q(U); (c) X(U); (d) X(U) and CP_Q-Autarky; (e) OLTC; (f) OLTC and CP_Q-Autarky.

Behaviour of Link-Grid in cases A, B and C:

Table A.41 HV-MV reactive power exchange of the small MV_Link-Grid for smoothed load profiles at the CP level, different cases, no control and various control strategies.

Control strategy	Q_t^{HV-MV} (kvar)		
	Case A	Case B	Case C
None	-3166.4324	-274.0876	-3158.5634
cos$\varphi(P)$	-3166.4324	11546.7229	-3158.5634
$Q(U)$	-1928.1602	1511.9364	-3710.0295
$X(U)$	-3166.4318	248.7131	-3158.5616
$X(U)$+	-4477.5800	-2081.4525	-3933.1527
OLTC	-3212.9555	-263.6931	-3145.0208
OLTC+	-4481.5044	-2784.5875	-3932.6640

Table A.42 Reactive power contribution of the CP_Link-Grids connected to the small MV_Link-Grid for smoothed load profiles at the CP level, different cases, no control and various control strategies.

Control strategy	$Q_{\Sigma,t}^{MV-CP}$ (kvar)		
	Case A	Case B	Case C
None	618.4366	1853.2531	999.4724
cos$\varphi(P)$	618.4366	3974.8352	999.4724
$Q(U)$	1453.9913	1515.7483	1001.1713
$X(U)$	618.4366	1848.5563	999.4724
$X(U)$+	0.0000	0.0000	0.0000
OLTC	618.9152	1853.2941	999.5357
OLTC+	0.0000	0.0000	0.0000

Table A.43 Reactive power contribution of the LV_Link-Grids connected to the small MV_Link-Grid for smoothed load profiles at the CP level, different cases, no control and various control strategies.

Control strategy	$Q_{\Sigma,t}^{MV-LV}$ (kvar)		
	Case A	Case B	Case C
None	727.8706	1475.6636	-147.5860
cos$\varphi(P)$	727.8706	10826.4782	-147.5860
$Q(U)$	1127.1403	3552.6617	-702.6286
$X(U)$	727.8711	1990.3126	-147.5842
$X(U)$+	36.8124	1528.7827	78.0662
OLTC	685.6193	1484.7638	-133.5151
OLTC+	37.5357	834.2631	79.2284

Table A.44 Reactive power contribution of the small MV_Link-Grid for smoothed load profiles at the CP level, different cases, no control and various control strategies.

Control strategy	$Q_{\Sigma,t}^{MV}$ (kvar)		
	Case A	Case B	Case C
None	-4512.7396	-3603.0043	-4010.4498
cos$\varphi(P)$	-4512.7396	-3254.5905	-4010.4498
$Q(U)$	-4509.2919	-3556.4736	-4008.5722
$X(U)$	-4512.7396	-3590.1558	-4010.4497
$X(U)$+	-4514.3924	-3610.2352	-4011.2189
OLTC	-4517.4900	-3601.7510	-4011.0413
OLTC+	-4519.0401	-3618.8506	-4011.8923

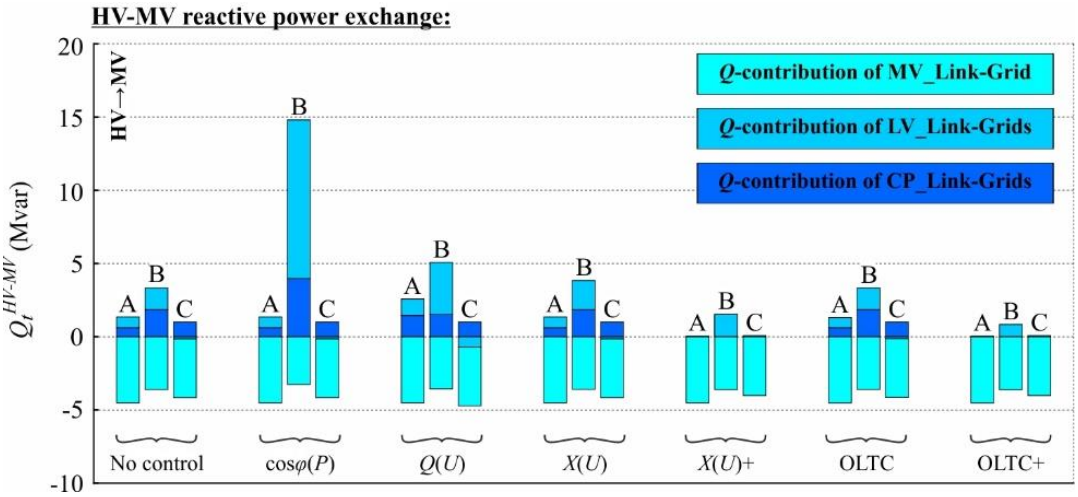

Fig. A.53 Composition of the HV-MV reactive power exchange of the small MV_Link-Grid for smoothed load profiles at the CP level, different cases, no control and various control strategies.

Table A.45 Active power loss within the small MV_Link-Grid for smoothed load profiles at the CP level, different cases, no control and various control strategies.

Control strategy	ΔP_t^{MV} (kW)		
	Case A	Case B	Case C
None	65.6263	522.4462	125.4512
cos$\varphi(P)$	65.6263	822.7866	125.4512
$Q(U)$	56.7900	546.8396	137.9468
$X(U)$	65.6263	527.0487	125.4512
$X(U)$+	81.2532	529.9529	134.0752
OLTC	62.9133	524.2177	124.9212
OLTC+	78.1092	535.3583	133.5975

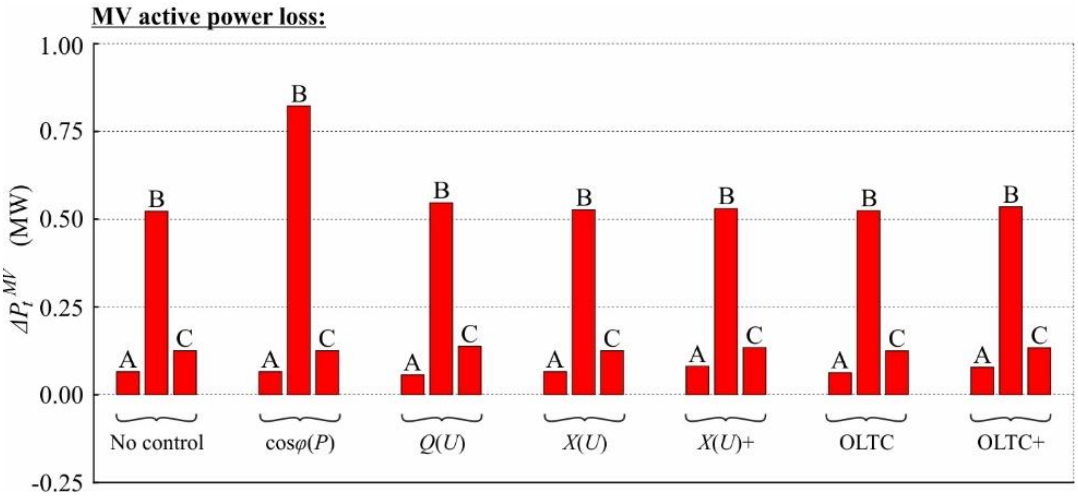

Fig. A.54 Active power loss within the small MV_Link-Grid for smoothed load profiles at the CP level, different cases, no control and various control strategies.

Large MV_Link-Grid

Model specification:

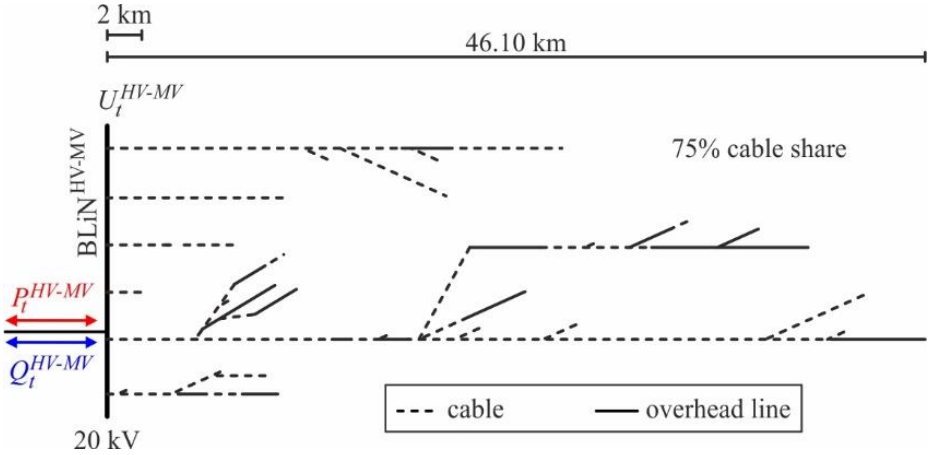

Fig. A.55 Simplified one-line diagram of the large MV_Link-Grid (real Austrian grid).

Table A.46 Model data of the large MV_Link-Grid for smoothed load profiles at the CP level.

Feeders	Nominal voltage			20 kV
	Number of feeders			6
	Total line length			267.151 km
	Total cable share			74.66 %
	Feeder length		Maximal Minimal	46.10 km 2.00 km
Connected lumped models	Link-Grids	CP	Commercial with smoothed load profiles	143
			Industrial with smoothed load profiles	2
		LV	Rural for smoothed load profiles in CP level	45
			Urban for smoothed load profiles in CP level	11
	Producers	Hydroelectric power plants	400 kW*	2
			300 kW*	1
			100 kW*	11
			60 kW*	1

* The hydroelectric power plants are modelled as voltage-independent PQ node-elements. They constantly inject 70 % of their maximal active power production over the entire time-horizon. They do not contribute any reactive power. Their upper and lower BVLs are set to 1.1 and 0.9 p.u. for the complete simulated time horizon.

Behaviour of Link-Grid without any Volt/var controls:

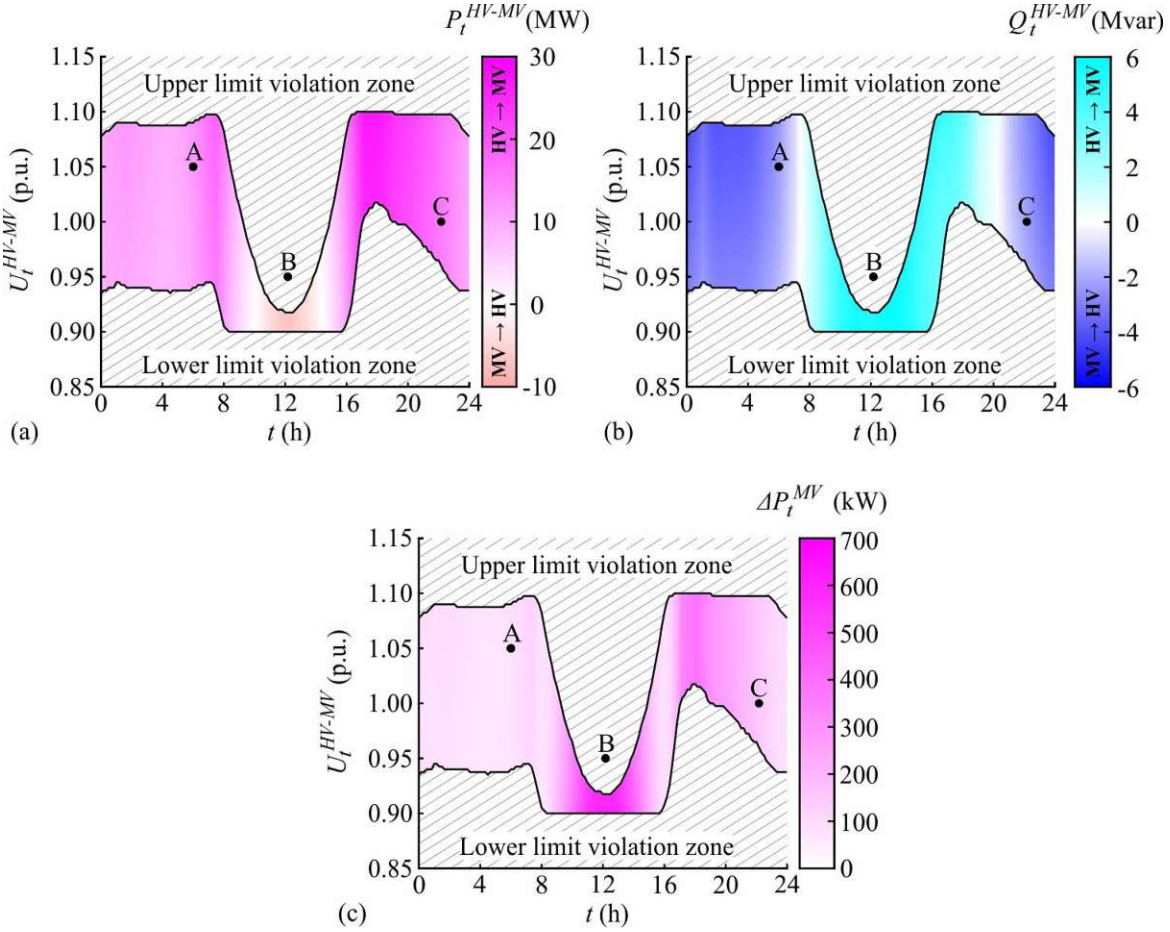

Fig. A.56 Daily behaviour of the large MV_Link-Grid without any Volt/var control for various voltages at the HV-MV boundary node and smoothed load profiles at the CP level: (a) HV-MV active power exchange; (b) HV-MV reactive power exchange; (c) MV active power loss.

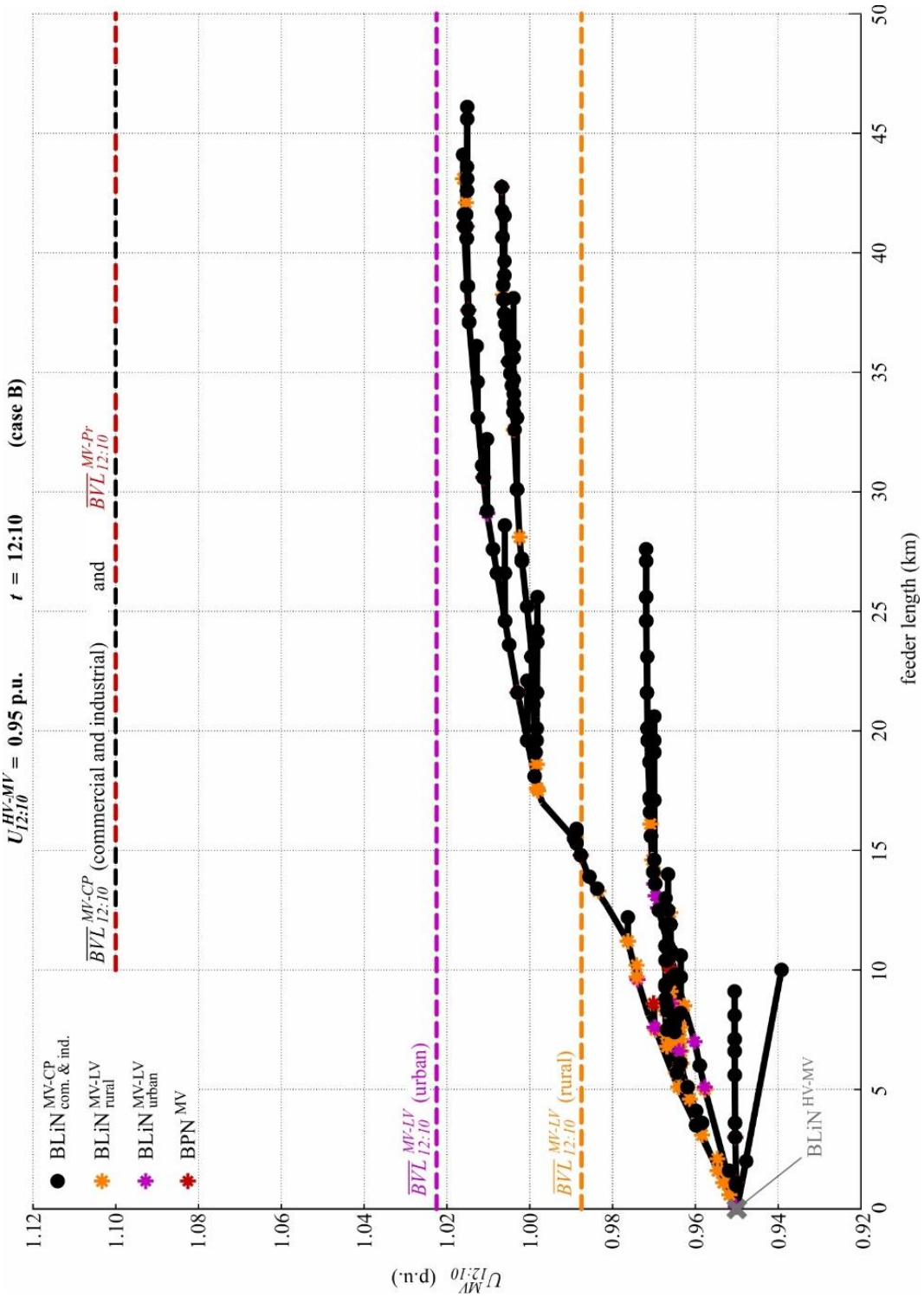

Fig. A.57 Voltage profiles of the large MV_Link-Grid's feeders without any Volt/var control at 12:10 for an HV-MV boundary voltage of 0.95 p.u. (case B) and smoothed load profiles at the CP level.

HV-MV reactive power exchange for different Volt/var controls:

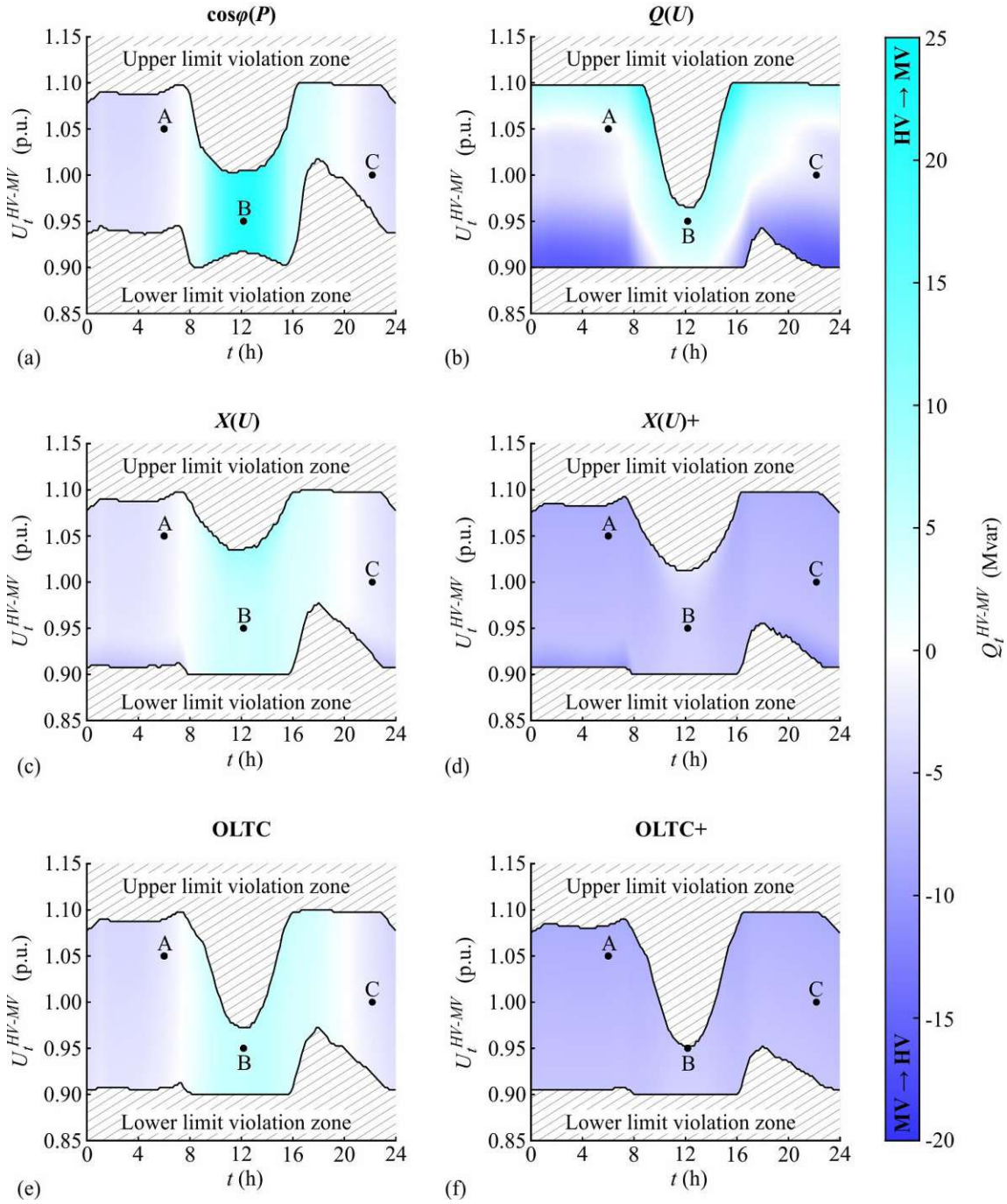

Fig. A.58 Daily HV-MV reactive power exchange of the large MV_Link-Grid for various voltages at the HV-MV boundary node, smoothed load profiles at the CP level, and different control strategies: (a) cosφ(P); (b) Q(U); (c) X(U); (d) X(U) and CP_Q-Autarky; (e) OLTC; (f) OLTC and CP_Q-Autarky.

MV active power loss for different Volt/var controls:

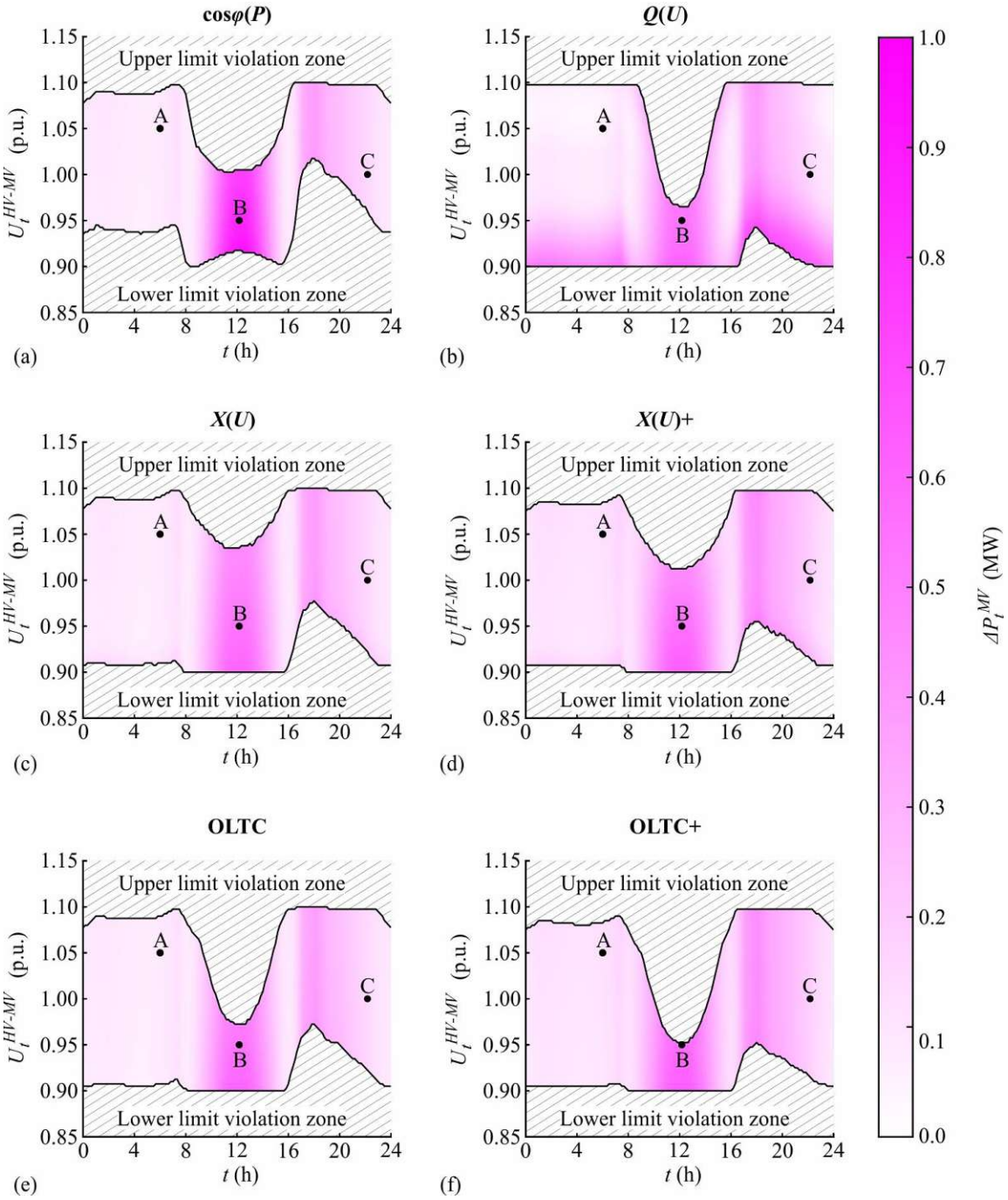

Fig. A.59 Daily active power loss within the large MV_Link-Grid for various voltages at the HV-MV boundary node, smoothed load profiles at the CP level, and different control strategies: (a) cosφ(P); (b) Q(U); (c) X(U); (d) X(U) and CP_Q-Autarky; (e) OLTC; (f) OLTC and CP_Q-Autarky.

Behaviour of Link-Grid in cases A, B and C:

Table A.47 HV-MV reactive power exchange of the large MV_Link-Grid for smoothed load profiles at the CP level, different cases, no control and various control strategies.

Control strategy	Q_t^{HV-MV} (kvar)		
	Case A	Case B	Case C
None	-2178.3268	5323.0076	-2288.3236
cos$\varphi(P)$	-2178.3268	21186.5807	-2288.3236
$Q(U)$	112.0730	6399.8174	-2589.4373
$X(U)$	-2178.3260	5519.1924	-2288.3210
$X(U)$+	-7480.6020	-4754.2448	-6577.2863
OLTC	-2234.5103	5326.7501	-2272.0105
OLTC+	-7484.4610	-5144.4723	-6576.9824

Table A.48 Reactive power contribution of the CP_Link-Grids connected to the large MV_Link-Grid for smoothed load profiles at the CP level, different cases, no control and various control strategies.

Control strategy	$Q_{\Sigma,t}^{MV-CP}$ (kvar)		
	Case A	Case B	Case C
None	4333.0964	9521.7222	4601.8610
cos$\varphi(P)$	4333.0964	13099.2043	4601.8610
$Q(U)$	5899.0375	9067.4411	4604.0249
$X(U)$	4333.0964	9514.0736	4601.8610
$X(U)$+	0.0000	0.0000	0.0000
OLTC	4334.1894	9521.7074	4601.9296
OLTC+	0.0000	0.0000	0.0000

Table A.49 Reactive power contribution of the LV_Link-Grids connected to the large MV_Link-Grid for smoothed load profiles at the CP level, different cases, no control and various control strategies.

Control strategy	$Q_{\Sigma,t}^{MV-LV}$ (kvar)		
	Case A	Case B	Case C
None	1015.8510	1887.8723	-212.1237
cos$\varphi(P)$	1015.8510	13708.7961	-212.1237
$Q(U)$	1720.6532	3389.1906	-514.2476
$X(U)$	1015.8518	2083.9526	-212.1211
$X(U)$+	54.1633	1398.7258	109.2150
OLTC	963.1898	1891.4090	-195.2761
OLTC+	54.9485	1011.2246	110.7794

Table A.50 Reactive power contribution of the large MV_Link-Grid for smoothed load profiles at the CP level, different cases, no control and various control strategies.

Control strategy	$Q_{\Sigma,t}^{MV}$ (kvar)		
	Case A	Case B	Case C
None	-7527.2742	-6086.5869	-6678.0609
cos$\varphi(P)$	-7527.2742	-5621.4196	-6678.0609
$Q(U)$	-7507.6177	-6056.8143	-6679.2146
$X(U)$	-7527.2742	-6078.8338	-6678.0609
$X(U)$+	-7534.7653	-6152.9706	-6686.5013
OLTC	-7531.8895	-6086.3663	-6678.6640
OLTC+	-7539.4095	-6155.6969	-6687.7617

Table A.51 Reactive power contribution of the producers connected to the large MV_Link-Grid for smoothed load profiles at the CP level, different cases, no control and various control strategies.

Control strategy	$Q_{\Sigma,t}^{MV-Pr}$ (kvar)		
	Case A	Case B	Case C
None	0.0000	0.0000	0.0000
cos$\varphi(P)$	0.0000	0.0000	0.0000
$Q(U)$	0.0000	0.0000	0.0000
$X(U)$	0.0000	0.0000	0.0000
$X(U)$+	0.0000	0.0000	0.0000
OLTC	0.0000	0.0000	0.0000
OLTC+	0.0000	0.0000	0.0000

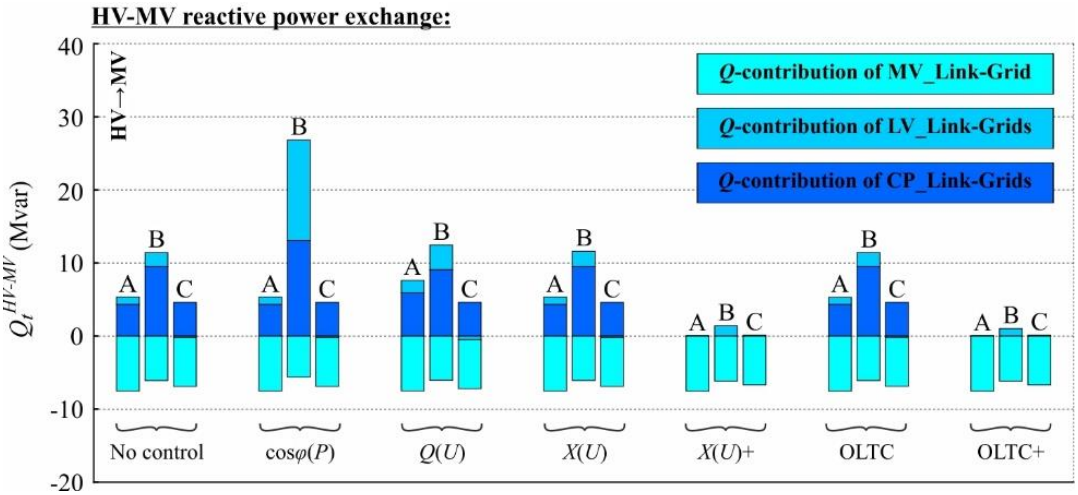

Fig. A.60 Composition of the HV-MV reactive power exchange of the large MV_Link-Grid for smoothed load profiles at the CP level, different cases, no control and various control strategies.

Table A.52 Active power loss within the large MV_Link-Grid for smoothed load profiles at the CP level, different cases, no control and various control strategies.

Control strategy	ΔP_t^{MV} (kW)		
	Case A	Case B	Case C
None	83.1072	536.9832	144.1819
cos$\varphi(P)$	83.1072	846.0916	144.1819
$Q(U)$	52.6137	538.5407	149.2351
$X(U)$	83.1072	536.4634	144.1819
$X(U)$+	121.4523	554.7991	181.1443
OLTC	81.9192	537.2434	143.6320
OLTC+	119.6531	572.3173	180.3358

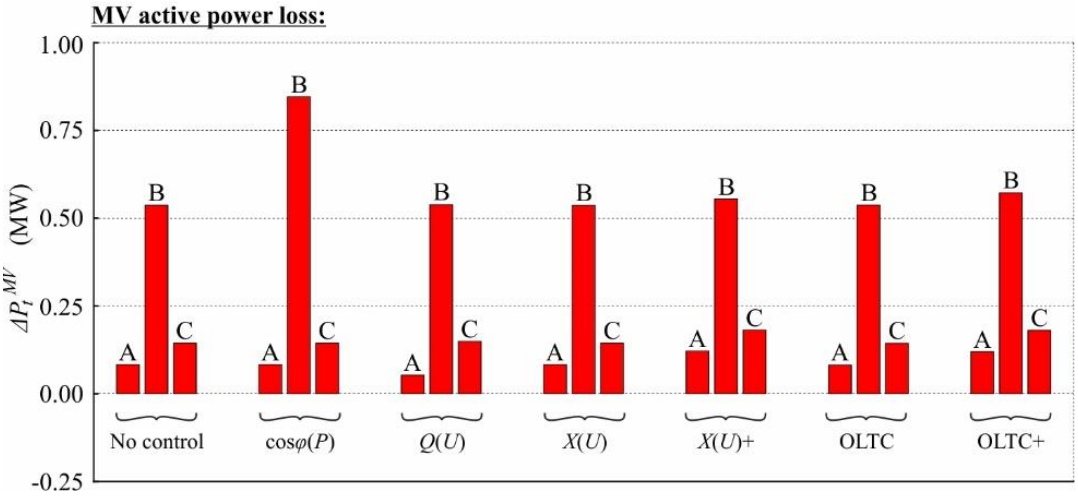

Fig. A.61 Active power loss within the large MV_Link-Grid for smoothed load profiles at the CP level, different cases, no control and various control strategies.

A.2 Volt/var control parametrisation

This appendix discusses the $Q(U)$ and OLTC parametrisation impact on the LV_Link-Grid's behaviour in detail.

A.2.1 Impact of $Q(U)$ parametrisation

The $Q(U)$-control characteristic must be adequately set to widen the BVL_t^{MV-LV} sufficiently, while avoiding unnecessary reactive power flows and oscillations. The maximal impact on the voltage is achieved when all PV inverters connected to the LV_Link-Grid contribute their maximal reactive power, either all in inductive or all in capacitive mode. However, the high reactive power flow increases the grid loss and the loading and propagates up to the superordinate MV_Link-Grid. Therefore, the characteristic should be set with a high slope gradient and a wide dead band to minimise the reactive power flows. But, too high slope gradients may lead to oscillations (Marggraf et al. 2017). Fig. A.62 shows two control characteristics used to analyse the impact of $Q(U)$ parametrisation on the behaviour of the rural LV_Link-Grid: Default and customised. The default characteristic is used in §3.6 to compare the different Volt/var control strategies and yields the results shown in Fig. 3.66b. The customised characteristic is parametrised to maximise the permissible voltage range at the $BLiN^{MV\text{-}LV}$ of the rural LV_Link-Grid for the given scenario while keeping the reactive power flows as low as possible; A higher slope gradient is used in this case.

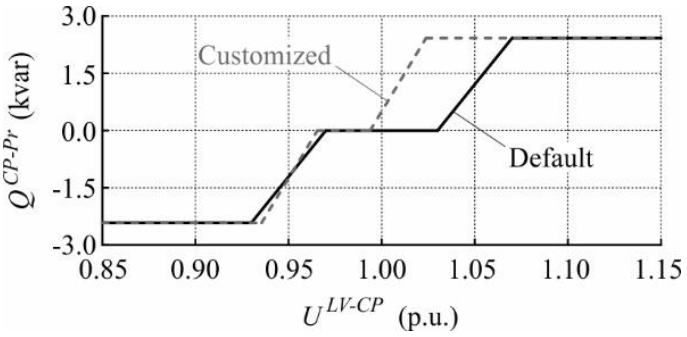

Fig. A.62 Default and customised control characteristics used to analyse the impact of $Q(U)$ parametrisation on the behaviour of the rural LV_Link-Grid.

The methodology used to customise the $Q(U)$-characteristic is illustrated in Fig. A.63. The goal is that all PV inverters contribute their maximal reactive power only when voltage limit violations occur. Simulating the scenario with smoothed load profiles defined in §3.6.2.1 for the customised characteristic yields the upper and lower BVL_t^{MV-LV} shown in Fig. A.63a.

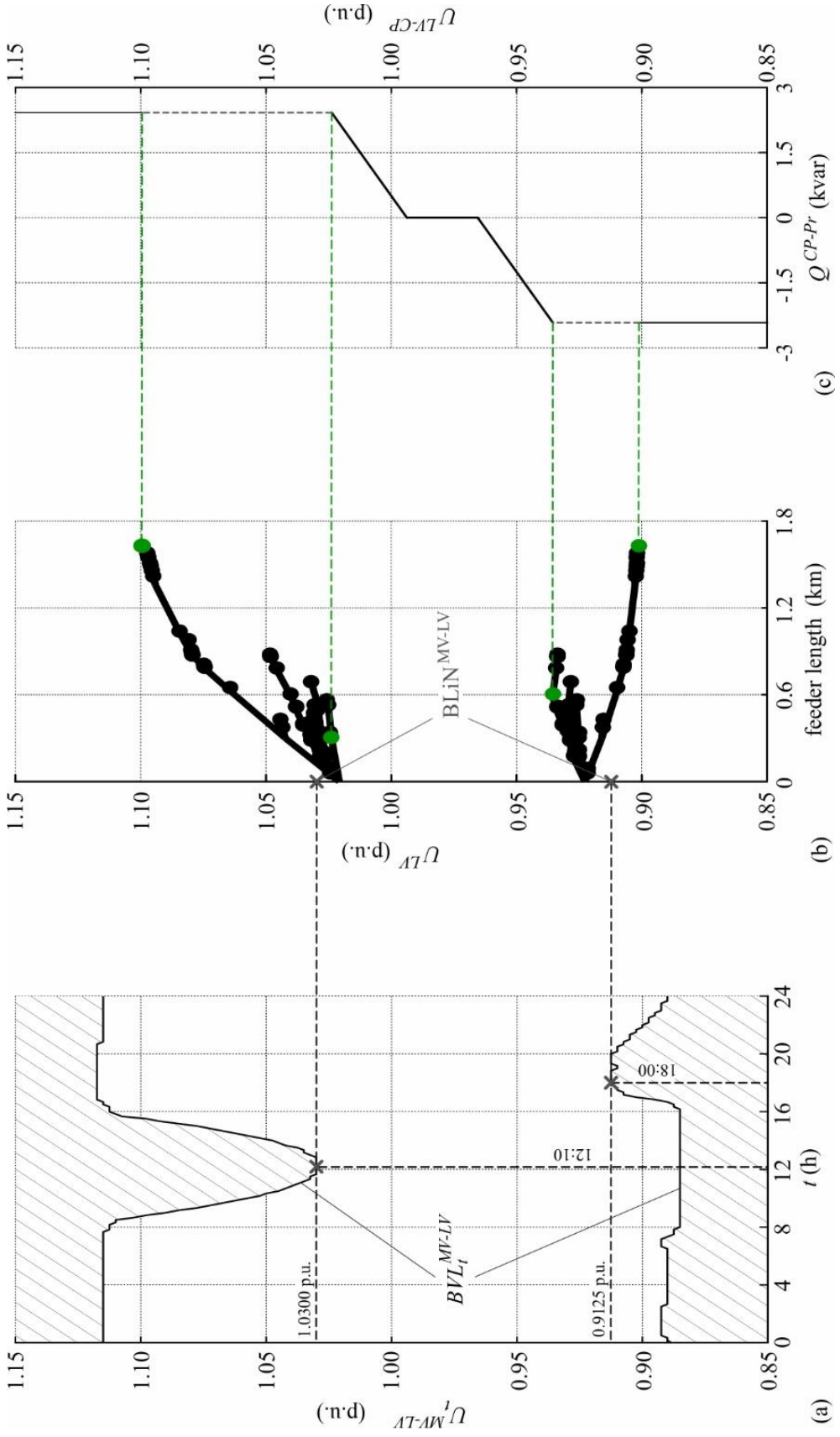

Fig. A.63 Methodology used to customise the $Q(U)$-characteristic for the rural LV_Link-Grid: (a) BVL resulting from the customised $Q(U)$-characteristic; (b) Voltage profiles violating the lower and upper BVL; (c) Customised $Q(U)$-characteristic.

The minimal boundary voltage that leads to upper limit violations within the LV_Link-Grid is 1.03 p.u. and appears at 12:10. Meanwhile, at 18:00 occurs the maximum boundary voltage that leads to lower limit violations, i.e. 0.9125 p.u. These two points are decisive for the control parametrisation, and the corresponding voltage profiles are shown in Fig. A.63b. The difference between the MV-LV boundary voltage, which is marked by a grey cross, and the voltage at the feeder beginning, results from the voltage drop over the DTR. Regarding the case with a lower limit violation, the inverters' capacitive behaviour increases the voltage along the feeders with overhead line share. In contrast, the voltage still decreases at the pure cable feeder due to the high active power consumption. For both cases, the $BLiN^{LV\text{-}CP}$ (which are also the connection nodes of the PV systems) with the lowest and highest voltage values are highlighted with green colour. It is clear to see in Fig. A.63c that all inverters contribute their maximal reactive power (hatched part of the characteristic). When the voltage at the $BLiN^{MV\text{-}LV}$ comes closer to its nominal value, no limits are violated, and some of the inverters reduce their var contribution, thus avoiding unnecessary reactive power flows.

The customised $Q(U)$-characteristic is an idealised case, as the CP power contributions are unknown in reality and vary for each day. But, it enables to theoretically analyse the optimal performance of the control strategy and the impact of its parametrisation on the grid behaviour. Fig. A.64 shows the daily Volt/var behaviour of the rural LV_Link-Grid with $Q(U)$-control for both characteristics.

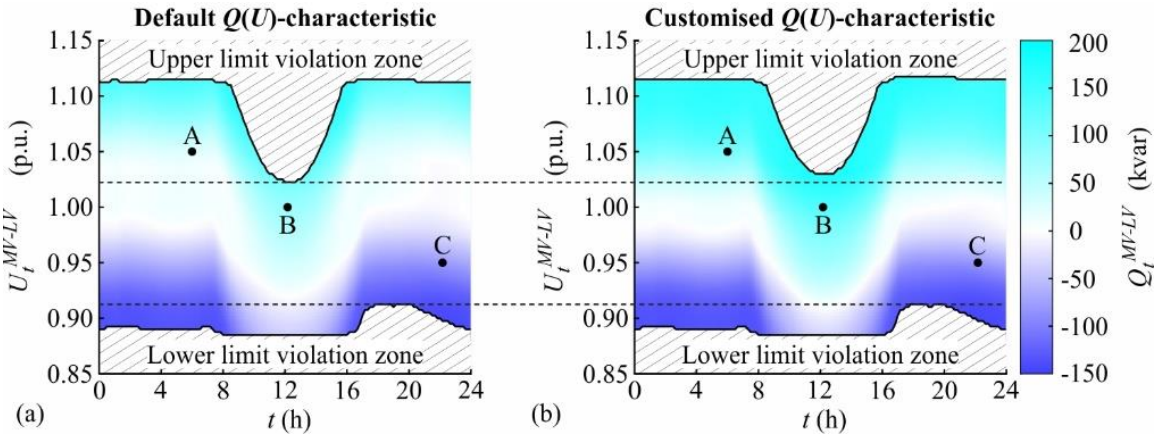

Fig. A.64 Daily MV-LV reactive power exchange of the rural LV_Link-Grid for various voltages at the MV-LV boundary node, smoothed load profiles at the CP level, $Q(U)$-control and different control characteristics: (a) Default; (b) Customised.

In comparison, the customised characteristic allows for higher MV-LV boundary voltages around midday and significantly increases the reactive power flows within a wide area of the voltage-time-plane. However, the inductive and capacitive areas, as well as the BVL_t^{MV-LV},

maintain their fundamental shape independently of the exact parametrisation. The reactive power flows over the BLiN$^{\text{MV-LV}}$ are compared for both $Q(U)$-characteristics in Table A.53.

Table A.53 Reactive power flow over the BLiN$^{\text{MV-LV}}$ of the rural LV_Link-Grid for smoothed load profiles at the CP level, different cases and distinct $Q(U)$-characteristics.

$Q(U)$-characteristic	Q_t^{MV-LV} (kvar)		
	Case A	Case B	Case C
Default	26.02	78.96	-74.98
Customised	107.83	137.24	-76.15

A.2.2 Impact of OLTC parametrisation

The OLTC maintains the voltage at the secondary bus bar of the DTR within a predefined voltage band, which must be adequately set to guarantee limit compliance at the LV level. The ideal parameters are found for the rural LV_Link-Grid and the defined scenario by excluding the DTR from the grid model, setting the BLiN$^{\text{MV-LV}}$ to its secondary bus bar, and calculating the upper and lower BVL_t^{MV-LV} of the resulting model for the case without any Volt/var control, Fig. A.65.

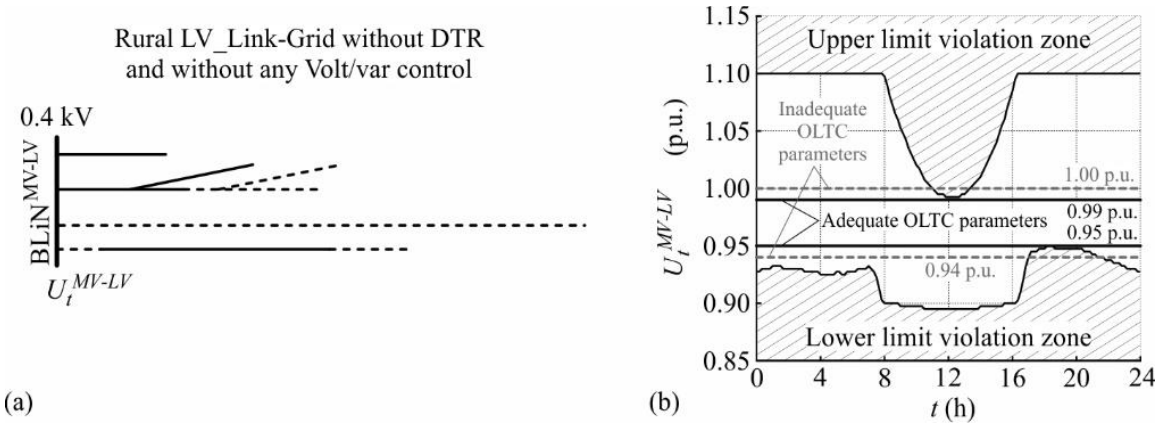

Fig. A.65 Rural LV_Link-Grid without DTR and Volt/var control: (a) Simplified one-line diagram of the grid; (b) Daily boundary voltage limits for smoothed load profiles at the CP level.

This analysis shows that no voltage limit violations occur within the LV grid when the secondary voltage stays within 0.95 and 0.99 p.u.; These values represent the adequate OLTC parameters. To study the impact of inadequate parameters, the wider voltage band between 0.94 and 1.00 p.u. is also considered in the following simulations. The OLTC parametrisation impact is analysed by calculating the lumped model of the rural LV_Link-Grid according to Fig. A.30 for both settings. Using the adequate OLTC parameters yields the results shown in Fig. A.66a.

The original BVL_t^{MV-LV}, i.e. those without any Volt/var control, are shifted mainly in parallel, without affecting the reactive power exchange significantly. When inadequate parameters are used, the BVL_t^{MV-LV} are also shifted in parallel, and additionally, upper and lower **limit violation islands** occur in the voltage-time-plane, Fig. A.66b. An increase of the MV-LV boundary voltage eliminates the upper limit violations at the LV level in the upper islands. In the lower ones, a reduction of the boundary voltage eliminates the lower limit violations.

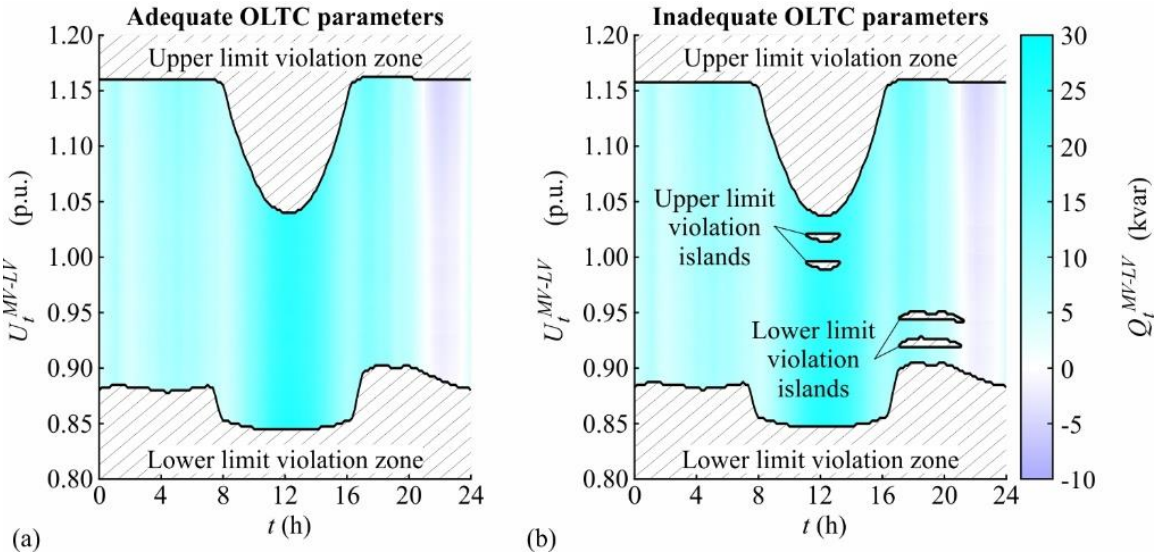

Fig. A.66 Daily MV-LV reactive power exchange of the rural LV_Link-Grid for various voltages at the MV-LV boundary node, smoothed load profiles at the CP level, OLTC and different control settings: (a) Adequate; (b) Inadequate.

To clarify the limit violation islands' occurrence, Fig. A.67 enlarges the limit violation islands and shows the voltage profiles of all feeders of the rural LV_Link-Grid with inadequate OLTC parameters at 18:00 for three different MV-LV boundary voltages: 0.9575 p.u. (case X), 0.9475 p.u. (case Y), and 0.9375 p.u. (case Z). In case X, the mid-position of the tap (3/5) is sufficient to maintain the voltage at the feeder beginning in the predefined band, which is set between 0.94 and 1.00 p.u. When the MV-LV boundary voltage decreases by 0.01 p.u., the CPs located at the feeder end violate their lower limit, case Y. Meanwhile, the voltage at the feeder beginning is 0.944 p.u., thus no change of the tap position is required. When the MV-LV boundary voltage further decreases, the tap changes its position to 4/5, eliminating the violations of the lower voltage limit, case Z.

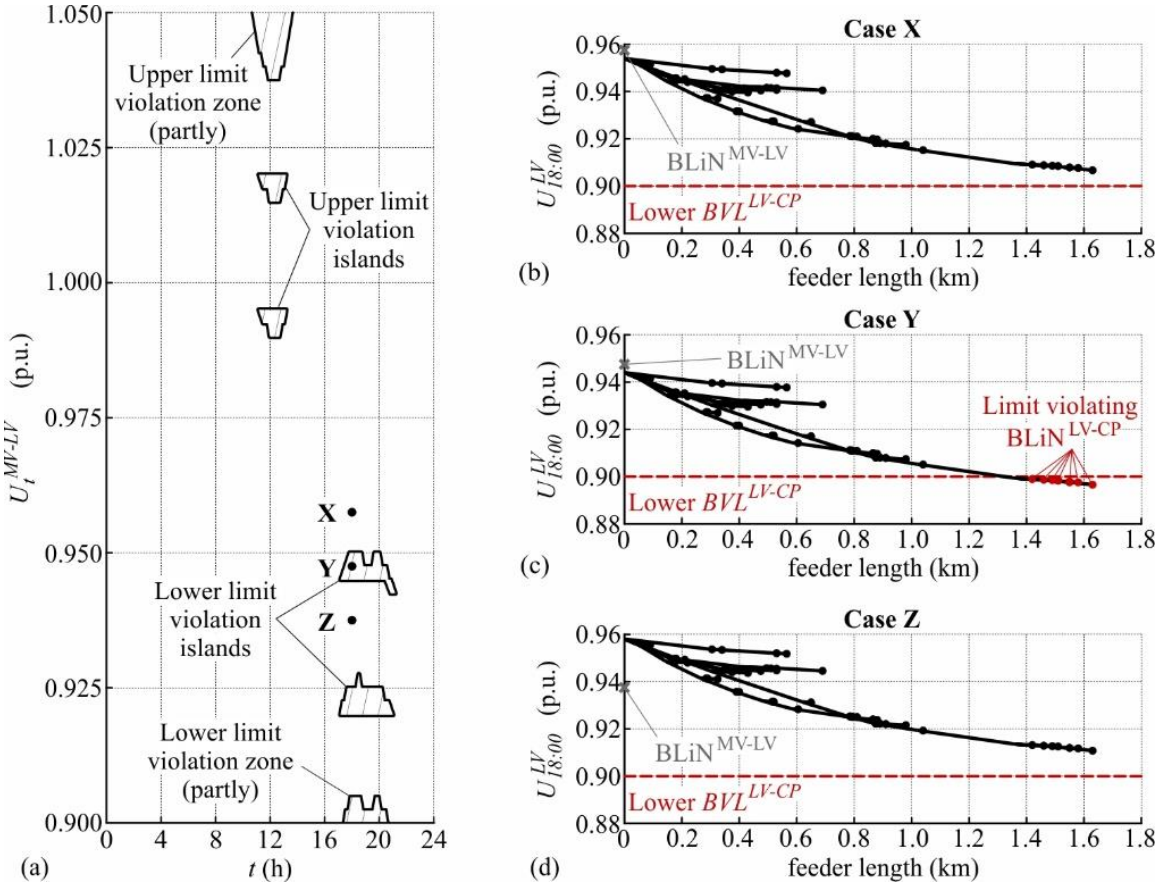

Fig. A.67 Occurrence of limit violation islands in the rural LV_Link-Grid with inadequate OLTC parameters: (a) Enlargement of the limit violation islands; (b-d) Voltage profiles of all feeders for cases X, Y and Z.

A.3 Volt/var control evaluation

This appendix provides the detailed definitions of the evaluation criteria used in §3.7 and the normalisation procedure used to enable their illustration within the evaluation hexagon.

A.3.1 Definition of technical evaluation criteria

The technical criteria are calculated for the (*U*,*t*)-plane spanned by the simulated time horizon of 24 hours and by the MV-LV boundary voltages between 0.9 and 1.1 p.u. (see Fig. 3.79). For brevity, the MV-LV boundary voltage (U_t^{MV-LV}) is denoted just as U in Equations (3.49) to (3.52).

Voltage limit violations

The voltage limit Violation Index (*VI*) is calculated for the regarded zone within the (*U*,*t*)-plane according to Equation (3.49).

$$VI_{U,t} = \frac{1}{N^{nodes}} \left(\sum_{j=1}^{m_{U,t}} \left(\frac{U_{U,t}^{\overline{viol},j}}{U_{nom}^{LV}} - 1.1 \text{ p.u.} \right) + \sum_{j=1}^{n_{U,t}} \left(0.9 \text{ p.u.} - \frac{U_{U,t}^{\underline{viol},j}}{U_{nom}^{LV}} \right) \right) \quad (3.49a)$$

$$VI = \sum_{\forall t} \sum_{\forall U} VI_{U,t} \quad (3.49b)$$

Where U and t are the MV-LV boundary voltage and the instant of time, respectively; N^{nodes} is the total number of LV grid nodes; $m_{U,t}$ is the number of the LV grid nodes that violate the upper voltage limit; $n_{U,t}$ is the number of the LV grid nodes that violate the lower voltage limit; $U_{U,t}^{\overline{viol},j}$ are the voltages of the LV grid nodes that violate the upper voltage limit; $U_{U,t}^{\underline{viol},j}$ are the voltages of the LV grid nodes that violate the lower voltage limit; And U_{nom}^{LV} is the nominal voltage of the LV level.

MV-LV reactive power exchange

The MV-LV reactive energy exchange (E^Q) is calculated for the regarded (*U*,*t*)-plane according to Equation (3.50) without considering the flow direction.

$$E^Q = \Delta t \cdot \sum_{\forall t} \sum_{\forall U} \left| Q_{U,t}^{MV-LV} \right| \quad (3.50)$$

Where $\Delta t = 10$ min is the temporal resolution of the smoothed load profiles; And $Q_{U,t}^{MV-LV}$ is the reactive power flow through the MV-LV boundary node.

Active power loss

The energy loss (ΔE) is calculated for the regarded (*U*,*t*)-plane according to Equation (3.51).

$$\Delta E = \Delta t \cdot \sum_{\forall t} \sum_{\forall U} \Delta P_{U,t}^{LV} \tag{3.51}$$

Where $\Delta P_{U,t}^{LV}$ is the active power loss within the LV_Link-Grid.

DTR loading

The average DTR loading ($Loading^{DTR,avg}$) is calculated for the regarded (U,t)-plane according to Equation (3.52).

$$Loading^{DTR,avg} = \frac{1}{N^t \cdot N^U} \cdot \sum_{\forall t} \sum_{\forall U} Loading_{U,t}^{DTR} \tag{3.52}$$

Where N^U, N^t are the numbers of MV-LV boundary voltages and instants of time, respectively, within the regarded (U,t)-plane.

A.3.2 Calculation of the evaluation hexagon data

The evaluation criteria defined in §A.3.1 are calculated for each control setup (indexed with c) and both LV_Link-Grids (indexed with g) catalogued in §A.1.2.2. Firstly, the evaluation hexagon is calculated for each LV_Link-Grid separately, and secondly, a common hexagon is calculated to enable the compact presentation of the final evaluation results.

Calculation of the separate hexagons

The technical evaluation criteria are normalised according to Equation (3.53) to enable their illustration in a common chart. The resulting normalised evaluation criteria lie within the interval [0, 1] and do not have any physical unit.

$$VI_{c,g}^{norm} = \frac{VI_{c,g}}{\max\limits_{c}\left(VI_{c,g}\right)} \tag{3.53a}$$

$$E_{c,g}^{Q,norm} = \frac{E_{c,g}^{Q}}{\max\limits_{c}\left(E_{c,g}^{Q}\right)} \tag{3.53b}$$

$$\Delta E_{c,g}^{norm} = \frac{\Delta E_{c,g}}{\max\limits_{c}\left(\Delta E_{c,g}\right)} \tag{3.53c}$$

$$Loading_{c,g}^{DTR,avg,norm} = \frac{Loading_{c,g}^{DTR,avg}}{\max\limits_{c}\left(Loading_{c,g}^{DTR,avg}\right)} \tag{3.53d}$$

Where $VI_{c,g}^{norm}$, $E_{c,g}^{Q,norm}$, $\Delta E_{c,g}^{norm}$, $Loading_{c,g}^{DTR,avg,norm}$ are the normalised values of the evaluation criteria of the control setup c and the LV_Link-Grid g (rural or urban).

Calculation of the common hexagon

The results of both LV_Link-Grids are superimposed according to Equation (3.54) to enable the compact presentation of the evaluation.

$$VI_c^{norm} = \frac{VI_{c,rural}^{norm} + VI_{c,urban}^{norm}}{2} \tag{3.54a}$$

$$E_c^{Q,norm} = \frac{E_{c,rural}^{Q,norm} + E_{c,urban}^{Q,norm}}{2} \tag{3.54b}$$

$$\Delta E_c^{norm} = \frac{\Delta E_{c,rural}^{norm} + \Delta E_{c,urban}^{norm}}{2} \tag{3.54c}$$

$$Loading_c^{DTR,avg,norm} = \frac{Loading_{c,rural}^{DTR,avg,norm} + Loading_{c,urban}^{DTR,avg,norm}}{2} \tag{3.54d}$$

Where VI_c^{norm}, $E_c^{Q,norm}$, ΔE_c^{norm}, $Loading_c^{DTR,avg,norm}$ are the normalised and superimposed values of the evaluation criteria for the control setup *c,* which are plotted in the common evaluation hexagon.

A.4 List of own publications

This appendix provides an overview of the author's scientific publications related to the topic of this dissertation.

A.4.1 Books

Ilo A, Schultis DL (2021) Holistic solution for Smart Grids based on LINK-Paradigm – Architecture, Energy Systems Integration, Volt/var chain process. Springer Nature, Cham. (in press)

A.4.2 Journal articles

Schultis DL, Ilo A (2019) Behaviour of Distribution Grids with the Highest PV Share Using the Volt/Var Control Chain Strategy. Energies, vol 12/20, 3865. https://www.mdpi.com/1996-1073/12/20/3865

Schultis DL (2019) Comparison of Local Volt/var Control Strategies for PV Hosting Capacity Enhancement of Low Voltage Feeders. Energies, vol 12/8, 1560. https://www.mdpi.com/1996-1073/12/8/1560

Ilo A, Schultis DL (2019) Low-voltage grid behaviour in the presence of concentrated var-sinks and var-compensated customers. Electric Power Systems Research, vol 171, pp 54-65. https://www.sciencedirect.com/science/article/abs/pii/S0378779619300434?via%3Dihub

Schultis DL, Ilo A, Schirmer C (2019) Overall performance evaluation of reactive power control strategies in low voltage grids with high prosumer share. Electric Power Systems Research, vol 168, pp 336-349. https://www.sciencedirect.com/science/article/abs/pii/S0378779618304127?via%3Dihub

Ilo A, Schultis DL, Schirmer C (2018) Effectiveness of Distributed vs. Concentrated Volt/Var Local Control Strategies in Low-Voltage Grids. Applied Sciences, vol 8/8, 1382. https://www.mdpi.com/2076-3417/8/8/1382

A.4.3 Conference papers

Schultis DL, Ilo A (2021) "Boundary Voltage Limits" – an instrument to increase the utilization of the existing infrastructures. CIRED 2021 Conference, Geneva, Switzerland, 20-23 September, 910. (accepted for publication)

Schultis DL, Petrusic S, Ilo A (2020) Modelling of low voltage grids with high PV share and Q(U)-control. CIRED 2020 Berlin Workshop, Berlin, Germany, 22-23 September, 360. https://publik.tuwien.ac.at/files/publik_290406.pdf

Schultis DL, Ilo A (2019) Adaption of the Current Load Model to Consider Residential Customers Having Turned to LED Lighting. 11th IEEE PES Asia-Pacific Power & Energy Engineering Conference, Macao, China, 1-4 December, pp 1-5. https://ieeexplore.ieee.org/document/8994535

Schultis DL, Ilo A (2019) A new Volt/var local control strategy in low-voltage grids in the context of the LINK-based holistic architecture. 11. Internationale Energiewirtschaftstagung an der TU Wien, Vienna, Austria, 13-15 February, pp 1-11. https://www.semanticscholar.org/paper/A-new-Volt-%2F-var-local-control-strategy-in-grids-

in-Schultis-Ilo/a4a1cbe2810c2bab641e7a7736d140ee72548657

Ilo A, Schirmer C, Schultis DL (2018) Robust Holistic Architecture for Smart Power Systems. CIRED Workshop on Microgrids and Local Energy Communities, Ljubljana, Slovenia, 7-8 June, 407. http://www.cired.net/publications/workshop2018/pdfs/Submission%200407%20-%20Paper%20(ID-20912).pdf

Schultis DL, Ilo A, Schirmer C (2018) Evaluation of Different Local Var Control Strategies in Low Voltage Grids. CIRED Workshop on Microgrids and Local Energy Communities, Ljubljana, Slovenia, 7-8 June, 454. http://www.cired.net/publications/workshop2018/pdfs/Submission%200454%20-%20Paper%20(ID-20915).pdf

A.4.4 Book chapters

Schultis DL (2020) Comparison of Local Volt/var Control Strategies for PV Hosting Capacity Enhancement of Low Voltage Feeders. Khumprom P, Bošnjaković M. Advances in Energy Research. Vide Leaf, Hyderabad. https://videleaf.com/product/advances-in-energy-research/

A.4.5 Datasets

Schultis DL (2019) Daily load profiles and ZIP models of current and new residential customers. Mendeley Data. https://data.mendeley.com/datasets/7gp7dpvw6b/1

Schultis DL, Ilo A (2018) TUWien_LV_TestGrids. Mendeley Data. https://data.mendeley.com/datasets/hgh8c99tnx/1